AD-A137 438 MORISON'S EQUATION AND THE WAVE FORCES ON OFFSHORE 1/3
STRUCTURES(U) SARPKAYA (TURGUT) CARMEL CA T SARPKAYA
DEC 81 NCEL-CR-82.008 N68305-80-C-0053

UNCLASSIFIED F/G 8/3 NL

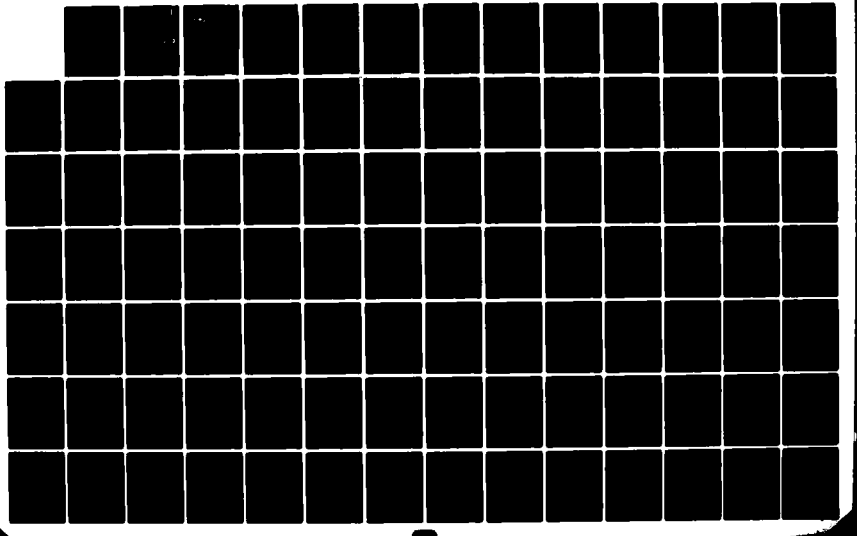

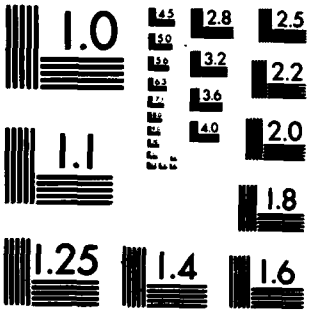

AD A137438

DTIC ACCESSION NUMBER

II

LEVEL

PHOTOGRAPH THIS SHEET

I

INVENTORY

Rpt. No. CR 82.008

Sarpkaya, Turgut

Dec '81

DOCUMENT IDENTIFICATION

N68305-80-C-0053

DISTRIBUTION STATEMENT A

Approved for public release;
Distribution Unlimited

DISTRIBUTION STATEMENT

ACCESSION FOR	
NTIS	GRA&I
DTIC	TAB
UNANNOUNCED	
JUSTIFICATION	
BY	
DISTRIBUTION /	
AVAILABILITY CODES	
DIST	AVAIL AND/OR SPECIAL
A/1	

DTIC
ELECTE
FEB 2 1984
S D
D

DATE ACCESSIONED

DISTRIBUTION STAMP

DATE RETURNED

84 02 02 013

DATE RECEIVED IN DTIC

REGISTERED OR CERTIFIED NO.

PHOTOGRAPH THIS SHEET AND RETURN TO DTIC-DDAC

DTIC FORM 70A
DEC 83

DOCUMENT PROCESSING SHEET

PREVIOUS EDITION MAY BE USED UNTIL STOCK IS EXHAUSTED.

CR 82.008

NAVAL CIVIL ENGINEERING LABORATORY
Port Hueneme, California

Sponsored by
NAVAL FACILITIES ENGINEERING COMMAND

MORISON'S EQUATION AND THE WAVE FORCES ON OFFSHORE STRUCTURES

December 1981

An Investigation Conducted by
Dr. Turgut Sarpkaya
25330 Vista del Pinos
Carmel, California

N68305-80-C-0053

Unclassified
SECURITY CLASSIFICATION OF THIS PAGE (When Data Entered)

REPORT DOCUMENTATION PAGE		READ INSTRUCTIONS BEFORE COMPLETING FORM
1. REPORT NUMBER CR 82.008	2. GOVT ACCESSION NO.	3. RECIPIENT'S CATALOG NUMBER
4. TITLE (and Subtitle) Morison's Equation and the Wave Forces on Offshore Structures		5. TYPE OF REPORT & PERIOD COVERED Final Sept 1980 - Sep 1981 6. PERFORMING ORG. REPORT NUMBER
7. AUTHOR(s) Turgut Sarpkaya		8. CONTRACT OR GRANT NUMBER(s) N68305-80-C-0053
9. PERFORMING ORGANIZATION NAME AND ADDRESS Dr. Turgut Sarpkaya 25330 Vista del Pinos, Carmel, CA 93923		10. PROGRAM ELEMENT, PROJECT, TASK AREA & WORK UNIT NUMBERS 62759N YF59.556.091.01.501
11. CONTROLLING OFFICE NAME AND ADDRESS Naval Civil Engineering Laboratory Port Hueneme, CA 93043		12. REPORT DATE December 1981 13. NUMBER OF PAGES 266
14. MONITORING AGENCY NAME & ADDRESS(if different from Controlling Office)		15. SECURITY CLASS. (of this report) Unclassified 15a. DECLASSIFICATION DOWNGRADING SCHEDULE

16. DISTRIBUTION STATEMENT (of this Report)

Approved for public release; distribution unlimited.

17. DISTRIBUTION STATEMENT (of the abstract entered in Block 20, if different from Report)

18. SUPPLEMENTARY NOTES

19. KEY WORDS (Continue on reverse side if necessary and identify by block number)
Morison's equation, Ocean waves, Wave forces, Drag coefficient, Inertia coefficient, Surface roughness, Transverse or lift force, Research needs

20. ABSTRACT (Continue on reverse side if necessary and identify by block number)
The origin and limitations of the Morison-O'Brien-Johnson-Schaff (MOJS) equation, the nature and decomposition of the time-dependent in-line force, the speculative generalizations of the MOJS equation to body shapes other than circular cylinders, to yawed cylinders, to wave-current combination, and to dynamic response of structures are discussed in detail. The background

DD FORM 1 JAN 73 1473 EDITION OF 1 NOV 65 IS OBSOLETE

Unclassified
SECURITY CLASSIFICATION OF THIS PAGE (When Data Entered)

and the limitations of the existing data are reviewed and the data from sinusoidally-oscillating planar flow about smooth and rough circular cylinders are chosen to critically assess the MOJS equation. Six methods are examined to delineate the limitations of the MOJS equation and to devise a new force expression. The final method used (the Fourier analysis of the residues) led to the formulation of a three-term and a four-term MOJS equation. It is shown through numerous examples that the new MOJS equation reduces the residue significantly for both smooth and rough circular cylinders, particularly in the drag-inertia dominated regime. Finally, the applicability of the new equation to the ocean conditions and the effect of spanwise coherence are discussed and numerous research projects are recommended for consideration. The suggestion is made that further improvement and understanding of the MOJS equation rest not only with carefully conducted laboratory investigations but also with additional ocean tests designed to shed light on several complicating influences such as the spanwise coherence of vortices and vortex interactions.

ACKNOWLEDGEMENT

This investigation has been sponsored by the Naval Civil Engineering Laboratory under contract No. N68305-80-C-0053.

The support and encouragement of Mr. Thomas M. Ward, the technical representative for the contract, are sincerely appreciated.

TABLE OF CONTENTS

LIST OF FIGURES

LIST OF TABLES

NOMENCLATURE*

A	Amplitude of flow oscillations
A_{mp}	Coefficients, [see Eq. (66)]
A_n	Fourier coefficients
A_p	Projected area per unit length
a	Acceleration
B_{mp}	Coefficients, [see Eq. (66)]
B_n	Fourier coefficients
B_n'	Fourier coefficients
C	Structural damping
C_a	Added mass coefficient
C_d	Drag coefficient
$\bar{C}_d$	Average drag coefficient in steady flow
C_{F*}	Force coefficient, [see Eq. (41)]
C_L	Lift coefficient
C_m	Inertia coefficient
C_{mp}	Coefficients, [see Eq. (66)]
c	Radius of circular cylinder
D	Diameter of body
d	Water depth
F	Force
F_c	Calculated force
F_{il}	In-line force
F_L	Transverse or lift force

*Additional symbols are defined as they appear in the text.

F_m	Measured force
f_v	Vortex shedding frequency
H	Wave height
K	Keulegan-Carpenter number, $K = 2\pi A/D = U_m T/D = \pi H/D$
K_s	Structural stiffness
k	Mean roughness height
L	Wave length
L_c	Length of circular cylinder
M	Mass per unit length
N	An integer
n	An integer
p, q	Coordinates of a vortex
R	Radius of sphere
Re	Reynolds number, $Re = U_m D/\nu$
St	Strouhal number (also denoted as S), $St = f_v D/U_m$ or $f_v D/\bar{V}$
s	Displacement of fluid
T	Period of flow oscillation
t	Time
U	Instantaneous velocity
U_m	Maximum velocity in a cycle
u	x-component of velocity
$\bar{V}$	Velocity of mean flow
x,y,z	Coordinate axis
z	Distance along the cylinder

α	Yaw angle
β	Frequency parameter, $\beta = Re/K = D^2/\nu T$
Γ	Circulation of vortex
ΔR	Residue
η	A proportionality factor
θ	angle, $\theta = 2\pi t/T$
Λ	$(C_m^* - C_m)/(KC_d)$ where C_m^* is the ideal potential flow value of C_m
μ	Dynamic viscosity
ν	Kinematic viscosity
ρ	Fluid density
σ	Goodness-of-fit parameter, [see Eq.(71)]
ϕ	Phase angle
ψ	Coherence-state factor
ω	Circular frequency

1.0 INTRODUCTION

Unsteady motion is of great interest in the solution of many applied technical problems in fluid mechanics, such as the motion of bodies through fluids, fluid motion in or about bodies, free-surface phenomena, and others. The variety and the complexity of the problems, particularly those involving separation, put their rigorous calculation beyond reach. In fact, a large number of practical and practically-inspired basic time-dependent flow problems exist for which ignorance reigns supreme. However, it will be misleading to invoke the unsteadiness of the ambient flow as the sole cause of all difficulties. In reality, the flow behind a bluff body, moving steadily through a fluid, is accompanied by large-scale unsteadiness. Thus, any type of unsteadiness of the ambient flow and/or of the motion of the body introduce additional changes in the characteristics of the flow.

The formation of a wake gives rise not only to a form drag, as would be the case if the motion were steady, but also to significant changes in the inertial forces. The velocity-dependent form drag is not the same as that for the steady flow of a viscous fluid, and the acceleration-dependent inertial resistance is not the same as that for an unseparated unsteady flow of an inviscid fluid. In other words, the drag and the inertial forces are inter-dependent as well as time-dependent. Although indirect, the role of viscosity is paramount in that its consequences are separation, vortex formation and shedding, and resultant alterations in the added mass. The specification of these various aspects provides a basis for the correlation of theoretically predicted and observed forces. Evidently, the coefficients obtained for unseparated unsteady flows are not applicable to occurrences in which the duration of flow in one direction is long enough and the body form blunt

enough for separation to occur. It is necessary to determine the relationships between various resistance components in terms of the unsteadiness of the ambient flow, the geometry of the body, the degree of the upstream turbulence, the roughness of the object, and the past history of the flow.

Clearly, it will not be a meaningful exercise to interpret the consequences of unsteadiness with preconceived notions or ideas carried over from steady flows. For example, in a sinusoidally-oscillating flow about a circular cylinder the periodic reversals of the flow inevitably lead to the forward and backward motion of the vortices whereas in steady flow the vortices shed (at a Strouhal frequency dependent on the Reynolds number) and are convected downstream. Thus, one is tempted to attribute the changes in drag to the vortex velocity fields and their 'unsteady' convection by the periodic flow. This is an obvious but nevertheless too simplistic explanation of the actual occurrences. Even for unidirectional time-dependent flows about bluff bodies, there are significant differences between the steady and unsteady flows in the levels of resistance experienced by the body. In general, it is more appropriate to regard each time-dependent flow situation as a new presence with all of its attendant consequences and not only in terms of its most obvious features. The wave motion about bluff bodies is such a time-dependent flow which demands quantitative analysis, ingenious experiments, and qualitative descriptions for the purpose of explaining the underlying causes of the physical effects and providing a model by which design can be reasonably performed.

2.0 THE ORIGIN OF THE MOJS EQUATION AND ITS LIMITATIONS

In a paper[1] submitted to the Petroleum Transactions of AIME on 23 October 1949, Morison, O'Brien, Johnson, and Schaaf (referred to hereafter as MOJS) wrote:

> "The force exerted by unbroken surface waves on a cylindrical object, such as a pile, which extends from the bottom upward above the wave crest, is made up of two components, namely: (1) A drag force proportional to the square of the velocity which may be represented by a drag coefficient having substantially the same value as for steady flow, and (2) A virtual mass force proportional to the horizontal component of the accelerative force exerted on the mass of water displaced by the pile. These relationships follow directly from wave theory and have been confirmed by measurements..."

Thus was born the MOJS equation, often referred to as the Morison equation. The authors also stated that "This paper is essentially a preliminary report submitted at this time because of the current importance of wave forces in the design of offshore structures[2]."

The MOJS equation was originally written as (retaining the nomenclature originally used by the authors)

$$dF = \left[C_M\left(\rho\frac{\pi D^2}{4}\right)\frac{\partial u}{\partial t} \pm C_D\frac{\rho D}{2}u^2\right]dz \qquad (1)$$

where dF represents the force exerted on a differential section, dz,

---

(1) See Morison et al., (1950), citation p. 77

(2) It is of some interest to note that the work of MOJS has been conducted under a contract with the U. S. Navy on a problem posed by the Bureau of Yards and Docks, the predecessor of the Naval Facilities Engineering Command.

in length; D, the pile diameter; ρ, water mass density; C_M, coefficient of mass; C_D, coefficient of drag; u, the horizontal component of the orbital velocity; and $\frac{\partial u}{\partial t}$, the acceleration (meaning local acceleration) of the water particles.

MOJS went on to express Eq. (1) in a form suitable for waves of small amplitude and carried out experiments in a wave flume with model piles hinged at the bottom. The necessary restraining force was measured at a known moment arm above the hinge. The coefficients C_D and C_M were obtained "by measuring the force when $\cos\theta$ or $\sin\theta$ are zero, respectively" (now known as the two-point method). According to MOJS "The experimental values of C_M and C_D showed some scattering but no trend as a function of d/L (still water depth/wave length), H/L (wave height/wave length) or Reynolds number. The average values obtained for runs with the pile on a horizontal bottom and without impulsive forces, were $C_M = 1.508 \pm 0.197$, $C_D = 1.626 \pm 0.414$. The Reynolds number, corresponding to the maximum surface orbital velocity, ranged from 0.22×10^4 to 1.11×10^4. The Reynolds number decreased from these maximum values both downward along the pile and with time. The drag coefficient of a cylinder varies not only with the Reynolds number but also with the turbulence of the incident stream. Values of C_D for cylinders in a steady stream of air or water within this range of Reynolds numbers vary from 0.65 to 1.20."

The MOJS paper represents in many ways a rather remarkable piece of engineering work. It is partly because of its historical importance and partly because many later works employed similar experimental and evaluation methods that the MOJS paper will be discussed in some detail.

1. MOJS recognized the importance of breaking waves and the impulsive

nature of the force exerted by breakers;

2. MOJS noted that "the orbit velocities are also unsymmetrical, the forward velocity at the crest exceeding the backward velocity in the trough by approximately 10 percent in a deep-water wave having a steepness ratio (H/L) of 0.02 and approximately 25 percent for a steepness ratio of 0.10";

3. Analysis of the data has been based upon a sinusoidal variation in velocity and, in effect, the asymmetrical velocity variation is represented in the empirical coefficients;

4. C_D and C_M were based on the total force (or moment) acting on the entire pile, evaluated as noted before. In view of this and in view of items (2) and (3), it is rather surprising that MOJS reported C_D and C_M with such scientific precision ($C_M = 1.508 \pm 0.197$ and $C_D = 1.626 \pm 0.414$);

5. The force expression is assumed "to follow directly from wave theory" and "confirmed by measurements." In fact, MOJS is stating that the force on a vertical "cylindrical object" (a circular cylinder or any other cylindrical object) is due to the horizontal component of the orbital velocity and the horizontal component of the local acceleration. Implications of this assumption are that (a) vertical components of the velocity and acceleration are of no importance; (b) the convective accelerations (horizontal and vertical) do not contribute to the force; (c) the horizontal force must be comprised of a velocity-dependent drag and an acceleration-dependent inertial force since the simple wave theory yields a velocity and an acceleration. It is not clear as to why the convective acceleration has been ignored, i.e., why did MOJS use only the local acceleration instead of total acceleration.

Clearly, every unsteady fluid motion has a time-dependent ambient velocity and ambient acceleration. Thus, it does not automatically follow that the instantaneous force is decomposable into a velocity-square dependent drag force and an acceleration-dependent inertial force. Even if such a

"separation of forces" were to be assumed, it does not follow that the forces should be added linearly, resulting in a simple linear-quadratic sum. One can state with hindsight that the choice of the particular form of the force expression seems to have been governed by the following criteria: (a) tangential velocities and accelerations cannot influence the flow appreciably; (b) the wave theory (small amplitude) yields normal velocities and local accelerations each of which must be separately and additively responsible for part of the force; (c) heuristic reasoning of the applicability of the force expression when applied to conditions of steady flow alone or accelerating flow alone (added mass concept in inviscid fluids); (d) analytical simplicity of the force expression (linear-quadratic sum); and (e) experimental justification of the results (within the range of parameters tested: $0.22 \times 10^4 < Re < 1.11 \times 10^4$, $4.14 < K = \pi H/D < 14.82$). For example, the assumption of constant C_D and C_M along the pile was justified by the results that "the experimental values of C_D and C_M showed some scattering but no trend as a function of d/L, H/L or Reynolds number." One can state, on the basis of current studies, that MOJS could have found variations in C_D and C_M with H/D had they measured the sectional forces on small segments of the pile rather than the total moment acting on the pile. However, even then they could not have found a systematic variation with the Reynolds number. MOJS did recognize the approximate nature of their equation and experimental results and certainly implied that an approximate equation was being calibrated with two empirical constants: "The force coefficients C_D and C_M reported here are regarded as sufficiently accurate for design purposes, provided that they are re-inserted in the equations from which they have been derived."

Further examination of the MOJS paper leads to a few other important facts. The sample oscillograph trace of MOJS (their Fig. 4), for $\pi H/D$ = 9.24 and Re = 4.85×10^3, shows that the moment trace exhibits cycle-to-cycle variations (in shape if not in maximum amplitudes). The paper does not contain the words "vortex", "boundary layer", "wake", "transverse force", "lift force", "spanwise coherence", "wave scatter", "diffraction", "direct measurement of velocities", etc. It follows that the MOJS equation does not deal with the causes of the in-line and transverse forces. The test pile was restrained at the top by two lateral springs. It is not known as to whether the pile underwent lateral oscillations. There is no discussion of the merits or shortcomings of the use of calculated velocities and accelerations. No attempt was made to measure the velocities directly. MOJS used very small piles where the diameter to wave length ratio (D/L) was much smaller than 0.2. Even though the wave scatter and diffraction effects were negligible, no mention of this fact was made. Clearly, the MOJS work was practically inspired, there was some urgency in obtaining some data ("The current importance of wave force in the design of offshore structures makes it desirable that the results to date be made available now"), and the investigation was carried out in an engineering spirit.

The impact of the MOJS equation has been profound. It established a blind trust for many years in the MOJS equation (in spite of the warnings of its originators). Many years had to pass by before the limits and capabilities of the MOJS equation were recognized. There was an awareness of the fact that what works in the laboratory may not work in the ocean environment. But this awareness was not translated into a clear assessment of the differences between the laboratory conditions and the environmental

conditions (e.g., wave nonlinearity and directionality, currents, natural roughness, etc.). Only during the past few years that the practically-inspired problems have been translated into important questions of basic fluid mechanics (see e.g., Sarpkaya and Isaacson 1981). During the interim period 1950 to 1975, design decisions were made about the flow conditions and the non-fluid-flow constraints where even broad features of fluid behavior are only vaguely perceived. The designs were based largely on general concepts, speculative generalizations of the MOJS equation, some reasoned arguments, proprietory coefficients, experience of the relevant flows, intuitive generalizations from existing designs and data, and special ad hoc experiments. Only during the last five years that extensive basic research came to the world of offshore engineering, partly in response to the demands and stimuli provided by the offshore engineering, partly by the challenge of the problems encountered, and partly by the ever increasing interest in time-dependent flows. Only the outstanding contribution of Keulegan and Carpenter in 1956 has been an exception to the foregoing.

Scientific fluid mechanics had to shun away the enormously complex and ill-defined problems of ocean engineering and searched for a well-posed and yet sufficiently relevant flow situation (e.g., the standing waves of Keulegan and Carpenter in a rectangular basin, sinusoidally-oscillating planar flow of Sarpkaya (1976) in a U-shaped water tunnel, etc.). Such an idealization of the flow is often an essential first step. Assuming the idealized flow situation can be understood through experiments, quantitative analysis, and qualitative descriptions, it must then be related back to the complexity of the actual ocean environment. One must be warned, however, that the search for well-posed oscillating flow situations and the new insights gained therefrom do not necessarily lead to the exploitation of

the findings in a useful way in the modelling of wave forces on offshore structures. If a more sophisticated MOJS equation brings no guarantee of better predictions outside the range of parameters and geometries on which the new model is based, then it is of little value to the ultimate user. Thus, it is important to emphasize that even though well-posed time-dependent flow situations are extremely important in uncovering the degree of importance of the parameters involved, in increasing our quantitative and qualitative understanding of the various flow mechanisms, and helping us to devise new models, there is definite need for data obtained and observations made directly in the ocean environment through precise instrumentation and appropriate data analysis. Ultimately, the design of offshore structures will not be improved solely due to the knowledge gained through the study of the well-posed problems, as if it were a one way approach, but rather through the interaction and reasonable marriage of the two approaches: basic studies and environmental measurements.

In summary, the MOJS equation was proposed as an approximate solution to a complex problem. Its justification is strictly pragmatic and rests with experimental confirmation. Some of the often repeated limitations of the MOJS equation are that it applies only to the prediction of in-line forces for D/L smaller than about 0.2; it does not apply uniformly well to all ranges of Re and K values; with average C_d and C_m (henceforth the subscripts will be denoted by lower case alphabets), the unsteadiness of the force resides only in the variation of u and du/dt with time; three-dimensional effects (e.g., spanwise correlation, flow shear, etc.) are ignored; the effect of the axial pressure gradient is ignored; the transverse force is not accounted for; it does not apply equally well to all cylinder shapes or bluff bodies; it cannot deal with the effects of orbital motion, yaw, body- or free-surface proximity, omnidirectionality of the waves and/or currents; in certain

ranges of K, ($8 < K < 25$), the MOJS equation yields relatively large residues even for a circular cylinder in sinusoidally oscillating planar flow (one must bear in mind the possibility that the large residue may be because of the said nature of the particular flow and the perfect spanwise coherence!); it has no provisions to deal with vortex and wake-return effects (history of the motion) which have been found in most experiments to cause cycle-to-cycle variations in the in-line force and non-stationary oscillations in the transverse force, and so on.

Both the form of the equation and the uncertainties that go into the characterization of the ocean environment are thought to be responsible for the differences between the measured and calculated forces. Clearly, it is not a meaningful exercise to relegate the errors only to one or the other. Thus, as far as the ocean environment is concerned, the MOJS equation, with calibrated coefficients, is tolerated in light of all other uncertainties and hidden and intentional safety factors that go into the design.

The MOJS equation may be examined more systematically through experiments with relatively more manageable flows where kinematics do not require the use of intermediate theories. In addition, many other difficulties arising from the change of kinematics with space, orbital motion, etc. may be avoided. The physical insight and the data acquired through observations and measurements may help to formulate an equation with, hopefully, fewer limitations and greater degree of power of prediction. In the final analysis it must meet the needs of the designer and not just the research needs of the fluid dynamicist.

3.0 THE NATURE AND DECOMPOSITION OF THE TIME-DEPENDENT IN-LINE FORCE

3.1 Basic Background

The most serious difficulty with the time-dependent flows lies in the description of the time-dependent force itself. Some insight may be gleaned into the nature and decomposition of this force from a remarkable paper by Stokes (1851) on the motion of pendulums. Stokes has shown that the force acting on a sphere oscillating in a liquid with the velocity $U = -A\omega \cos\omega t$ is given by

$$F(t) = \frac{\rho\pi D^3}{6}\left(\frac{1}{2} + \frac{9}{2}\sqrt{\frac{2\mu}{\rho\omega D^2}}\right)\frac{dU}{dt} + 3\pi\mu DU\left(1 + \frac{1}{2}\sqrt{\frac{\rho\omega D^2}{2\mu}}\right) \qquad (2)$$

This force is composed of two parts: an inertial force and a drag force, linearly-dependent on acceleration and velocity, respectively. Evidently, the fluid motion is assumed to be unseparated. Both components of the force depend on viscosity.

The decomposition of the time-dependent force into the two said components is somewhat arbitrary. The same force may be decomposed into three or four parts and each part may be given a separate meaning. For example, one may write

$$F(t) = \frac{1}{2}\left(\frac{\rho\pi D^3}{6}\right)\frac{dU}{dt} + 3\pi\mu DU + \frac{9}{2}\left(\frac{\rho\pi D^3}{6}\right)\sqrt{\frac{2\mu}{\rho\omega D^2}}\,\frac{dU}{dt} + \frac{3}{2}\pi\mu DU\sqrt{\frac{\rho\omega D^2}{2\mu}} \qquad (3)$$

in which the first term on the right-hand side represents the added-mass (its ideal value) times acceleration; the second term, the linear viscous resistance to the steady motion of a sphere at very low Reynolds numbers (say $Re < 1$); the third term, either the effect of history or the motion on the inertial force or simply the viscous effects in harmonic motion on

the acceleration-dependent forces; and the last term, the history effect on the linear drag or the increase in skin friction and pressure drag due to oscillations. Also, one may combine the last two terms and regard them as history-dependent modifications to the ideal and the instantaneous steady-state values of the inertia and drag forces.

In Stokes sphere problem where the Reynolds number is very small, drag is proportional to the first power of velocity. In the MOJS equation

$$dF = [0.5\rho D C_d |U|U + \rho C_m (\pi D^2/4) dU/dt]dz \qquad (4)$$

where u^2 is now changed to $|U|U$ and $\partial u/\partial t$ to dU/dt, drag is proportional to the square of the velocity since the flow is separated and the drag is primarily due to pressure rather than the skin friction. Thus, one may regard the MOJS equation as an heuristic extension to separated time-dependent flows of the solution obtained by Stokes, with the understanding that the validity of the extension and the limits of its application will have to be determined experimentally.

The fact that the drag and inertia coefficients in the MOJS form of the resistance equation depend on both the Reynolds number ($Re = U_m D/\nu$ where $U_m = A\omega$) and the relative amplitude A/D or $K = 2\pi A/D$ may be demonstrated by writing the MOJS equation and the Stokes solution for a sinusoidally oscillating flow ($U = -U_m \cos\omega t$) about a sphere at rest as

$$\frac{F}{\frac{1}{2}\rho\frac{\pi D^2}{4}U_m^2} = -C_d |\cos\omega t| \cos\omega t + \frac{8\pi}{3}\frac{1}{K}C_m \sin\omega t \qquad (5)$$

and

$$\frac{F}{\frac{1}{2}\rho\frac{\pi D^2}{4}U_m^2} = -\frac{24}{Re}\left(1 + \frac{1}{2}\sqrt{\pi\frac{Re}{K}}\right)\cos\omega t + \frac{8\pi}{3K}\left(\frac{3}{2} + \frac{9}{2}\sqrt{\frac{K}{Re}}\right)\sin\omega t \qquad (6)$$

Equation (6) yields

$$C_d = \frac{24}{Re}\left(1 + \frac{1}{2}\sqrt{\pi\frac{Re}{K}}\right) = \frac{24}{Re}\left(1 + \frac{1}{2}\sqrt{\pi\beta}\right) \tag{7}$$

and

$$C_m = \frac{3}{2} + \frac{9}{2}\sqrt{\frac{1}{\pi}\frac{K}{Re}} = \frac{3}{2} + \frac{9}{2}\sqrt{\frac{1}{\pi\beta}} \tag{8}$$

where $\beta = Re/K = D^2/\nu T$ and $T = 2\pi/\omega$.

C_d and C_m for the Stokes force depend on both K and Re. However, there is a unique relationship between C_d and C_m, dependent only on Re, i.e.,

$$\left(\frac{C_d}{24/Re} - 1\right)\left(C_m - \frac{3}{2}\right) = \frac{9}{4} \tag{9}$$

where 24/Re is the steady-flow drag coefficient for a sphere in the Stokes regime and the constant 3/2 is the ideal value of C_m for a sphere. Thus, in unseparated flow the oscillations increase both the drag and the inertia coefficient above their corresponding steady-state values. Experiments show that only for small values of K and β does C_m exceed its potential flow value (Sarpkaya 1976a).

3.2 The Fourier Analysis of Keulegan and Carpenter

The first systematic evaluation of the drag and inertia coefficients was made by Keulegan and Carpenter (1958) at relatively low Reynolds numbers through measurements on submerged horizontal cylinders and plates placed in the node of a standing wave. In this study, the theoretically derived rather than measured values of velocities and accelerations were used.

Keulegan and Carpenter expressed the force in terms of a Fourier series assuming the force to be an odd-harmonic function of $\theta = 2\pi t/T$ as

$$2F/(\rho DU_m^2) = 2[A_1 \sin\theta + A_3 \sin 3\theta + A_5 \sin 5\theta + \cdots$$
$$B_1 \cos\theta + B_3 \cos 3\theta + B_5 \cos 5\theta + \cdots] \quad (10)$$

Keulegan and Carpenter were able to reconcile Eq. (10) with that proposed by MOJS by writing Eq. (10) in the following form

$$2F/(\rho DU_m^2) = \frac{\pi^2}{K} C_m \sin\theta + 2[A_3 \sin 3\theta + A_5 \sin 5\theta + \cdots]$$
$$-C_d |\cos\theta| \cos\theta + 2[B_3' \cos 3\theta + B_5' \cos 5\theta + \cdots] \quad (11)$$

in which U is assumed to be given by $U = -U_m \cos\theta$. Evidently, Eq. (11) reduces to the MOJS equation, i.e., to

$$2F/(\rho DU_m^2) = \frac{\pi^2}{K} C_m \sin\theta - C_d |\cos\theta| \cos\theta \quad (12)$$

provided that the coefficients C_m and C_d are independent of θ, i.e., each term has the same constant value (dependent on K and Re) and A_n and B_n are zero for n equal to greater than 3.

The Fourier averages of C_d and C_m are obtained by multiplying both sides of Eq. (12) once with $\cos\theta$ and once with $\sin\theta$ and integrating between the limits $\theta=0$ and $\theta=2\pi$. This procedure yields,

$$C_d = -\frac{3}{4}\int_0^{2\pi} \frac{F \cos\theta}{\rho DU_m^2} d\theta \quad (13)$$

$$C_m = \frac{2U_m T}{\pi^3 D}\int_0^{2\pi} \frac{F \sin\theta}{\rho DU_m^2} d\theta \quad (14)$$

The drag and inertia coefficients may also be obtained through the use of the method of least squares, two-point values, least-squares for higher order parameters, etc. (see Sarpkaya and Isaacson 1981). The details of these methods will not be presented here since they are not of particular relevance to the discussion on hand.

One can show through the use of Eq. (12) that the rate of change of force with time is zero at the time of maximum acceleration and is proportional to C_m/KT at the time of maximum velocity. Thus, the determination of C_m, in particular through the use of force at the time of maximum acceleration, depends on the particular values of C_m, K, and T, and may not be quite accurate. In general, it is recommended that either the Fourier-averaged or the least-squares averaged force-transfer coefficients be used for sinusoidally oscillating flows.

Keulegan and Carpenter's pioneering efforts to reconcile the Fourier decomposition of the in-line force with that proposed by MOJS gave rise to numerous questions ,i.e. (a) Does the MOJS equation with two time-invariant Fourier-averaged coefficients represent the time-dependent in-line force with sufficient accuracy for all values of the governing parameters? (b) Could the time-dependence of the force be relegated only to the time dependence of the flow kinematics? (c) What are the governing parameters? (d) How could the difference between the measured and calculated forces be accounted for? (e) Should one use time-dependent force coefficients assuming that the nature of the 2-term MOJS equation permits a meaningful correlation between the variable coefficients and the governing parameters (no history effects)? (f) Could one use time-invariant coefficients and account for the disparities between the measured and calculated forces through the use of additional terms ($A_n \sin n\theta$, $B_n \cos n\theta$)? (g) What are the reasons for the observed differences between the measured and calculated forces (for circular cylinders as well as other body shapes)? (h) Could the in-line as well as transverse forces be predicted through the use of the fundamental equations of motion and proper numerical techniques? (i) What is the effect of additional variables and conditions such as roughness, yaw, proximity, orbital motion, etc.?

These questions, formulated with 30 years of hindsight, remained unresolved. However, they have helped to replace the blind trust in the MOJS equation with a recognition of its limits as well as capabilities.

Keulegan and Carpenter have demonstrated that the 2-term MOJS equation with constant coefficients does not accurately represent the measured force for all values of $K = U_m T/D$ (now known as the Keulegan-Carpenter number). They have attempted to explain the role played by K and the vortices on the variation of the force and the force coefficients. The relatively low range of Reynolds numbers encountered in their experiments did not permit them to detect the effect of the Reynolds number ($Re = U_m D/\nu$) on the drag and inertia coefficients. Much later Sarpkaya (1976) re-examined the Keulegan-Carpenter data and has shown conclusively that the force-transfer coefficients (C_d, C_m, C_L, etc.) depend not only on the Keulegan-Carpenter number but also on the Reynolds number, relative roughness, etc.

3.3 Additional Considerations

The experiments of Keulegan and Carpenter as well as some others conducted subsequently have demonstrated clearly that even the motion of a relatively more manageable time-dependent flow (sinusoidally-oscillating planar flow) is extremely complex and the simplicity of the ambient flow helps to alleviate only the uncertainties associated with the kinematics of the flow (relative to the ocean environment) but not the complexities of the phenomenon associated with the motion of the vortices. Thus, even the use of a planar oscillating flow did not resolve all of the problems associated with the nature of the MOJS equation.

In 1963 Sarpkaya has shown through the use of the generalized Lagally's theorem and the discrete vortex model that the total resistance for a circular

cylinder in a flow with unidirectional constant acceleration may be written as

$$F = 0.5\rho U^2 D\, G(s/D) + 0.25\pi\rho D^2 (dU/dt)\, H(s/D) \qquad (15)$$

where U is the instantaneous velocity; s, the displacement of the ambient flow ($s = 0.5Ut$); and G(s/D) and H(s/D) are two functions dependent on the relative displacement s/D. Equation (15) suggested that the total force, for at least this particular flow, may be written as

$$F = 0.5\rho D C_d U^2 + \rho C_m (\pi D^2/4)(dU/dt) \qquad (16)$$

The dependence of C_d and C_m on the Reynolds number does not appear in Eq. (16) because Eq. (16) has been developed through the use of the inviscid flow assumption.

Equation (16) strongly suggests that C_d and C_m for the in-line force and C_L for the lift force (or transverse force) may be related to the relative displacement s/D, Reynolds number, and the relative roughness. This possibility has not been explored so far. Such a method will make C_d and C_m, and C_L functions of time. Hence, the time-dependence of the force will not reside only in the variation of U and dU/dt with time but also in the variation of the force coefficients with time or relative displacement (measured, say, from the time when U = 0). The variability of the force coefficients will be discussed more later.

Subsequent to Stokes studies, the forces on a sphere moving in a viscous fluid in an arbitrary manner were investigated by Boussinesq (1885) and also by Basset (1888). They found that the force experienced by a sphere at a given time depends, in general, on the entire history of its acceleration as well as the instantaneous velocity and acceleration. To a first order of approximation, this is given by

$$F = 6\pi\mu RU + 0.5(4\pi R^3/3)\rho(dU/dt) + 6R^2(\pi\mu\rho)^{1/2}\int_0^t \frac{dU/dt'}{t - t'}\,dt' \qquad (17)$$

where the last term represents the history effect. It should be stressed that Eq. (17) only has qualitative relevance to the MOJS equation since the entire analysis is based on the assumption of unseparated viscous flow at very low Reynolds numbers. The history term gives an indication of how the variation of acceleration influences the resistance in viscous unseparated flow about a sphere undergoing arbitrary motions and what is important when this effect is incorporarted into a mathematical model of the flow resistance. For a strictly sinusoidal flow, the integration of the history term yields two parts which may be combined with the first two terms of Eq. (17) to yield Eq. (6). One may, therefore, conclude that for a strictly sinusoidal motion of a sphere or cylinder, the two-term MOJS equation is well founded provided that the flow is unseparated and the drag and inertia coefficients are determined in terms of the Reynolds number and the Keulegan-Carpenter number. However, it does not immediately follow from the foregoing that the MOJS equation is well-founded for the case of separated simple harmonic flow about a bluff body. To be sure, the effect of the history term may be incorporated into the drag and inertia coefficients with no loss of generality for the strictly sinusoidal motion. However, C_d and C_m cannot be taken as time-invariant constants, dependent only on K and Re (for a smooth cylinder). It is a well-known fact that the MOJS equation does not accurately represent the measured force with time-invariant constants, particularly in the so-called drag-inertia dominated regime ($8 < K < 20$). In other words, C_d and C_m must be regarded as functions of time also.

A simple dimensional analysis of the flow under consideration shows that

$$2F/(\rho D U_m^2) = f(U_m T/D,\ U_m D/\nu,\ k/D,\ t/T) \tag{18}$$

Equation (18) says nothing about the form of the functional relationship. Thus, it is incorrect to state that the MOJS equation is well founded for separated sinusoidal flow about a circular cylinder if C_d and C_m are assumed to be functions of K, Re, k/D, and t/T. Only when the MOJS equation is assumed to be valid, one can combine Eq. (18) with the MOJS equation to obtain

$$C_d = f_1(K,\ Re,\ k/D,\ t/T) \quad \text{and} \tag{19}$$

$$C_m = f_2(K,\ Re,\ k/D,\ t/T) \tag{20}$$

A closer examination of the instantaneous force records show that even the Eqs. (19) and (20) are not sufficient to account for the non-stationary nature of the lift force (chordwise and spanwise coherences) and the cycle-to-cycle variations of the in-line force, due to lack of two-dimensionality of the separated flow. Thus, one must include at least the length-to-diameter ratio of the cylinder among the parameters in Eqs. (19) and (20) to account for the spanwise coherence. Other effects caused by the individual test conditions (end effects, wall boundary layers, etc.) and the measurement techniques are likely to affect the variations of C_d, C_m, C_L, etc.

For more general time-dependent flows the effect of the history term cannot be incorporated into the variations of C_d and C_m and the justification for the MOJS equation is strictly pragmatic. For periodic non-sinusoidal flows (e.g., Stokes waves), the use of the MOJS equation simply implies that the history effects are accounted for by the variations of C_d and C_m. For ocean waves of varying amplitude and period (if not direction also) the history effects resulting from the cycle-to-cycle variation of the ambient flow

kinematics cannot be taken into account by the two-term MOJS equation even if C_d and C_m are assumed to depend on K, Re, k/D, and t/T. Thus, the use of the MOJS equation together with the in-line wave forces measured in the ocean environment to determine two time-invariant coefficients necessarily lead to large scatter even if all sources of measurement errors were to be eliminated or minimized. Suffice it to recapitulate that a cylinder subjected to variable wave forces is like a cylinder experiencing an equally variable time-dependent motion. Ocean data cannot be accurately analyzed with the two-term MOJS equation alone (with time-invariant or time-dependent coefficients) without taking into account the effect of the history of the motion, at least through the use of a third term.

Two additional matters need to be discussed before concluding the discussion of the nature and decomposition of the in-line force.

It has been stated that the assumption of the validity of the MOJS equation for a planar sinusoidal flow about a bluff body leads to $C_d = f_1(K, Re, k/D, t/T)$ and $C_m = f_2(K, Re, k/D, t/T)$. There is no simple way to deal with these expressions even for the most manageable time-dependent flows. Another and perhaps the only other alternative is to eliminate time as an independent variable and consider suitable time-invariant averages as given by Eqs. (13) and (14). Thus, one has

$$[C_d, C_m, C_L, ...] = f_i(K, Re, k/D) \tag{21}$$

For periodically oscillating flows the Reynolds number is not necessarily the most suitable parameter. The primary reason for this is that U_m appears in both K and Re. Thus, replacing Re by $\beta = D^2/\nu T = Re/K$ in Eq. (21), one has

$$C_i(\text{a coefficient}) = f_i(K, \beta, k/D) \tag{22}$$

in which β is called the 'frequency parameter' introduced by Sarpkaya (1976a)

who used it first to demonstrate the fact that the Keulegan-Carpenter data depend on Re as well as on K, (see also Sarpkaya and Isaacson 1981).

Finally, it is of some importance to note that the time-dependent force F for the most general case may be written as

$$F = f(\rho, D, L_c, U, \nu, k, \alpha, dU/dt, d^2U/dt^2, ...) \tag{23}$$

which may be reduced to

$$F/(0.5\rho DL_cU^2) = f(UD/\nu, L_c/D, k/D, \alpha, \frac{D}{U^2}\frac{dU}{dt}, \ldots, \frac{D^n}{U^{n+1}}\frac{d^nU}{dt^n}) \tag{24}$$

in which L_c is the body length and α is the yaw angle. Obviously, there is a giant step between Eq. (24) and the MOJS equation, written as,

$$F(t)/(0.5\rho DL_cU^2) = C_d \frac{U|U|}{U^2} + \frac{\pi}{2} C_m \frac{D}{U^2}\frac{dU}{dt} \tag{25}$$

or as

$$F(t)/(0.5\rho DL_cU_m^2) = C_d \frac{U|U|}{U_m^2} + \frac{\pi}{2} C_m \frac{D}{U_m^2}\frac{dU}{dt} \tag{26}$$

For a planar sinusoidal flow represented by $U = -U_m \cos\theta$, Eq. (26) reduces to

$$F(t)/(0.5\rho DL_cU_m^2) = -C_d|\cos\theta|\cos\theta + \frac{\pi^2}{K} C_m \sin\theta \tag{27}$$

A comparison of Eqs. (24) and (27) shows that the unknown effects of L_c/D, k/D, α, and $(D^n/U^{n+1})(d^nU/dt^n)$ are all incorporated into the two time-invariant coefficients. It is no surprise that the large discrepancies among studies with the prototype structures are attributed to factors such as random nature of the ocean waves, wave theories used, currents, free-surface effects, the sweeping back of the wake over one segment of the structure after being generated at another segment under different flow conditions, etc. Evidently, all of these factors are important and contribute to the observed discrepancies

in C_d, C_m, C_L, etc. However, it is equally important to realize that the form of the MOJS equation or the particular force decomposition assumed in the determination of C_d, C_m, etc. is just as responsible for the said discrepancies. There are no simple approaches to quantifying these effects and to providing qualitative descriptions and none is likely to appear in the near future.

4.0 SPECULATIVE GENERALIZATIONS OF THE MOJS EQUATION

4.1 General Comments

The MOJS equation was originally written as

$$dF = [C_m(\pi\rho D^2/4)\partial U/\partial t \pm C_d(\rho D U^2/2)]dz \qquad (1)$$

and was intended for the determination of "the force exerted by unbroken surface waves on a cylindrical object, such as a pile, which extends from the bottom upward above the wave crest,..." Shortly thereafter it became

$$dF = [C_m(\pi\rho D^2/4)\partial U/\partial t + C_d(\rho D U|U|/2)]dz \qquad (28)$$

The change from $\pm U^2$ to $U|U|$ did not in any way require additional assumptions beyond and above those already embodied in the original equation.

A further generalization was made by replacing D by a characteristic cross-sectional area A per unit length, and $\pi D^2/4$ by volume $\forall$ per unit length for structural elements other than circular cylinders. The local acceleration has been occasionally replaced by the total acceleration dU/dt (with probably little difference in the analysis of the ocean test data). Thus, the MOJS equation became

$$dF = [C_m\rho\forall\, dU/dt + C_d(\rho A U|U|)/2]dz \qquad (29)$$

This modification implies that the MOJS equation is equally valid or no less valid for other body shapes. This is rather conjectural for several reasons. If the drag and inertia coefficients are determined in exactly the same manner for each body through the use of one of the existing methods (e.g., Fourier averaging, least-squares, etc.), Eq. (29) is relatively more applicable to a circular cylinder than to a plate normal to the flow. In fact, Keulegan and Carpenter (1958) have shown that "for the plate data the remainder (meaning $A_3\sin 3\theta,\ldots,$ $B_3'\cos 3\theta,\ldots$) may not be disregarded, in particular when the

period number (meaning K) is small." The reason for this is that the form and character of the wake (wake width, strength of the vortices, etc.) and hence the history effects depend on the body shape. Thus, the approximations made regarding the constancy of C_d and C_m and the negligibility of the history effects are relatively more justified for streamlined bodies than for bodies with sharp edges (bluffer bodies). Strong vortices in the near wake give rise to large variations in all wake characteristics, to varying degrees of importance, during their shedding and backward convection (particularly at or near the times of maximum velocity). This, in turn, increases the deviation of the instantaneous values of C_d and C_m from their time-invariant values and gives rise to large errors in the predicted force. Thus, for body shapes where the strength of the vortices and the manner in which they interact with the body are such that higher harmonics of notable energy are produced, the MOJS equation is likely to produce poorer results. It is clear from the foregoing that the simplicity of the generalization of the MOJS equation from Eq. (28) to Eq. (29) is deceptive and invites a whole host of new problems. Furthermore, it should be noted that both Eq. (28) and Eq. (29) imply that the elemental force dF may be calculated for an elemental length dz and integrated over the entire length of the cylinder (either by assuming C_d and C_m remains constant, as in the original formulation of the MOJS equation, or more appropriately by assuming C_d and C_m depend on the local values of Re, K, and k/D). Even the use of the local values of C_d and C_m is not without some additional assumptions. The nonuniformity of the flow along the body (even without the effect of the orbital motion) may alter the strength, shedding, and the spanwise coherence of vortices. Thus, the local values of C_d and C_m may differ from those obtained with planar sinusoidal flow under identical Re, K, and k/D values.

The MOJS equation was subsequently written in vectorial form (Borgman 1958) for a vertical cylinder as

$$F = \begin{Bmatrix} F_x \\ F_y \end{Bmatrix} = 0.5\rho C_d D \begin{Bmatrix} V_x \\ V_y \end{Bmatrix} \sqrt{V_x^2 + V_y^2} + \frac{\pi}{4}\rho D^2 C_m \begin{Bmatrix} a_x \\ a_y \end{Bmatrix} \qquad (30)$$

where V_x and V_y are the velocity components in the x-y plane which is normal to the cylinder axis. It is important to note that the velocity and acceleration vectors are not collinear. Equation (30) does not require additional assumptions beyond those required for Eq. (29) provided that it is applied either to a vertical pile or more appropriately to a circular cylinder in planar oscillatory flow. The form of the Eq. (30) may suggest incorrectly that it may be applied to a horizontal cylinder in waves (wave crests parallel to the cylinder axis) with C_d and C_m values identical to those for a vertical pile.

For a horizontal cylinder in a uniform flow field with $V_x = -V_{xm}\cos\theta$ and $V_y = -V_{ym}\sin\theta$, Eq. (30) reduces to

$$2F_x/(\rho D V_{xm}^2) = (\pi^2 D/V_{xm}T)C_m \sin\theta - C_d \sqrt{\cos^2\theta + (V_{ym}/V_{xm})^2 \sin^2\theta}\, \cos\theta \qquad (31)$$

and

$$2F_y/(\rho D V_{ym}^2) = (\pi^2 D/V_{ym}T)C_m \sin\theta - C_d \sqrt{(V_{xm}/V_{ym})^2 \cos^2\theta + \sin^2\theta}\, \sin\theta \qquad (32)$$

Equations (31) and (32) state that the instantaneous in-line force in the x- and y-directions is equal to the sum of the projections, on the respective axis, of the instantaneous values of the total-velocity-square dependent drag force and the total-acceleration-dependent inertial force. This implies that the flow over a cycle may be regarded as a juxtaposition of planar flows

with instantaneous velocities and accelerations given by

$$q = \sqrt{V_{xm}^2 \cos^2\theta + V_{ym}^2 \sin^2\theta} \tag{33a}$$

and

$$a = \sqrt{V_{xm}^2 \sin^2\theta + V_{ym}^2 \cos^2\theta} \tag{33b}$$

The vortices do not move with the velocity of the ambient flow and the wake does not rotate about the cylinder at the same rate as the ambient velocity vector. In other words, one must be aware of the fact that the writing of the MOJS equation in vectorial form does not necessarily imply that the behavior of the wake can be correctly represented by it. The drag and the inertia coefficients for a horizontal cylinder in waves are considerably different from those for a vertical cylinder at the corresponding K, Re, and k/D values.

Equations (31) and (32) cannot be written using only the x- or only the y-component of the velocity in the MOJS equation. This will assume that the drag component of the in-line force is proportional to the square of the projected velocity rather than to the square of the instantaneous total velocity. Finally, it is because of the assumptions noted above that the drag components of the forces given by Eqs. (31) and (32) become linear for $V_{xm} = V_{ym}$ (fluid particles undergoing circular orbits).

4.2 Yaw Effects

The need to predict the forces acting on yawed cylinders subjected to wave motion gave rise to another speculative generalization of the MOJS equation. The effect of the body orientation on resistance has been the subject of extensive investigation in steady flows. It has not been possible to correlate the in-plane normal force and the out-of-plane transverse force with a single Reynolds number (see Sarpkaya and Isaacson 1981). Evidently, for a zero angle of attack (flow parallel to the axis of the cylinder), the

appropriate Reynolds number is based on the length measured along the body. For a 90-degree angle of attack (flow normal to the axis of the body), the appropriate Reynolds number is based on the diameter of the body. Between the two situations, it is not possible to define a simple characteristic length and hence a universal Reynolds number which will correlate the force-transfer coefficients for all angles and flow regimes.

Hoerner (1965) proposed the independence- or crossflow-principle or the 'cosine law' which states that the normal pressure forces are independent of the tangential velocity for subcritical values of Re_n (based on the normal component of velocity U_n). The 'flow independence principle' has been commonly accepted for subcritical flow conditions (laminar boundary layers), but rejected for transcritical flows (Hoerner 1965). The recent wind tunnel data by Norton et al. (1981) show that the flow-independence principle is valid, at least for cylinder inclinations up to 50 degrees (the angle between the cylinder axis and the ambient flow velocity), as long as the Reynolds number Re_n, based on the normal component of the velocity, remains entirely within either the subcritical or postcritical flow regime (turbulent boundary layers). However, should Re_n drop from postcritical to transcritical as the angle of inclination is decreased, one would expect the independence principle to fail.

The time-dependent flows, in general, and the wave motion, in particular, about oblique cylinders present even more complex problems. The use of the independence principle or the assumption that shedding frequency is proportional to $\cos^2\theta$ may be a gross simplification of the behavior of flow in the near wake. Under these circumstances only experiments can lead to some understanding of the problem and to the evolution of appropriate calculation methods. At present neither the method of decomposition of velocities and/or forces nor the drag

and inertia coefficients appropriate to each method of force decomposition are clear. Furthermore, there are not enough systematic experiments with waves or with harmonic flows to guide the analysis or to justify the generalization of the MOJS equation to yawed cylinders.

Wade and Dwyer (1976) examined four methods, generally accepted by the industry, for calculating wave forces on normal and inclined tubular members. Horizontal and vertical wave-induced water-particle kinematic vectors were used in each of the wave force methods on two deep water platforms to compare the horizontal base shear and overturning moments (for a detailed discussion of these see Sarpkaya and Isaacson 1981). Such comparisons, however valuable, are not sufficient to assess the validity of one method over the others since Wade and Dwyer used identical but constant drag and inertia coefficients (C_d = 0.6, C_m = 2 for one test structure and C_d = 0.6 and C_m = 1.4 for the other test structure) and since the base shear and over-turning moment represent the sum of the forces and moments over many members at various angles of inclination, interference, etc. Thus, the generalization of the MOJS equation to inclined members through

$$\begin{Bmatrix} F_x \\ F_y \\ F_z \end{Bmatrix} = 0.5\rho C_d D|W_n| \begin{Bmatrix} u_{nx} \\ u_{ny} \\ u_{nz} \end{Bmatrix} + \frac{\pi}{4} \rho C_m D^2 \begin{Bmatrix} \dot{u}_{nx} \\ \dot{u}_{ny} \\ \dot{u}_{nz} \end{Bmatrix} \tag{34}$$

together with the C_d and C_m values appropriate to the normal cylinder at the corresponding Reynolds numbers ($Re = |W_n|D/\nu$) and Keulegan-Carpenter numbers ($K = |W_n|T/D$) is highly speculative. One must bear in mind that in oscillatory and wavy flows the Reynolds number may vary from subcritical to postcritical and one cannot expect the conclusions resulting from the steady flow tests

(either at subcritical or postcritical Re) to hold true, particularly in the drag-inertia dominated regime. Furthermore, it is not clear that a two-term MOJS equation may be forced to represent the measured force on inclined members, with C_d and C_m determined through some reasonable method. As in the case of cylinders bluffer than a circular cylinder (e.g., a plate or square cylinder) the effect of the history term or the magnitude of the residue (the difference between the measured and calculated force) may be quite large.

The recent unpublished data by Sarpkaya (1982) have shown that the independence principle is not valid for either smooth or rough inclined cylinders in sinusoidally oscillating planar flows. Considerable additional work is required in order to acquire some understanding of the wave forces on oblique members and, hopefully, to establish uniformly accurate and acceptable design criteria.

4.3 Waves and Currents

Another speculative generalization of the MOJS equation concerns the combined waves and currents. It is ordinarily assumed (as recommended by the American Petroleum Institute) that the MOJS equation applies equally well to periodic flow with a mean velocity and that C_d and C_m have constant, current-invariant, Fourier- or least-squares averaged values equal to those applicable to rigid, stationary cylinders in wavy flows. This, in turn, implies that C_d and C_m are independent of the biassed convection of vortices and its attendant consequences. The fact that this is not necessarily so is clearly evidenced by the measurements of Mercier (1973), Sarpkaya (1977) and Verley and Moe (1979). Thus, the effect of the current-harmonic-flow combination on the motion of vortices and on the force-transfer coefficients must be carefully examined in light of available data and the limits of

application of the MOJS equation to such flows must be assessed a new. The latter is particularly important in view of the fact that the drag and inertia coefficients in ocean tests (where there are always some currents and body motion) are evaluated through the use of the MOJS equation (note that the values of C_d and C_m may vary considerably from one half wave cycle to another because of the current-induced biassing of the wake and vortex formation and that neither set of coefficients may be identical with those obtained without current).

It has been customary to express the in-line force either as

$$F = 0.5\rho C_{dc}(\bar{V}-U_m\cos\theta)|\bar{V}-U_m\cos\theta| + (\pi\rho C_{mc}D^2/4)\, dU/dt \qquad (35)$$

where $\bar{V}$ represents the current and $U = -U_m\cos\theta$, or more generally as

$$F = 0.5\rho C_{dc}(\bar{V}+U_w)|\bar{V}+U_w| + (\pi\rho C_{mc}D^2/4)\, dU_w/dt \qquad (36)$$

where U_w is the wave velocity, added vectorially to the current velocity (some designers use the projection of the current velocity on the wave velocity and assume the sum of the two to be in the direction of wave).

The generalization of the MOJS equation to Eq. (35) or Eq. (36) is not warranted and is not supported by experimental data. Clearly, extensive work is needed to determine the role played by the current, the validity of the MOJS equation, the appropriate force-transfer coefficients, etc., not only for fluid mechanical and practical design purposes but also to ascertain the validity of the method of analysis of the data obtained in the ocean tests through the use of Eq. (35). The use of a speculative generalization, unproven even under idealized circumstances, to analyze data so as to prove the validity of the generalization itself is not very meaningful.

In the foregoing the waves and currents were assumed to superpose linearly. In general certain changes in wave characteristics arise from the superposition of waves and currents (Longuet-Higgins and Stewart 1961). When a wave train propagates into a region of local current, the wave amplitude decreases and the wave length increases if the current and the waves are in the same direction. However, if the current and the waves are in opposing directions, the wave amplitude increases and wave length decreases. A theoretically critical point is reached as the current velocity becomes equal and opposite to one half of the local wave group velocity. The wave energy at this critical velocity can no longer be propagated against the current and the wave amplitude theoretically approaches infinity. In fact, the waves break long before they reach such a limit. The wave-current interaction problem has not been studied in sufficient detail. Thus, even the proper kinematical inputs into the MOJS equation are unknown when the waves and currents are combined.

4.4 Effects of Dynamic Response

The need to analyze the hydroelastic response of structures gave rise to a further generalization of the MOJS equation.

Assuming a single member (normal to the wave direction) of mass M, structural damping C, and stiffness K_s, the equation of motion is written as

$$M\ddot{x} + C\dot{x} + K_s x = \rho\forall\dot{U} + \rho(C_m-1)\forall(\dot{U}-\ddot{x}) + 0.5\rho C_d A_p|U-\dot{x}|(U-\dot{x})$$

$$= \rho\forall C_m\dot{U} - \rho(C_m-1)\forall\ddot{x} + 0.5\rho C_d A_p|U-\dot{x}|(U-\dot{x}) \qquad (37)$$

in which U and $\dot{U}$ represent the velocity and acceleration of the fluid; and x, $\dot{x}$, $\ddot{x}$ represent, respectively, the displacement, velocity, and acceleration of the structural member in the direction of U. Equation (37) may also be

written as

$$(M + \rho C_a \forall)\ddot{x} + C\dot{x} + K_s x = \rho \forall C_m \dot{U} + 0.5\rho C_d A_p |U-\dot{x}|(U-\dot{x}) \qquad (38)$$

where $C_a = C_m - 1$, as usual, and $(M + \rho C_a \forall)$ now represents the structural mass, water inside the pipe, and the added mass.

The approximations involved in the formulation of Eq. (37) are far more than those relating to the wave-current combination because of the simple fact that now both U and x are functions of time. In fact, there is no experimental verification of Eq. (37) at any Reynolds number, Keulegan-Carpenter number, and $\dot{x}/U$ ratio. It is based on a reasonable-sounding argument and it reduces to the correct limiting forms for $\dot{x} = \ddot{x} = 0$ and for $U = \dot{U} = 0$. Perhaps the only other justification for the use of Eq. (37) is that there is a need for it and yet there are no better alternatives to meet the demands of this need. As far as the industrial applications are concerned the basic research sees the need but a little late and always a little too idealized.

In spite of its uncertain limitations, Eq. (37) is further manipulated to suit the needs of calculation. For example, in order to apply spectral methods, the drag term is often linearized with an equivalent linearization technique (for details see Sarpkaya and Isaacson 1981). The approximations are further compounded, with ever increasing degree of uncertainty, by applying Eq. (37) to the dynamic response of a number of normal and inclined members. For example, the total force at a node of a structure is obtained by summing the contributions of the members contained in the nodal tributary zone (the region halfway above and below the node). The use of the projected area method rather than the independence principle yields an expression for the force acting on the j-th member in zone i as,

$$P_i(t) = \sum_j \left[\rho(C_{mij}-1)\frac{\pi}{4}D_{ij}^2 L_{ij}(\dot{U}_{ij}-\ddot{x}_i) + \rho\frac{\pi}{4}D_{ij}^2 L_{ij}\dot{U}_{ij} + 0.5\rho C_{dij} D_{ij} L_{ij} |U_{ij}-\dot{x}_i|(U_{ij}-\dot{x}_i)\right] \quad (39)$$

where C_{dij}, C_{mij} are the unknown drag and inertia coefficients for the member ij, and D_{ij} and L_{ij} are the diameter and the projected length of the tubular members at node level i.

The generalization of the MOJS equation to the form given by Eq. (39), over a period of 30 years, is at best speculative and is not based on sound data. It will take many years and much research either to verify it or to devise a new equation to replace it. It is rather unfortunate that the urgent needs of the industry and the passage of time rather than scientific data are helping to consolidate the use of this most speculative generalization of the MOJS equation.

5.0 THE SEARCH FOR A NEW MOJS EQUATION

5.1 Background and an Assessment of the Existing Data

The extensive discussion of the original MOJS equation and its various generalizations has shown that (i) a great deal of additional research is needed, both in the laboratory and in the field, to assess critically the validity or the limitations of each generalization; (ii) there is not, at present enough meaningful analysis or data to attempt to improve every form of the MOJS equation; and (iii) the understanding of the limitations and the improvement of the MOJS equation for the simplest possible flow and body combination should be the first step towards the development of an equation of greater generality and hence towards the understanding, analysis, and interpretation of the data obtained under more complex conditions.

The first step towards the search of a new MOJS equation began with the selection of the most suitable flow situation and the body shape. It became quickly apparent that there are essentially three types of flow situations for which some data of varying degrees of quality, covering various ranges of the governing parameters, exist. These are: (a) data obtained with vertical cylinders in laboratory wave channels, often with small amplitude waves; (b) data obtained in the ocean environment either through the instrumentation of the existing platforms or through the use of small scale platforms built specifically for test purposes (e.g., Exxon's Ocean Test Structure, and NMI's Christchurch Bay Tower); and (c) data obtained with sinusoidally oscillating planar flow about smooth and rough circular cylinders (Sarpkaya 1976a, 1976b).

The data obtained with small amplitude laboratory waves were found to be unsuitable for the purpose under consideration. The reasons for this are as follows: (a) the range of Reynolds numbers and Keulegan-Carpenter numbers is

quite limited; (b) both Re and K vary with depth (as well as with time); (c) often the total in-line force acting on the entire pile, rather than that on small segments, is measured; (d) the kinematics of the flow, calculated through a suitable wave theory, is of questionable accuracy; and (e) the orbital motion of the particles and the variation of K and Re along the pile, in the range of K values where the original MOJS equation is least accurate, complicates the problem considerably.

There are two major sources of data obtained in the ocean environment: Ocean Test Structure of Exxon and the Christchurch Bay Tower of the National Maritime Institute of England.

5.2 Ocean Test Structure Data

A large scale experiment was undertaken by Exxon Production Research (EPR) Company to evaluate present wave force calculation procedures for fixed, space-frame structures. This highly instrumented 20x40x120 ft platform was installed in 66-ft water depth in the Gulf of Mexico. Data obtained include local wave forces on clean and barnacle-covered sensors, local wave kinematics, total base shear and over-turning moment on the structure, forces on a simulated group of well conductors, and impact forces on a member above the mean water level.

Heideman et al. (1979) used two methods to evaluate the drag and inertia coefficients. The first was the least-squared-error procedure for each half-wave cycle. The instantaneous in-line velocity in the MOJS equation included both the wave velocity and the projection of the current velocity. The second method consisted of the evaluation of C_d over short segments of waves in which drag force was dominant and of C_m over short segments of waves in which inertia force was dominant. The in-line force was taken as the projection of the

normal force on the velocity vector. The normal force was measured with wave force transducers (WFT) of 16 inch O.D. and 32 inch length, built into the vertical legs at the four corners of the structure, at a depth of -15 ft. The normal water velocity was measured with an electromagnetic current meter (ECM) located 4.67 ft from the WFT axis, i.e., ECM was at 3.5 D from the WFT axis.

The force coefficients exhibited large scatter particularly for $K < 20$. The scatter decreased considerably in the range $20 < K < 45$. It is not clear whether this is a genuine reduction in scatter or whether it is a consequence of the fewer data points in the drag-dominated regime.

Heideman et al., attributed the scatter in C_d and C_m to random wake encounters. It is postulated that if the cylinder encounters its wake on the return half cycle but the current meter does not, then the actual incident velocity will be greater than measured and the apparent C_d calculated from the measured force and velocity will be higher than the true C_d. Conversely, if the current meter encounters the wake on the return half cycle but the cylinder does not, then the apparent C_d will be too low. Clearly, the encounter of the wake with the current meter and the biassing of the wake by the current are extremely important. This is evidenced by the fact that the values of C_d and C_m vary considerably from one half wave cycle to another even for the same wave. Thus, it is desirable to evaluate C_d and C_m with due consideration to the effect of current, wave spreading, and the irregularities superimposed on each wave.

Heideman et al. concluded that (a) the MOJS equation with constant coefficients can be made to fit measured local forces and kinematics satisfactorily over individual half wave cycles; (b) most of the scatter in the C_d

results can be explained by the random wake encounter concept; (c) local deviations in apparent C_d are not spatially correlated in any given wave; (d) C_d results from Sarpkaya's experiments (1976) represent an upper band to C_d values that may be expected in random three-dimensional oscillatory flow; (e) for $Re < 2x10^5$, the apparent C_d depends on surface roughness and, for members that are nearly in the orbit plane, on K; (f) asymptotic C_d results from the test data in random three-dimensional oscillatory flow are consistent with steady flow data for the same relative roughness; and (g) C_m is greater for smooth cylinders than for rough cylinders, while the reverse is true for C_d.

The OTS data of EPR are extremely valuable in assessing the combined effect of the environmental conditions on the force-transfer coefficients but not well-defined enough to assess the reasons for the deviation of the measured forces from those predicted by the MOJS equation in the drag-inertia dominated regime. This is primarily due to the existence of currents and the omnidirectionality of the waves and currents. As noted earlier, the first original version of the MOJS equation and not its speculative generalizations to the wave-current combination should be examined. Finally, it should be noted that the OTS signal conditioning units had four pole active (Butterworth) filters with an upper cut-off frequency of 3 Hz. However, all data had the same phase relationship due to input filters. Nevertheless, the force components at frequencies higher than the cut-off frequency are lost. Thus, the OTS data are not suitable either for the frequency domain analysis or for the analysis of impact forces (wave slamming) acting on the horizontal members of the structure. Primarily for the reasons cited above, and to a lesser extent, because of the general unavailability of the said data, the use of the OTS data has been precluded from further consideration.

5.3 CHRISTCHURCH BAY TOWER DATA

The tower is located at about 12 miles from a maintenance base at Lymington and the Marine Trials Base of the National Maritime Institute (UK) at Hythe, on Southampton water. It consists of two steel vertical columns, a platform, and an instrumentation module, supported by a reinforced concrete base. The main column is surrounded by five separate but adjacent sleeves of 9.2 ft diameter which measure the horizontal loading due to waves and currents as a function of depth. The wave staff is fitted with four force sleeves of 1.6 ft diameter which are mounted at similar heights to the lower force sleeves on the main column. In addition, the pressure is measured at 24 positions around a circumference of the middle sleeve and also at a single position on each of the other four force sleeves on the main column. The wave staff also carried perforated ball instruments for measuring wave particle motions, and a capacitance wire for measuring the wave elevation. For additional details see Wheatley (1976).

The wave force data from the Christchurch Bay Tower have been analyzed by Bishop (1978, 1979, 1980) and Standing (1980).

Starting from the MOJS equation, Bishop (1978) has shown that

$$\overline{F^2} = (0.5\rho DLC_d)^2\,\overline{U^4} + (0.25\pi\rho LD^2C_m)^2\overline{(dU/dt)^2} \qquad (40)$$

where the bars denote the mean values of the squares of the respective measured quantities integrated over one or more discrete cycles or over a long enough interval to include several cycles in an irregular sea. The coefficients C_d and C_m are determined from any one or more pairs of equations set up from different samples of the measurements. As would be expected, the variability in the coefficients due to highly variable effects and irregularities in the

incident wave train is averaged out by taking larger sampling times. Bishop found that C_d and C_m [as defined by Eq. (40)] are quite stable for integration intervals larger than about 4 minutes and show increasing variations as the integration interval is reduced. The best fit values of C_d and C_m differed between the two runs evaluated and also for the main column and the wave staff of the test facility. For the wave staff, C_d was 0.73 and C_m = 1.22 for one run and 1.66 for the other run. For the main column, C_d was forced to 1.0 and C_m was about 1.85. The Reynolds number ranged from 10^5 to 10^6 and the Keulegan-Carpenter number from 2 to 30. There appeared to be significant differences in the force coefficients due to current, for both the wave staff and the main column. The difference was largest on the smaller wave staff. Bishop noted that "the variations of the coefficients can be attributed to genuine hydrodynamic effects but also to imperfections in the experimental and analysis techniques. No attempt has been made to attribute the variations to individual causes..."

In 1980 Bishop defined a new force coefficient C_{F*} as

$$C_{F*} = \sqrt{\frac{\overline{F^2}}{(0.5\rho DL)^2[\overline{U^4} + (\pi D/2)^2(\overline{dU/dt})^2]}} \tag{41}$$

where $\overline{F^2}$ is defined by Eq. (40). In addition, Bishop (1980) defined K as

$$K_* = (2\pi/0.866D)[\overline{U^4}/\overline{\dot{U}^2}]^{1/2} \tag{42}$$

and reduced Eq. (41) to

$$C_{F*} = \left[\frac{C_d^2 + C_m^2(\pi^2/0.866K_*)^2}{1 + (\pi^2/0.866K_*)}\right]^{1/2} \tag{43}$$

Clearly, for large values of K_* (drag dominated regime) $C_{F*} \rightarrow C_d$ and for small

values of K_* (inertia dominated regime) $C_{F*} \rightarrow C_m$. It is seen that "C_{F*} can be derived from existing data which have been processed to give C_d and C_m values but it cannot be obtained precisely from drag-based total force coefficients." Bishop described an approximate conversion to overcome this difficulty. At any rate, C_{F*} requires first the evaluation of C_d and C_m and it is not clear at this time as to what purpose C_{F*} can serve in an appraisal of the MOJS equation, particularly in the drag-inertia dominated regime. Note that Eqs.(40) through (43) already assume the validity of the MOJS equation with constant coefficients.

Standing (1980) described a wave-by-wave analysis of some of the selected portions of the Christchurch Bay data. 16-second samples of data were judiciously selected for analysis from two runs recorded during a storm in September 1976. The time histories of force and velocity were first Fourier-transformed into the frequency domain, components above 0.5 Hz were removed, and the time histories reconstituted by inverse transformation. The MOJS equation was fitted to the measured in-line force through the use of a least-squares fitting technique to derive C_d and C_m in a narrow range of Reynolds numbers between 3×10^5 and 7×10^5.

The results obtained by Standing showed considerable scatter even though the analyzed samples were chosen subjectively by visual inspection. As noted by Standing "a much larger degree of scatter might be expected if samples had been chosen entirely at random." Standing tentatively concluded that in many cases the MOJS equation provided a good fit to the measured in-line force. In general main column forces fitted less well than wave staff forces possibly due to the "spatial separation between force sleeves on the main column and the velocity sensors", "spikes and rapid fluctuations on the acceleration record...", "disturbances to the velocity field caused by structural components

in the vicinity of the velocity sensor", "inadequacies of the MOJS equation, particularly associated with vortex-shedding effects", etc. The force-transfer coefficients showed no consistent variation with K in the range appropriate to each individual column.

It appears from the foregoing that the Christchurch Bay data are in need of further analysis which will bring into focus the effects of currents, wave nonlinearity, vortex shedding, wake biassing, etc., on the force-transfer coefficients. At present, there does not seem to be any possibility of using the said data in a meaningful way for a critical assessment and improvement of the MOJS equation.

The foregoing points out certain simple facts concerning the evaluation of the force-transfer coefficients from laboratory and field tests. Firstly, the collection of full-scale data from structures at sea is difficult and involves considerable uncertainty. Secondly, the interpretation of the results in terms of suitable parameters is subject to ambiguity. In fact, the drag and inertia coefficients obtained through the use of one method should not be compared with those obtained through the use of another one. Thirdly, the flow is definitely three-dimensional and its consequences cannot be evaded by measuring sectional forces rather than the total force on the entire pile. Finally, the experimental conditions in the ocean environment cannot be controlled or repeated. These facts coupled with equally complex human factors entering into the acquisition, evaluation, and the style and degree of completeness of the dissemination of the information generated lead to considerable scatter in the drag, inertia, and lift coefficients. Apparently, the appreciation of the facts leading to the scatter does not necessarily enable one to quantify these factors or remedy the situation but it gives the designer at least a sense of understanding and security within the scope of his overall

design philosophy. Additional in situ measurements may help to calibrate the MOJS equation for application to more or less similar conditions in a given region but they are not likely to help to uncover the degree of importance of the parameters involved. Evidently, the answer lies neither in the use of the steady-flow drag coefficients with an inertia coefficient near its ideal value nor in the use of the coefficients obtained with relatively idealized and controlled experiments without an appreciation of the mitigating effects of the ocean environment. It would be unreasonable to argue on the one hand that steady-flow coefficients should be used at high K and Re values and on the other hand to argue that even for relatively high K values, one must expect significant differences between oscillatory and uniform incident flow.

It is a well-known fact that the flow conditions in the real environment do not resemble either steady flow or harmonically oscillating flow or two-dimensional wavy flow (orbital motion, sweeping of the wake to and fro over the body, and the spectral nature of waves and currents).

The true purpose of relatively-idealized experiments (e.g., uniform harmonic flow about circular cylinders) is not to provide coefficients for immediate use in the design of offshore structures but rather, and more importantly, to determine whether the linear combination of a linear inertial force with a nonlinear drag force can predict, with sufficient accuracy, the measured time-dependent forces. Should this prove to be the case, one can then determine the role played by each controllable parameter in the evaluation of the coefficients quantifying the drag and inertial forces. This by no means ensures that the said two-term linear superposition will continue to hold true for more complex flow kinematics and body shapes to the same degree of accuracy as in idealized experiments in the flow regimes defined by K and Re.

It has already been pointed out that the MOJS equation does not correctly

predict the measured force in the drag-inertia dominated regime even for a harmonically oscillating planar flow (the possibility must be kept in mind that this may be because of the harmonically oscillating nature of the flow). It is not expected that it will hold better for more complex flows. However, the reduced spanwise coherence of the vortices may give rise to a time-dependent force which may resemble to that predicted by the MOJS equation with two time-averaged coefficients.

The improvement of the MOJS equation is clearly desirable with the addition of one or more terms. Even then the revised form of the equation may be suitable only for the conditions on which the revision is based. It appears that the comparison of the numerous drag and inertia coefficients obtained from the ocean tests, particularly in the range $8 < K < 20$, is not a realistic and fluid-mechanically satisfying exercise. Clearly, both the form of the MOJS equation and the uncertainties that go into the characterization of the ocean environment are jointly responsible for the differences between the measured and calculated forces.

5.4 Sinusoidally Oscillating Planar Flow

The set of data finally chosen for a detailed study of the MOJS equation was that obtained with a sinusoidally oscillating planar flow. In 1976 Sarpkaya (1976a, 1976b) reported the results of a comprehensive series of experiments with a sinusoidally oscillating flow about smooth and rough circular cylinders and demonstrated clearly the dependence of C_d, C_m, and C_L on the Reynolds number, Keulegan-Carpenter number, and the relative roughness. During the past six years, these data have stimulated a great deal of research activity and gave rise to a number of questions: Are these data applicable to the design of offshore structures, what is the effect of the orbital motion

of the particles, do the data apply to horizontal cylinders, why are the drag coefficients for rough cylinders so large, are there blockage effects, do the in-line and transverse forces vary significantly from cycle to cycle, does the MOJS equation hold true for all values of K and Re, why is the added mass coefficient sometimes negative, etc.? These questions were in general valid and required a great deal of additional research for their clarification and resolution.

In view of the foregoing Sarpkaya (1981) repeated his 1976 experiments in a larger U-shaped oscillating flow tunnel. The length of the U-shaped tunnel (Sarpkaya 1976) has been increased from 30 ft to 35 ft and its height from 16 ft to 22 ft. The cross section of the 35 ft long test section has been increased from 3 ft by 3 ft to 3 ft by 4.7 ft. Furthermore, the oscillation mechanism has been completely modified so that mono-harmonic oscillations can be generated and maintained indefinitely at the desired amplitude.

The velocity in the tunnel has been determined through the use of a capacitance wire, hotfilm anemometer, perforated ball, magnetic flow meter, an accelerometer (which measured the instantaneous acceleration of flow in the test section), and by visual measurement of the water level at its highest and lowest points in the legs of the tunnel. It is safe to state that the velocity could not have been measured more accurately. The only other means by which the velocity could have been measured was the use of a laser device. In view of the fact that the other means of measurement yielded the ambient velocity within 2 percent of each other it was decided to forsake the laser system.

The signal from the force transducers was simultaneously recorded in analog form and also fed to an HP scanner-voltmeter system which digitized the analog signal at time intervals corresponding to 0.5 degrees. The data

were stored in floppy discs and fed to an HP-9845B computer. The data were then analyzed cycle-by-cycle, averaging two consecutive cycles, averaging three consecutive cycles, etc., up to 50 cycles. It was firmly established that the cycle-by-cycle analysis yielded drag coefficients whose maximum and minimum were within 5 percent of the 50-cycle averaged values for all K and Re values. These data have been reported by Sarpkaya (1981), Bakmis (1981) and Raines (1981) and formed the basis of the present analysis together with the data reported earlier by Sarpkaya (1976a, 1976b).

It should be noted in passing that Sarpkaya (1981) has shown that: (a) the inroads towards the understanding of wave-induced forces and the establishment of a fluid-mechanically sound wave-force methodology require extremely careful experiments over a broad range of K, Re, and k/D values; (b) the drag and inertia coefficients vary dramatically with time, particularly in the drag-inertia dominated regime; (c) the averaged negative added mass is a consequence of the averaging process and does not actually contradict reality; (d) roughness can and does significantly increase the drag coefficient in harmonic flow over circular cylinders; and that (e) the original MOJS equation yields relatively large residues in the drag-inertia dominated regime (as reflected by the mismatch between the measured and calculated forces, see Figs. 1-10). In this regime, where the complex problems associated with the motion of relatively few vortices are much pronounced, the MOJS equation tries to reproduce the time-dependent force using constant, averaged, force-transfer coefficients which do not account for the history of the motion or the rapid changes in the flow which produce components at higher frequencies, mainly at odd harmonics of the basic. Thus, it must be either modified or a new unified force equation be developed.

6.0 METHODS OF ANALYSIS

6.1 Introduction

Six methods were considered for the representation or evaluation of the time-dependent force in terms of appropriate parameters. These consisted of: (1) evaluation of the instantaneous values of C_d and C_m; (2) evaluation of C_d and C_m in terms of the relative displacement s/D and the Reynolds number; (3) use of the discrete vortex model; (4) evaluation of the instantaneous force; (5) evaluation of the effect of the instantaneous lift force on the in-line force; and (6) the Fourier analysis of the residues. These methods will now be described in some detail.

6.2 Methods 1 and 2: Instantaneous and Relative Displacement Analysis of C_d and C_m

Equation (15), rewritten here as,

$$\frac{2F}{\rho D U_m^2} = \frac{|U|U}{U_m^2} G(s/D) + \frac{\pi}{2} \frac{D}{U_m^2} \frac{dU}{dt} H(s/D) \qquad (44)$$

suggests that C_d and C_m in the MOJS equation may be evaluated as time-dependent coefficients as functions of s/D where s is the displacement of the fluid i.e.,

$$C_d = G(s/D) \qquad (45a)$$

$$C_m = H(s/D) \qquad (45b)$$

It is also thought that G and H will depend on the Reynolds number, relative roughness, etc. This can be done in various ways each of which offer extremely voluminous and at best difficult-to-use information. Furthermore, this method already assumes the validity of the form of the MOJS equation and tries to fit the measured force to it by properly choosing the appropriate values of C_d and C_m at each instant. Strictly speaking, the use of the MOJS equation to determine $C_d(\theta)$ and $C_m(\theta)$ is not quite correct for non-periodic flows because of the

presence and variation with time of an additional history term. In sinusoidal flows, as in the case under consideration, the effect of the history term can be incorporarted into C_d and C_m without any loss of generality. Sarpkaya (1981) did in fact evaluate $C_d(\theta)$, $C_m(\theta)$, and $C_L(\theta)$ for a number of representative tests and showed that the said coefficients exhibit dramatic variations with θ. Ideally, such calculations can be carried out for the available data and $C_d(\theta)$, $C_m(\theta)$, and $C_L(\theta)$ may be provided either in terms of the instantaneous values of K and Re or in terms of $K = U_m T/D$ and $Re = U_m D/\nu$. Evidently, this information is difficult to use and provides no additional information about the form of the MOJS equation. In order to circumvent these difficulties, it was assumed that C_d and C_m may be decomposed into two parts. One part representing their Fourier averages and the other part representing the dependence on s/D of the deviation of the instantaneous values of C_d and C_m from their Fourier-averaged values, i.e.,

$$C_d = C_{df} + C_d(s/D) \tag{46a}$$

$$C_m = C_{mf} + C_m(s/D) \tag{46b}$$

For a sinusoidally oscillating flow represented by $U = -U_m\cos\theta$, the displacement s is given by $s = -A\sin\theta$. Noting that at $\theta = 0$, $U = -U_m$ and that a fluid particle moved a distance of $s = A$ from the instant of $U = 0$, the displacement was written as $s = A(1 - \sin\theta)$. Then the MOJS equation was written as

$$2F/(\rho D U_m^2) = (\pi^2/K)[C_{mf}+C_{ms}(s/D)^n]\sin\theta - [C_{df}+C_{ds}(s/D)^n]|\cos\theta|\cos\theta \tag{47}$$

where C_{df} and C_{mf} represent the usual Fourier averages as given by Eqs. (13) and (14); C_{ds} and C_{ms}, two new coefficients representing the variations in C_d and C_m; $s/D = (K/2\pi)(1-\sin\theta)$; and n, an unknown power of the relative

displacement. It was hoped that n will be a constant, and the coefficients C_{ds} and C_{ms} will depend only on $Re = U_m D/\nu$ and $K = U_m T/D$, and k/D. Thus, knowing C_{mf}, C_{df}, C_{ms}, and C_{ds} in terms of K, Re, and k/D, one will be able to calculate the variation of F with time with no additional coefficients. It was further hoped that the additional terms containing C_{ds} and C_{ms} will account for the dramatic effects brought about by the shedding of the vortices, particularly in the drag-inertia dominated regime.

Numerous tests have been evaluated using n = 1, n = 2, and n = 3 and the appropriate values of C_{ds} and C_{ms} were determined. The results have shown that C_{ds} and C_{ms} did not in any systematic manner correlate with Re, K, and k/D for any value of n, and the residue did not significantly change relative to that resulting from the original MOJS equation. This was particularly true for the residues near $\theta = \pi/2$ and $3\pi/2$, since at these angles or times $\theta = 0$, and Eq. (47) is identical to the original MOJS equation. Subsequently, it was throught that there should be a phase difference between the instantaneous force and the instantaneous displacement, similar to that between the maximum force and maximum velocity. Then $\sin\theta$ in s/D was replaced by $\sin(\theta+\phi)$. The new form of the equation required the evaluation of C_{ds}, C_{ms}, and ϕ, as a function of K, Re, and k/D for a given value of n. Calculations, too numerous to mention here, have shown that the scatter in the variations of C_{ds}, C_{ms}, and ϕ cannot be accounted for through this method. This unsuccessful approach was finally discontinued.

6.3 Method No. 3: Discrete Vortex Analysis

The use of the discrete vortex model was seriously considered since this method proved to be quite successful for steady flow about stationary and transversely oscillating circular cylinders (Sarpkaya 1963, 1979, Sarpkaya and

Shoaff 1979, Clements and Maull 1975). However, the use of the said method for sinusoidally oscillating flow about a circular cylinder met with numerous difficulties: (a) the position of the separation points; (b) the relationship between the time-dependent boundary layer, separation points, and the near wake; (c) the rate of decay of circulation; (d) Reynolds number effect; and finally, (e) computer time.

No fluid-mechanically satisfactory method has been discovered to relate the position of the mobile separation points to the evolution of the wake and the boundary layers. The assumption of fixed separation points and a constant rate of shedding of vorticity proved to be a useless exercise at best. The use of discrete vortices with constant strength always yielded an inertia coefficient of $C_m = 2$ (for a circular cylinder). This was clearly unsatisfactory. It has been shown by Sarpkaya (1963) that the in-line and transverse forces exerted on a circular cylinder immersed in a time-dependent ambient flow with m number of growing and moving vortices arbitrarily situated outside the cylinder are given by

$$F_{il} = -\sum_{k=1}^{m} \rho\Gamma_k(v_k - v_{ki}) + \sum_{k=1}^{m} \rho q_{ki} \frac{\partial\Gamma_k}{\partial t} + 2\pi\rho c^2 \frac{\partial U}{\partial t} \tag{48a}$$

and

$$F_L = \sum_{k=1}^{m} \rho\Gamma_k(u_k - u_{ki}) - \sum_{k=1}^{m} \rho p_{ki} \frac{\partial\Gamma_k}{\partial t} \tag{48b}$$

in which Γ_k represents the strength of the k-th vortex; v_k and v_{ki}, the y-component of the velocities of the k-th vortex and its image; u_k and u_{ki}, the x-component of the k-th vortex and its image; p_{ki} and q_{ki}, the x- and y-coordinates of the image of the k-th vortex; t, time; $\partial\Gamma_k/\partial t$, the rate of change of circulation of the k-th vortex; c, the radius of cylinder (D = 2c); and $\partial U/\partial t$,

the local acceleration of the ambient flow.

Normalizing Eqs. (48a) and (48b) with $0.5\rho DU_m^2 = \rho cU_m^2$, where U_m is now a characteristic velocity of the ambient flow, one has

$$F_{il}/(\rho cU_m^2) = -\sum_{k=1}^{m} \frac{\Gamma_k}{U_m c}\left(\frac{v_k}{U_m} - \frac{v_{ki}}{U_m}\right) + \sum_{k=1}^{m} \frac{q_{ki}}{c} \frac{\partial(\Gamma_k/U_m c)}{\partial(U_m t/c)} + 2\pi \frac{\partial(U/U_m)}{\partial(U_m t/c)} \tag{49a}$$

and

$$F_L/(\rho cU_m^2) = \sum_{k=1}^{m} \frac{\Gamma_k}{U_m c}\left(\frac{u_k}{U_m} - \frac{u_{ki}}{U_m}\right) - \sum_{k=1}^{m} \frac{p_{ki}}{c} \frac{\partial(\Gamma_k/U_m c)}{\partial(U_m t/c)} \tag{49b}$$

Equations (48a) through (49b) show that the evaluation of the in-line and transverse forces require the instantaneous strength, position, and velocity of the vortices, even if one were to ignore the rate of change of circulation with time. Ordinarily, one can determine the above variables by starting the flow impulsively from rest and performing calculations for a large number of steps until one reaches a quasi-steady state. For a sinusoidally oscillating flow about a circular cylinder this is not yet possible due to the deficiencies of the model associated with the boundary layers, separation points, and their interaction with the wake. More importantly, however, one has no experimental information regarding the rate of change of circulation of the individual vortices (see Sarpkaya and Shoaff 1979). It is clear from Eq. (48a) or Eq. (49a) that the assumption of $\partial\Gamma_k/\partial t = 0$ leads, by virtue of the last terms in the said equations, to $C_m = 2$ at all times. This is clearly unacceptable and shows that $\partial\Gamma_k/\partial t$ is not to be ignored.

The fact that there are no means to model the rate of change of circulation with time without making arbitrary assumptions or introducing ad-hoc circulation decay functions, no direct means to relate the boundary layer, separation points, and the wake in periodically reversing flows, no means to incorporate the effect of viscosity (Reynolds number dependence), (save for the arbitrary assumption of

a diffusing vortex core whose radius is assumed to be a function of the Reynolds number), and no means to intelligently model the effect of roughness led to the abandonment of the application of the discrete vortex model to the flow under consideration.

6.4 Method No. 4: Instantaneous Force Analysis

This method is based on Eq. (24) which may be reduced to

$$C(\theta) = 2F/(\rho D L_c U^2) = f[UD/\nu,\ L_c/D,\ k/D,\ \alpha,\ (D/U^2)\partial U/\partial t] \qquad (50)$$

if one ignores the effect of higher order derivatives of U and, of course, the free-surface effects. For smooth, unyawed cylinders (ignoring the effect of yaw), $C(\theta)$ is seen to be a function of UD/ν and $(D/U^2)\partial U/\partial t$. Clearly, $C(\theta)$ varies from zero to infinity; UD/ν, from $-U_m D/\nu$ to $+U_m D/\nu$; and $(D/U^2)\partial U/\partial t$, from minus infinity to plus infinity for $U = -U_m \cos\theta$.

The coefficient $C(\theta)$ has been calculated for numerous smooth-cylinder tests, at $\Delta\theta = 1$ degree intervals, together with the corresponding values of UD/ν and $(D/U^2)\partial U/\partial t$. The purpose of the calculation was to prepare a three-dimensional plot of the three variables involved. This proved to be a nearly impossible task primarily because of the extreme variations of the limits of the said parameters. In addition, such a plot offered nothing new about the physics of the problem.

6.5 Method No. 5: Analysis of the Effect of Lift Force on In-Line Force

The fact that the variations in the in-line force may be related to the growth, shedding, and subsequent convection of the vortices may be used to improve the MOJS equation. In steady flow past a circular cylinder, the drag coefficient fluctuates with a frequency twice the vortex shedding frequency and with an amplitude which may be related to the amplitude of the lift force

by

$$C_d = \bar{C}_d + \eta C_L \sin(4\pi f_v t + \phi) \tag{51}$$

where $\bar{C}_d$ is the mean drag coefficient; η, a proportionality constant; C_L, a representative lift coefficient (maximum, rms, etc.); f_v, the vortex shedding frequency; and ϕ, the phase angle. It is of course recognized that f_v is not clearly definable at all Reynolds numbers and that the Strouhal number defined by $St = f_v D/\bar{V}$ is about 0.2 at subcritical Reynolds numbers, and about 0.3 at postcritical Reynolds numbers. In the critical and transcritical regimes, a broad band of power spectral density is usually observed for a rigidly held cylinder (see e.g., Sarpkaya and Shoaff 1981).

For sinusoidally oscillating flow, Sarpkaya (1976) suggested that a third term may be added to the MOJS equation as

$$2F/(\rho D U_m^2) = (\pi^2/K) C_m \sin\theta - C_d |\cos\theta| \cos\theta - \eta C_L \cos(3\theta - \phi) \tag{52}$$

Sarpkaya (1976) has performed preliminary calculations with Eq. (52) to demonstrate that the eddy-induced in-line force oscillations can account for most of the error in the predictions of the MOJS equation in the range of K values from about 10 to 20. The preliminary studies have been pursued further with the impetus received from the exploratory studies of Verley (1981) and Bearman et al. (1981) regarding the variation of the lift force, particularly at large K values.

The lift force was written as

$$F_L = 0.5\rho D U^2 C_L \sin 2\pi f_v t \tag{53}$$

and it was assumed that the instantaneous Strouhal number $St = f_v D/U$ is nearly constant. Then $f_v = SU/D$, (St is replaced by S for sake of simplicity), and

$$F_L = 0.5\rho D C_L U_m^2 (\sin^2\theta) \sin(2\pi S U t/D) \tag{54}$$

assuming now $U = U_m \sin\theta$. Since Ut/D represents the relative displacement of the fluid from the start (say t = 0), one may write

$$Ut/D = \int_0^t (U_m/D)\, \sin(2\pi t/T)dt = (U_m T/2\pi D)(1 - \cos\theta) \qquad (55)$$

or

$$C_L(\theta) = 2F_L/(\rho D U_m^2) = C_L(\sin^2\theta)\sin[KS(1 - \cos\theta)] \qquad (56)$$

where C_L is a representative lift coefficient for a given K, Re, and k/D (expressed either in terms of its maximum or rms value); and $C_L(\theta)$, the amplitude and frequency-modulated instantaneous lift coefficient. The angle θ starts from zero at each half cycle, i.e., $0 < \theta < \pi$.

Equation (56) is expected to produce lift-force variations which resemble those obtained experimentally only at relatively high K values where the quasi-steady-state assumption may be valid for the purpose under consideration. Comparisons have shown that even at high K values Eq. (56) produces $C_L(\theta)$ values which resemble only occasionally those obtained experimentally, primarily because of the random nature of the shedding of vortices and the strong effect of this randomness on the transverse force. Figures 11 through 20 show the results of sample calculations, carried out assuming $C_L = 1$ and S = 0.2. These calculations need to be pursued further in order to explore the characteristics of the lift force, particularly at lower K values.

The recognition of the fact that the effect of the shedding and subsequent convection of vortices on the fluctuations of the in-line force is somewhat less pronounced, compared with the similar effect on the transverse force, it was thought advisable to account for the residue in the in-line force through the use of an expression similar to that given by Eq. (52), i.e.,

$$2F/(\rho D U_m^2) = (\pi^2/K)C_m \sin\theta - C_d \cos\theta|\cos\theta| + \\ + nC_L \sin(\theta-\phi)|\sin(\theta-\phi)|\sin[NKS\{1 - \cos(\theta-\phi)\}] \qquad (57)$$

where ϕ is a phase angle and N, the frequency-modulation factor. Numerous calculations have been performed to determine η, ϕ, and N, particularly in the range of K values from 10 to 20. The results were quite encouraging (see Figs. 21 and 22) and it appeared that it would be possible to relate η, ϕ, and N to $K = U_m T/D$ and $Re = U_m D/\nu$ in minimizing the residue between the measured and calculated forces. The calculations have not been pursued further partly because the coefficients C_L (the rms value of the lift coefficient in terms of K, Re, and k/D) were not available for the desired range of K and Re values and partly because of time constraints. This approach should be pursued further through the use of the simultaneous records of the in-line and transverse forces. In doing so, it might be desirable to carry out a spectral analysis of the lift force and to write Eq. (57) as

$$2F/(\rho D U_m^2) = (\pi^2/K)\, C_m \sin\theta - C_d |\cos\theta| \cos\theta + \sum_{i=1}^{p} \eta_i C_{L_i} \sin(\theta-\phi) |\sin(\theta-\phi)| \sin[N_i KS\{1-\cos(\theta-\phi)\}] \qquad (58)$$

in order to include the contribution of the fundamental frequency and at least its first harmonic. This will help to clarify not only the role played by the lift force on the in-line force but also the role played by the shedding and convection of vortices on the evolution of the lift force itself. However, the question of the randomness of vortex shedding remains open. One must introduce either a coherence-state factor (perfect, partial, ocean conditions, etc.) or a probability-function multiplier into the third term of Eq. (58). As noted earlier, one of the mitigating effects of the ocean environment is to reduce the coherence length of the vortices and hence the effect of the shedding and convection of the vortices on the fluctuations of the in-line force.

6.6 Method No. 6 - Analysis of the Residues

As noted earlier, Keulegan and Carpenter expressed the time-dependent force as [see Eq. (11)],

$$2F/(\rho DU_m^2) = (\pi^2/K)C_m\sin\theta - C_d|\cos\theta|\cos\theta + \Delta R \tag{59}$$

where ΔR represents the residue given by

$$\Delta R = C_3\cos(3\theta - \phi_3) + C_5\cos(5\theta - \phi_5) + \ldots\ldots \tag{60}$$

Keulegan and Carpenter considered only the first term in Eq. (60) in the form

$$\Delta R = A_3\sin 3\theta + B_3\cos 3\theta \tag{61}$$

and evaluated A_3 and B_3, and showed that they are functions of K, within the range of their K and Re values ($3 < K < 120$ and $5700 < Re < 29300$). Keulegan and Carpenter noted that "for period parameters, K, in the neighborhood of the critical, $U_mT/D = 15$, the representation of forces is more exact by using Eq. (59)" together with Eq. (61). They did not pursue the matter further.

The obvious disadvantage of this expanded form of the MOJS equation [Eqs. (59) and (61)] is that it now requires the evaluation of four coefficients, namely, C_d, C_m, and either C_3 and ϕ_3 or A_3 and B_3. Even then the calculated and measured forces do not always correspond partly due to the existence of other harmonics and partly due to the pronounced effect of the randomness of the shedding, spanwise coherence, and the motion of a few vortices, vice large number of vortices. This, in turn, requires the addition of two more terms involving C_5 and ϕ_5. Clearly, the determination of the dependence of six coefficients on the parameters characterizing the phenomenon is a nearly impossible task and is not very practicable for the design of offshore structures, even if one were to confine his attention to smooth circular cylinders alone! It is partly because of this reason and partly because of the

uncertainties in the input parameters (velocities and accelerations) that the two-term MOJS equation has been used over the past thirty years in spite of its known limitations (at least under laboratory conditions). The inaccuracies resulting from the use of the said equation have been compensated partly by the mitigating effects of the ocean environment (reduced spanwise coherence, omnidirectionality of the waves and currents distribute the residue over a broad band of frequencies, making the predictions of the MOJS equation come closer to those measured) and partly by the designer through the use of hidden and intentional safety factors.

In view of the foregoing it was decided to explore the possibility of revising the MOJS equation with the following constraints: (a) the revision should be fluid-mechanically meaningful; (b) the revised form of the equation should contain no more than the two coefficients already in use, namely, C_d and C_m; (c) the coefficients of the additional terms should be related to C_d and C_m (since they too are functions of K, Re, and k/D) through a careful spectral and Fourier analysis of the residues; and (d) the revised form of the equation should reduce to the MOJS equation in the drag and inertia dominated regimes.

With the objectives cited above, the residues of the in-line forces acting on 11 smooth and 11 rough circular cylinders, ranging from 2- to 7-inches in diameter have been subjected to extensive spectral analysis through the use of standard techniques. The results have shown that all harmonics from 2 through 15 (the upper limit of the frequency considered) appear in the spectral analysis of the residue, with varying degrees of importance (see Tables 1 through 10 where only the first 10 residues are listed). However, the third and fifth harmonics are far more important than the remaining ones, at least for the sinusoidally oscillating flow under laboratory conditions (see Figs. 23 and 24

where the values of C_3 and C_5, averaged over each K, are shown for all tests for the purpose of illustrating the region of importance of each coefficient).

It is thus apparent that the MOJS equation must be modified to minimize the residue and that this modification should involve the third and the fifth harmonics. It is with this realization that the MOJS equation was written as a sum of Eqs. (59) and (60) as

$$2F/(\rho DU_m^2) = (\pi^2/K)C_m\sin\theta - C_d|\cos\theta|\cos\theta + C_3\cos(3\theta - \phi_3) + C_5\cos(5\theta - \phi_5) \qquad (62)$$

Then the attention has been concentrated on the determination of C_3, ϕ_3, C_5, and ϕ_5 with the constraints cited earlier. This, in turn, required an extensive search for a functional relationship between the said coefficients and the known parameters C_d, C_m, K, Re, and k/D.

For relatively small smooth cylinders and Reynolds numbers, Keulegan and Carpenter have already shown that A_3 and B_3 are functions of K, as were their C_d and C_m values, according to their conclusions, [Sarpkaya (1976a) has shown much later that the C_d and C_m values of Keulegan and Carpenter depend also on Re]. A similar analysis of the A_3 and B_3 values of Keulegan and Carpenter has shown that both A_3 and B_3 depend not only on K but also on Re.

The data used in the present analysis also have shown that C_3, ϕ_3, C_5, and ϕ_5 depend on K, Re, and k/D. Note that K, Re, and k/D are the same independent parameters which determine the Fourier-averaged values of C_d and C_m, as shown clearly by Sarpkaya (1976a, 1976b). Detailed study of the said four coefficients have shown that it is preferable to explore their dependence on K, C_d, and C_m rather than on K, Re, and k/D. Evidently, the two approaches are mathematically identical. Thus, one has

$$C_i = C_i(K, C_d, C_m) \ , \quad i = 3, 5 \tag{63a}$$

$$\phi_i = \phi_i(K, C_d, C_m) \ , \quad i = 3, 5 \tag{63b}$$

By virtue of Eqs. (63a) and (63b), the residue is solely dependent on K, C_d, and C_m. Significant effort has been devoted to determining the form of the above relationships by numerous correlations. Here only the final result and not the year-long efforts will be described.

It is a well-known fact that in harmonic flow the ratio of the maximum inertia force to the maximum drag force is given by the MOJS equation as $\pi^2 C_m/KC_d$. Thus, the ratio of the deviation of the maximum inertial force from its ideal value to the maximum drag force is proportional to

$$\Lambda = (2 - C_m)/(KC_d) \tag{64}$$

It must be noted in passing that C_m exceeds its ideal potential-flow value for small values of K and β, as noted earlier in connection with the discussion of Stokes solution. However, in the region of K values from about 8 to 20, this increase is not of special importance and the ideal value of C_m for a circular cylinder may be taken equal to 2. For other shapes of bodies Λ may be written as

$$\Lambda = (C_m^* - C_m)/(KC_d) \tag{65}$$

where C_m^* is the ideal value of the inertia coefficient for the particular body.

It is clear that Λ approaches zero for both the small and large values of K and is unique for a given K, Re, and k/D. Thus, unique relationships should exist between the coefficients C_i, ϕ_i and Λ and K. Numerous attempts have shown that $C_i\sqrt{\Lambda}$, and $\phi_i\sqrt{\Lambda}$ are indeed unique functions of K for all smooth and rough cylinders (within the range of data and the experimental scatter). Figures 25 through 28 show the variations of $C_3\sqrt{\Lambda}$, $\phi_3\sqrt{\Lambda}$, $C_5\sqrt{\Lambda}$, and $\phi_5\sqrt{\Lambda}$ as a

function of K. The scatter in these figures is primarily due to the sensitivity of the four coefficients (i.e., the sensitivity of the residue) to spanwise coherence and the somewhat random shedding of the vortices in the intermediate range of the Keulegan-Carpenter numbers. In spite of the scatter of the data, the relationships are quite satisfactory.

Figures 25 through 28 show that $C_3\sqrt{\Lambda}$, $\phi_3\sqrt{\Lambda}$, $C_5\sqrt{\Lambda}$, and $\phi_5\sqrt{\Lambda}$ reach their extreme values at about K = 12.5. It must be noted that the relationships between these parameters and K should have a probabilistic character because of the complex motion of the vortices and the non-stationary nature of the motion. The following simple distribution has been chosen to relate $C_3\sqrt{\Lambda}$, ..., $\phi_5\sqrt{\Lambda}$ and K

$$M_p = A_{mp} + B_{mp}\, e^{C_{mp}(K - 12.5)^2} \tag{66}$$

in which M denotes either C or ϕ; p, the index 3 or 5; and A_{mp}, B_{mp}, and C_{mp}, three constants for the relationships between $M_p\sqrt{\Lambda}$ and K. A parametric analysis of these coefficients for the best fit of the predictions of Eq. (66) to the experimental data has shown that

$$\begin{array}{lll} A_{c3} = 0.01 & B_{c3} = 0.10 & C_{c3} = -0.08 \\ A_{\phi 3} = 0.05 & B_{\phi 3} = 0.35 & C_{\phi 3} = -0.04 \\ A_{c5} = 0.0025 & B_{c5} = 0.053 & C_{c5} = -0.06 \\ A_{\phi 5} = 0.25 & B_{\phi 5} = 0.60 & C_{\phi 5} = -0.02 \end{array} \tag{67}$$

These are considered as universal constants and are not dependent on K, Re, and k/D for a circular cylinder.

The four-term MOJS equation may now be written as

$$2F/(\rho DU_m^2) = (\pi^2/K)C_m\sin\theta - C_d|\cos\theta|\cos\theta +$$

$$\Lambda^{-1/2}\{A_{c3}+B_{c3}\exp[C_{c3}(K-12.5)^2]\}\cos\left\{3\theta-\Lambda^{-1/2}\{A_{\phi3}+B_{\phi3}\exp\right.$$

$$\left.[C_{\phi3}(K-12.5)^2]\}\right\} + \Lambda^{-1/2}\{A_{c5}+B_{c5}\exp[C_{c5}(K-12.5)^2]\}$$

$$\cos\left\{5\theta- \Lambda^{-1/2}\{A_{\phi5} + B_{\phi5}\exp[C_{\phi5}(K-12.5)^2]\}\right\} \qquad (68)$$

It is clear from Eq. (68) as well as from Figs. 25 through 28 that the residue, as represented by the last two terms in Eq. (68), diminishes rapidly for K smaller than about 7 and larger than about 20. In other words, Eq. (68) reduces to the two-term MOJS equation for all practical purposes outside the drag-inertia dominated regime. The additional terms cause an amplitude and frequency modulation in the in-line force, in a manner similar to that provided by Eq. (58), and reflect the role played by the growth and motion of vortices on the in-line force.

6.6.1 The Predictions of the New MOJS Equation

Figures 29a through 71c show the results obtained with the new MOJS equation. Note that the original MOJS equation [Eq. (12)] is called "the two-term MOJS equation." The one obtained with the addition of only $C_3\cos(3\theta-\phi_3)$ is called "the three-term MOJS equation", i.e.,

$$2F/(\rho DU_m^2) = (\pi^2/K)C_m\sin\theta - C_d|\cos\theta|\cos\theta + \Lambda^{-1/2}\{0.01 + 0.10\ e^{-0.08(K-12.5)^2}\}$$

$$\cos\left\{3\theta - \Lambda^{-1/2}\{0.05 + 0.35\ e^{-0.04(K-12.5)^2}\}\right\} \qquad (69)$$

Finally, the one obtained with the addition of $[C_3\cos(3\theta-\phi_3) + C_5\cos(5\theta-\phi_5)]$

is called "the four-term MOJS equation" [Eq. (68)] or more specifically,

$$2F/(\rho D U_m^2) = (\pi^2/K)C_m \sin\theta - C_d|\cos\theta|\cos\theta +$$

$$\Lambda^{-1/2}[0.01 + 0.10\ e^{-0.08(K-12.5)^2}]\cos\{3\theta - \Lambda^{-1/2}[0.05 + 0.35\ e^{-0.04(K-12.5)^2}]\}$$

$$+ \Lambda^{-1/2}[0.0025 + 0.053\ e^{-0.06(K-12.5)^2}]\cos\{5\theta - \Lambda^{-1/2}[0.25 + 0.60\ e^{-0.02(K-12.5)^2}]\} \quad (70)$$

The first figure in each set, such as Fig. 29a, shows a comparison of the normalized measured force with that predicted by the two-term MOJS equation. In addition, the residue, i.e., the difference between the normalized measured and calculated forces, is shown in each figure. The second figure in each set, such as Fig. 29b, shows a comparison of the normalized measured force with that predicted by the three-term MOJS equation together with the new residue (the difference between the normalized measured force and the normalized calculated force through the use of the three-term MOJS equation). Finally, the third figure in each set, such as Fig. 29c, shows a comparison of the normalized measured force with that predicted by the four-term MOJS equation together with the corresponding residue. It should be noted that Figs. 29 through 71 are arranged in the order of increasing Keulegan-Carpenter numbers. A detailed study of the particulars of each figure shows that the results cover a wide range of Keulegan-Carpenter numbers, Reynolds numbers, and relative roughnesses.

It is clear from Figs. 29 through 71 that the three-term MOJS equation and in particular the four-term MOJS equation reduce the residue significantly. In some cases, the difference between the measured and calculated forces is smaller than the experimental error.

The reduction in residue may be quantified through the use of various "goodness-of-fit" parameters (Sarpkaya 1976a). In the present study, the following definition has been adopted and evaluated for each run:

$$\sigma = 100 \sqrt{\frac{\frac{1}{T}\int_0^T (F_m - F_c)^2 \, dt}{\frac{1}{T}\int_0^T F_m^2 \, dt}} \tag{71}$$

in which F_m represents the measured force and F_c, the calculated force. The results have shown that in the drag-inertia dominated regime the two-term MOJS equation [Eq. (12)] yields σ values ranging from about 10 to 25. The three-term MOJS equation [Eq. (69)] reduces σ by about 50 percent ($5 < \sigma < 10$). Finally, the four-term MOJS equation [Eq. (68) or Eq. (70)] reduces σ by about 80 percent ($1 < \sigma < 5$) relative to the two-term MOJS equation. In fact, the results have shown that the predictions of Eq. (70) are as good as those based on the actual values of the Fourier components of the residue. In other words, Eq. (70) represents quite accurately the behavior of the residue and in many cases as accurately as its Fourier components. Clearly, no functional relationship, representing $C_3\cos(3\theta-\phi_3)$ and $C_5\cos(5\theta-\phi_5)$, can provide a better correlation between the measured and calculated forces than the one where the actual values of C_3, ϕ_3, C_5, and ϕ_5 are used in the third and fourth terms of Eq. (62), as determined from the Fourier analysis of the residue.

The form of the residue suggests that all harmonics of the fundamental play some role even though the third and fifth harmonics are predominant. This fact is evidenced by the results shown in Tables 1 through 10.

It is clear from the foregoing that a perfect match between the measured

and calculated force can be obtained only if one takes into account the contributions of all harmonics. From a practical point of view this is rather difficult and certainly not justified in view of the uncertainties associated with the kinematics of the flow field, spanwise coherence of the vortices, nonstationary nature of the occurrences, nonuniform surface roughness, and the possible dynamic response of the body to the fluid forces imposed on it. It is primarily because of these reasons that the modified MOJS equation has been restricted to four terms.

The new version of the MOJS equation contains only the two coefficients already in use, namely, C_d and C_m. Furthermore, the Fourier averages of C_d and C_m are still given by Eqs. (13) and (14). Thus, Eq. (68) satisfies practically all the constraints imposed on its evaluation.

6.6.2 A Critical Assessment of the New MOJS Equation [Eq. (68)]

Equation (68) is based on the results obtained with a sinusoidally oscillating flow about smooth and rough circular cylinders. The in-line forces used in the analysis of the residues corresponded to the flow conditions where the spanwise coherence of the vortices was as perfect as possible, as reflected by the magnitude and periodicity of the corresponding transverse forces. It is a well know fact that the vortices shed from a cylinder is neither straight nor parallel to the axis of the cylinder even in steady flow. Variation of the spanwise characteristics of vortices has a profound effect on the instantaneous loading of the cylinder. Relatively poor correlation of the flow in the spanwise direction gives rise to a lift force which is lower than that resulting from a fully-correlated vortex shedding. It has been shown by Wilkinson (1981) that the lift acting on a given length of cylinder is a function both of the aspect ratio of the

body configuration and the aspect ratio of the portion of cylinder on which the loads are being considered. In general, the three-dimensional lift coefficient (based on a finite length of cylinder) is smaller than the two-dimensional lift coefficient (based on a small section of the cylinder). Thus, the determination of a lift coefficient from the measurement of forces acting on a finite length of a cylinder has only limited value unless the spanwise coherence of the flow field is known in terms of the governing parameters and the end conditions. It is because of this reason that the in-line forces used in the development of Eq. (68) corresponded to the flow conditions where the spanwise coherence of vortices was as perfect as possible, as reflected by the magnitude and periodicity of the corresponding transverse forces at both ends of the test cylinders.

In sinusoidally oscillating planar flow the coherence of the vortices and the interaction between vortices from the two sides of the reciprocating wake are much stronger than those in wave flows in the ocean environment. Even then the occasional lack of coherence of vortex shedding in sinusoidally oscillating planar flows gives rise to intermittent transverse forces (Maull and Milliner 1978, Sarpkaya and Isaacson 1981). This is particularly true for the drag-inertia dominated regime. In any case, however, the intermittency of the transverse force in wave flows is much higher than that in sinusoidally-oscillating planar flows.

The in-line force is certainly affected by the intermittent nature of the transverse force and by the variations in the coherence length. However, the dependence of the in-line force on the characteristics of vortex shedding (intermittency, spanwise coherence, interaction between vortices) is considerably less than that of the transverse force.

The reduced spanwise coherence decreases the peak value of the in-line force and the amplitude of secondary oscillations imposed on it by the shedding, interaction, and convection of vortices. In other words, the reduction of the spanwise correlation results in the distribution of the energy of the secondary oscillations over a broader band of frequencies. This results in smaller drag and inertia coefficients. The drag coefficient is more sensitive than the inertia coefficient since the force in Eq. (13) is multiplied by $\cos\theta$ and since the largest effects of vortex shedding and spanwise coherence occur near the times of maximum velocity, i.e., when $\cos\theta$ is near its maximum.

It is evident from the foregoing that additional research is needed to quantify the effect of spanwise coherence on the in-line and transverse forces and, in turn, on the drag, inertia, and lift coefficients. It is also evident that the data obtained in the ocean environment must necessarily reflect not only the consequences of currents, nonuniform roughness, nonuniform waves, body inclination, dynamic response, proximity, etc., but also the effect of the variation of the spanwise coherence. The scatter in the ocean-data-based drag, inertia, and lift coefficients may be brought to order by measuring the spanwise pressure distribution over the length of the force sleeve and reporting the said coefficients together with the corresponding coherence length, expressed suitably in terms of the fluctuating pressures.

The effect of the reduced spanwise coherence on the predictions of Eq. (68) has been examined in detail by considering in-line forces for which the transverse forces at the two ends of the test cylinder did not correlate (either in phase and/or in magnitude). The results have shown that the

predictions of the original MOJS equation are better than expected and that Eq. (68) holds true provided that M_p in Eq. (66) is replaced by $M_p^* = \Psi M_p$ where Ψ is a factor expressing the influence of the reduced spanwise correlation on the in-line force ($0 < \Psi < 1$), i.e.,

$$M_p^* = \Psi[A_{mp} + B_{mp}\exp\{C_{mp}(K - 12.5)^2\}] \tag{69}$$

where the meaning and the numerical values of A_{mp}, B_{mp}, and C_{mp} remain unchanged and are given by Eq. (67). Clearly, the foregoing amounts to the replacement of C_3, ϕ_3, C_5, and ϕ_5 by $C_3^* = \Psi C_3$, $\phi_3^* = \Psi\phi_3$, $C_5^* = \Psi C_5$, and $\phi_5^* = \Psi\phi_5$.

Figures 72a through 73c show in-line force samples with reduced spanwise coherence and their comparison with the predictions of the two-term MOJS equation, three-term MOJS equation, and the four-term MOJS equation, [$\Psi = 0.3$ was used in Eqs. (68) and (69)]. Evidently, the reduction of the spanwise coherence removes large scale oscillations from the in-line force and thereby creates conditions to which the original MOJS equation is more applicable. It is also evident that there is very little difference between the predictions of the three-term MOJS equation and the four-term MOJS equation. Thus, as far as the ocean-based data are concerned, the use of the three-term MOJS equation with the appropriate spanwise-correlation factor Ψ is more than adequate. At present, there is no ocean test data with spanwise and chordwise pressure distributions to relate Ψ to the local flow conditions. Suffice it to note that the reduction of the correlation length, among other factors, smoothens the exacerbating effects of the vortex induced forces, reduces the magnitude of the force-transfer coefficients, and makes the predictions of the original MOJS equation more credible.

It is evident from the foregoing that the better the spanwise coherence of vortices, as in the case of planar oscillatory flows, the poorer the predictions of the original MOJS equation, particularly in the drag-inertia dominated regime. This is because of the fact that the better the spanwise coherence, the larger the transverse force and hence the larger the amplitude of the lift-induced oscillations in the in-line force. Also, the more regular the transverse force, the narrower the band of frequencies at which the energy of secondary oscillations and hence the residue are concentrated. However, even in planar oscillatory flows the shedding and subsequent interaction of vortices are not perfectly deterministic. There are variations not only from cycle to cycle but also in each half cycle. Consequently, the in-line force in a given cycle is not representable by an odd-harmonic function, i.e., by a function where $F(\theta) = -F(\theta+\pi)$, (see e.g., Fig. 34a where the in-line force does not return to its initial value at the end of the cycle). On the other hand, the mathematical models [Eqs. (12), (69), and (70)] are based on odd-harmonic functions (see e.g., the force traces predicted by the three-term and four-term MOJS equation in Figs. 34b and 34c, respectively). Thus, the residue, representing the difference between the measured force (a non-odd-harmonic function) and the calculated force (an odd-harmonic function), is a non-odd-harmonic function. In other words, the residue does not ordinarily and necessarily return to its initial value at the end of the cycle (see e.g., Fig. 38c). These observations point out once again the exacerbating effects of the vortex motion in time-dependent flows and the fact that as far as the vortices are concerned each encounter is a new experience, however slight the differences may be.

In concluding the assessment of the new MOJS equation, it must be pointed out that Eq. (68) or Eq. (70) does not apply to yawed cylinders, to wave-current combinations, to flexible cylinders, and to the flow conditions involving free-surface and/or body-proximity effects. At present, there is not enough data to critically assess the speculative generalizations of the original MOJS equation and the improvements which must be made on them.

7.0 CONCLUSIONS

1. The origin of the MOJS equation and its limitations have been discussed in detail and it has been concluded that the choice of the particular form of the force expression seems to have been governed by the following criteria: (a) tangential velocities and accelerations cannot influence the flow appreciably; (b) the wave theory yields normal velocities and accelerations each of which must be separately and additively responsible for part of the force; (c) heuristic reasoning of the applicability of the force expression when applied to conditions of steady flow alone or accelerating flow alone; (d) analytical simplicity of the force expression (linear-quadratic sum); and (e) experimental justification of the then available results.

2. The MOJS equation is an approximate solution to a complex problem. Its justification is strictly pragmatic and rests with experimental confirmation. It applies only to the prediction of in-line forces for D/L smaller than about 0.2 (no diffraction effects); it does not apply uniformly well to all ranges of Reynolds number and Keulegan-Carpenter number; with average C_d and C_m, the unsteadiness of the force resides only in the variation of the velocity and acceleration with time; three-dimensional effects are ignored; the effect of the axial pressure gradient is disregarded; the transverse force is not accounted for; it cannot deal with the effects of orbital motion, yaw, body- and/or free-surface proximity effects, and the omnidirectionality of the waves and currents; and in certain ranges of flow it gives rise to relatively large residues. The magnitude of the residue (i.e., the difference between the measured and calculated force) in the drag-inertia dominated regime increases with increasing spanwise coherence of vortices.

3. A critical study of the nature and decomposition of the time-dependent in-line force has shown that the MOJS equation is not well-founded even for a sinusoidally-oscillating planar flow. The effect of the history of the motion must be represented by one or more additional terms. For a strictly sinusoidal motion the effect of the history term may be incorporated into the drag and inertia coefficients with no loss of generality.

4. The speculative generalizations of the original MOJS equation has been reviewed in detail and it has been concluded that (a) the MOJS equation is not equally valid for all shapes of bodies and types of flows; (b) its use to predict the forces acting on yawed cylinders through the use of the "independence principle" has not been subjected to experimental verification; (c) the generalization of the MOJS equation to predict the in-line forces due to combined waves and currents is unproven and remains as a pure speculation; and finally, (d) the generalization of the MOJS equation to the prediction of the dynamic response of structures is not supported by experimental data.

5. The background of the existing data (from wave channels, ocean tests, and oscillating planar flows) has been reviewed in detail and it has been concluded that the inroads towards the understanding of the limitations of the MOJS equation require extremely careful experiments over a broad range of Keulegan-Carpenter numbers, Reynolds numbers, and relative roughnesses. Neither the Ocean Test Structure data of EPR nor the Christchurch Bay Tower data of NMI are well-defined enough to assess the reasons for the deviation of the measured forces from those predicted by the MOJS equation in the drag-inertia dominated regime. This is primarily due to the lack of information regarding spanwise coherence. Furthermore, the existence of currents and

the omnidirectionality of the waves and currents do not allow one to assess critically the original version of the MOJS equation. The evaluation of the OTS and CBT data require the use of the speculative generalization of the original MOJS equation to the wave-current combination.

6. The MOJS equation should be revised with the following constraints: (a) the revision should be fluid-mechanically meaningful; (b) the revised form of the equation should contain no more than the two coefficients already in use, namely, C_d and C_m; (c) the coefficients of the additional terms should be related to C_d and C_m (since they too are functions of K, Re, and k/D) through a careful spectral and Fourier analysis of the residues; and (d) the revised form of the equation should reduce to the MOJS equation in the drag and inertia dominated regimes.

7. Six methods were considered for the representation or evaluation of the time-dependent force in terms of appropriate parameters. These consisted of: (i) the evaluation of the instantaneous values of the drag and inertia coefficients, (ii) evaluation of the drag and inertia coefficients in terms of the relative displacement of the fluid and the Reynolds number, (iii) use of the discrete vortex model, (iv) evaluation of the instantaneous force, (v) evaluation of the effect of the instantaneous lift force on the in-line force, and finally, (vi) the Fourier analysis of the residues. Among these two methods were found to be most promising, namely, the evaluation of the effect of the instantaneous lift force on the in-line force and the Fourier analysis of the residues. It has been concluded that the available data will not permit the further exploration of the former method at this time.

8. The residues have been analyzed in great detail. The results have shown that all harmonics appear in the spectral analysis of the residue, with varying degrees of importance. However, the third and fifth harmonics are

far more important than the remaining ones, at least for the sinusoidally oscillating flow about smooth and rough circular cylinders. The use of the in-line forces corresponding to the flow conditions where the spanwise coherence was as perfect as possible (as reflected by the magnitude and phase of the corresponding transverse forces at both ends of the test cylinders) resulted in the correlation of the coefficients of the third and fifth harmonics of the residue with the Keulegan-Carpenter number and the ratio of the deviation of the maximum inertial force from its ideal value to the maximum drag force, i.e., $\Lambda = (C_m^* - C_m)/(KC_d)$. This resulted in a new MOJS equation [Eq. (68) or Eq. (70)] whose validity for smooth and rough cylinders has been shown through numerous comparisons with the measured in-line forces and through the calculation of new residues together with the corresponding values of the "goodness-of-fit" parameter σ [Eq. (71)]. The results have shown that the three-term MOJS equation [Eq. (69)] reduces σ by about 50 percent and the four-term MOJS equation [Eq. (70)], by about 80 percent. In fact, the predictions of Eq. (70) are as good as those based on the actual values of the Fourier components of the residue.

9. The new MOJS equation has been critically assessed regarding its applicability to ocean test data and it has been concluded that (a) the in-line force is affected by the intermittent nature of the transverse force and by the variations in the coherence length; (b) it is necessary to introduce a spanwise correlation factor into the new MOJS equation in order to compare its predictions with the data obtained from ocean tests; (c) the reduction of the correlation length, among other factors, smoothens the exacerbating effects of the vortex-induced forces, reduces the magnitude of the force-coefficients, and makes the predictions of the original MOJS

equation more credible; (d) the better the spanwise coherence, the larger the residue in the drag-inertia dominated regime; (e) the sinusoidally-oscillating planar flow accentuates the failings of the original MOJS equation whereas the wave flow tends to minimize them; (f) the scatter in the drag, inertia, and lift coefficients derived from ocean experiments may be brought to order by measuring the spanwise pressure distribution over the length of the force sleeve and correlating the force-transfer coefficients with the corresponding coherence length, expressed suitably in terms of the fluctuating pressures.

8.0 RECOMMENDATIONS

1. Extensive research is needed to justify each and every generalization of the original MOJS equation. Specifically, laboratory and ocean experiments are required to determine (a) the kinematics of the wave and current interactions, (b) the wave and current induced forces on smooth and rough circular cylinders, (c) the forces acting on yawed cylinders and the merits of the "independence principle", and (d) to examine critically the generalization of the MOJS equation to the prediction of the dynamic response of structures.

2. The measurement of in-line and transverse forces alone is no longer sufficient. Extensive research is needed to quantify the effect of spanwise coherence on the in-line and transverse forces and, in turn, on the drag, inertia, and lift coefficients. This will require the measurement of spanwise and chordwise pressure distributions over cylinders.

3. The determination of the effect of lift-induced oscillations on the in-line force is extremely important. The merits of Eq. (58) must be explored through the use of the simultaneous records of the in-line and transverse forces not only for the improvement of the MOJS equation but also for the assessment of the role played by the spanwise coherence of vortices.

4. The contributions of all harmonics of the residue cannot be taken into consideration. From a practical point of view this is rather difficult and certainly not justified in view of the uncertainties associated with the kinematics of the flow field, spanwise coherence of vortices, nonstationary nature of the occurrences, nonuniform surface roughness, and the possible dynamic response of the body to the fluid forces imposed on it. It is because of these reasons that the modified MOJS equation should be restricted to three terms [Eq. (58) or Eq. (69)].

5. Flow kinematics under storm driven seas are random and three-dimensional. Experiments must be carried out both in the laboratory and in the ocean environment to simulate all of the important features of storm driven seas at Reynolds numbers larger than 10^6.

6. Basic research should be pursued to determine the role played by the shedding and interaction of vortices in time-dependent flow about non-circular bluff bodies. Such studies will enhance our understanding of the MOJS equation and the limitations of its generalizations.

9.0 REFERENCES

Bakmis, C., (1981), "Harmonic Flow About Cylinders," Thesis submitted to the Naval Postgraduate School, Monterey, Calif.

Basset, A. B., (1888), "On the Motion of a Sphere in a Viscous Fluid," Phil. Trans., Royal Society of London, Vol. 179, pp. 43-63.

Bearman, P. W., Graham, J. M. R., Naylor, P., and Obasaju, E. D., (1981), "The Role of Vortices in Oscillatory Flow About Bluff Cylinders," Proceedings of the International Conference on Hydrodynamics in Oceans, held at Trondheim in August 1981.

Bishop, J. R., (1978), "The Mean Square Value of Wave Force Based on the Morison Equation," National Maritime Institute Report No. R-40.

Bishop, J. R., (1979), "RMS Force Coefficients Derived from Christchurch Bay Wave Force Data," National Maritime Institute Report No. R-62.

Bishop, J. R., Tickell, R. G., and Gallagher, K. A., (1980), "The UK Christchurch Bay Project; A Review of Results," OTC Paper No. 3796, Houston, TX.

Borgman, L. E., (1958), "Computation of the Ocean-Wave Forces on Inclined Cylinders," Trans. American Geophysical Union, Vol. 39, pp. 885-888.

Boussinesq, J., (1885), "On the Resistance Offered by an Infinite Stationary weightless Liquid to the variable Motion of a Solid Sphere," Compt. Rend., Vol. 100, pp. 935-937.

Clements, R. R. and Maull, D. J., (1975), "The Representation of Sheets of Vorticity by Discrete Vortices," Prog. Aero. Sci., Vol. 16, pp. 129-146.

Heideman, J. C., Olsen, O. A., and Johansson, P. I., (1979), "Local Wave Force Coefficients," Civil Engineering in the Oceans IV, ASCE, pp. 684-699.

Hoerner, S. F., (1965), Fluid-Dynamic Drag. 2nd ed. Book published by the Author, New Jersey.

Keulegan, G. H. and Carpenter, L. H., (1958), "Forces on Cylinders and Plates in an Oscillating Fluid," Journal of the National Bureau of Standards, Vol. 60, No. 5, pp. 423-440.

Longuet-Higgins, M. S. and Stewart, R. W., (1961), "The Changes in Amplitude of Short Gravity Waves on Steady Non-Uniform Currents," Journal of Fluid Mechanics, Vol. 10, pp. 529-549.

Maull, D. J. and Milliner, M. G., (1978), "Sinusoidal Flow Past a Circular Cylinder," Coastal Engineering, Vol. 2, pp. 149-168.

Mercier, J. A., (1973), "Large Amplitude Oscillations of a Circular Cylinder in a Low-Speed Stream," Ph. D. Dissertation submitted to the Stevens Institute of Technology.

Morison, J. R., O'Brien. M. P., Johnson, J. W., and Schaaf, S. A., (1950), The Forces Exerted by Surface Waves on Piles," Petroleum Trans., AIME, Vol. 189, pp. 149-157.

Norton, D. J., Heideman, J. C., and Mallard, W. W., (1981), "Wind Tunnel Tests of Inclined Circular Cylinders," OTC Paper No. 4122, Houston, TX.

Raines, T. S., (1981), "Harmonic Flow About Smooth and Rough Cylinders," Thesis submitted to the Naval Postgraduate School, Monterey, CA.

Sarpkaya, T., (1963), "Lift, Drag, and Added Mass Coefficients for a Circular Cylinder in a Time-Dependent Flow," Journal of Applied Mechanics, Vol. 30, No. 1, Trans. ASME, Vol. 85, Series E., pp. 13-15.

Sarpkaya, T., (1976a), "Vortex Shedding and Resistance in Harmonic Flow About Smooth and Rough Circular Cylinders at High Reynolds Numbers," Report No. NPS-59SL76021, Naval Postgraduate School, Monterey, CA.

Sarpkaya, T., (1976b), "In-line and Transverse Forces on Smooth and Sand-Roughened Cylinders in Oscillatory Flow at High Reynolds Numbers," Report No. NPS-69SL76062, Naval Postgraduate School, Monterey, CA.

Sarpkaya, T., (1977), "Unidirectional Periodic Flow About Bluff Bodies," Report No. NPS-69SL77051, Naval Postgraduate School, Monterey, CA.

Sarpkaya, T., (1979), "Vortex-Induced Oscillations - A Selective Review," Journal of Applied Mechanics, Trans. ASME., Vol. 46, pp. 241-258.

Sarpkaya, T., (1981), "A Critical Assessment of Morison's Equation," Proceedings of the International Conference on Hydrodynamics in Oceans, held in Trondheim in August 1981.

Sarpkaya, T. and Isaacson, M., (1981), Mechanics of Wave Forces on Offshore Structures, Van Nostrand Reinhold Company, New York.

Sarpkaya, T. and Shoaff, R. L., (1979), "Inviscid Model of Two-Dimensional Vortex Shedding by a Circular Cylinder," AIAA Journal, Vol. 17, pp. 1193-1200.

Sarpkaya, T., (1982), "Harmonic Flow About Smooth and Rough Inclined Circular Cylinders," (to be presented at the OTC meeting in Houston, TX.).

Standing, R. G., (1980), "Wave-by-Wave Analysis of Data from Christchurch Bay Wave Force Experiment," National Maritime Institute Report No. R-86.

Stokes, Sir George Gabriel, (1851), "On the Effect of Internal Friction on Fluids on the Motion of Pendulums," Cambridge Phil. Trans. IX.

Verley, R. L. P., (1981), "A Simple Model of Vortex-Induced Forces in Waves and Oscillating Currents," (to be published in the Applied Ocean Engineering).

AD-A137 438 MORISON'S EQUATION AND THE WAVE FORCES ON OFFSHORE STRUCTURES(U) SARPKAYA (TURGUT) CARMEL CA T SARPKAYA DEC 81 NCEL-CR-82.008 N68305-80-C-0053 2/3

UNCLASSIFIED F/G 8/3 NL

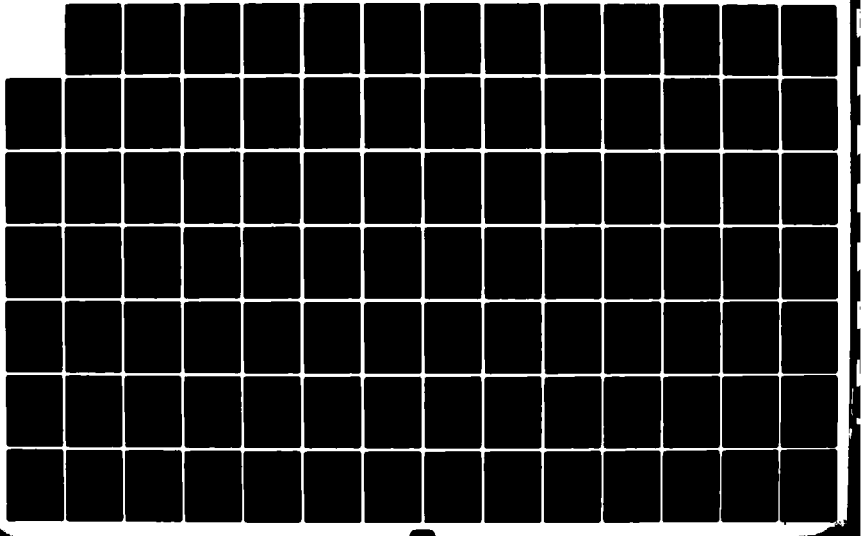

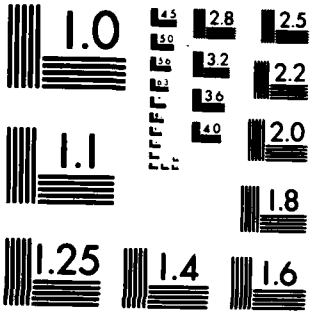

Verley, R. L. P. and Moe, G., (1979), "The Forces on a Cylinder Oscillating in a Current," River and Harbour Laboratory, The Norwegian Institute of Technology, Report No. STF60 A 79061.

Wade, B. G. and Dwyer, M., (1976), "On the Application of Morison's Equation to Fixed Offshore Platforms," OTC Paper No. 2723, Houston, TX.

Wheatley, J. H. W., (1976), "A British Offshore Facility," Trans. Roy. Inst. of Naval Architects, RINA, Vol. 118.

Wilkinson, R. H., (1981), "Spanwise Correlation and Loading, Part II," Aeronautical Quarterly, May 1981, pp. 111-125.

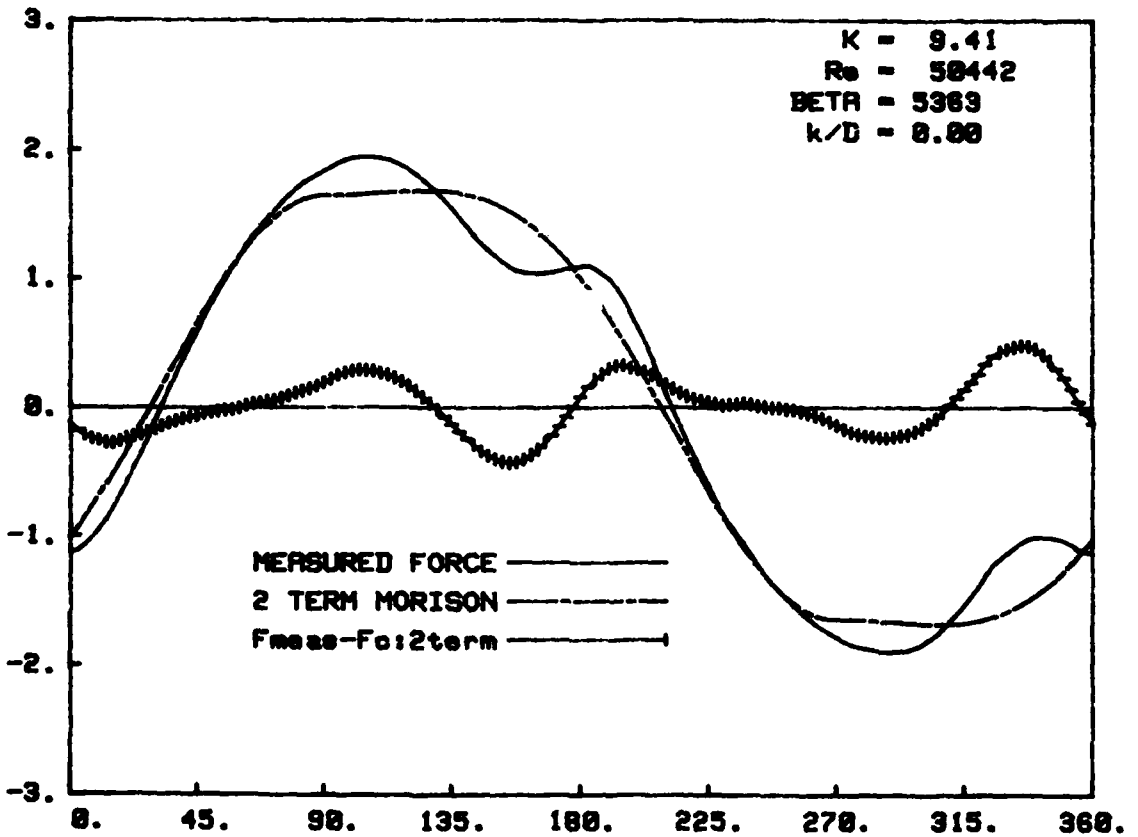

Fig. 1 Comparison of measured and calculated forces, K = 9.41

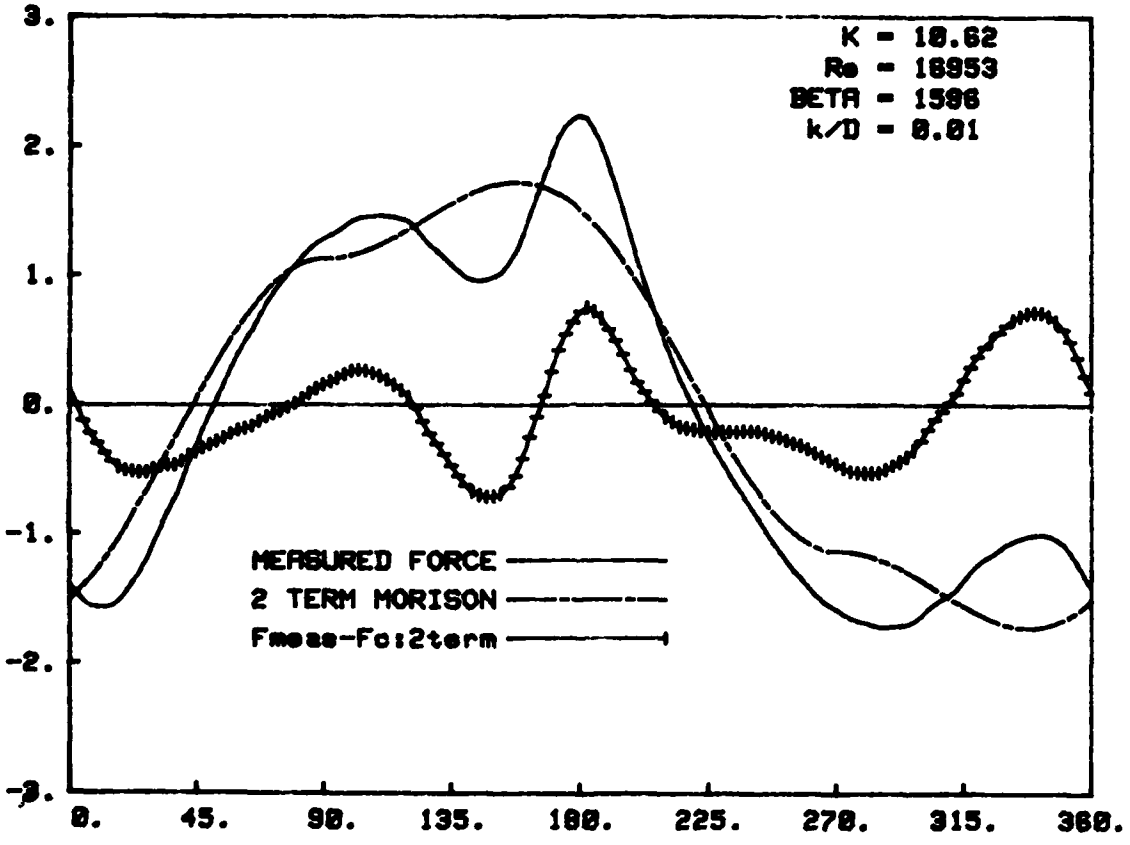

Fig. 2. Comparison of measured and calculated forces, K = 10.62

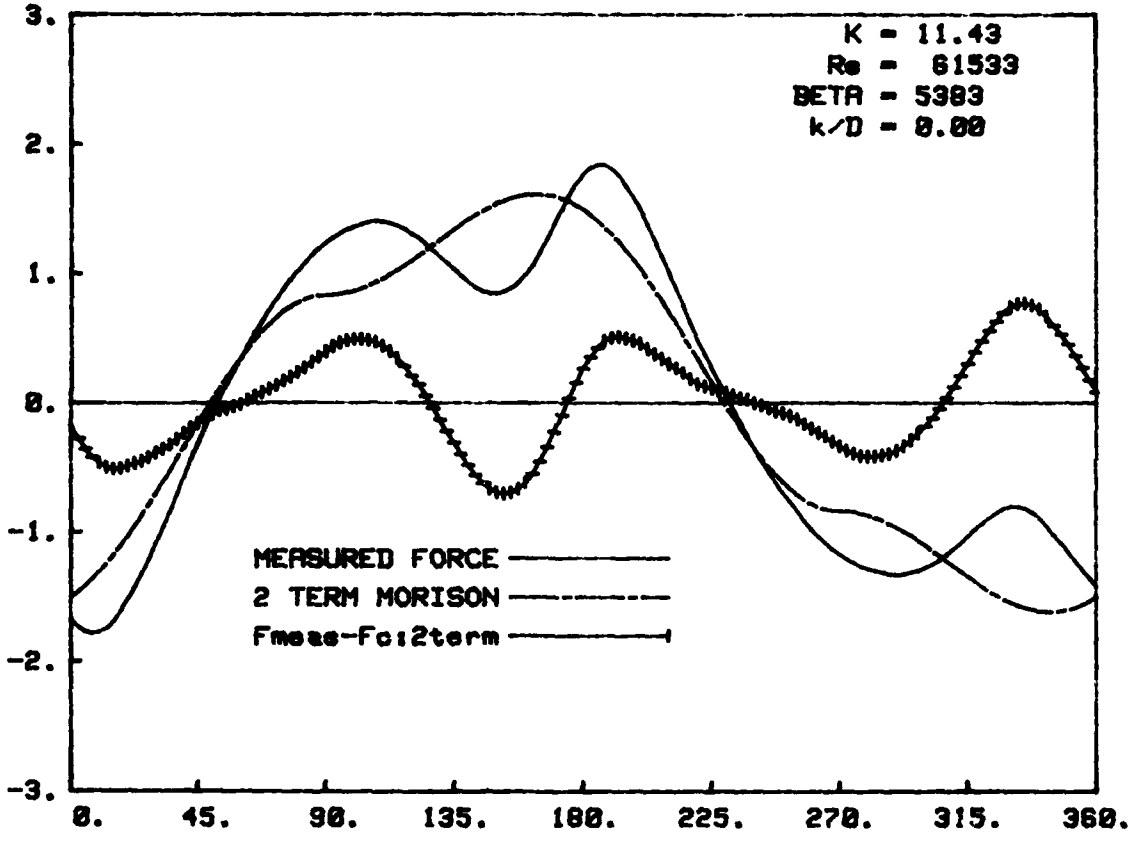

Fig. 3. Comparison of measured and calculated forces, K = 11.43

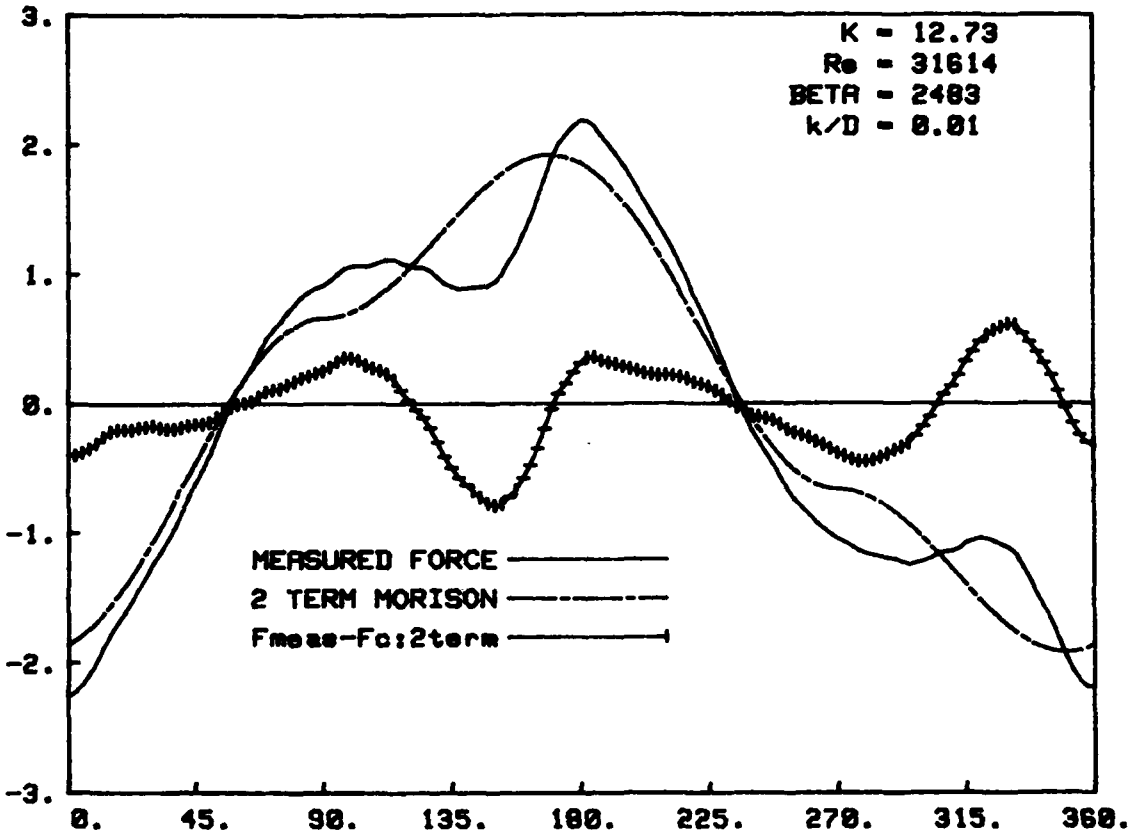

Fig. 4. Comparison of measured and calculated forces, K = 12.73

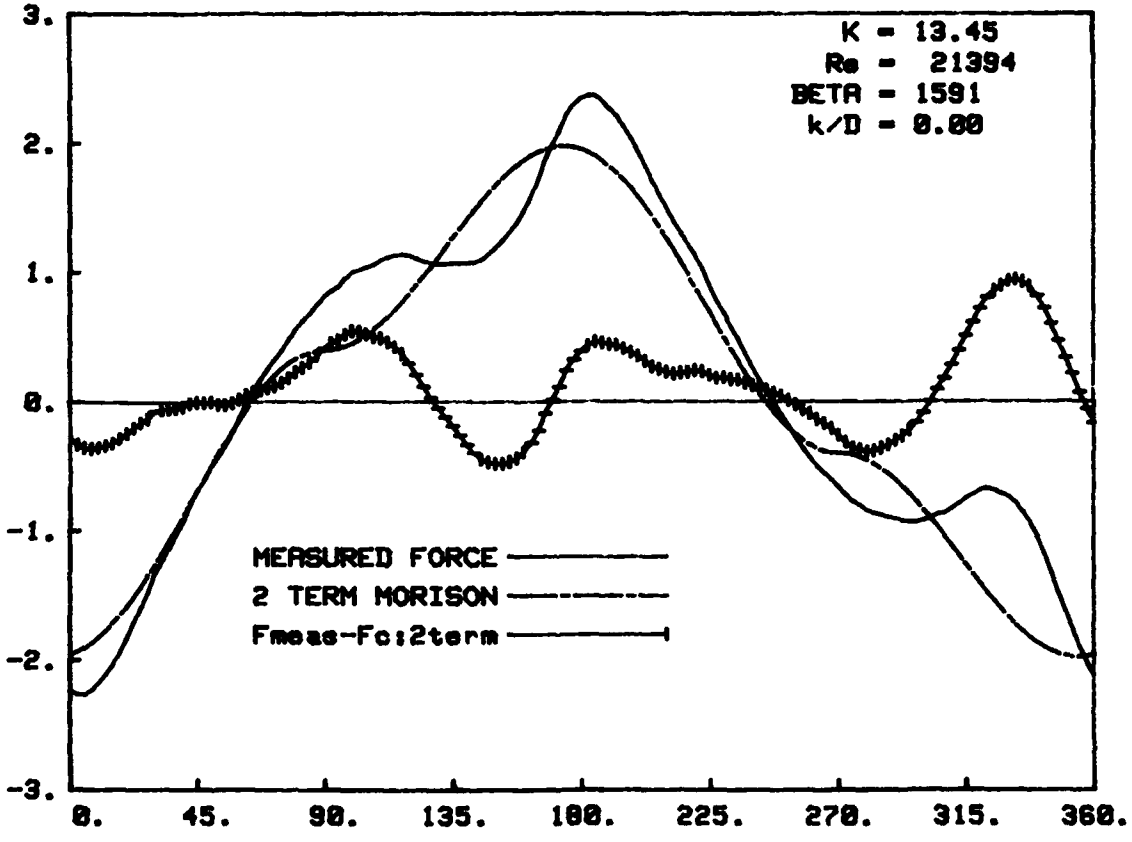

Fig. 5. Comparison of measured and calculated forces, K = 13.45

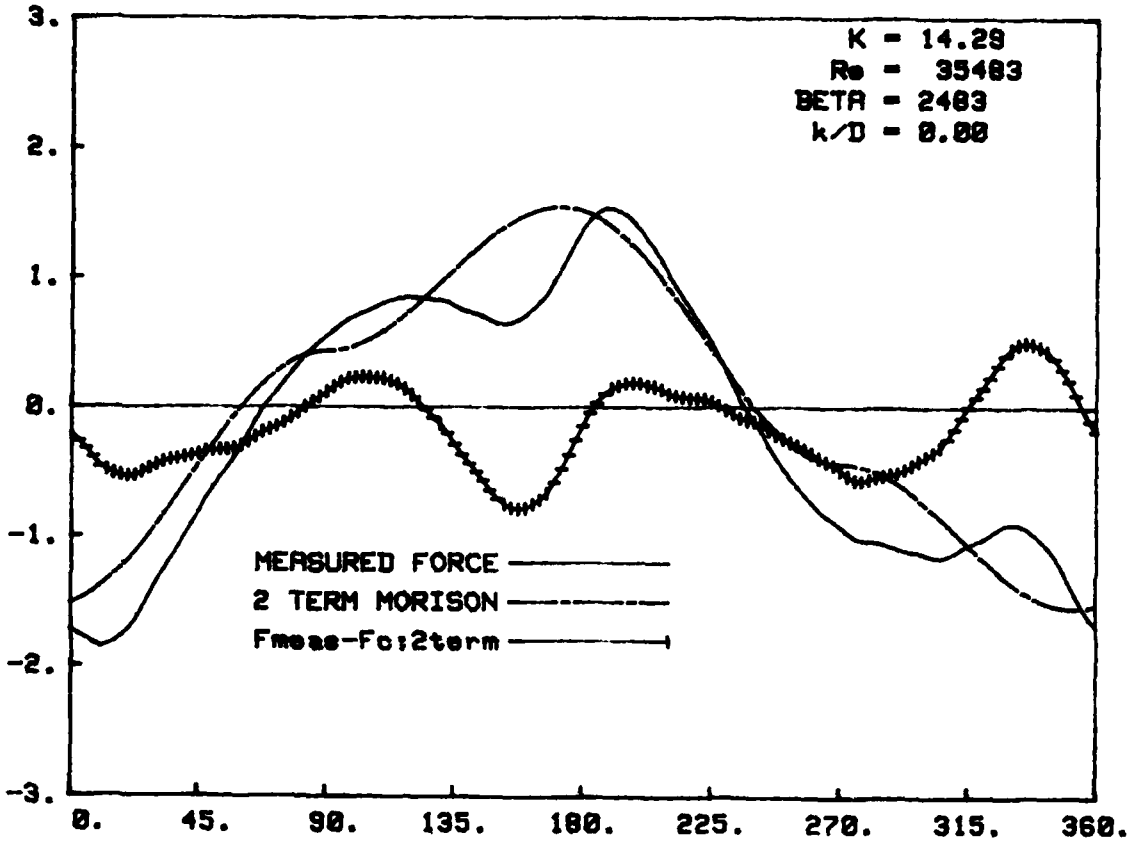

Fig. 6. Comparison of measured and calculated forces, K = 14.29

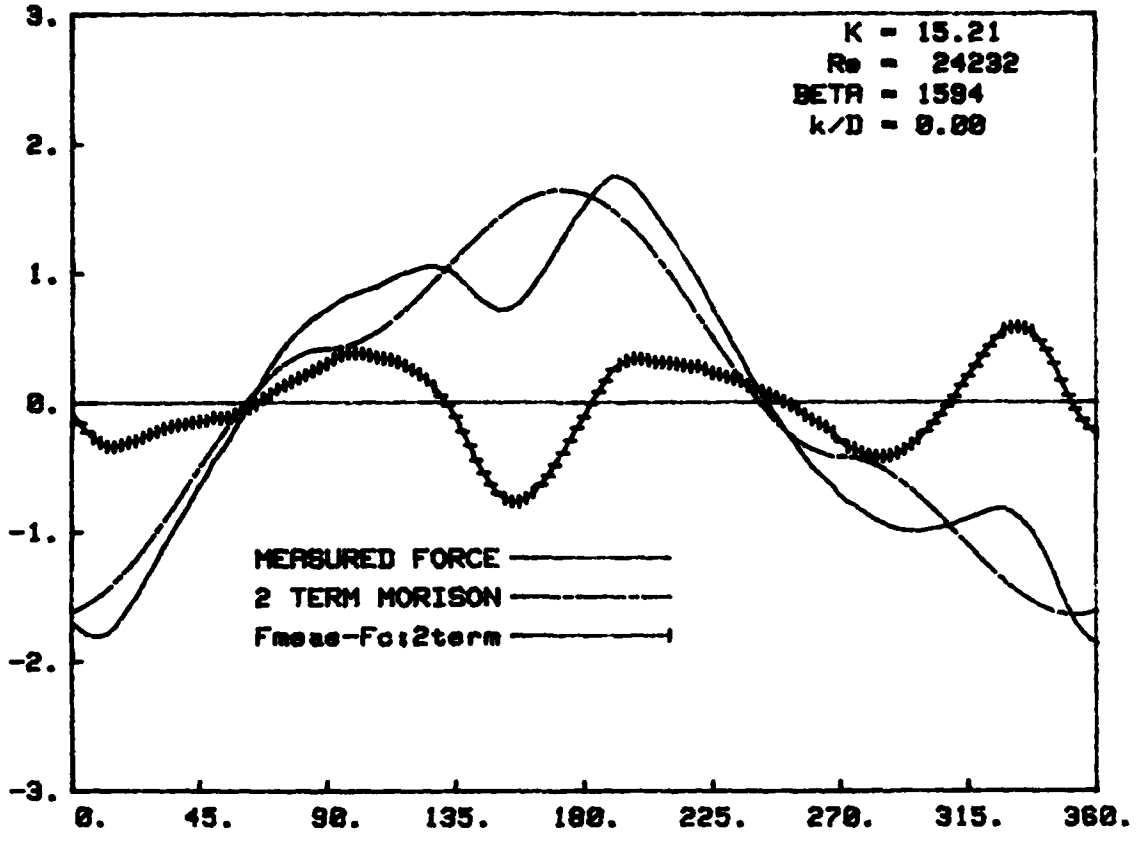

Fig. 7. Comparison of measured and calculated forces, K = 15.21

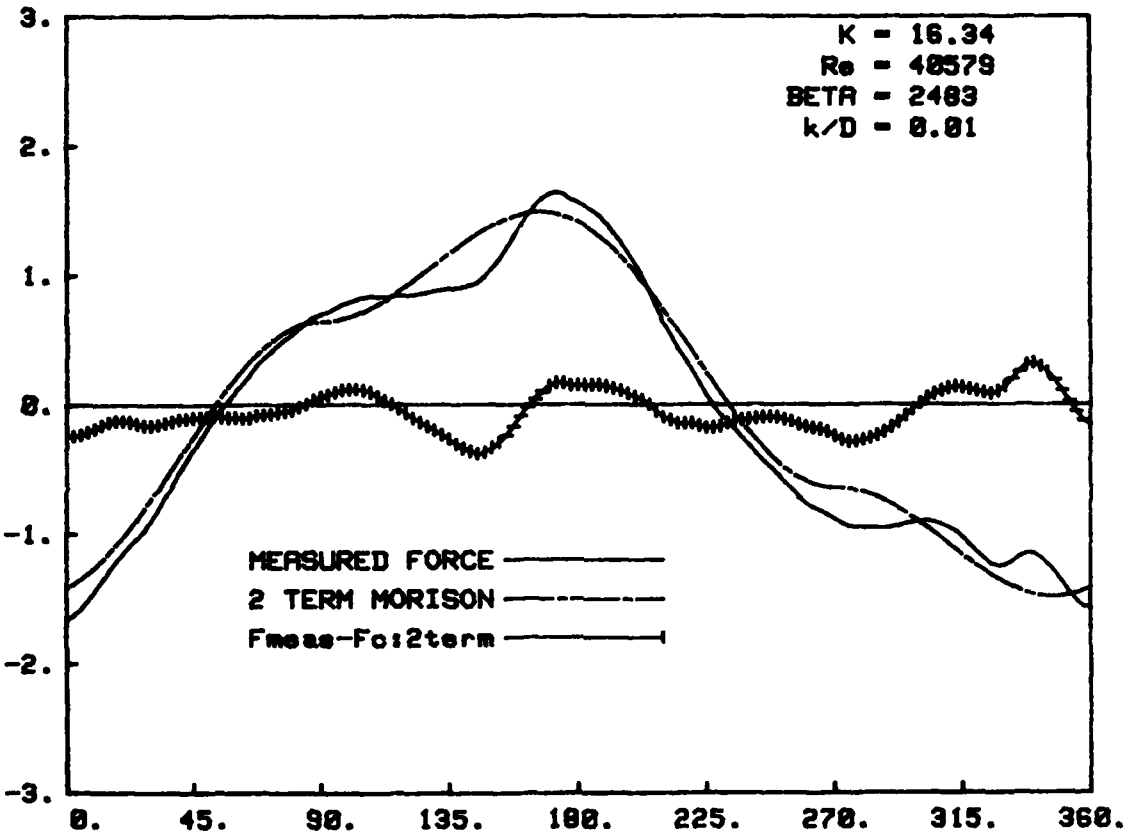

Fig. 8. Comparison of measured and calculated forces, K = 16.34

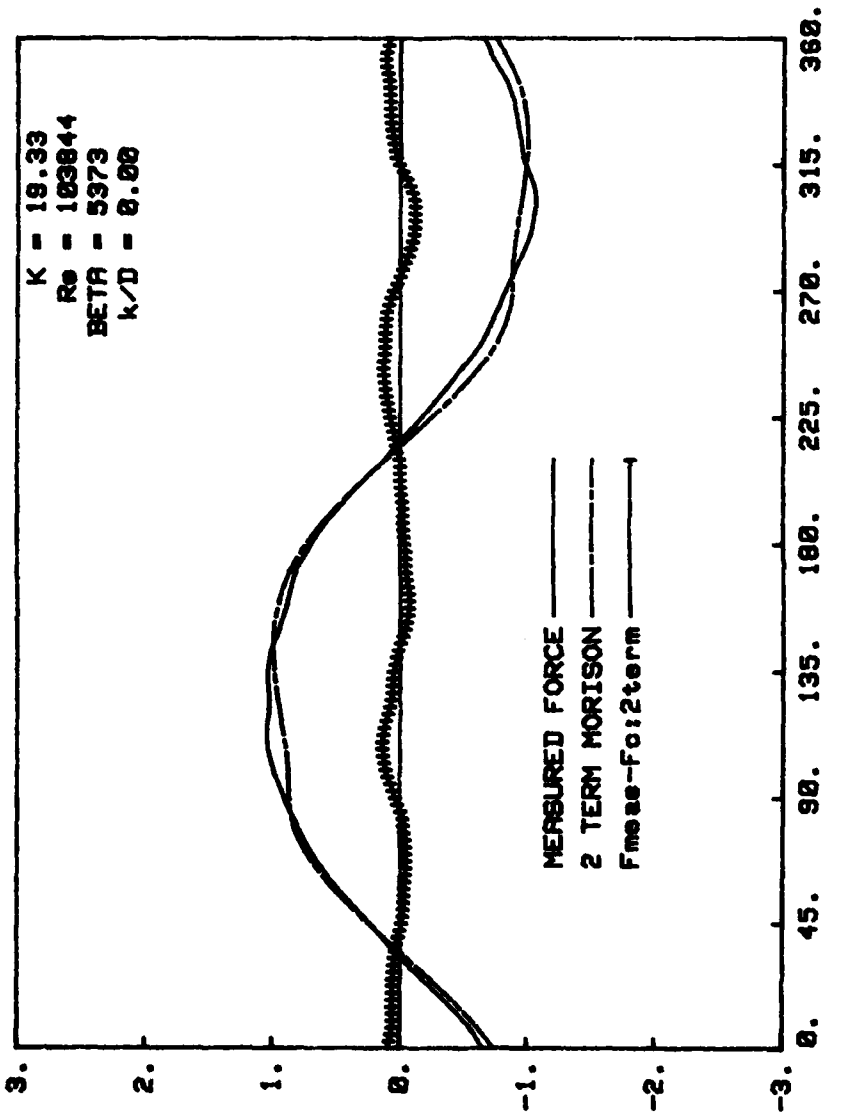

Fig. 9. Comparison of measured and calculated forces, K = 19.33

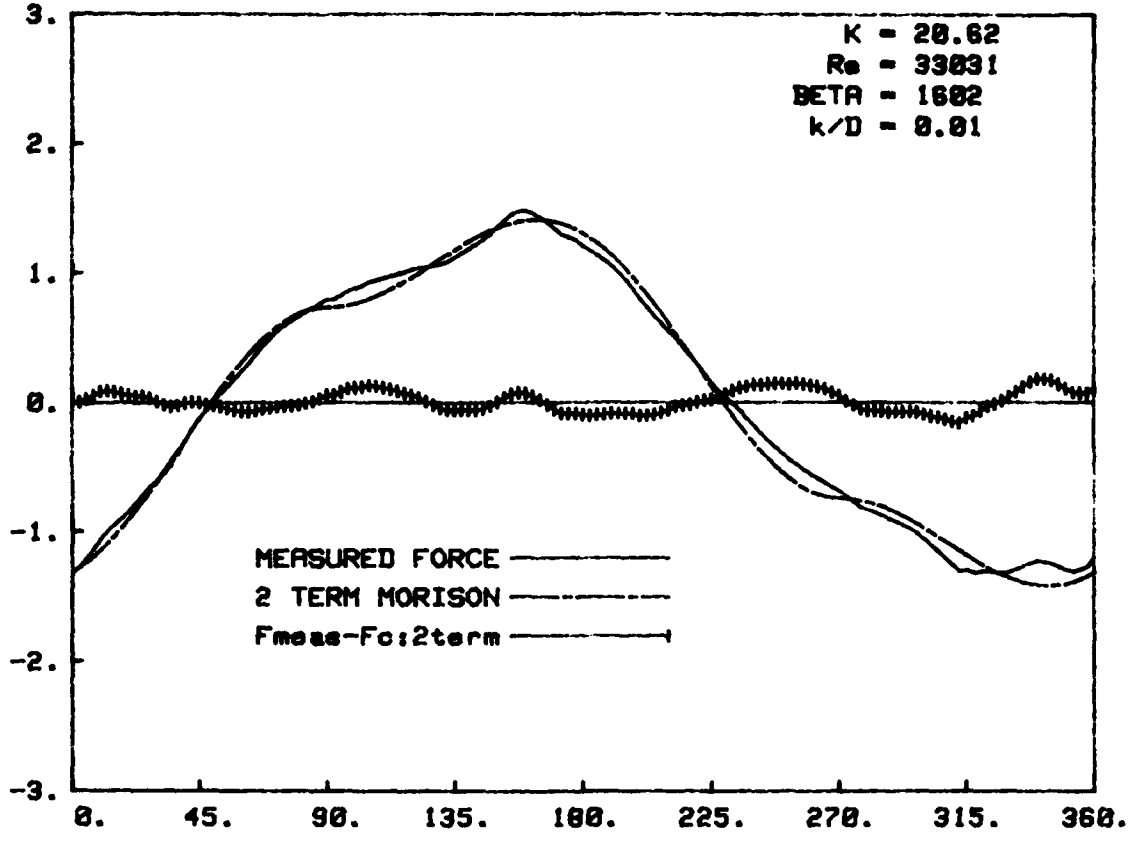

Fig. 10. Comparison of measured and calculated forces, K = 20.62

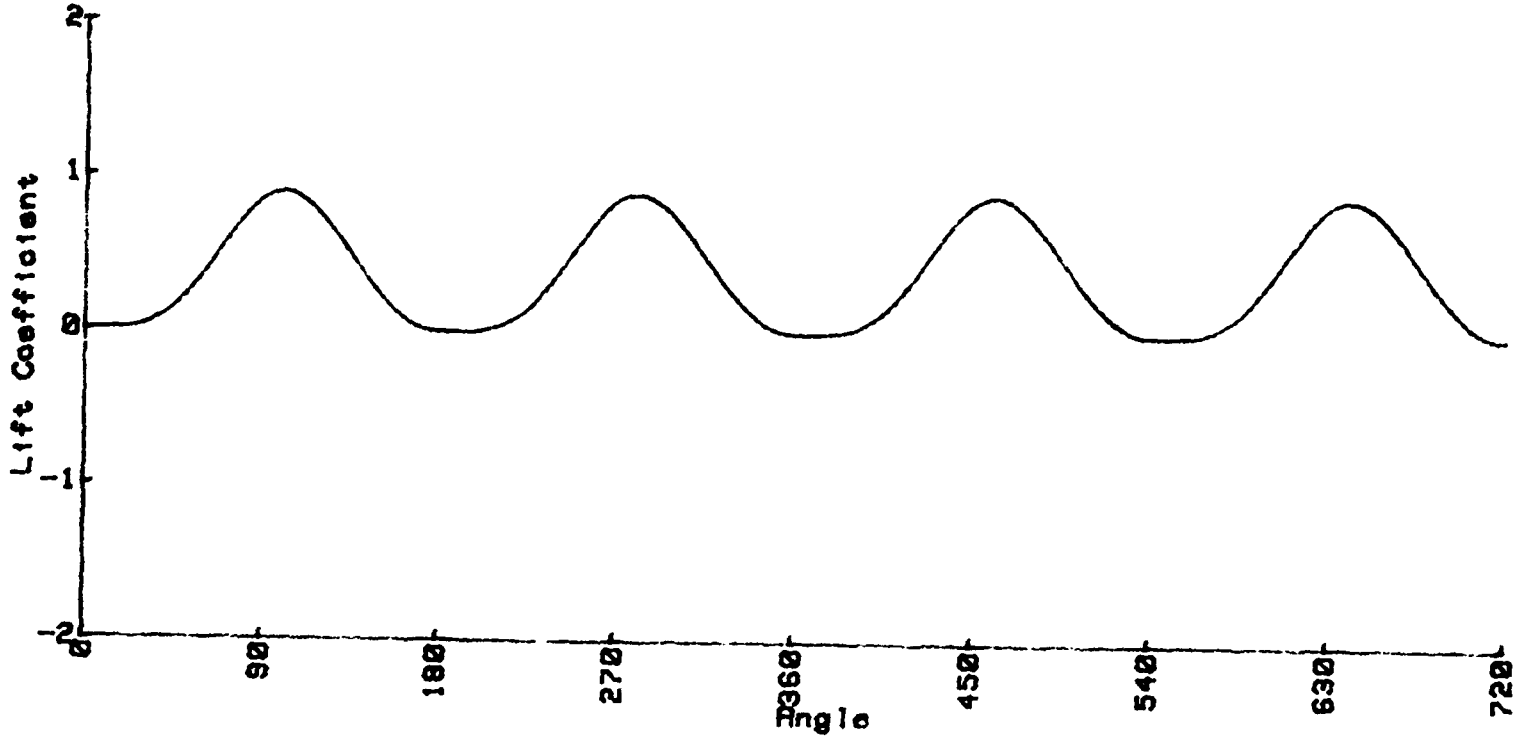

Fig. 11 Similation of the lift coefficient for K =5

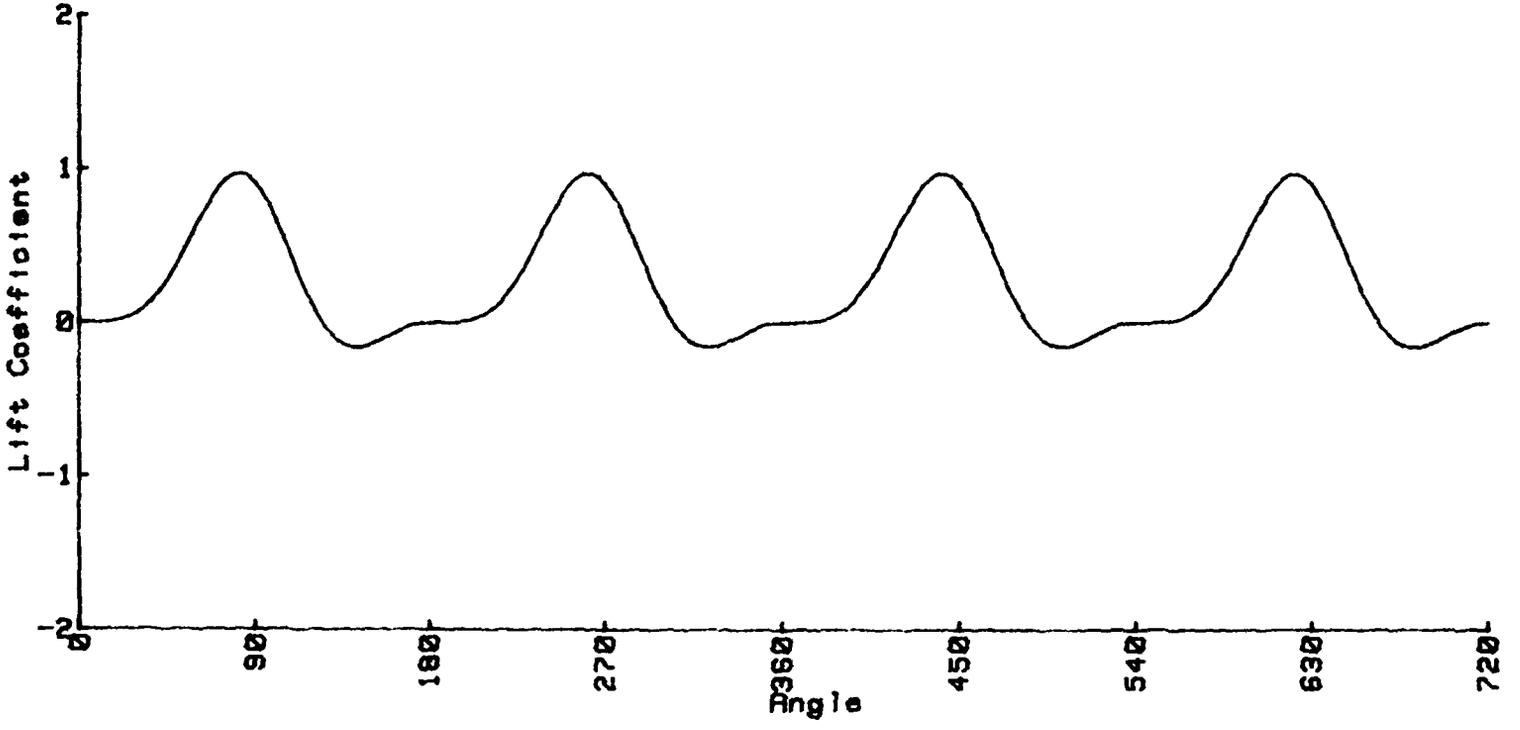

Fig. 12 Simulation of the lift coefficient for K = 10

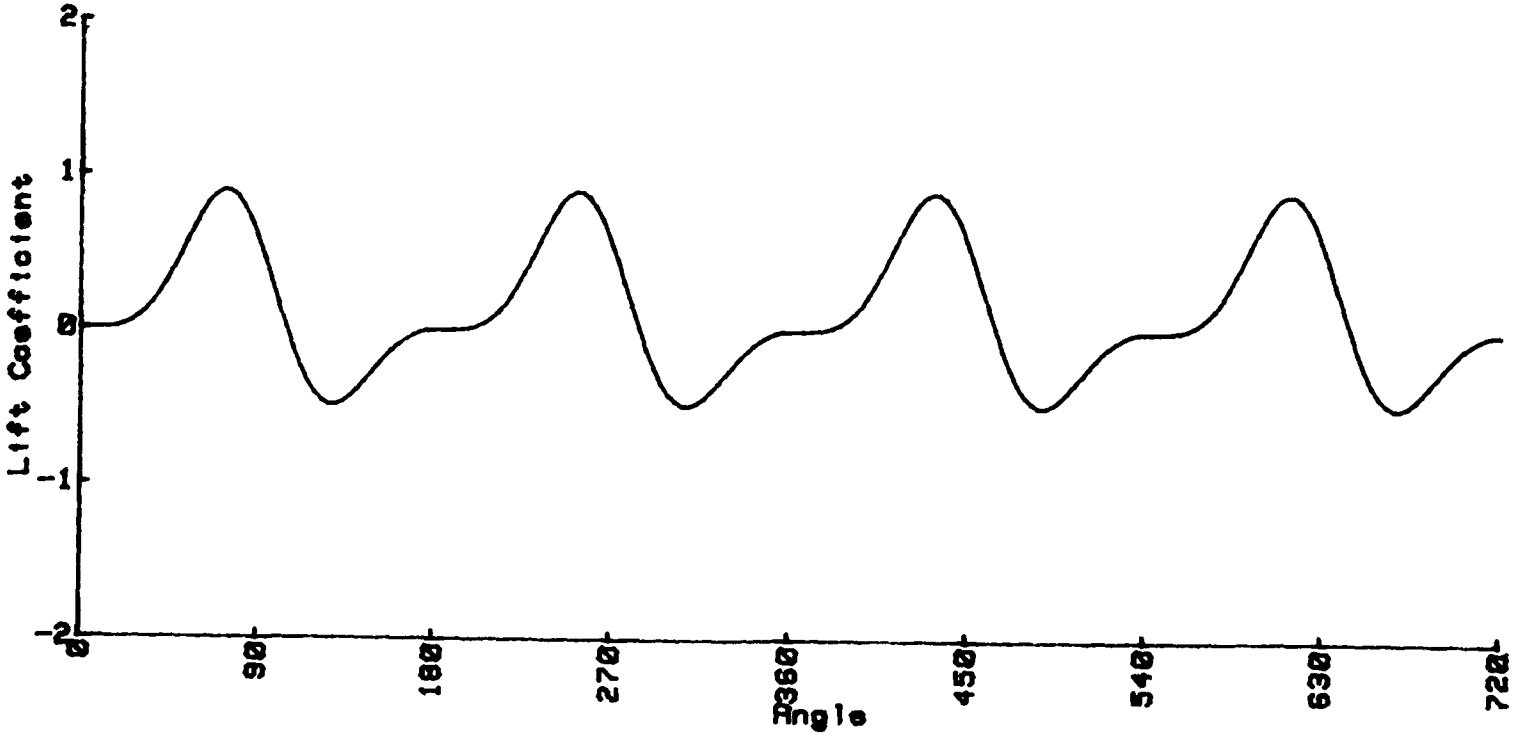

Fig. 13 Simulation of the lift coefficient for K = 12.5

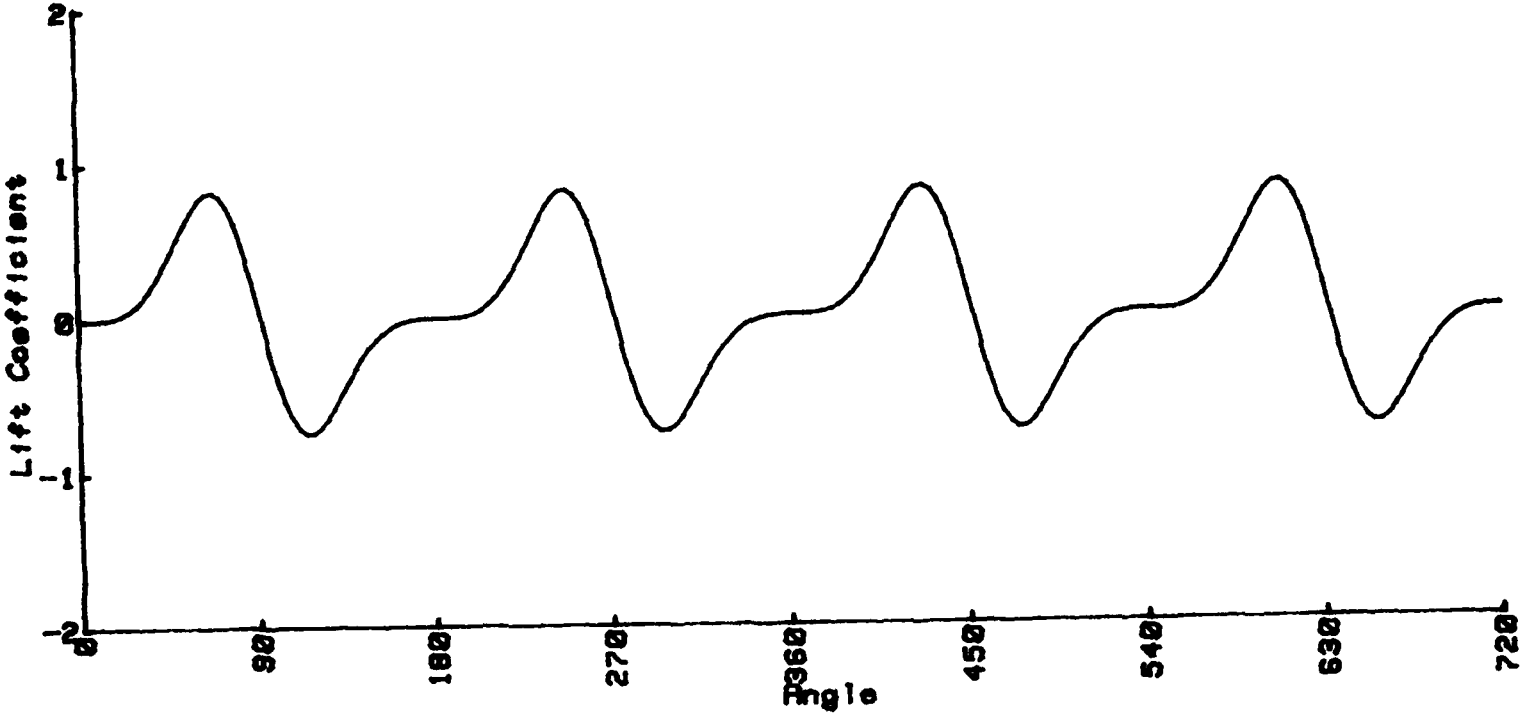

Fig. 14 Simulation of the lift coefficient for K = 15

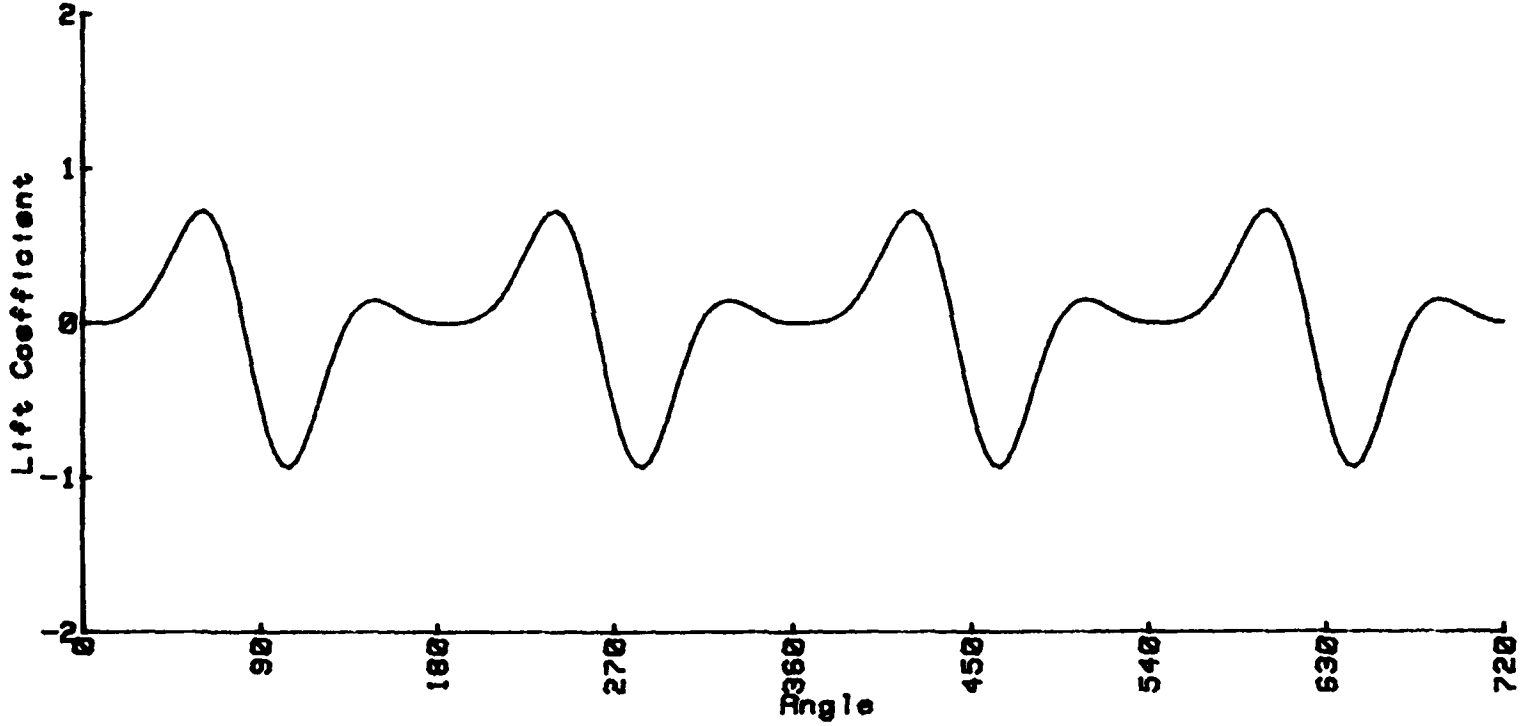

Fig. 15 Simulation of the lift coefficient for K = 18.5

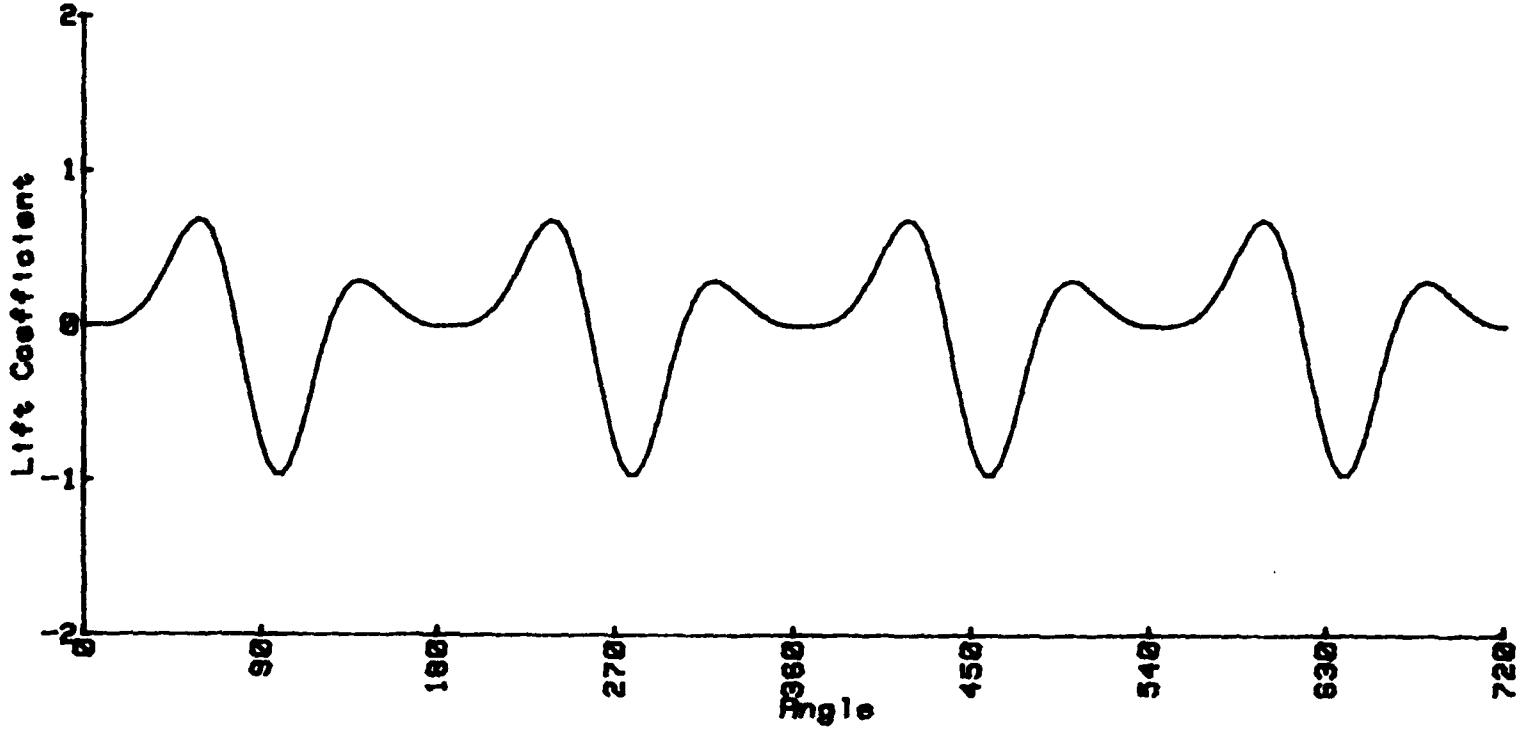

Fig. 16 Simulation of the lift coefficient for K = 20

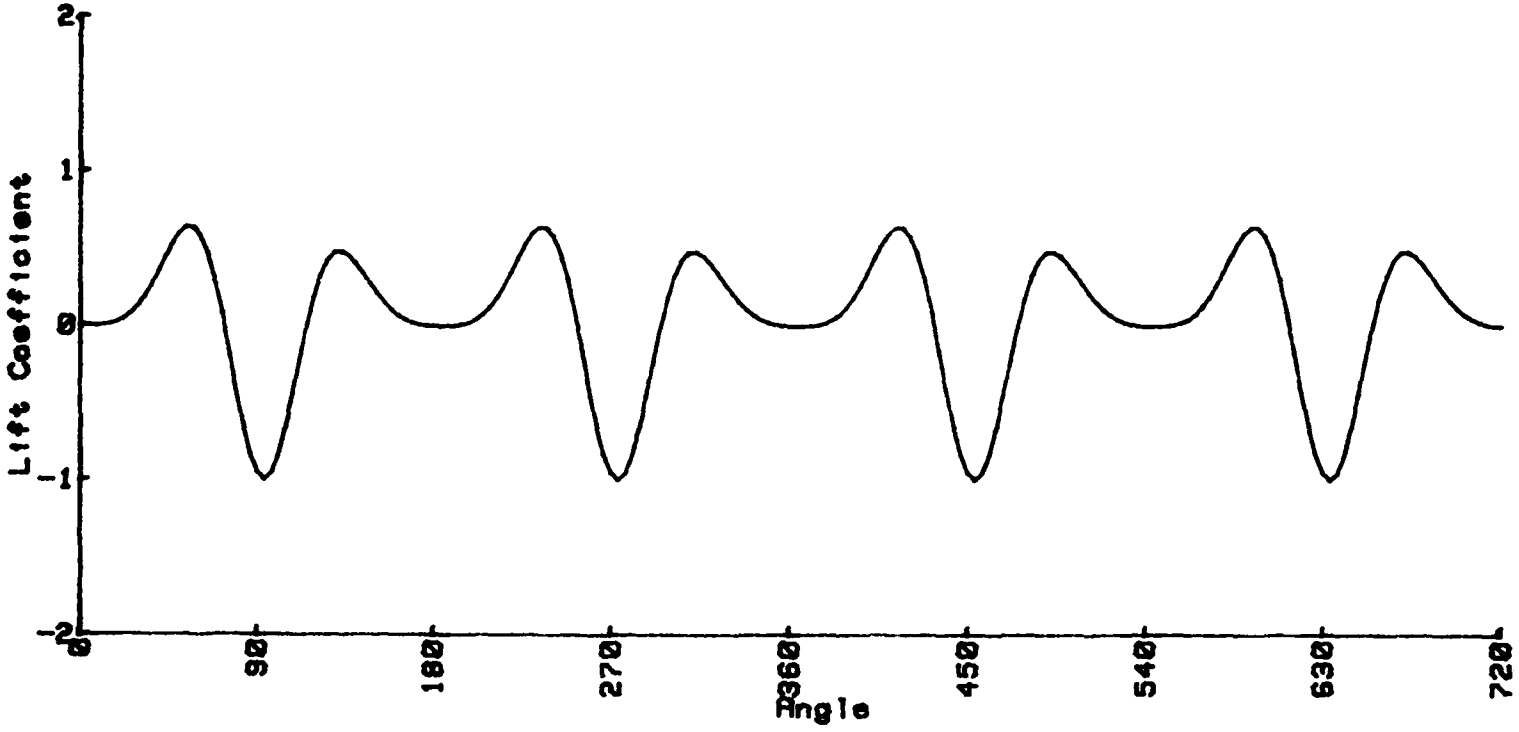

Fig. 17 Simulation of the lift coefficient for K = 22

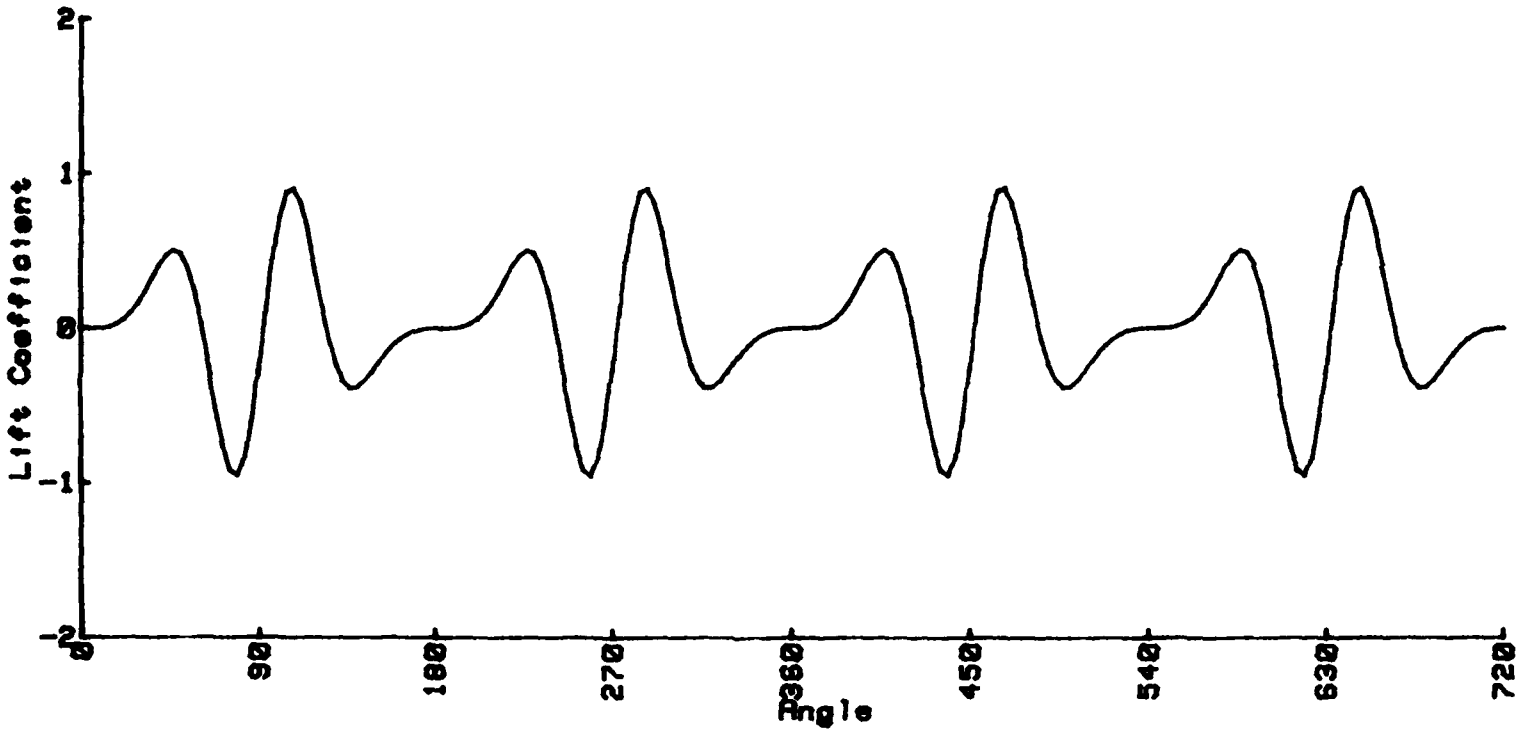

Fig. 18 Simulation of the lift coefficient for K = 30

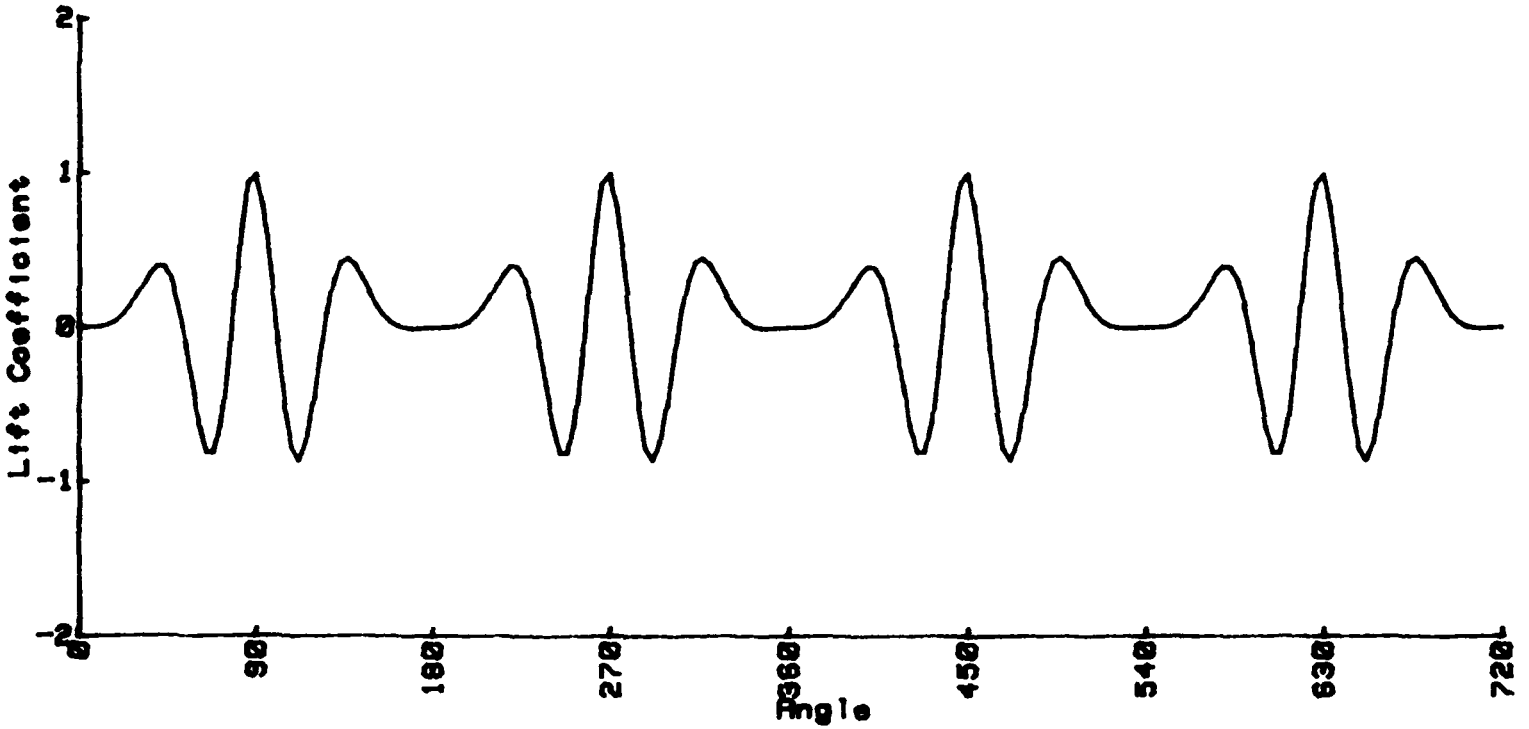

Fig. 19 Simulation of the lift coefficient for K = 40

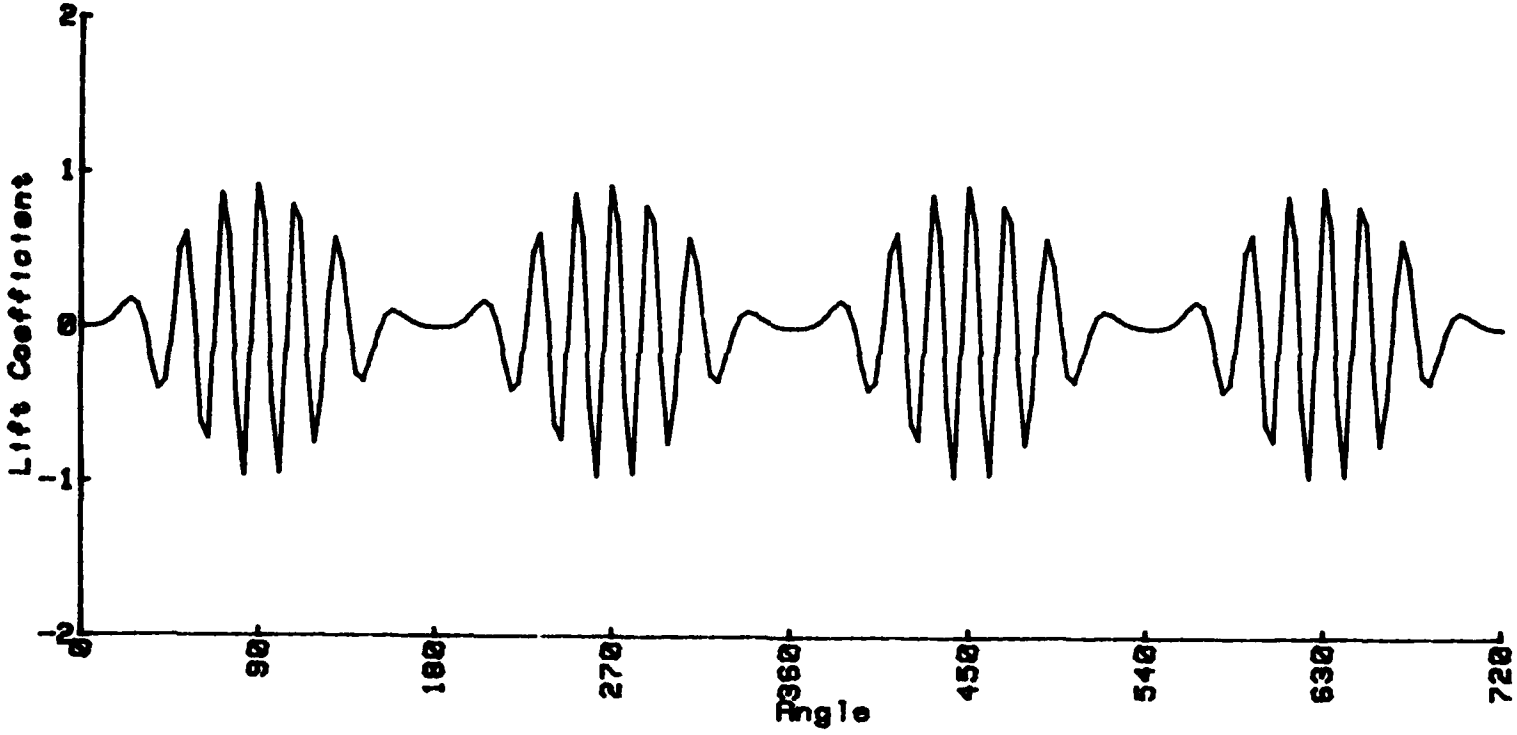

Fig. 20 Simulation of the lift coefficient for K = 100

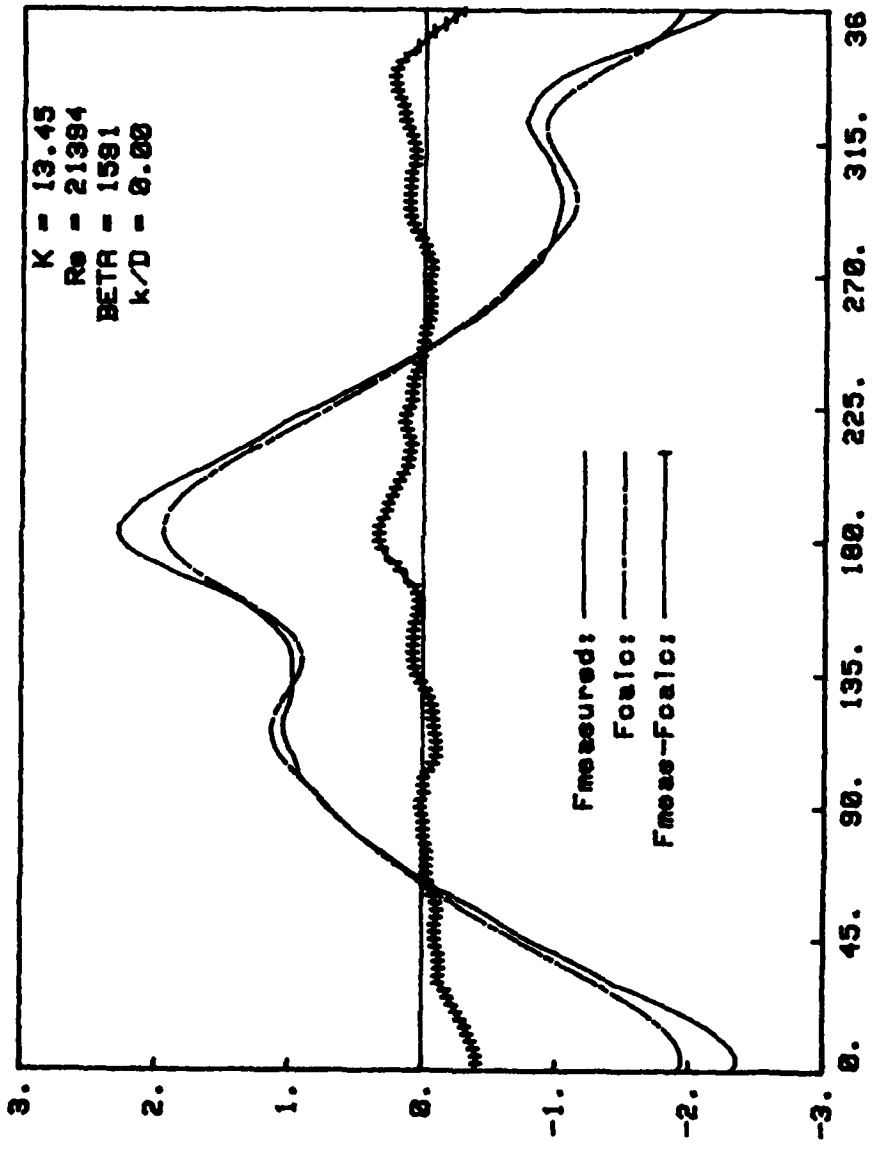

Fig. 21 Comparison of measured and simulated forces (Method No. 5), ($K = 13.45$, $C_L = 0.7$, $N = 1$, $S = 0.27$, $\phi = 45$ deg.)

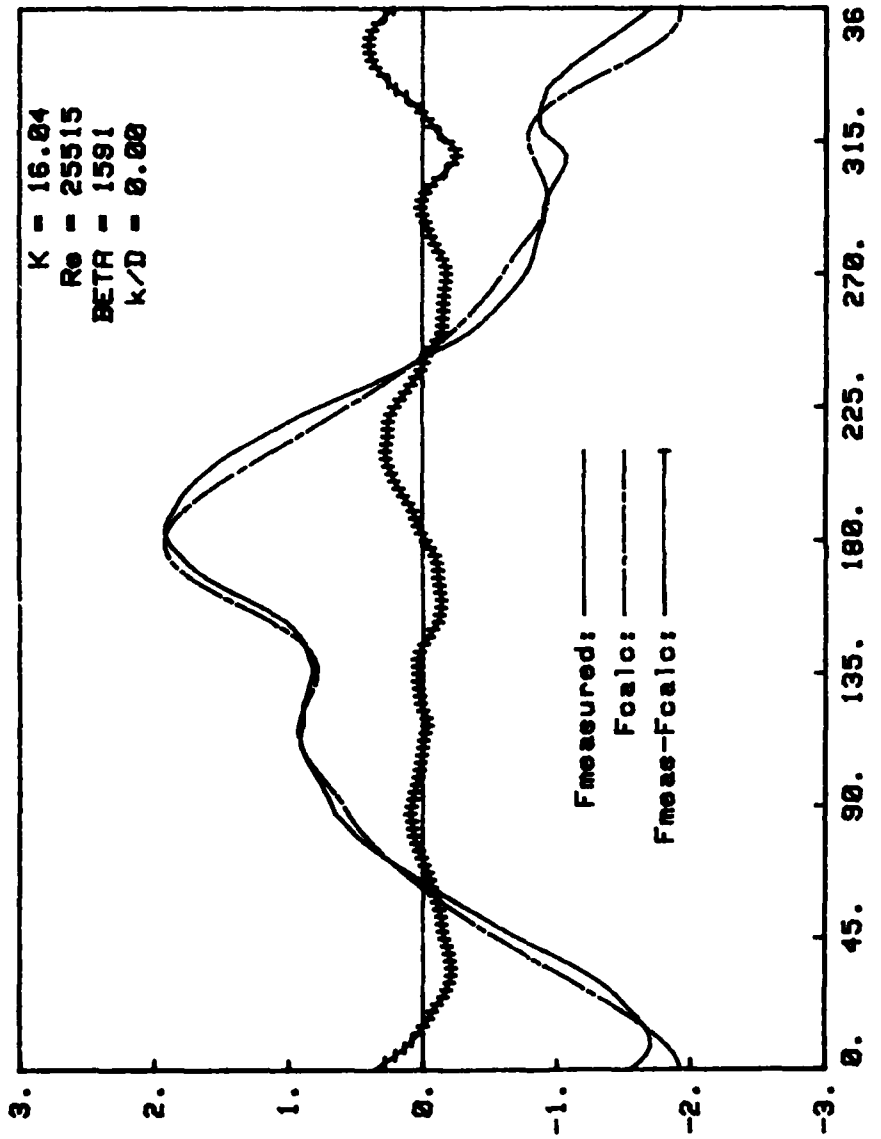

Fig. 22 Comparison of measured and simulated forces (Method No. 5), ($K = 16.04$, $C_L = 0.5$, $N = 1$, $S = 0.27$, $\phi = 50$ deg.)

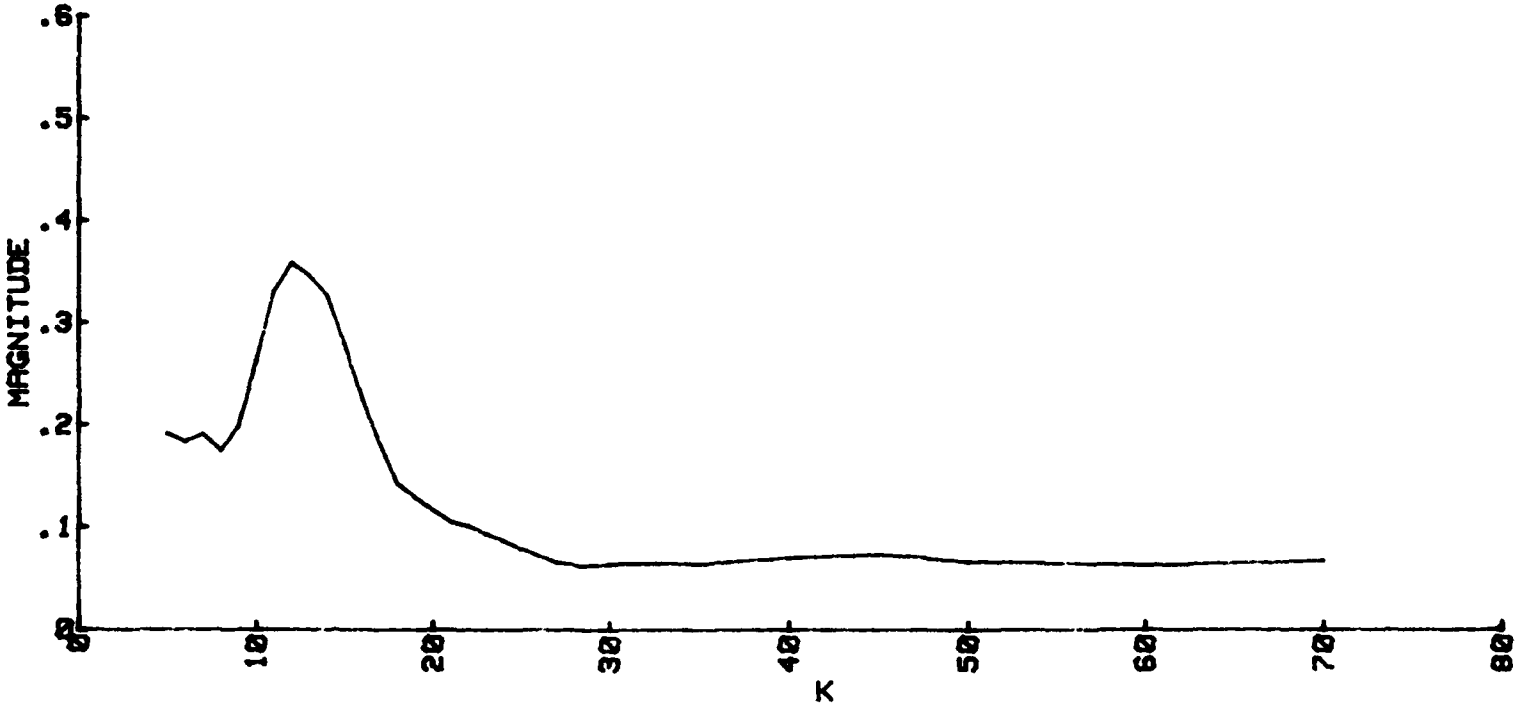

Fig. 23 The coefficient C_3 versus K, (averaged over each K)

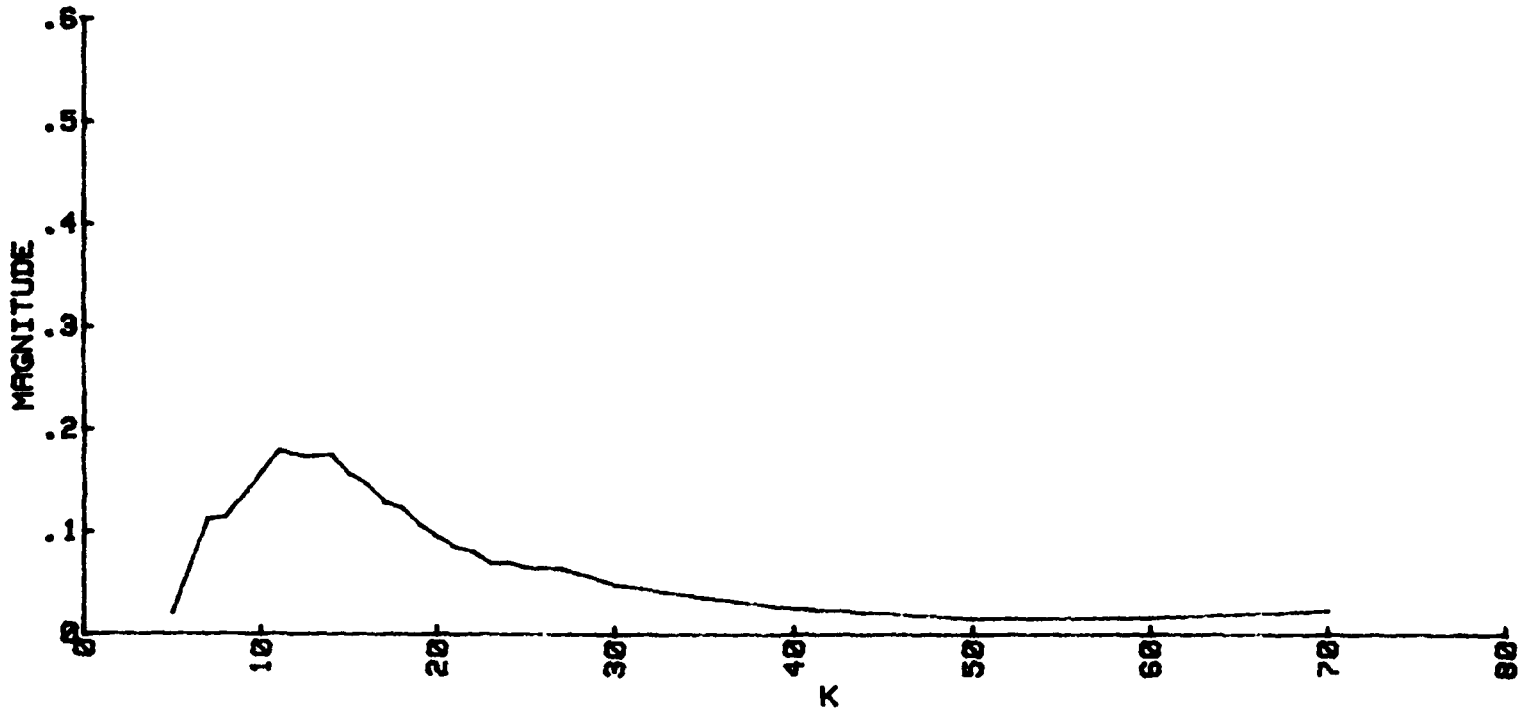

Fig. 24 The coefficient C_5 versus K, (averaged over each K)

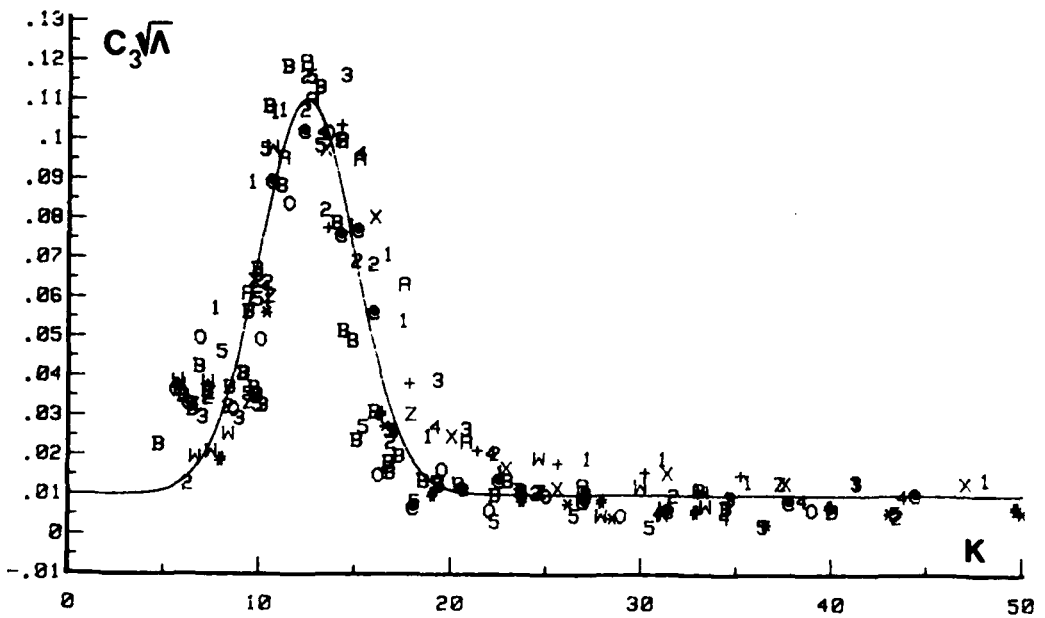

Fig. 25 The variation of $C_3\sqrt{\Lambda}$ with K (experimental data and analytical model)

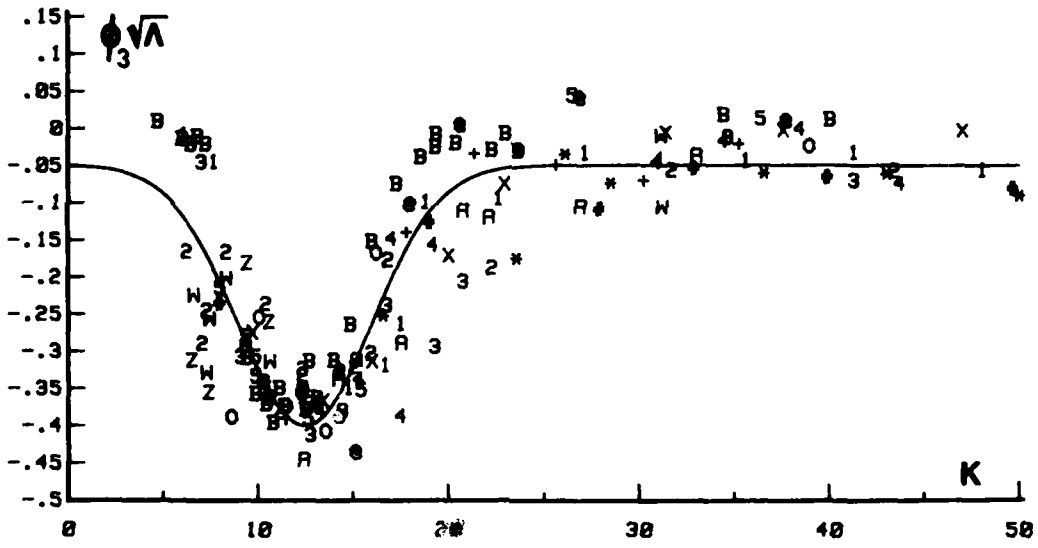

Fig. 26 The variation of $\phi_3\sqrt{\Lambda}$ with K (experimental data and analytical model)

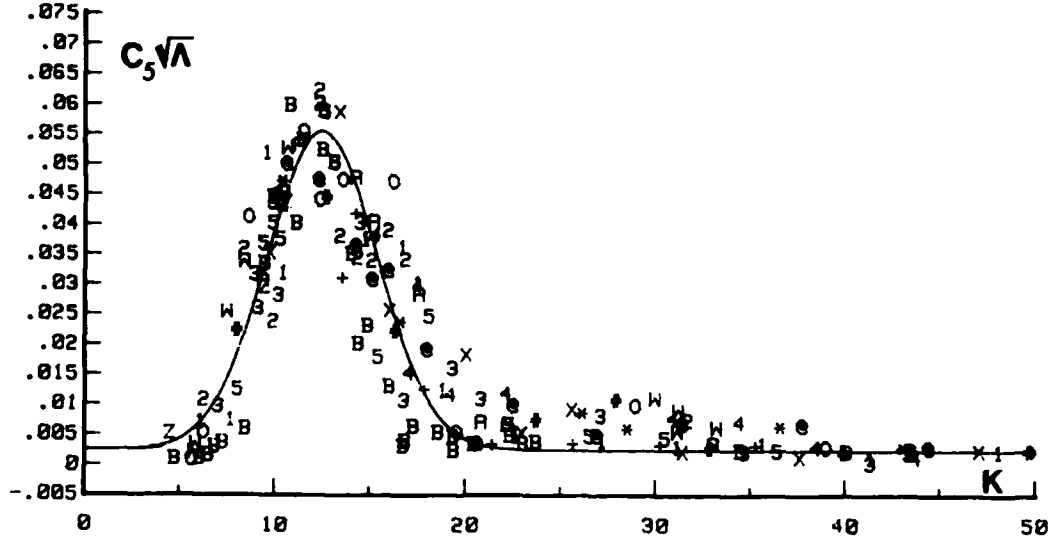

Fig. 27 The variation of $C_5\sqrt{\Lambda}$ with K (experimental data and analytical model)

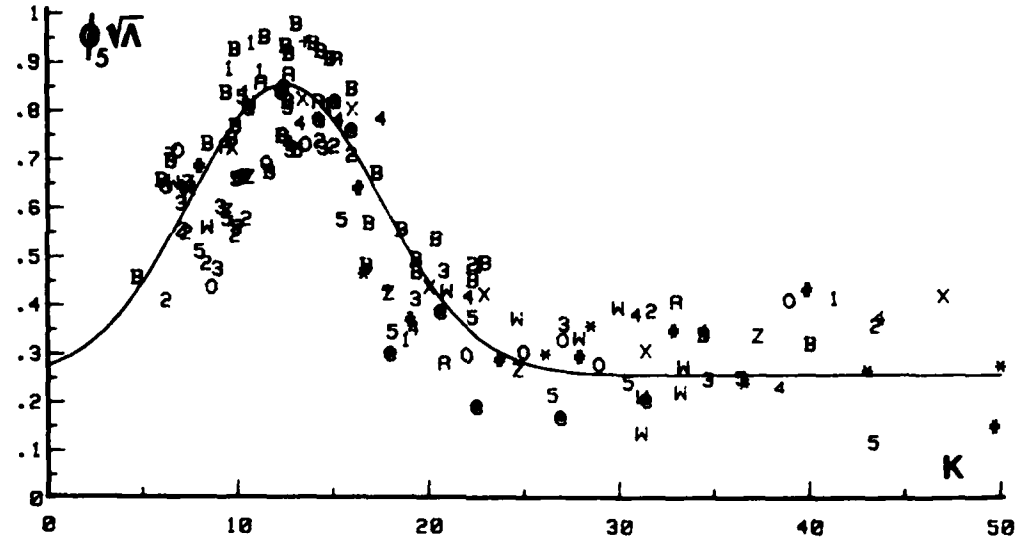

Fig. 28 The variation of $\phi_5\sqrt{\Lambda}$ with K (experimental data and analytical model)

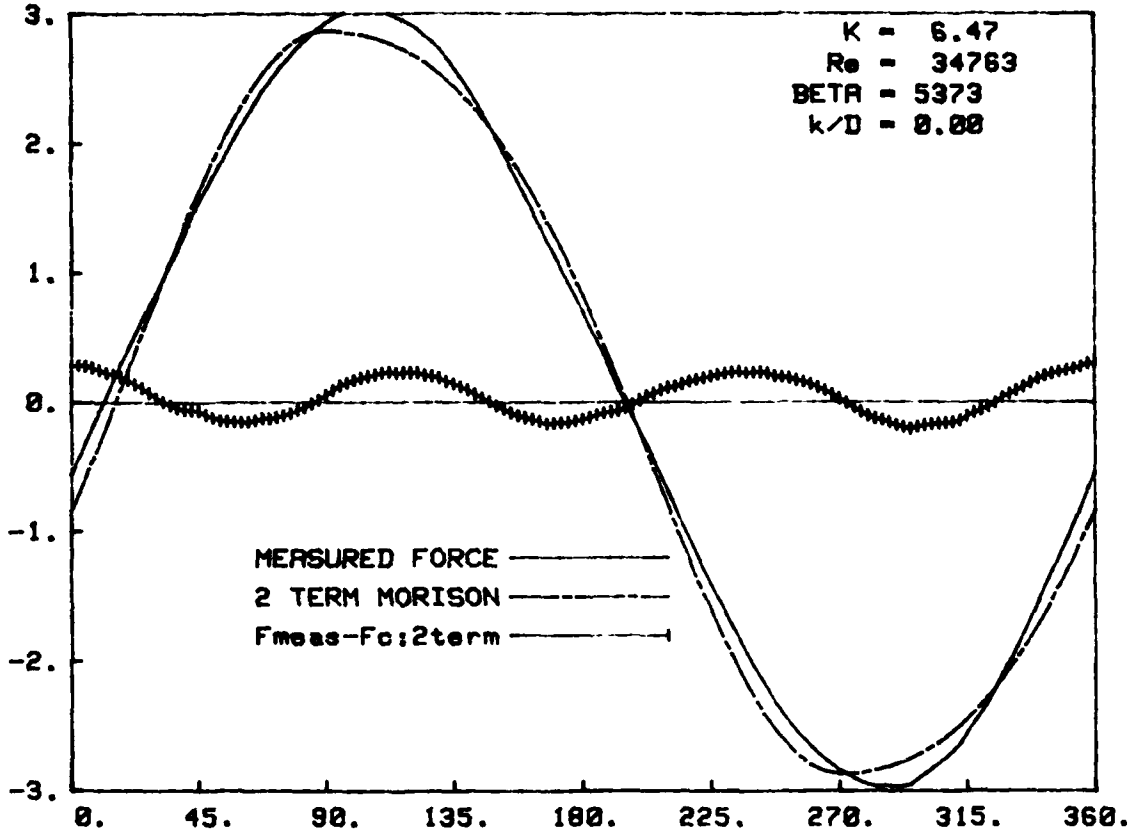

Fig. 29a Comparison of measured and calculated forces (Two-term MOJS Eq.)
K = 6.47

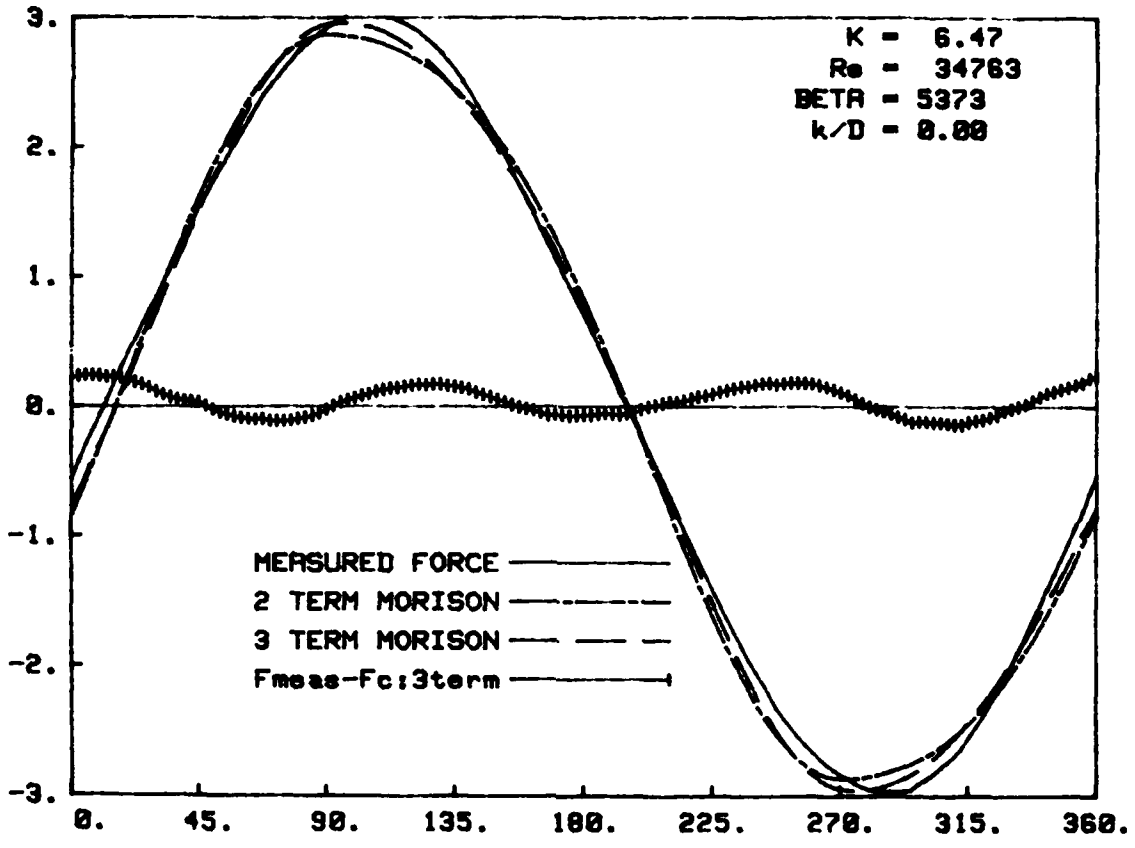

Fig. 29b Comparison of measured and calculated forces (Three-term MOJS Eq.)
K = 6.47

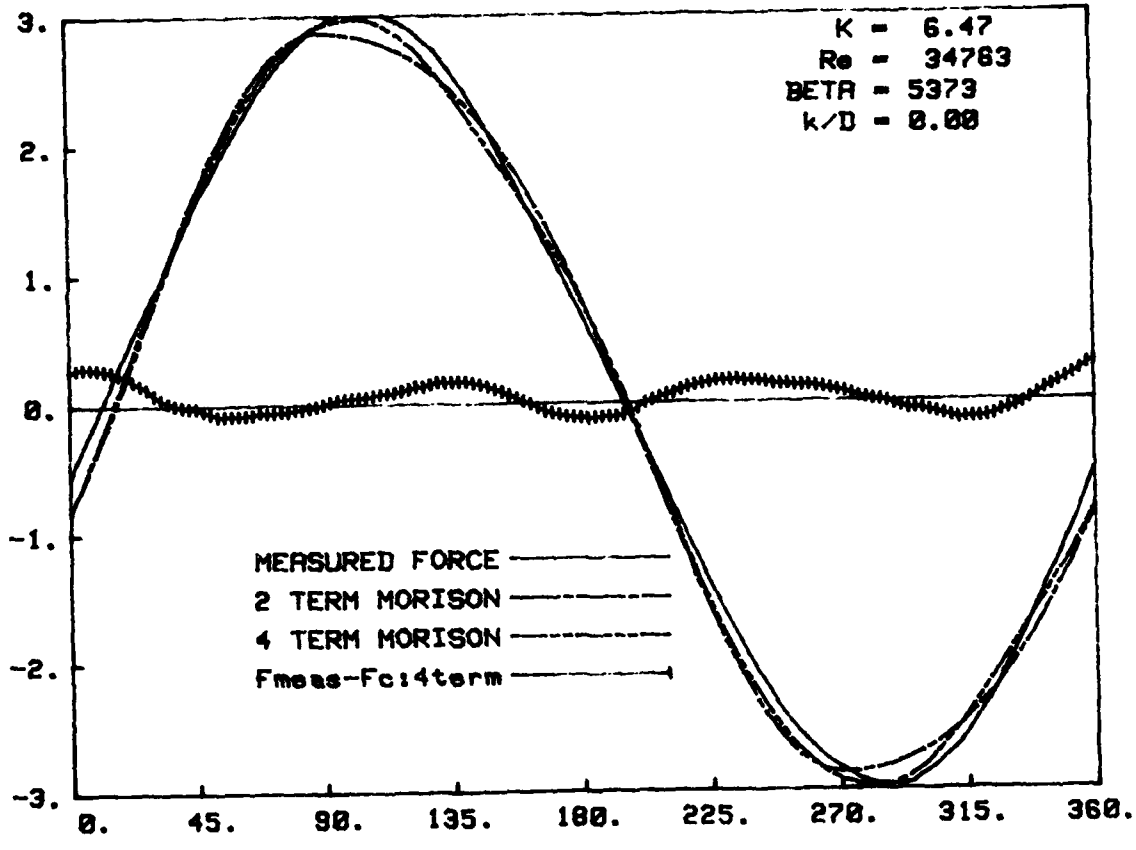

Fig. 29c Comparison of measured and calculated forces (Four-term MOJS Eq.)
K = 6.47

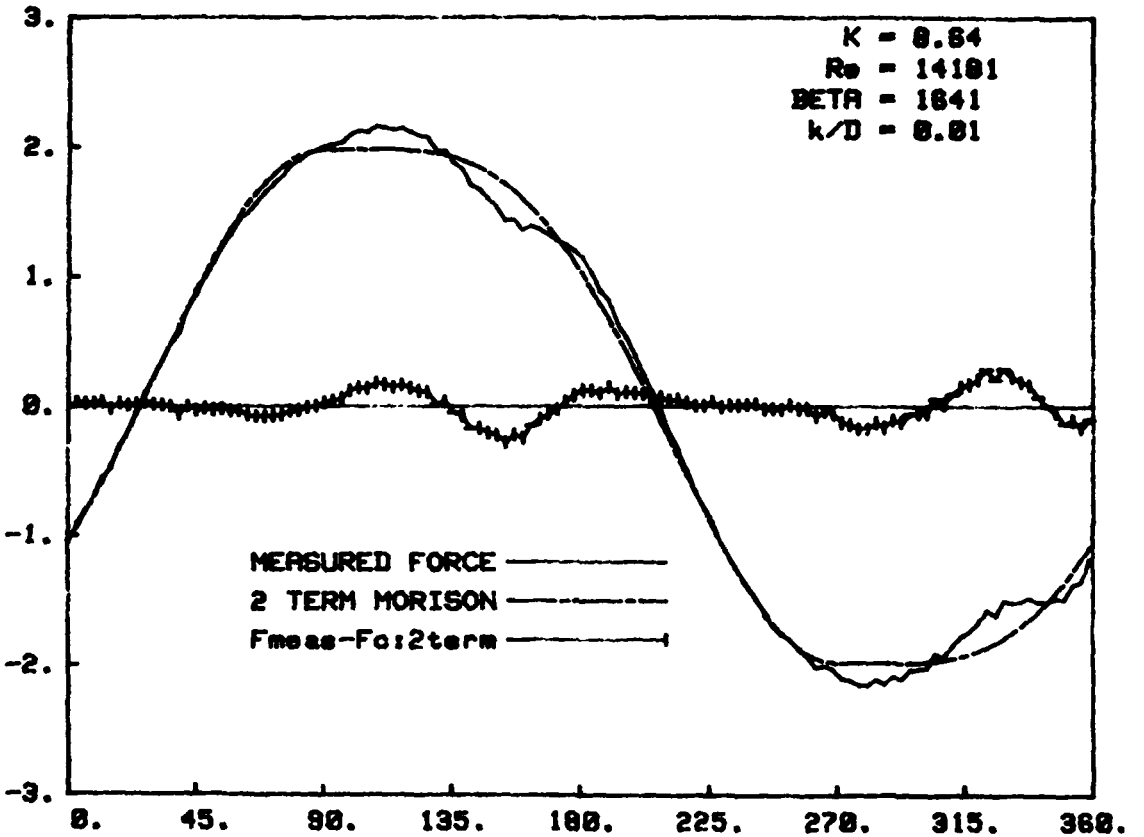

Fig. 30a Comparison of measured and calculated forces (Two-term MOJS Eq.)
K = 8.64

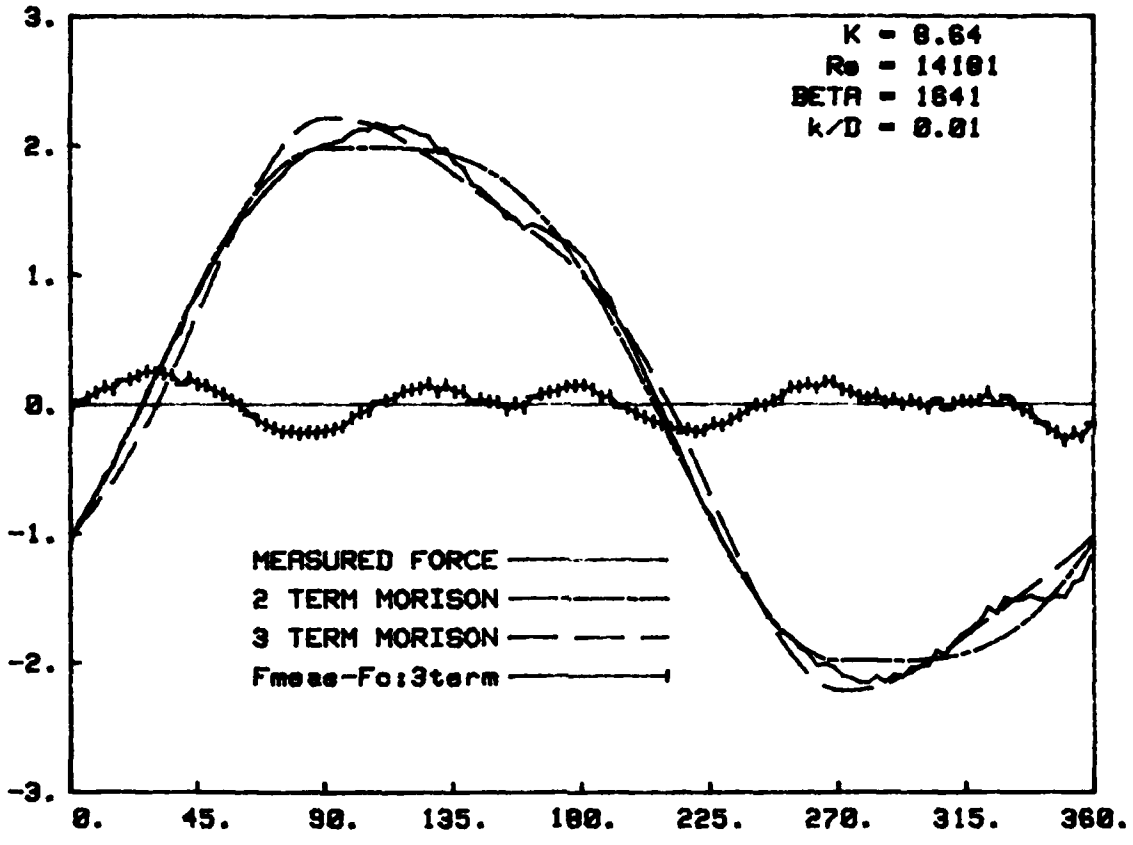

Fig. 30b Comparison of measured and calculated forces (Three-term MOJS Eq.)
K = 8.64

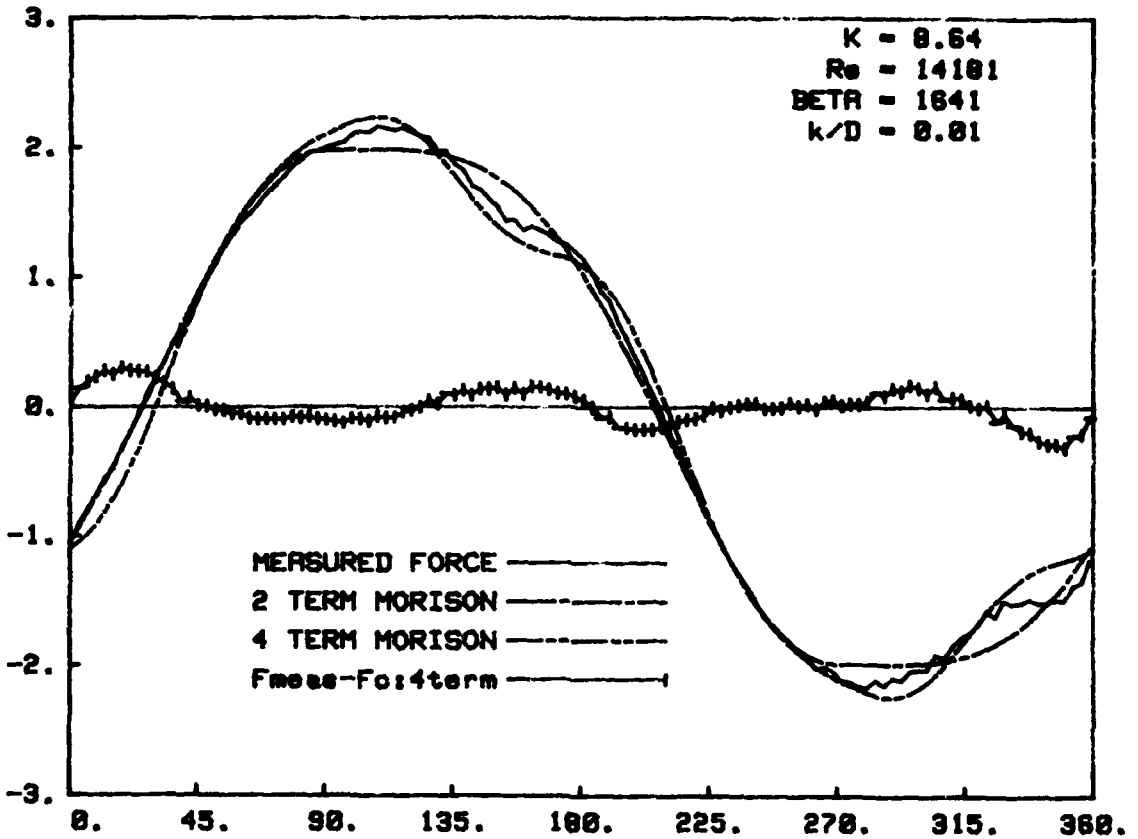

Fig. 30c Comparison of measured and calculated forces (Four-term MOJS Eq.)
K = 8.64

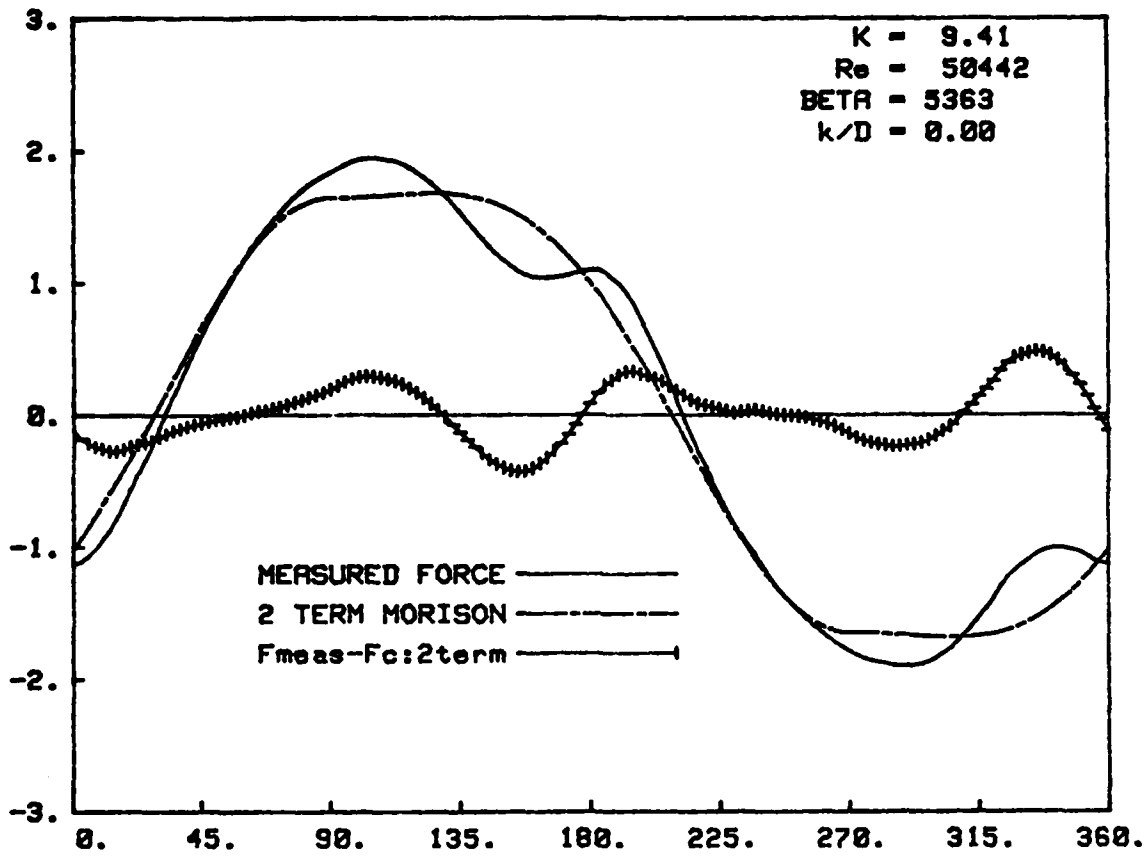

Fig. 31a Comparison of measured and calculated forces (Two-term MOJS Eq.)
K = 9.41

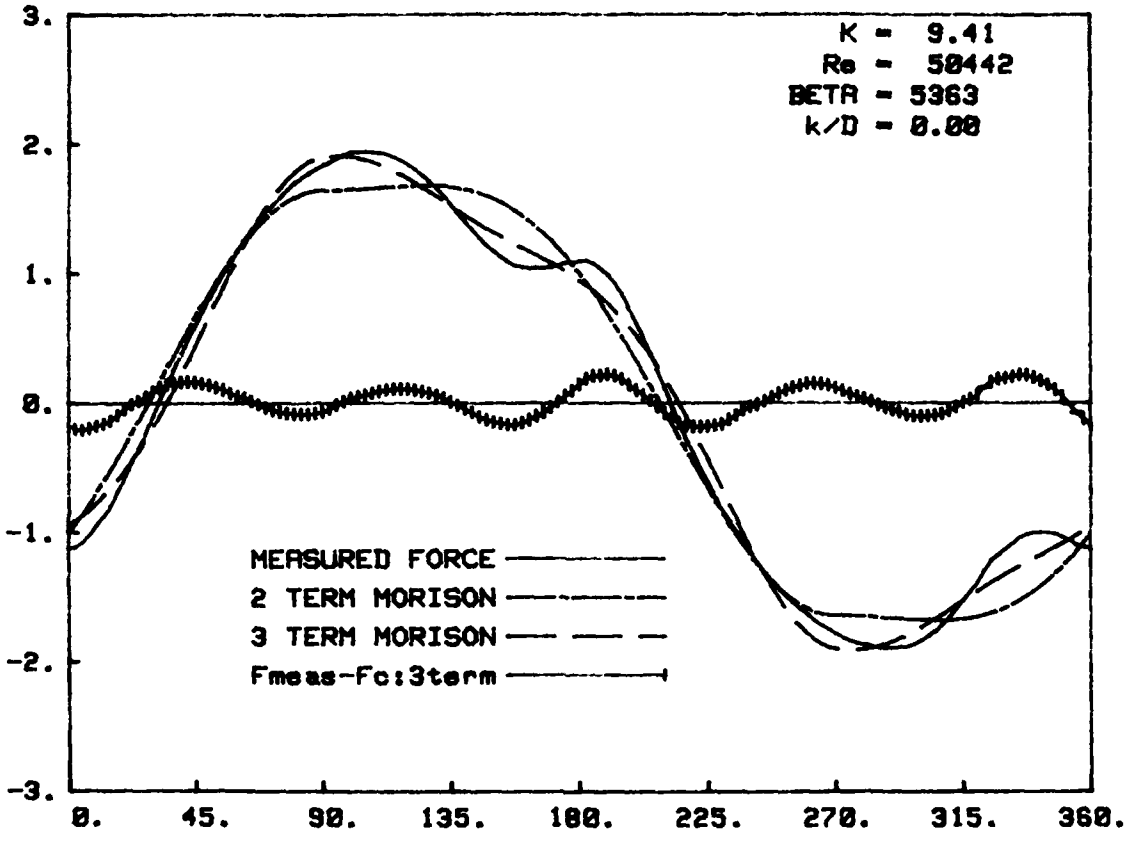

Fig. 31b Comparison of measured and calculated forces (Three-term MOJS Eq.)
K = 9.41

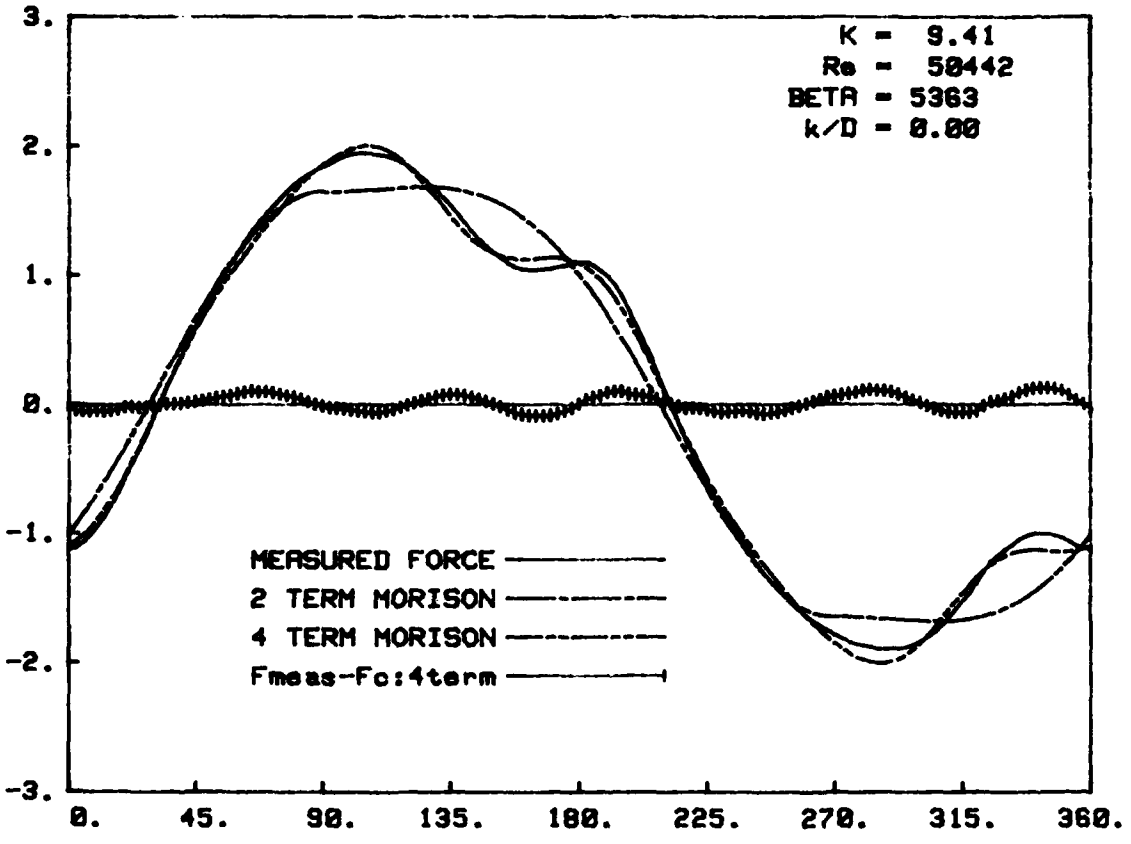

Fig. 31c Comparison of measured and calculated forces (Four-term MOJS Eq.)
K = 9.41

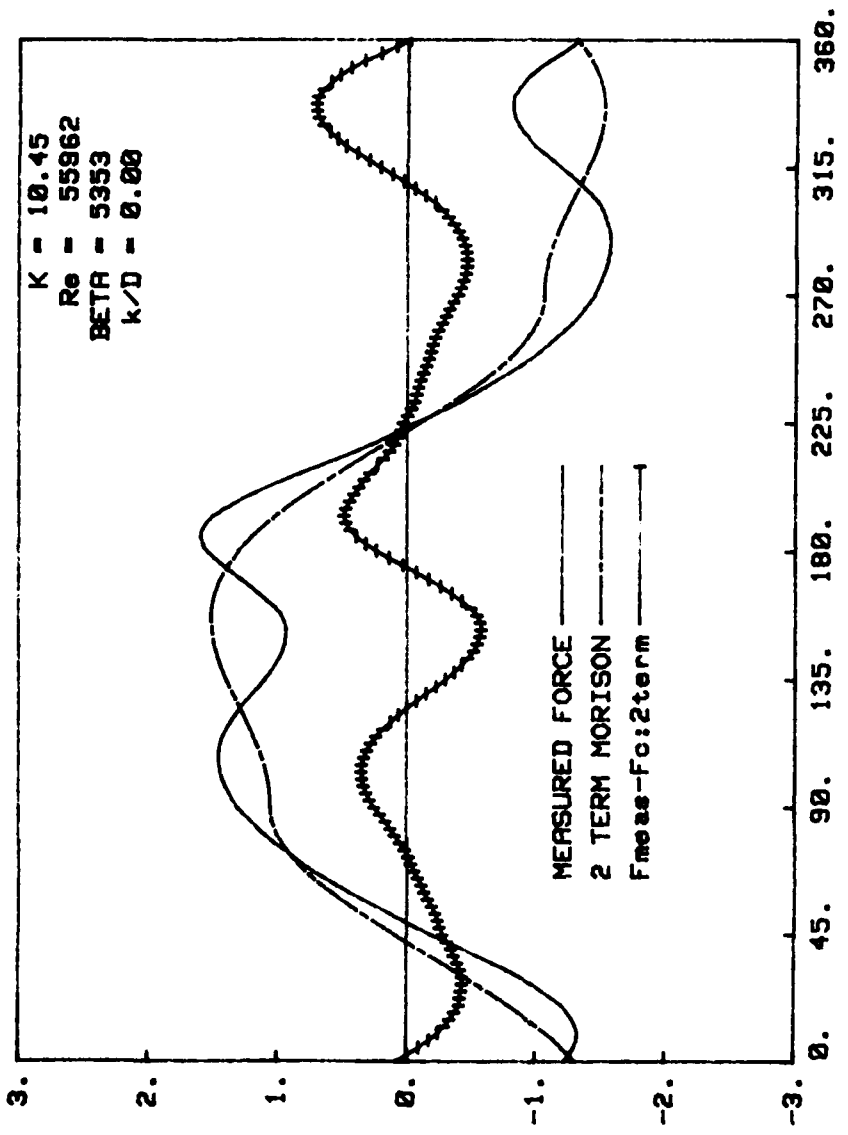

Fig. 32a Comparison of measured and calculated forces (Two-term MOJS Eq.)
K = 10.45

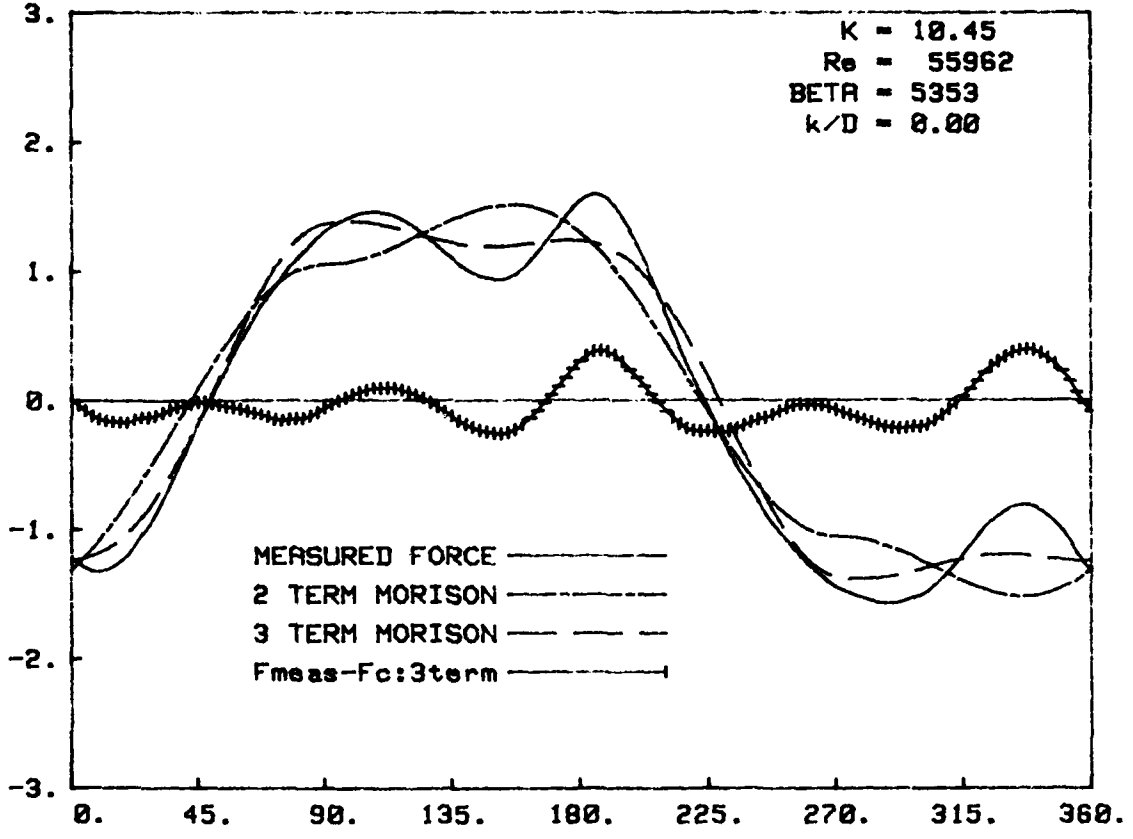

Fig. 32b Comparison of measured and calculated forces (Three-term MOJS Eq.)
K = 10.45

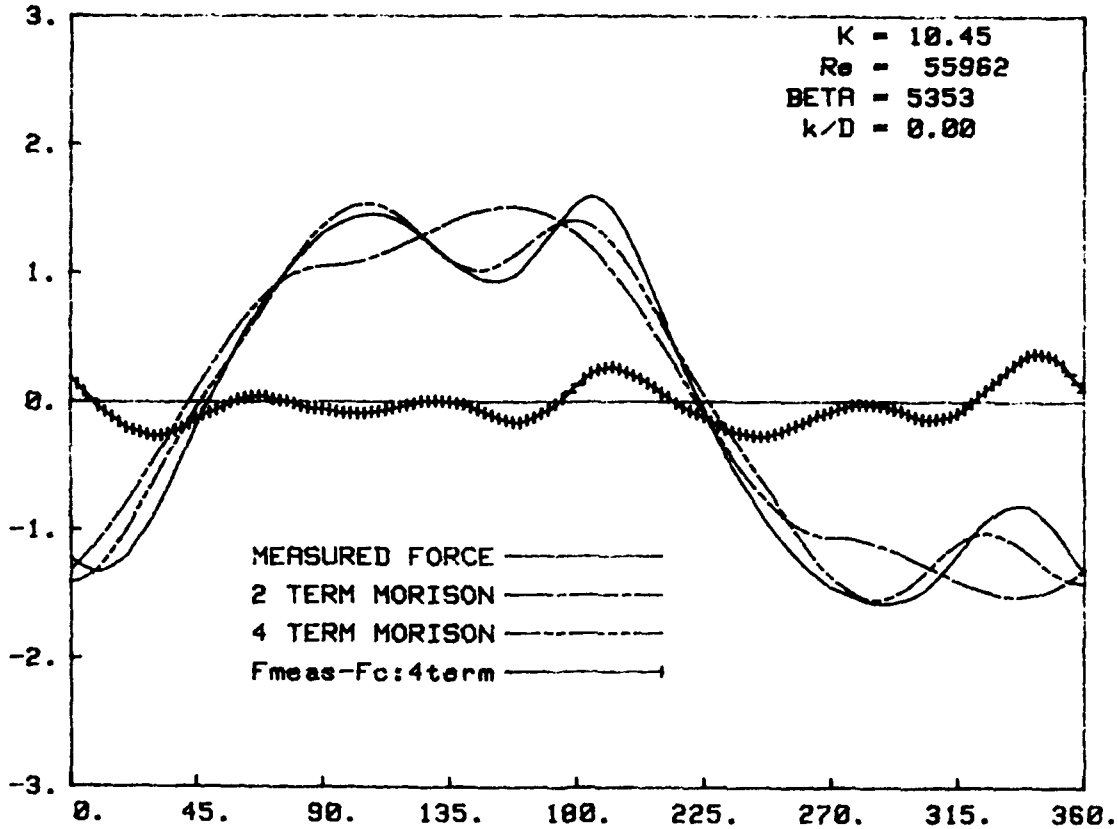

Fig. 32c Comparison of measured and calculated forces (Four-term MOJS Eq.)
K = 10.45

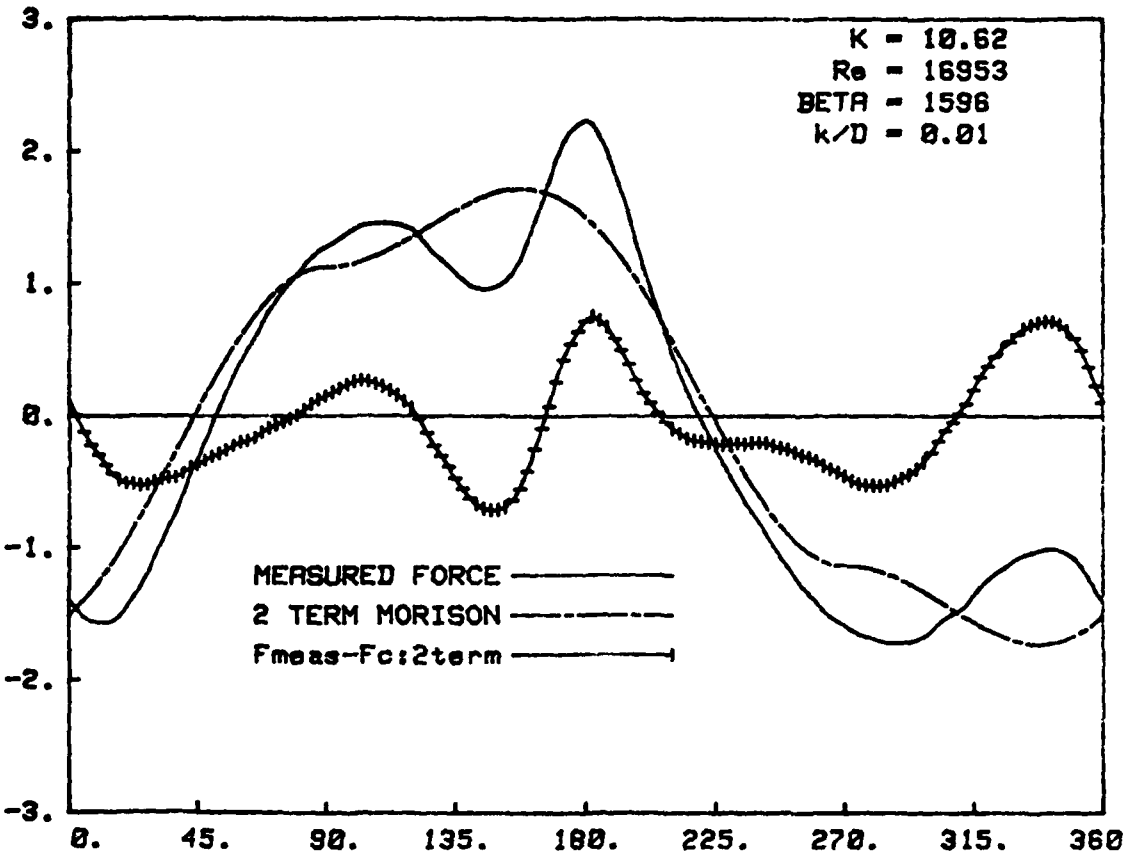

Fig. 33a Comparison of measured and calculated forces (Two-term MOJS Eq.)
K = 10.62

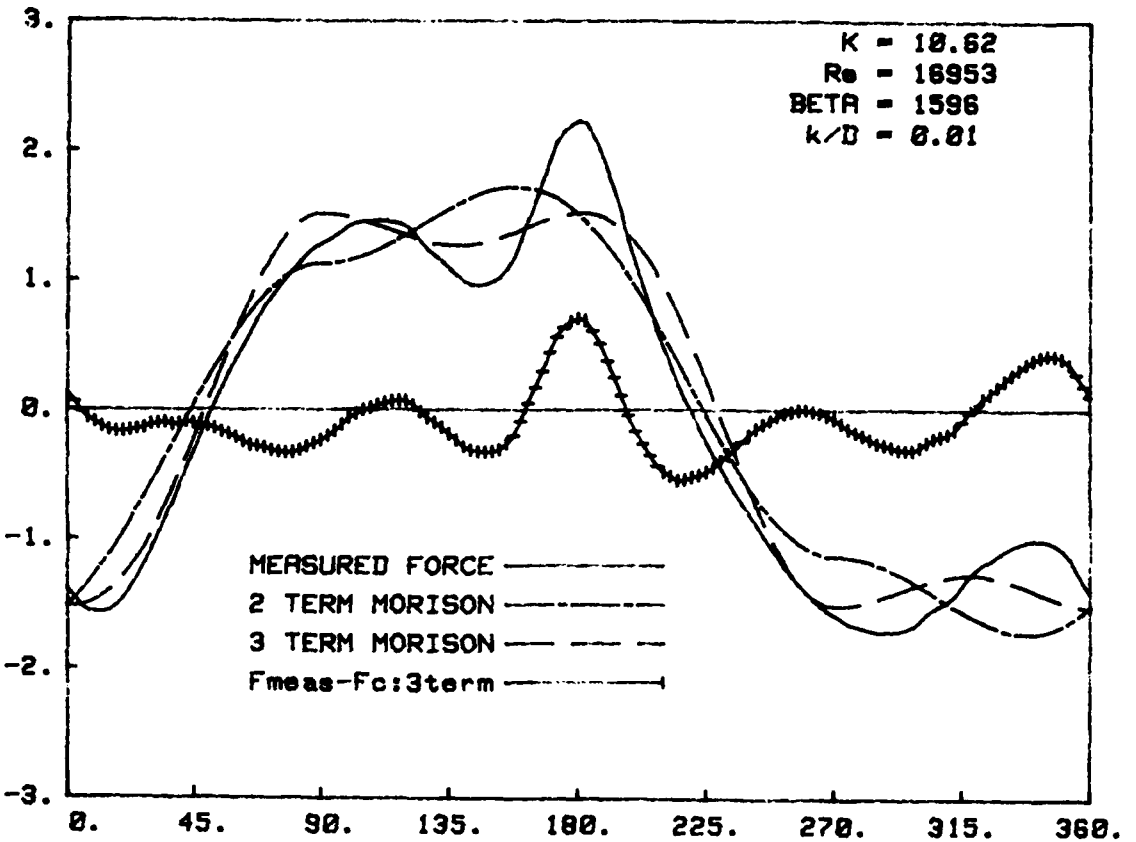

Fig. 33b Comparison of measured and calculated forces (Three-term MOJS Eq.)
K = 10.62

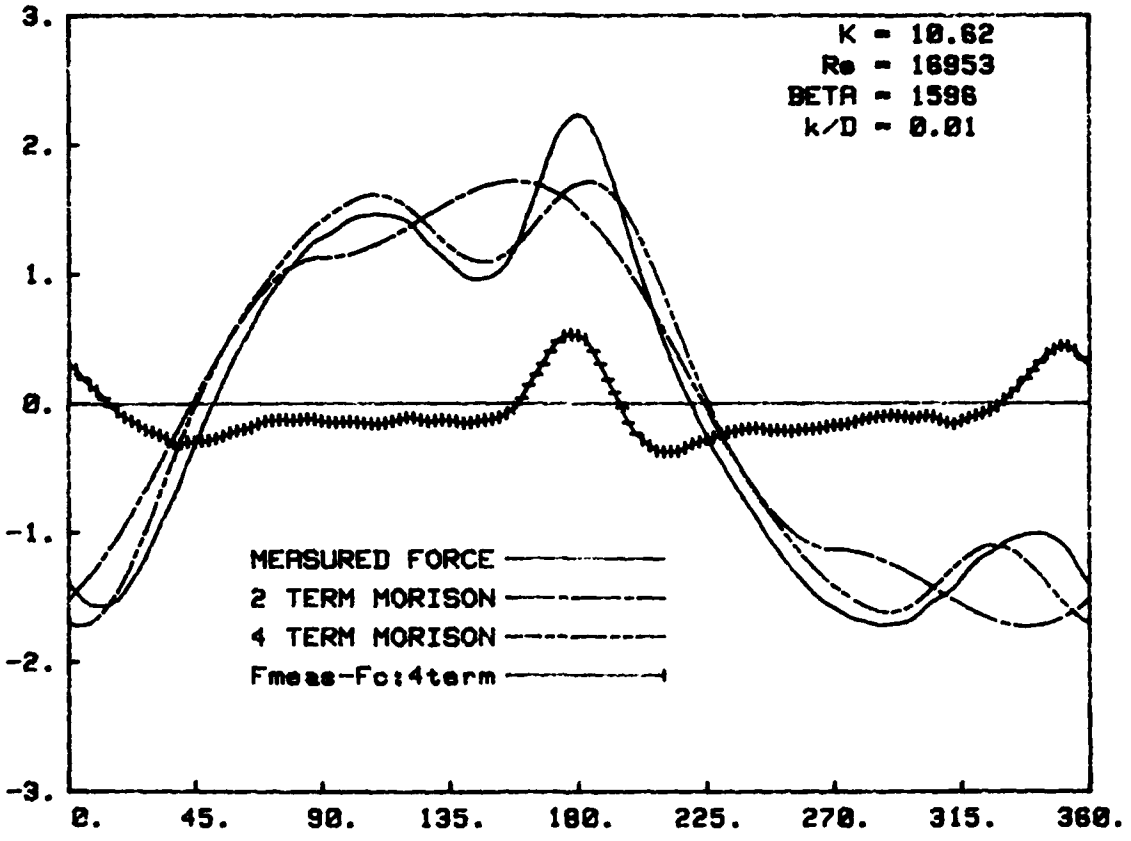

Fig. 33c Comparison of measured and calculated forces (Four-term MOJS Eq.)
K = 10.62

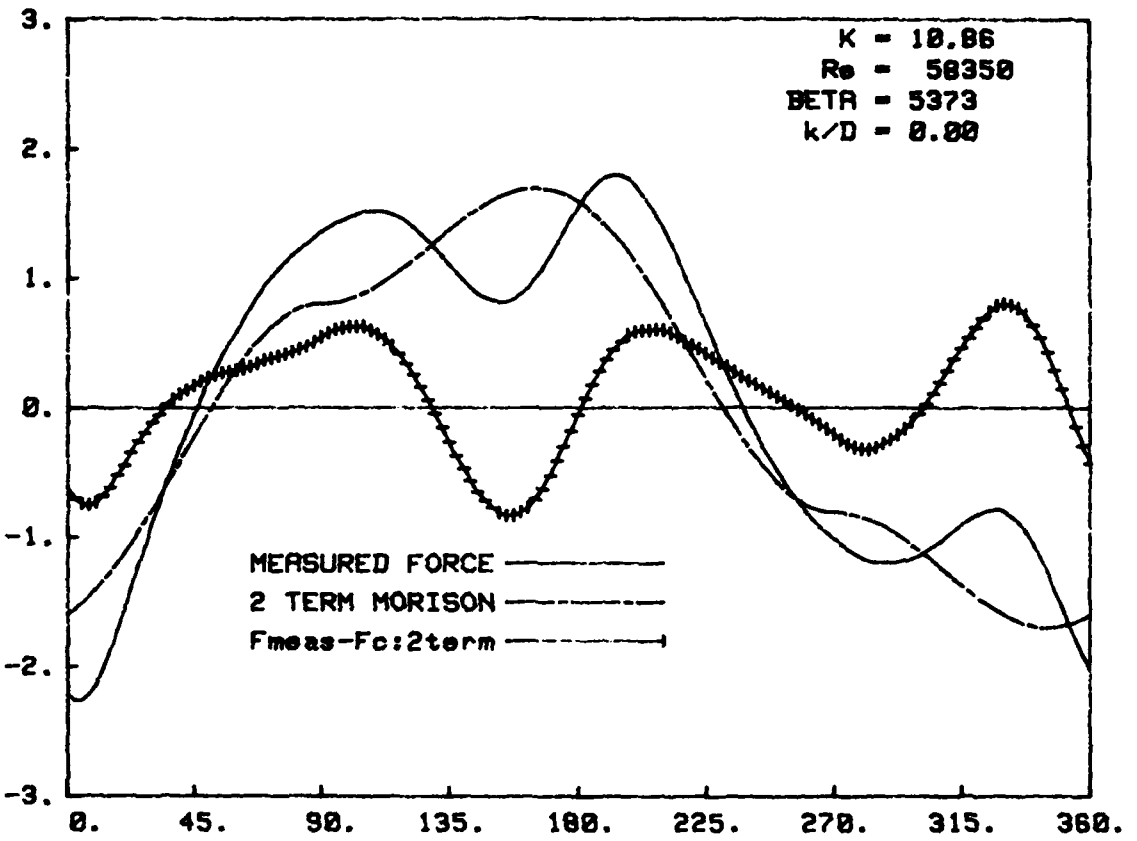

Fig. 34a Comparison of measured and calculated forces (Two-term MOJS Eq.)
K = 10.86

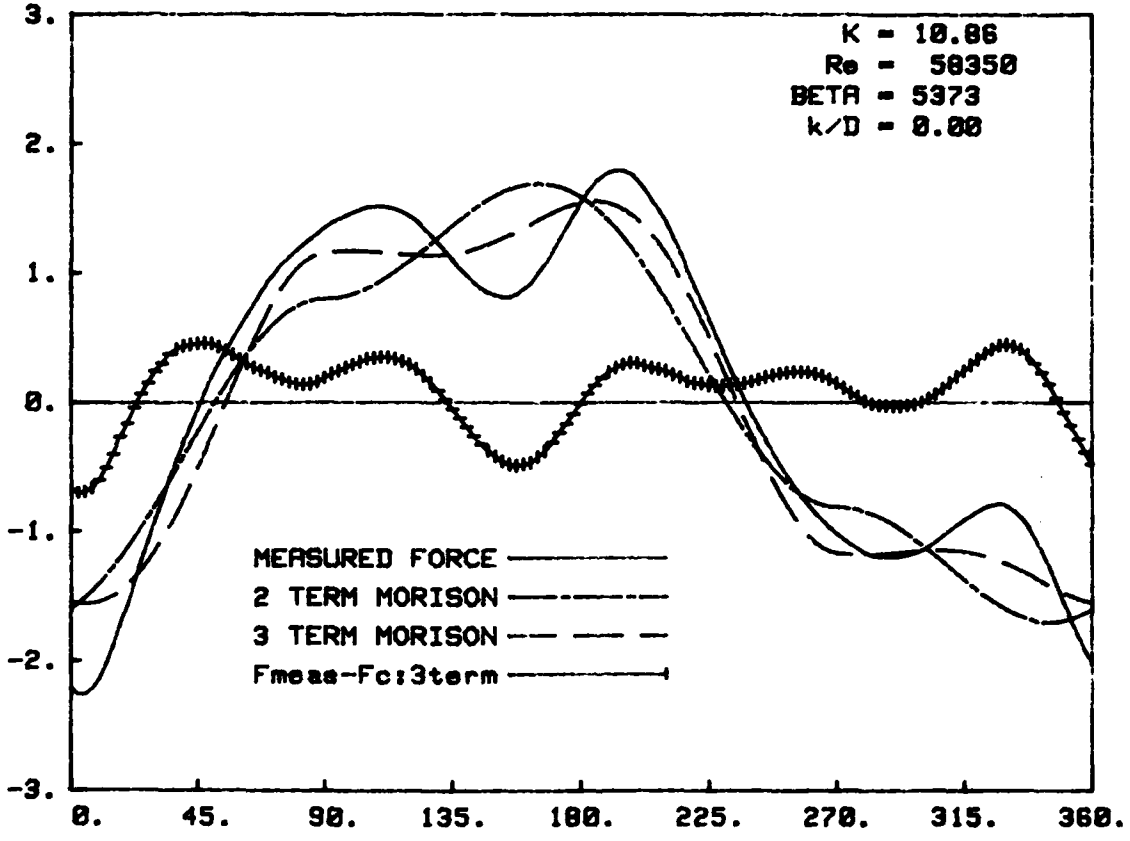

Fig. 34b Comparison of measured and calculated forces (Three-term MOJS Eq.)
K = 10.86

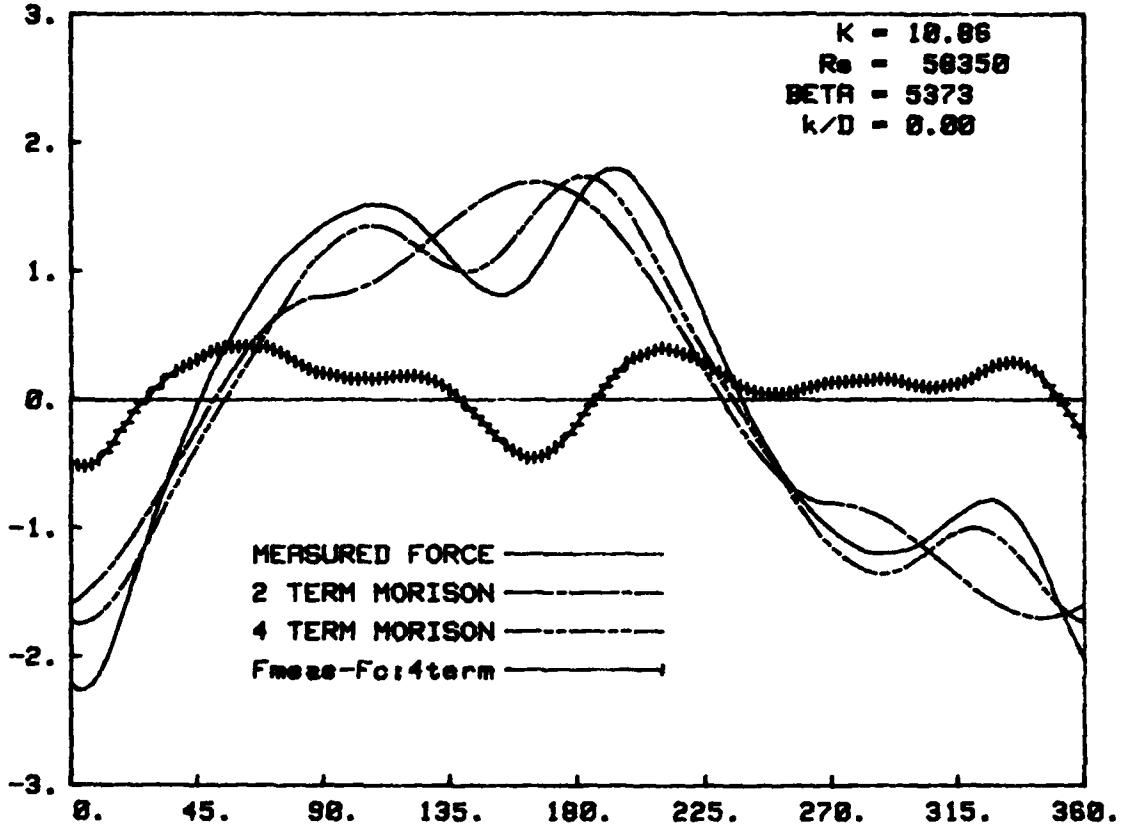

Fig. 34c Comparison of measured and calculated forces (Four term MOJS Eq.)
K = 10.86

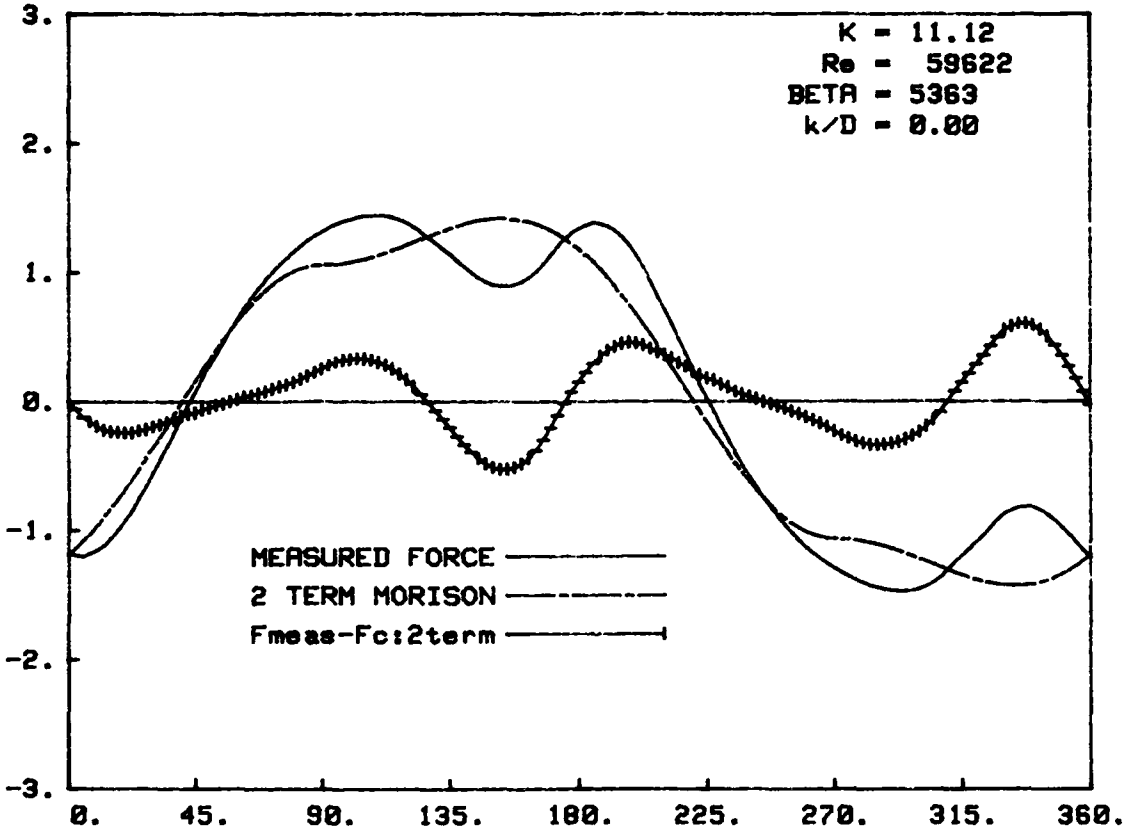

Fig. 35a Comparison of measured and calculated forces (Two-term MOJS Eq.)
K = 11.12

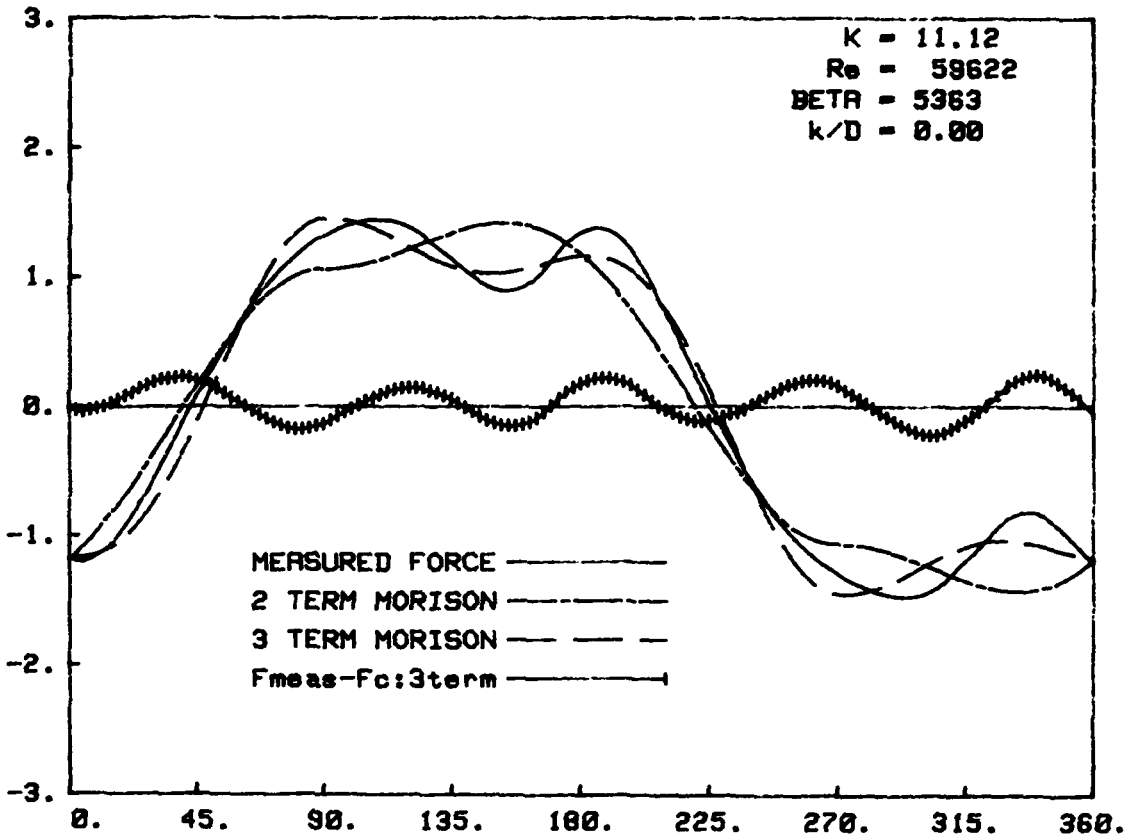

Fig. 35b Comparison of measured and calculated forces (Three-term MOJS Eq.)
K = 11.12

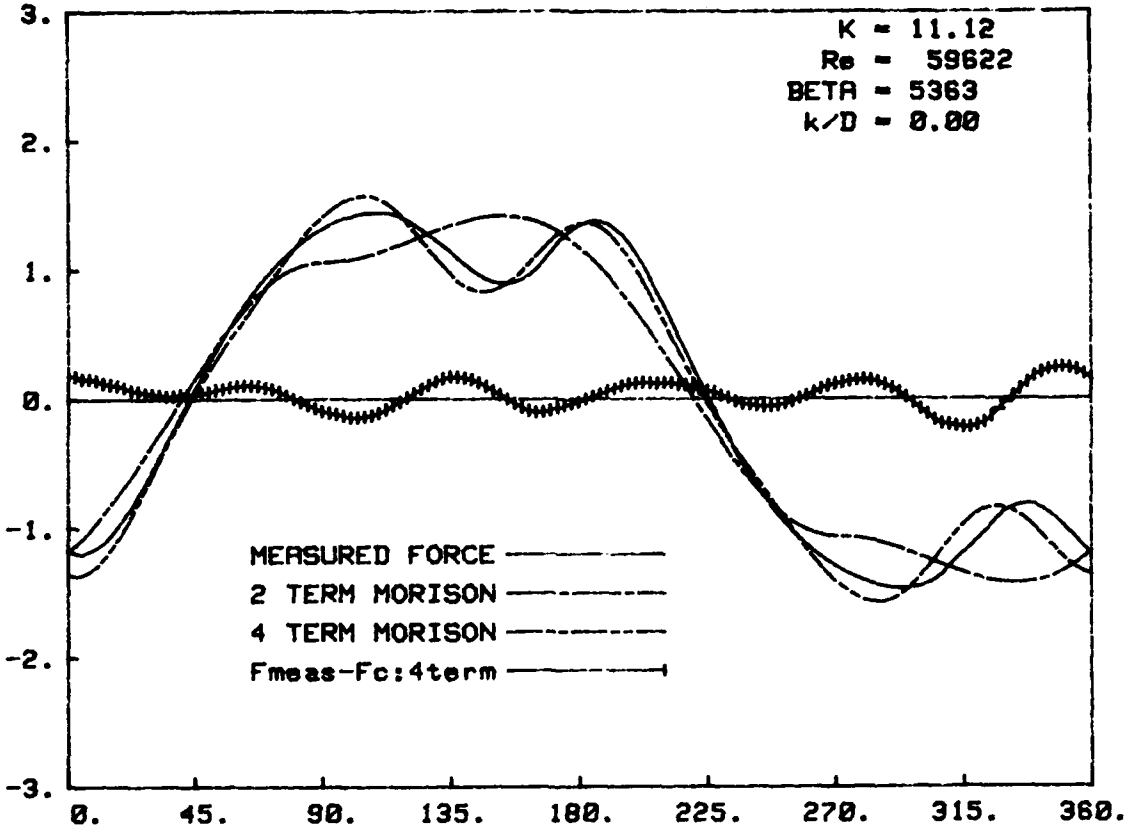

Fig. 35c Comparison of measured and calculated forces (Four-term MOJS Eq.)
K = 11.12

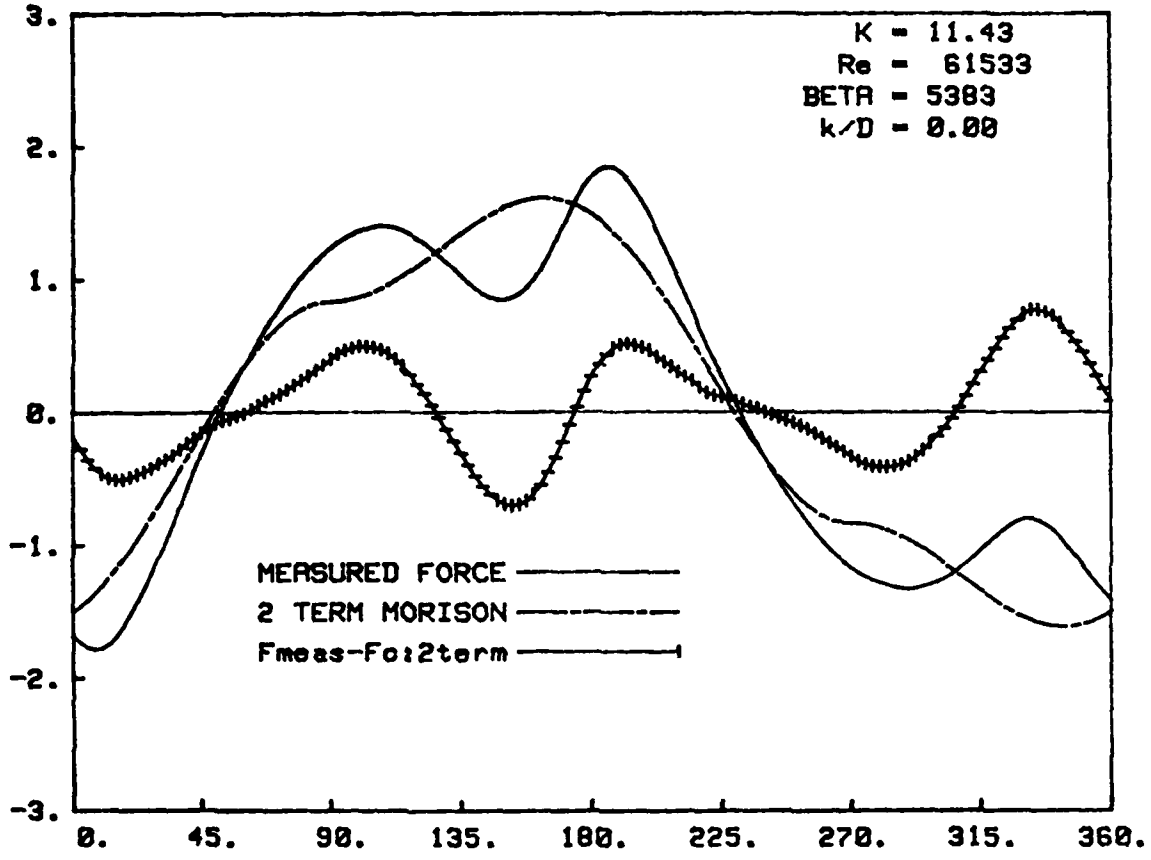

Fig. 36a Comparison of measured and calculated forces (Two-term MOJS Eq.)
K = 11.43

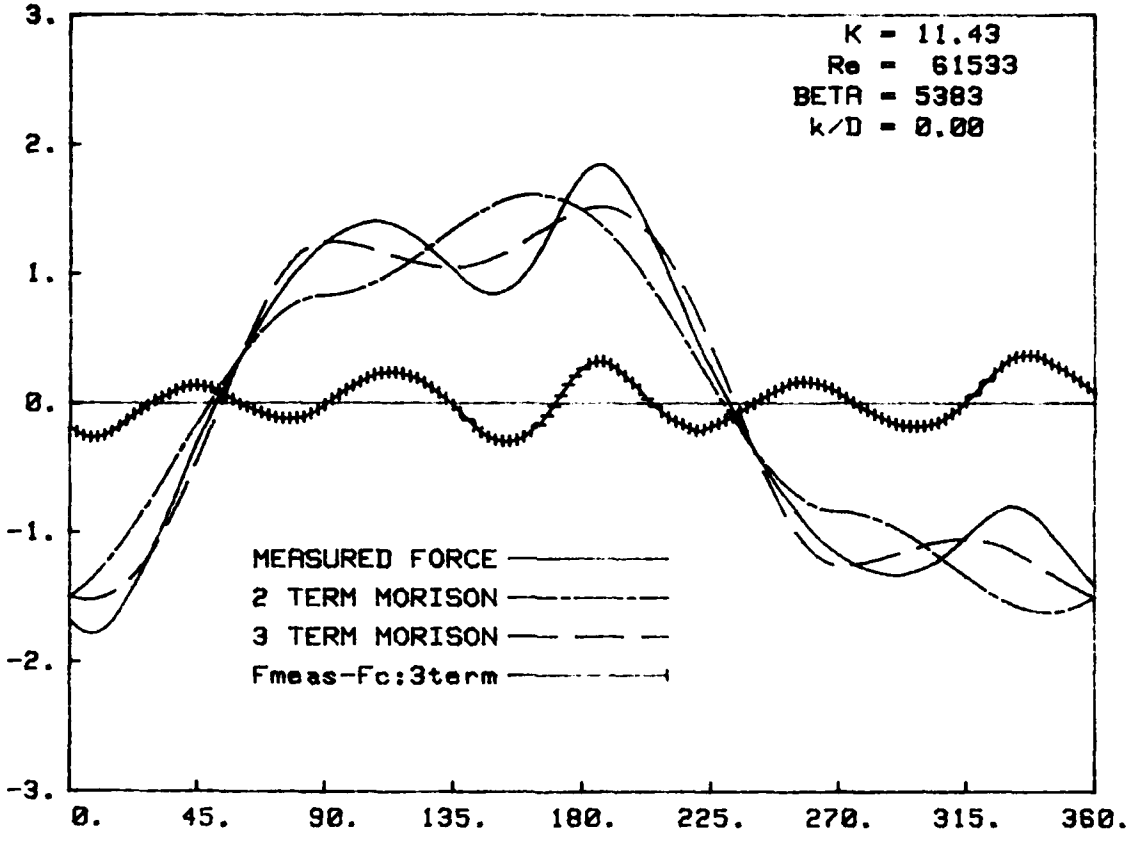

Fig. 36b Comparison of measured and calculated forces (Three-term MOJS Eq.)
K = 11.43

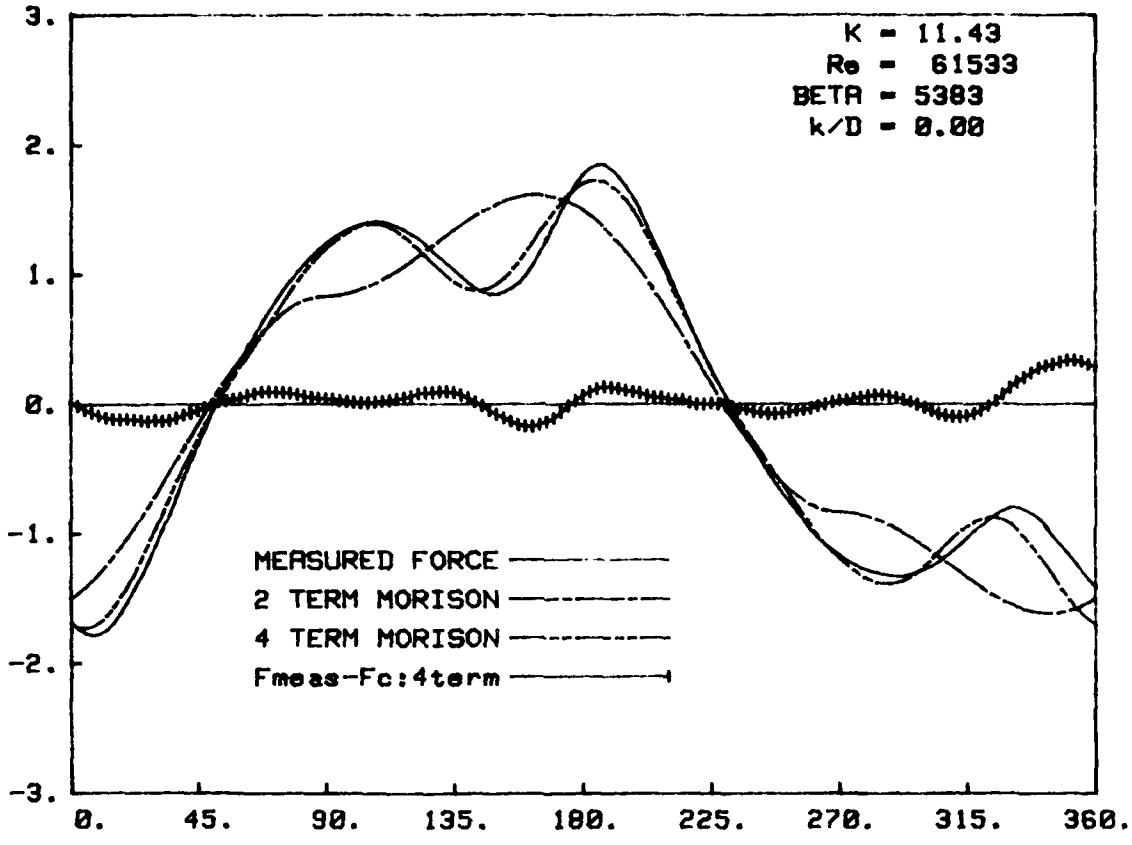

Fig. 36c Comparison of measured and calculated forces (Four-term MOJS Eq.)
K = 11.43

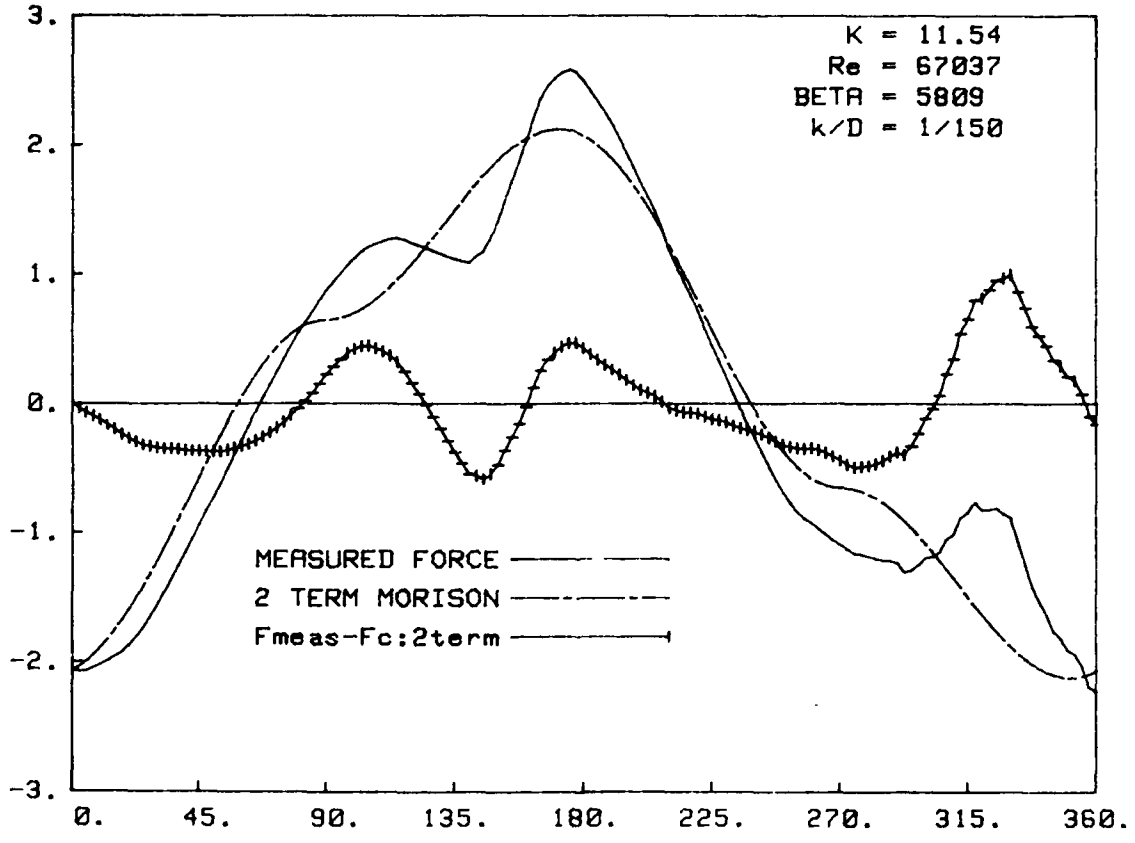

Fig. 37a Comparison of measured and calculated forces (Two-term MOJS Eq.)
K = 11.54

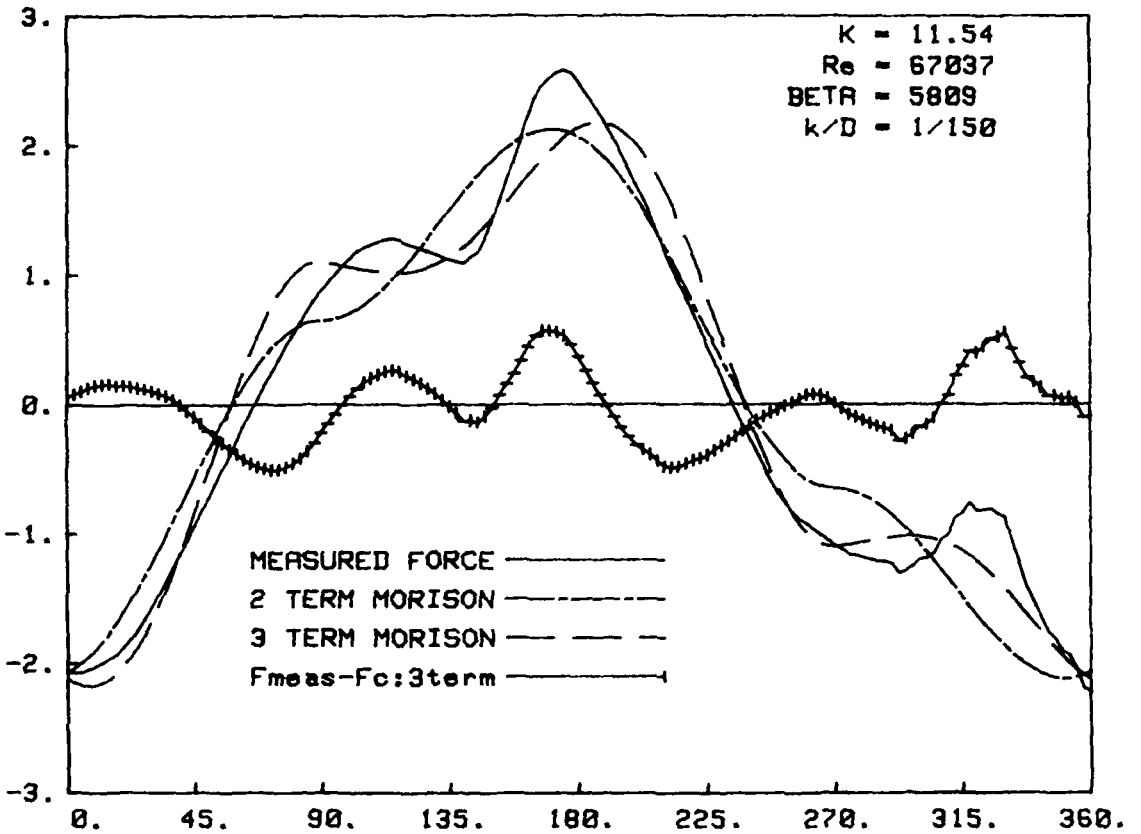

Fig. 37b Comparison of measured and calculated forces (Three-term MOJS Eq.)
K = 11.54

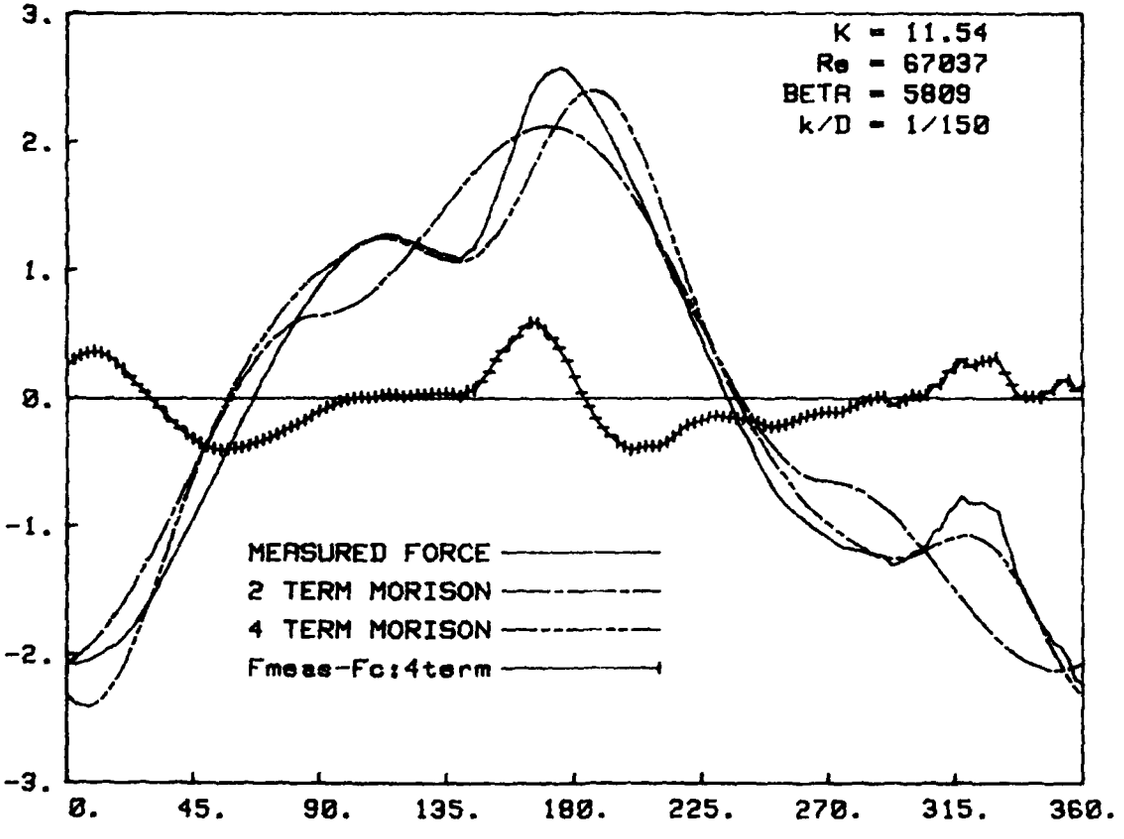

Fig. 37c Comparison of measured and calculated forces (Four-term MOJS Eq.)
K = 11.54

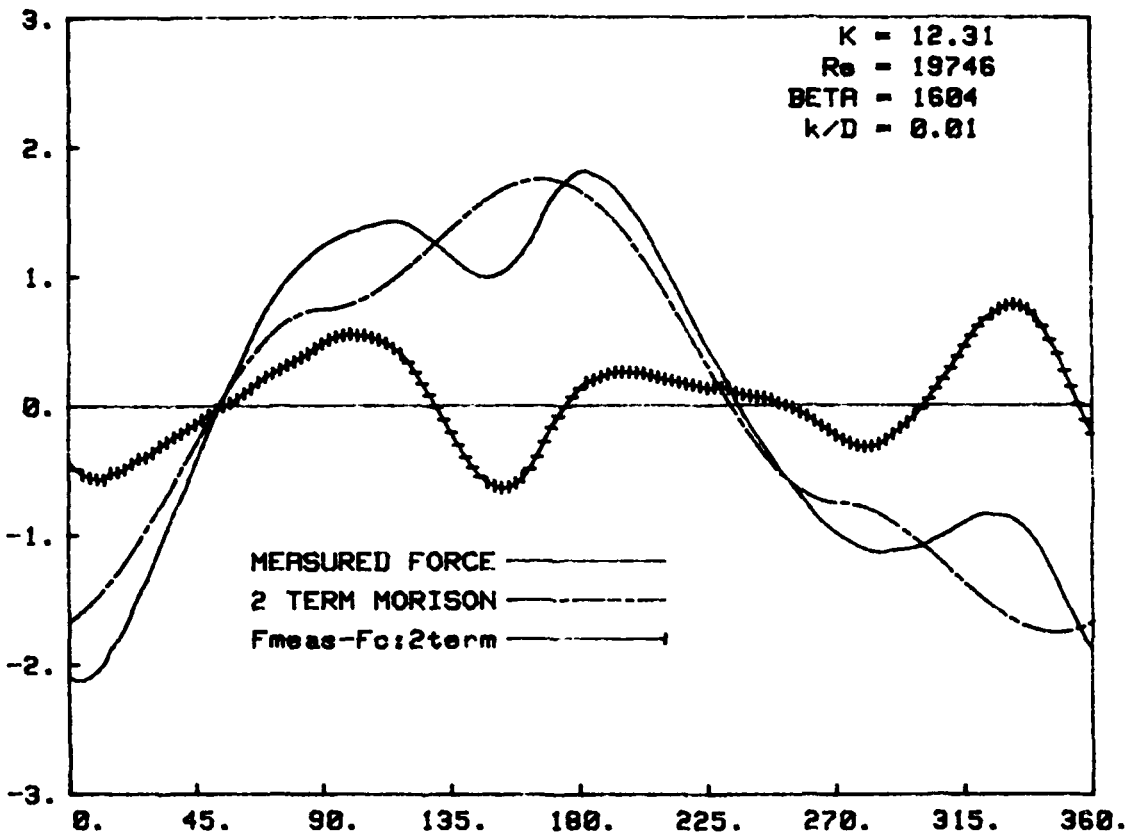

Fig. 38a Comparison of measured and calculated forces (Two-term MOJS Eq.)
K = 12.31

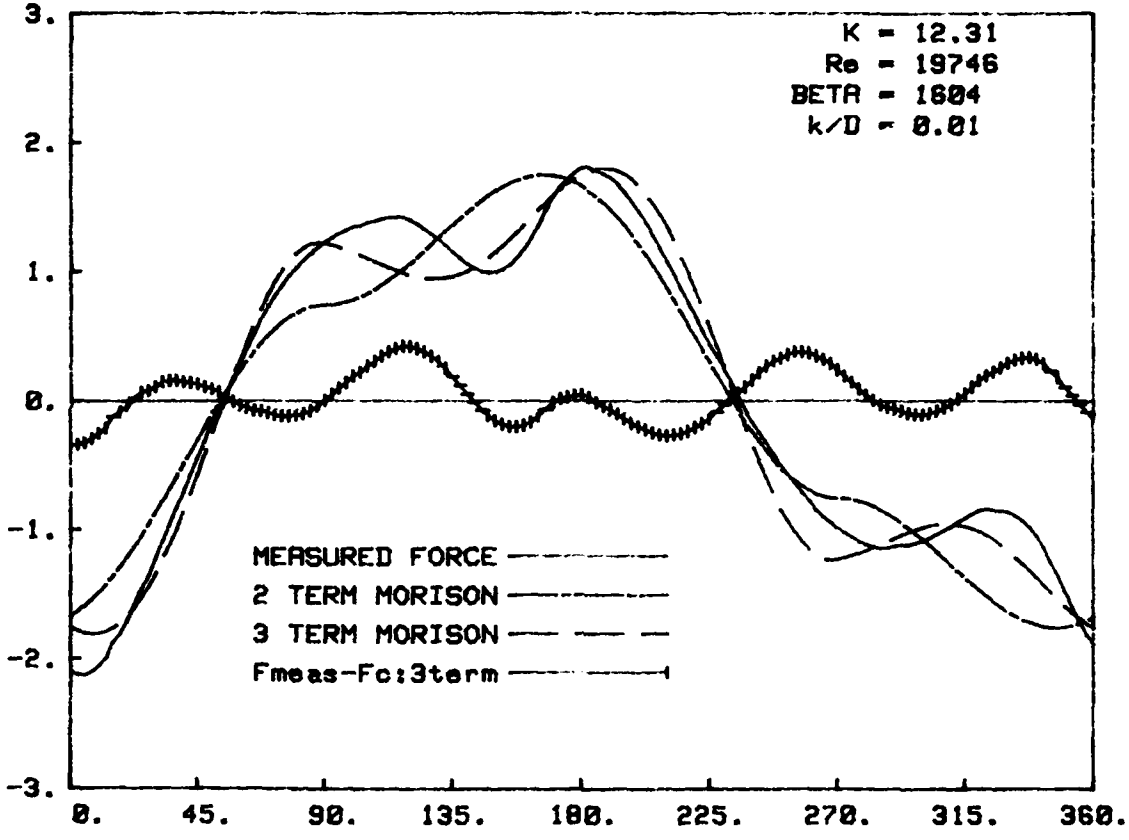

Fig. 38b Comparison of measured and calculated forces (Three-term MOJS Eq.)
K = 12.31

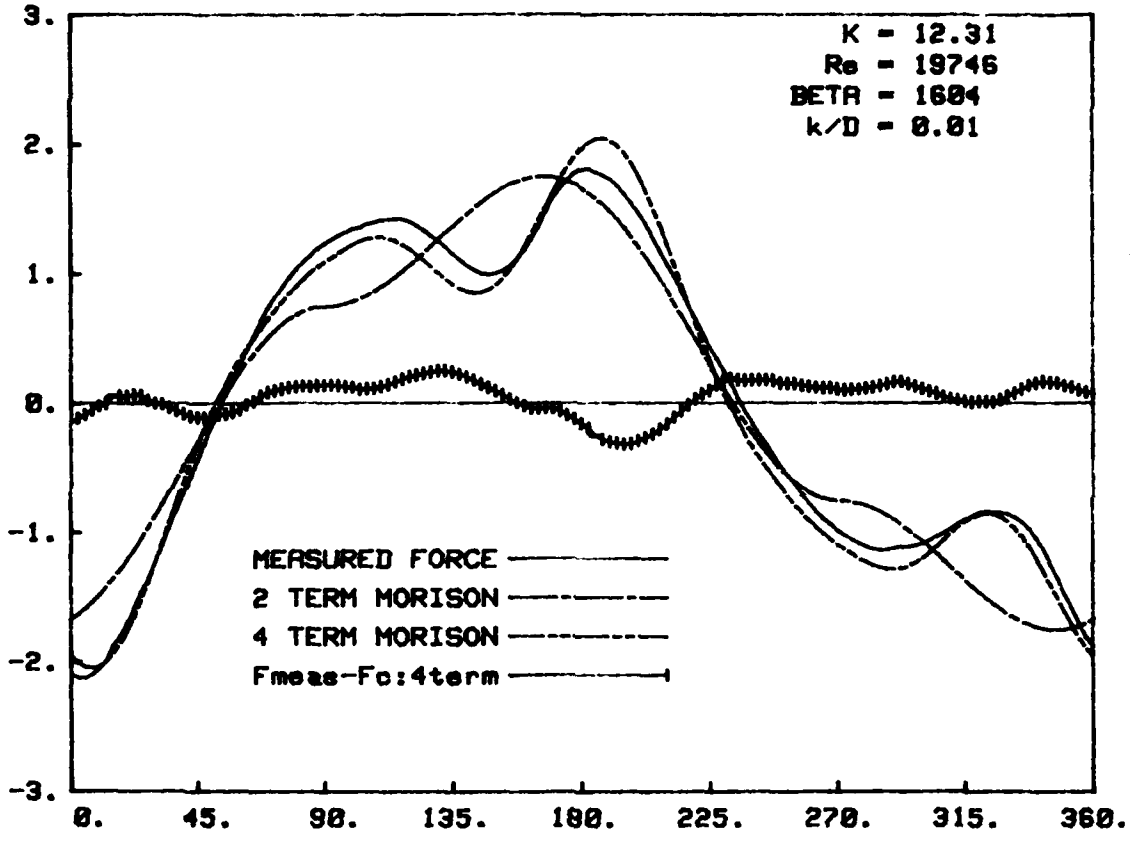

Fig. 38c Comparison of measured and calculated forces (Four-term MOJS Eq.)
K = 12.31

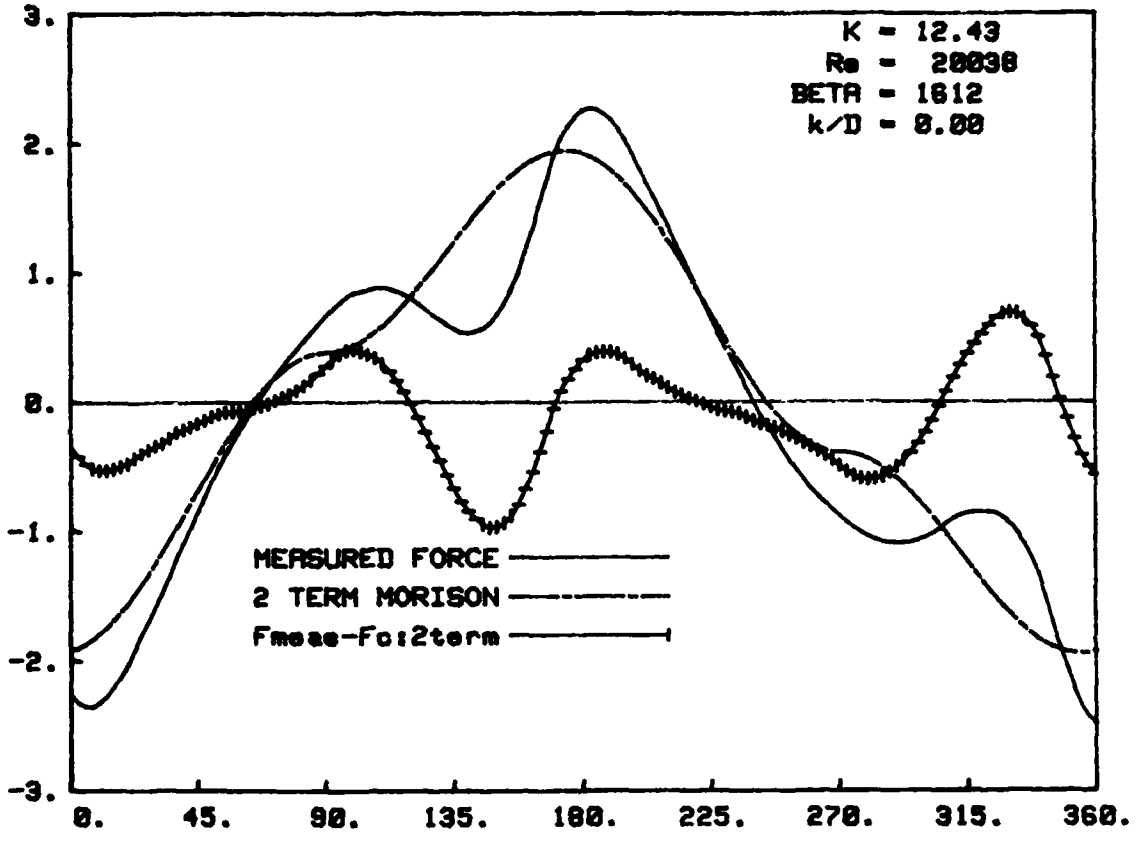

Fig. 39a Comparison of measured and calculated forces (Two-term MOJS Eq.)
K = 12.43

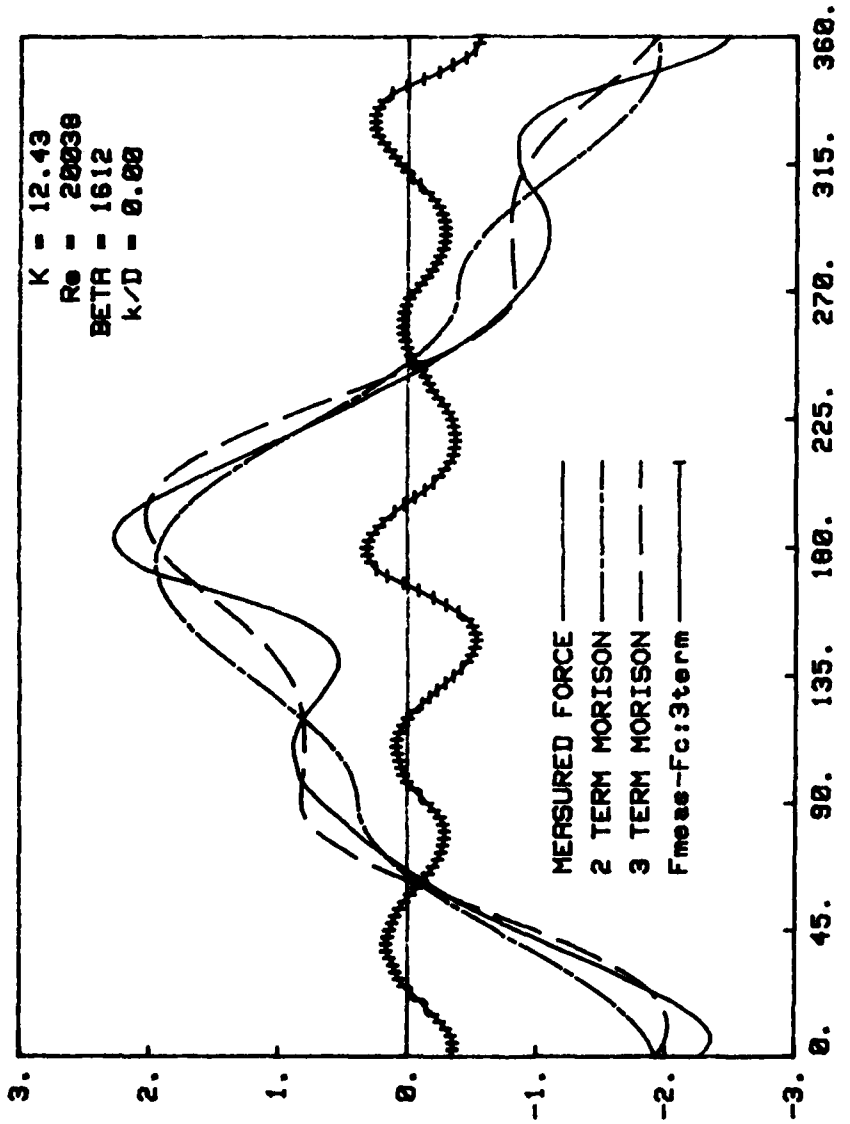

Fig. 39b Comparison of measured and calculated forces (Three-term MOJS Eq.)
K = 12.43

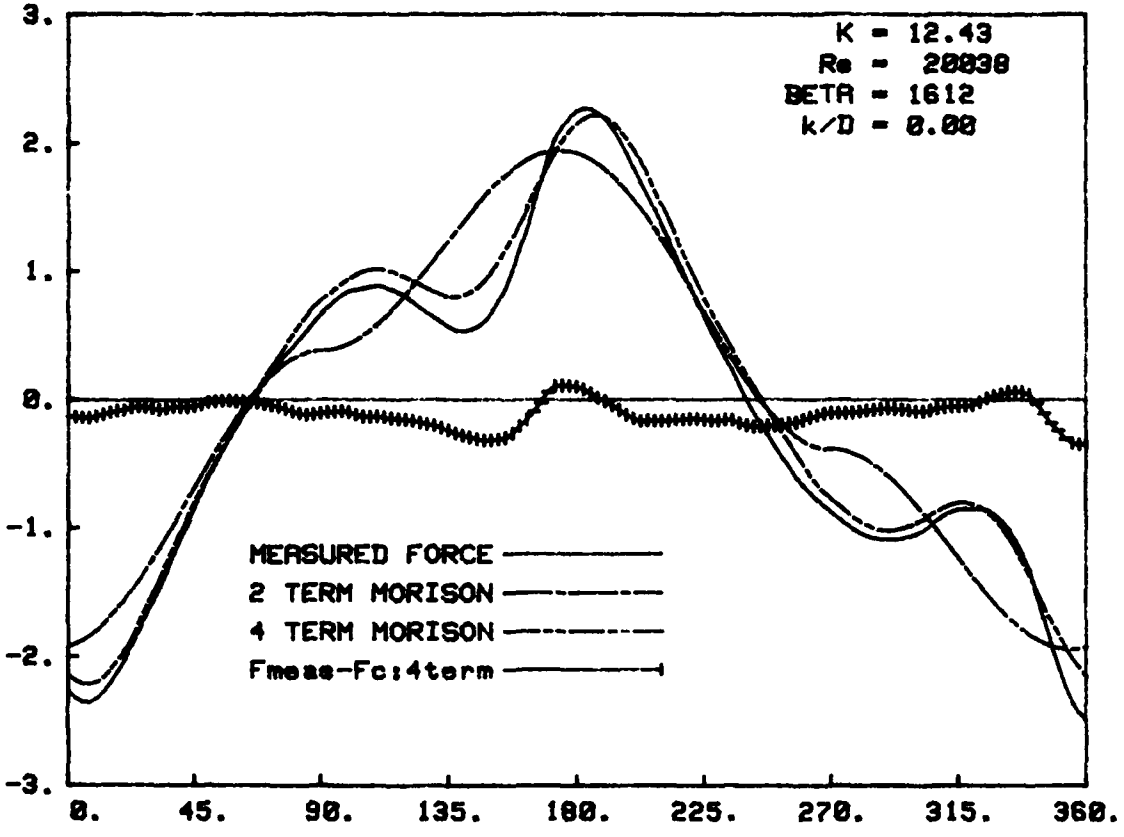

Fig. 39c Comparison of measured and calculated forces (Four-term MOJS Eq.)
K = 12.43

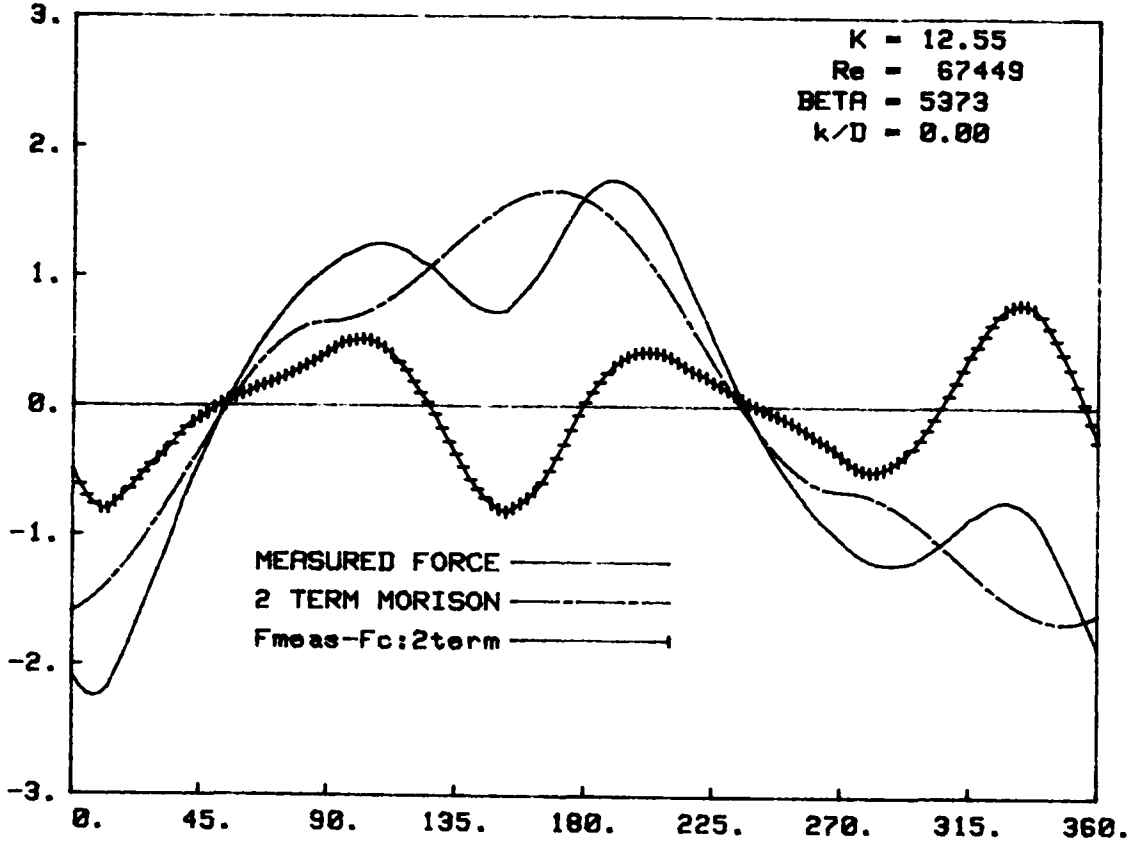

Fig. 40a Comparison of measured and calculated forces (Two-term MOJS Eq.)
K = 12.55

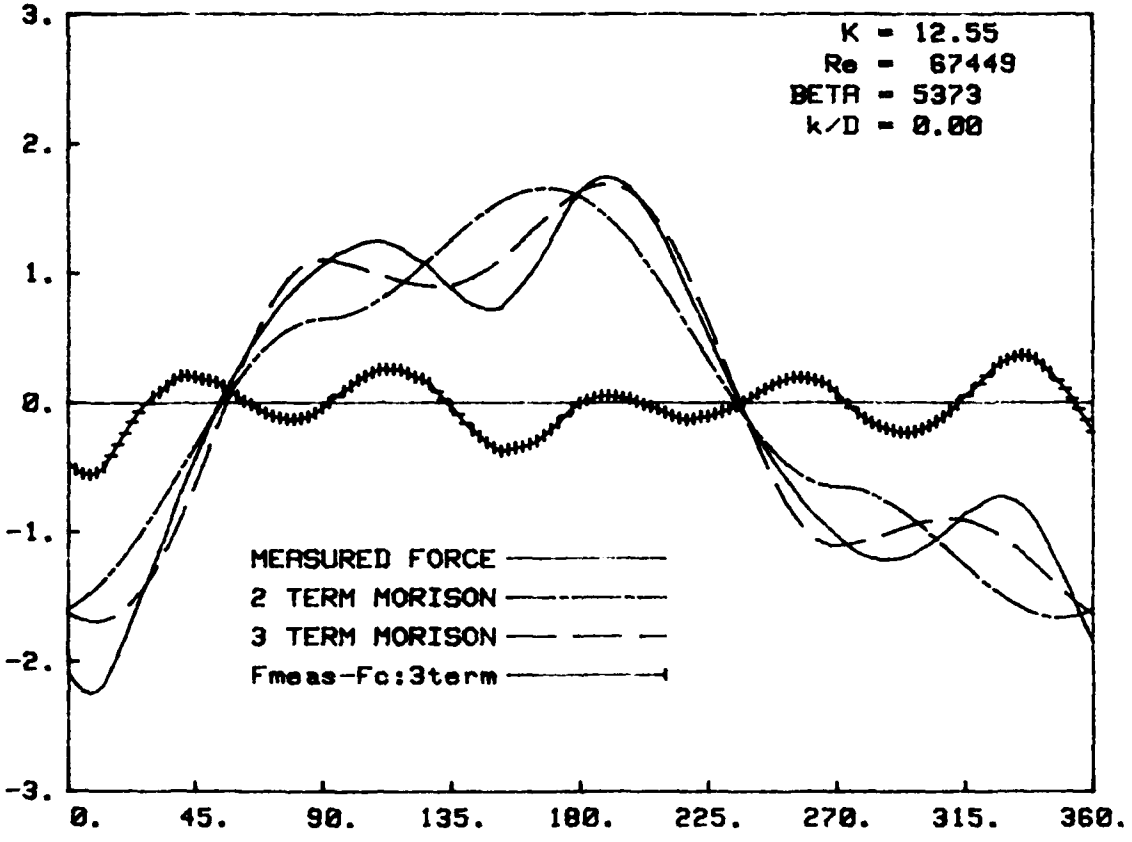

Fig. 40b Comparison of measured and calculated forces (Three-term MOJS Eq.)
K = 12.55

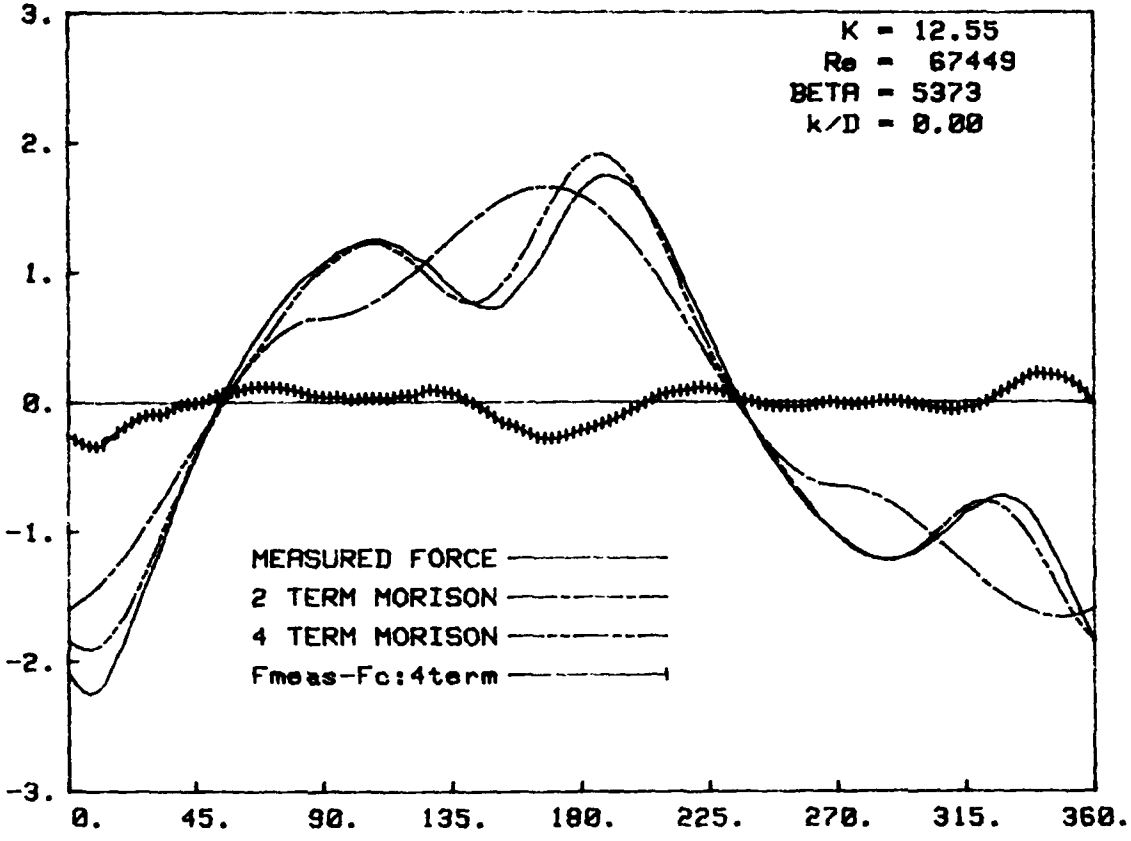

Fig. 40c Comparison of measured and calculated forces (Four-term MOJS Eq.)
K = 12.55

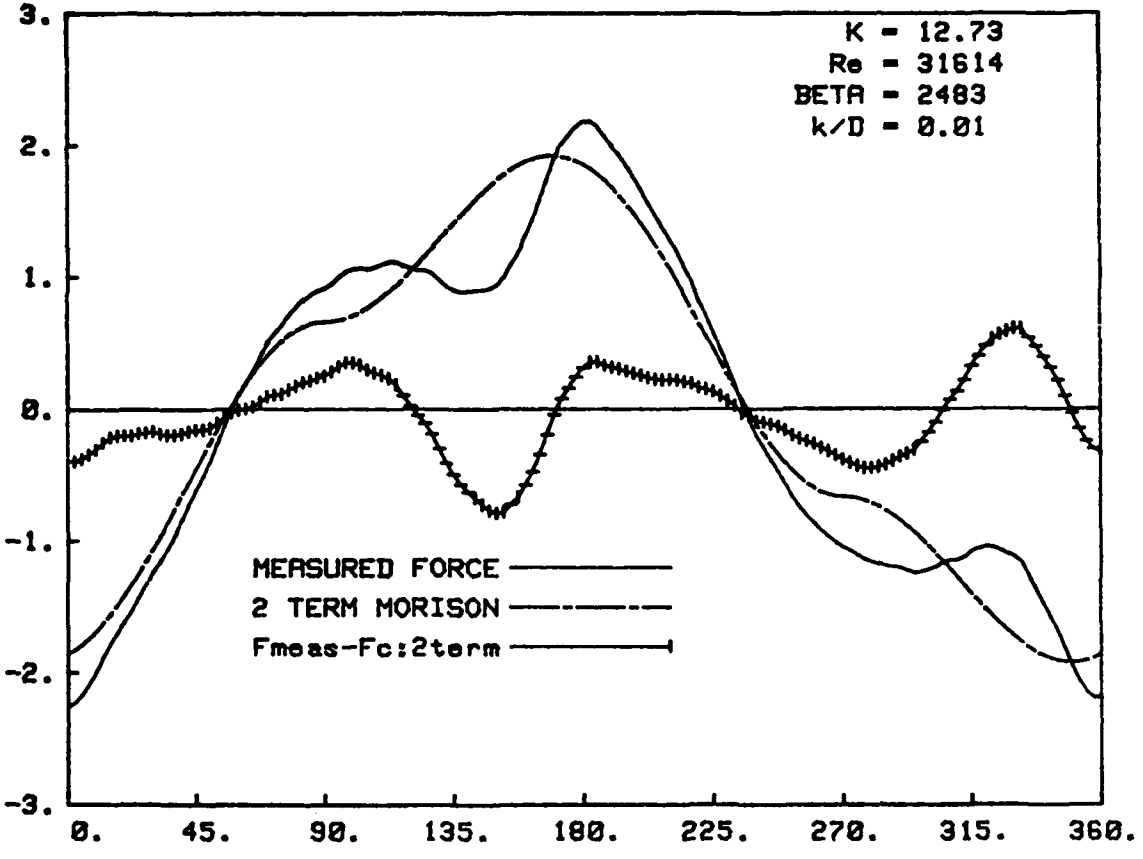

Fig. 41a Comparison of measured and calculated forces (Two-term MOJS Eq.)
K = 12.73

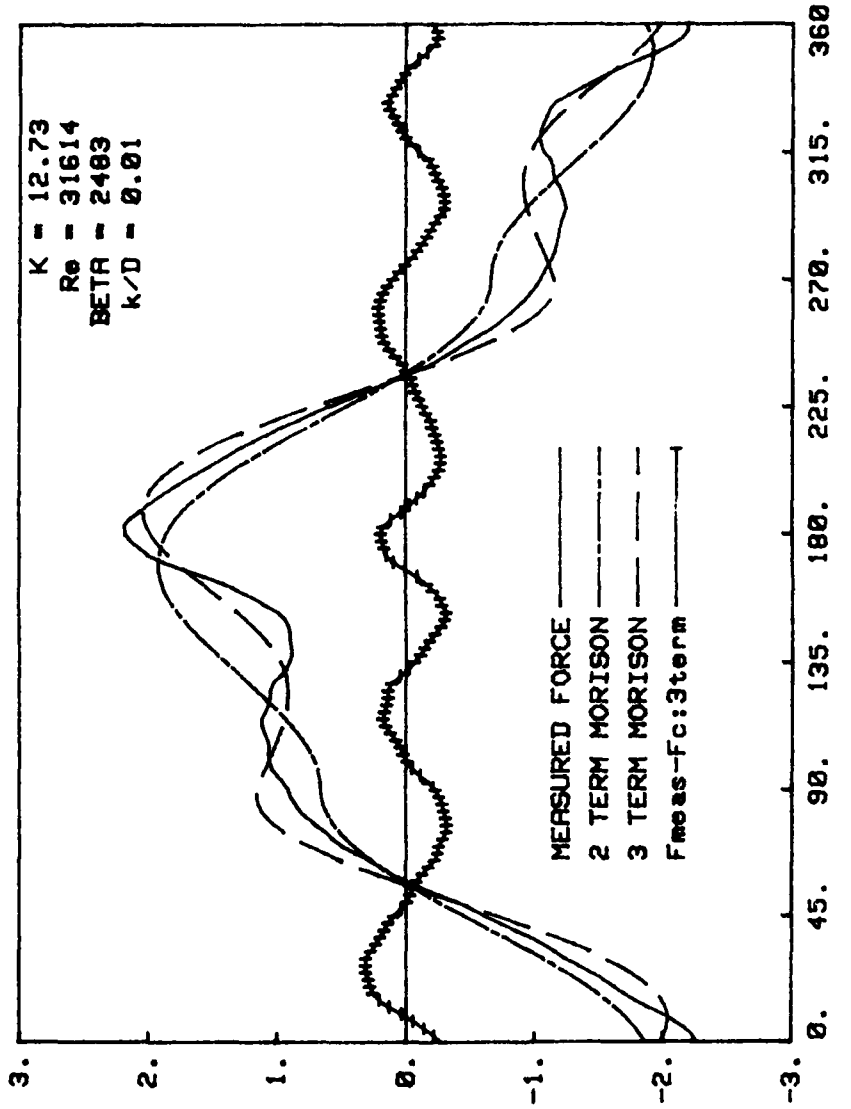

Fig. 41b Comparison of measured and calculated forces (Three-term MOJS Eq.)
K = 12.73

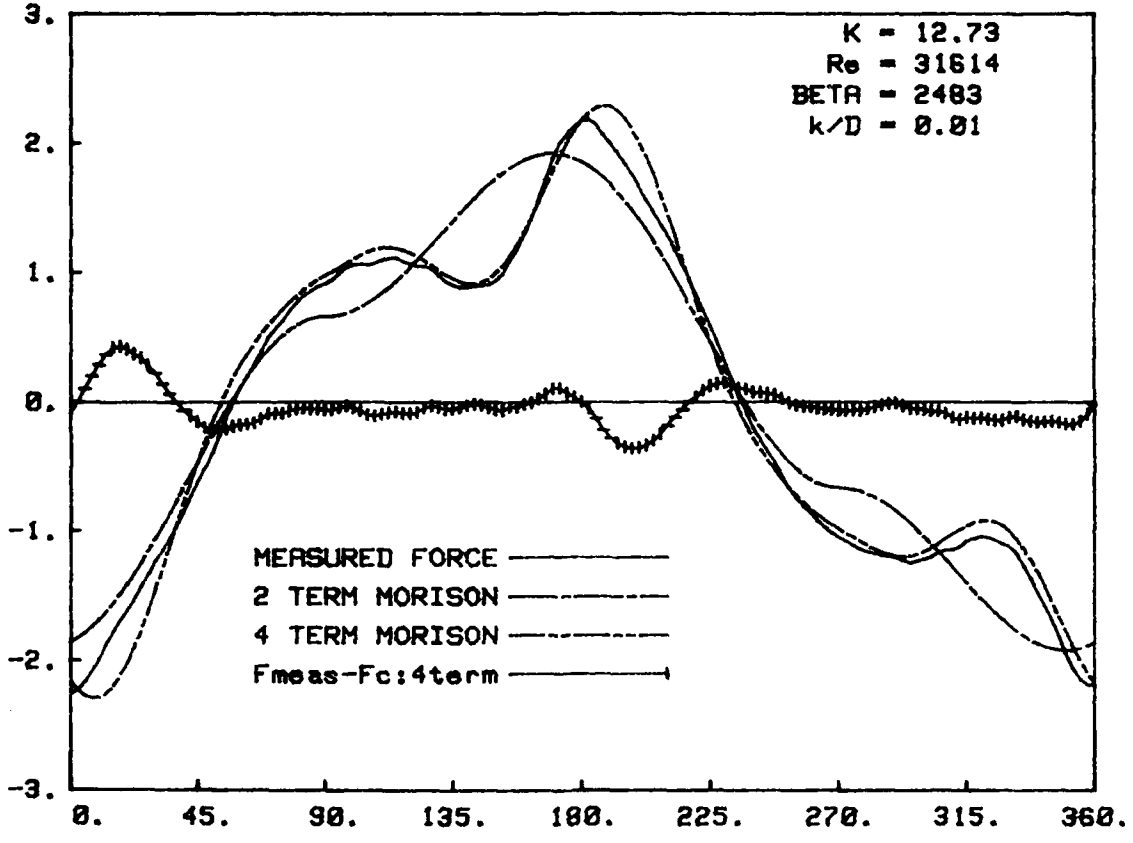

Fig. 41c Comparison of measured and calculated forces (Four-term MOJS Eq.)
K = 12.73

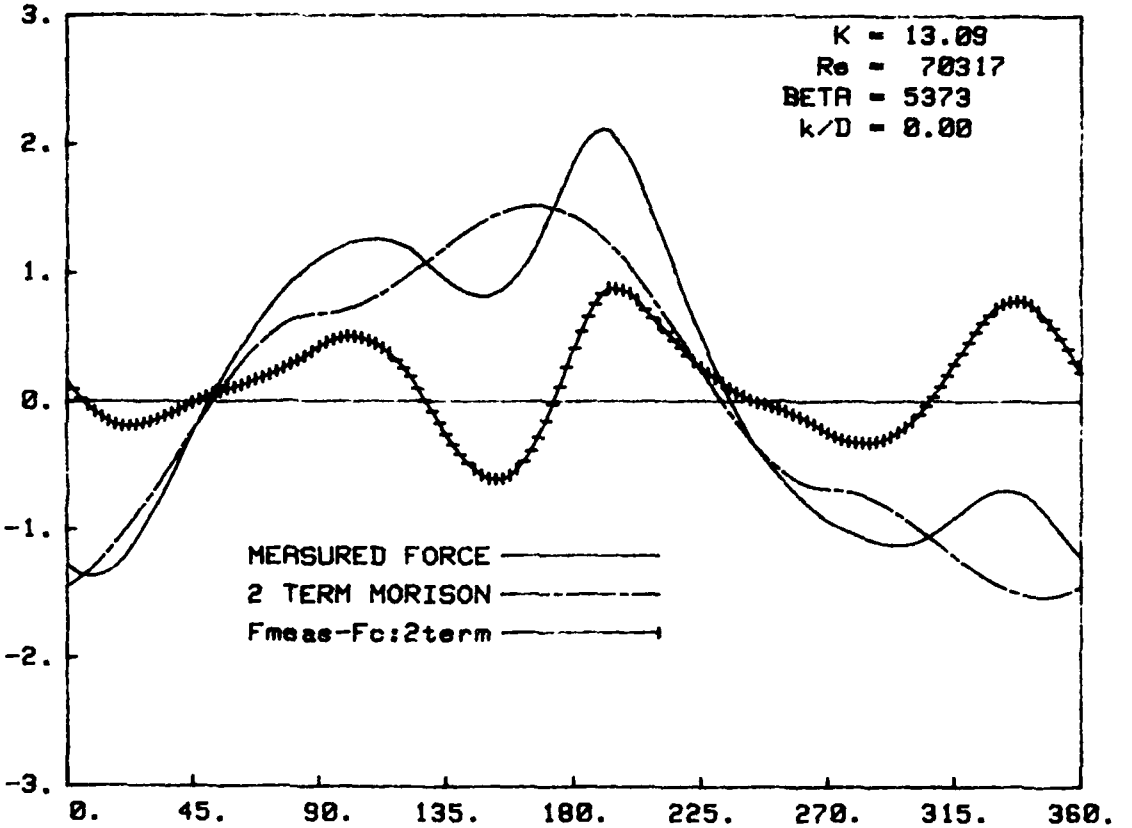

Fig. 42a Comparison of measured and calculated forces (Two-term MOJS Eq.)
K = 13.09

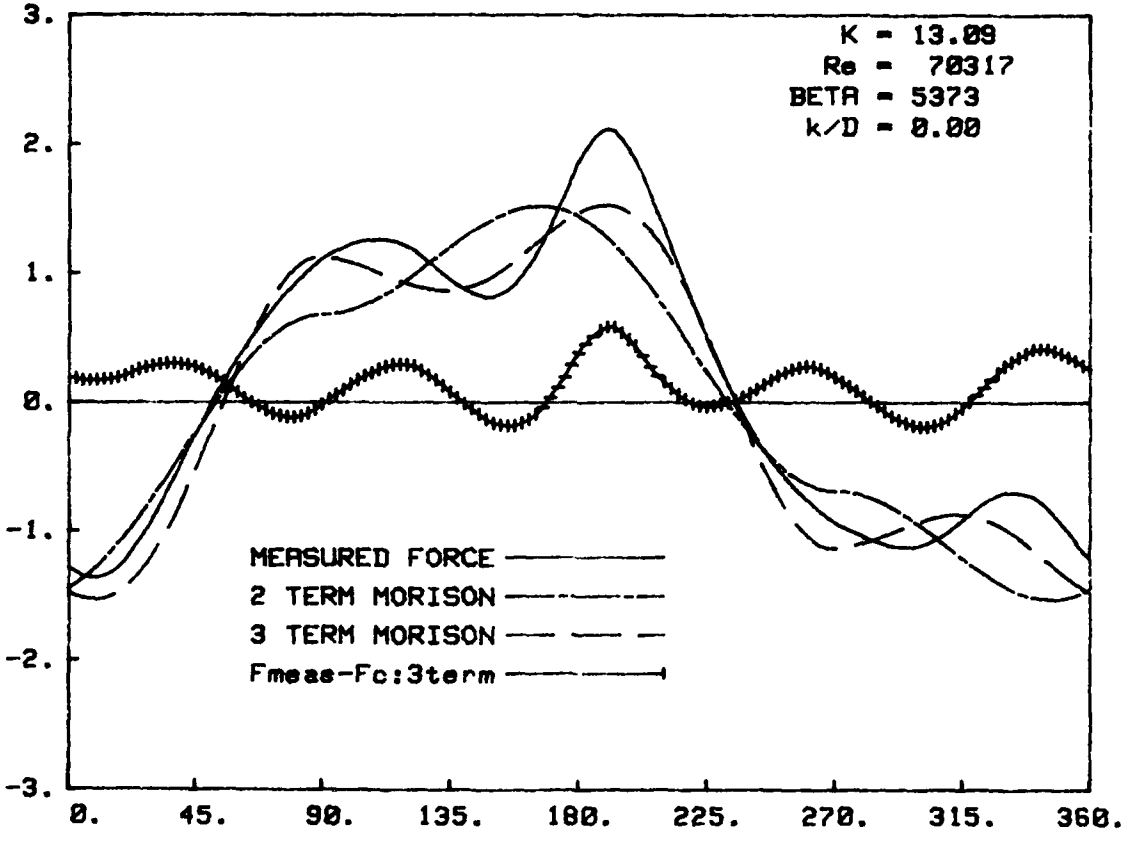

Fig. 42b Comparison of measured and calculated forces (Three-term MOJS Eq.)
K = 13.09

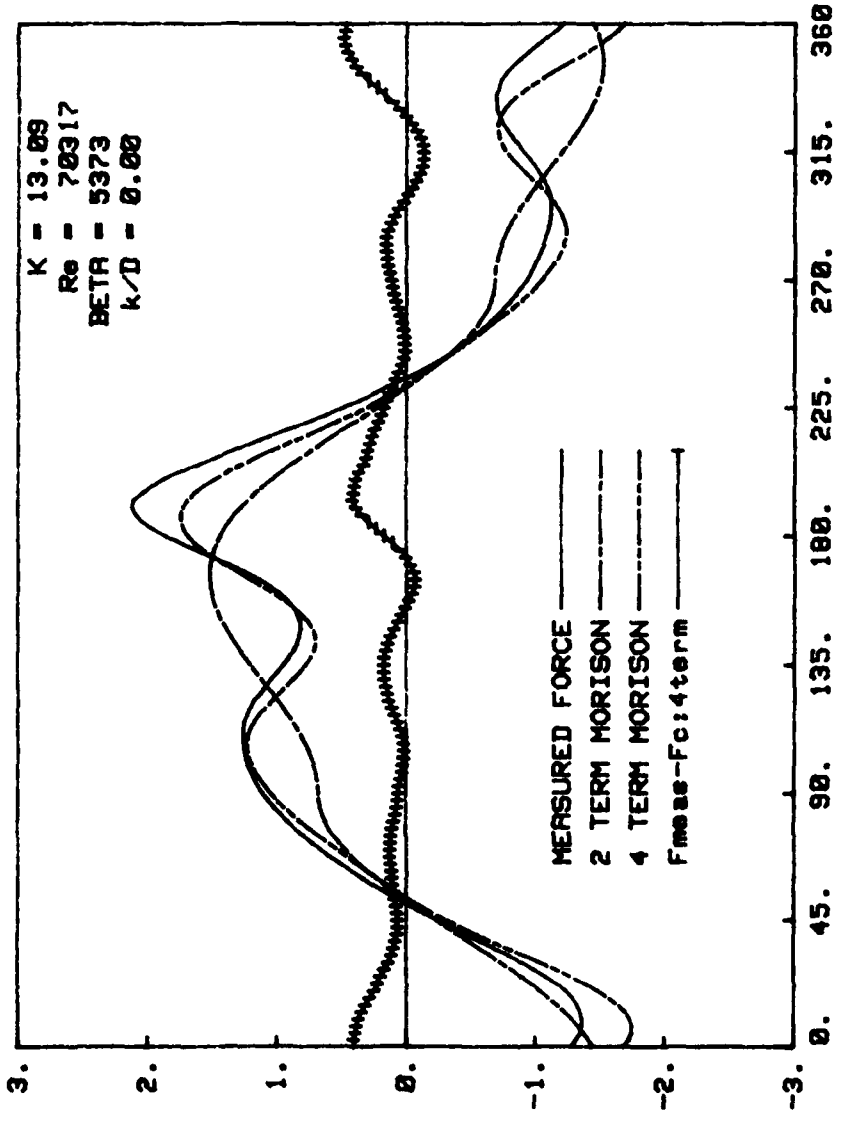

Fig. 42c Comparison of measured and calculated forces (Four-term MOJS Eq.)
K = 13.09

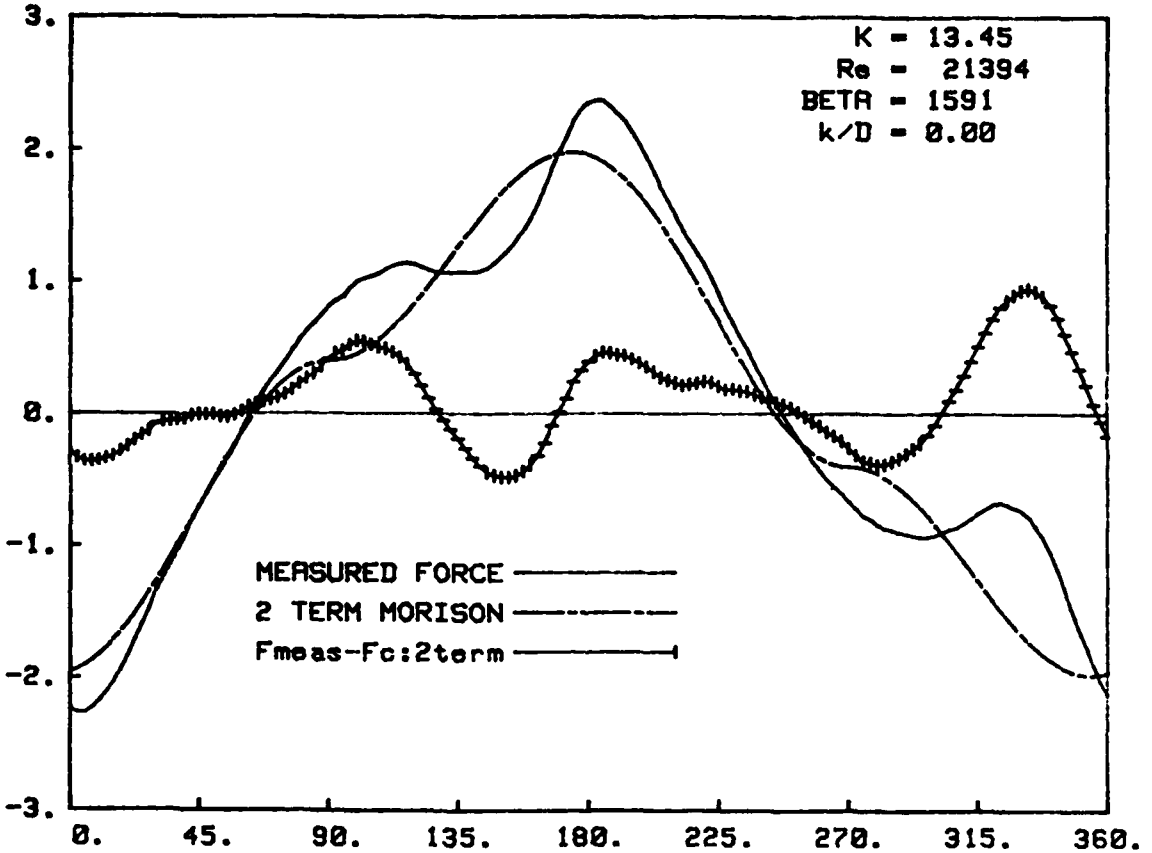

Fig. 43a Comparison of measured and calculated forces (Two-term MOJS Eq.)
K = 13.45

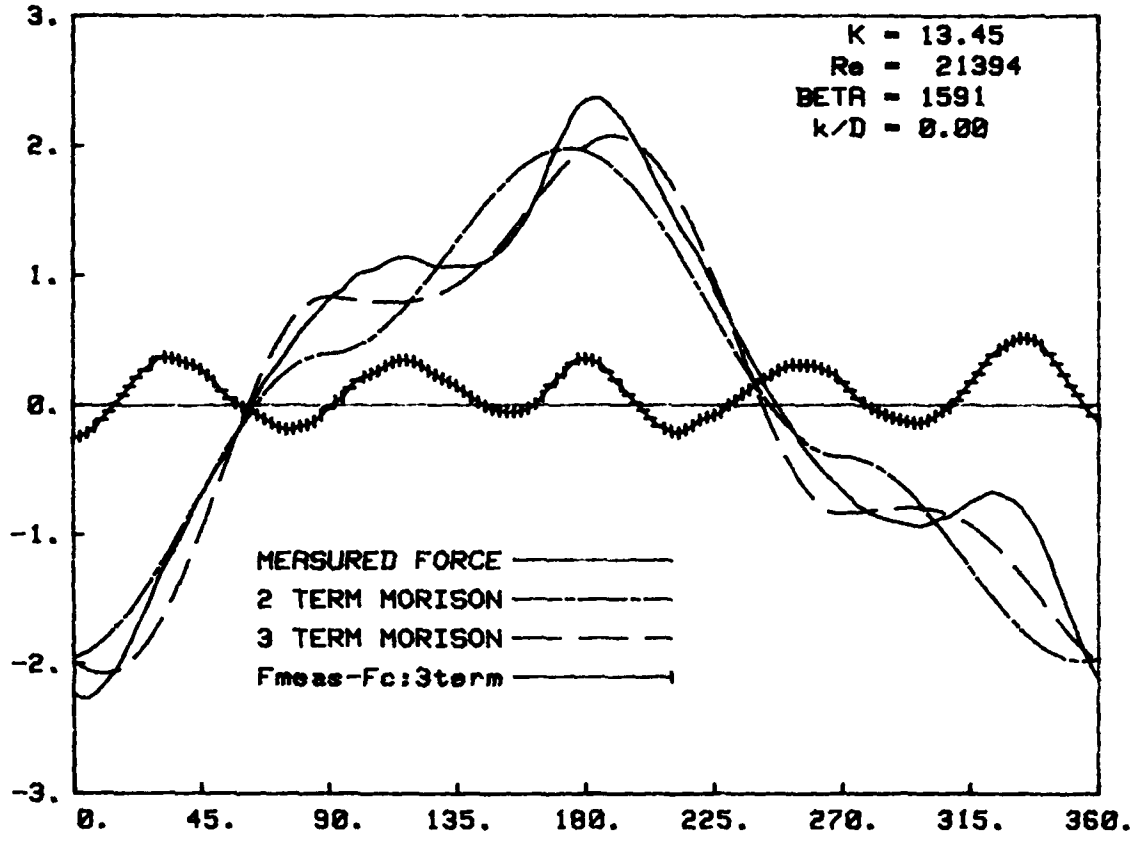

Fig. 43b Comparison of measured and calculated forces (Three-term MOJS Eq.)
K = 13.45

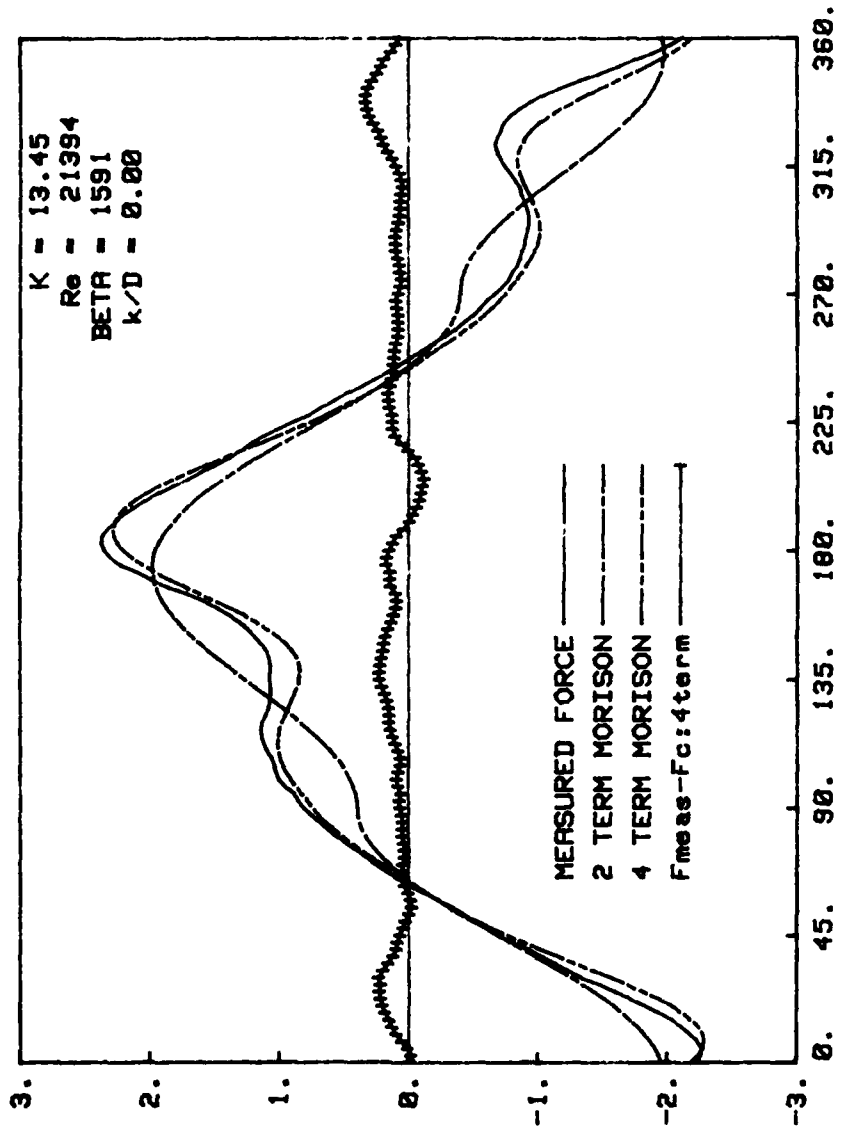

Fig. 43c Comparison of measured and calculated forces (Four-term MOJS Eq.)
K = 13.45

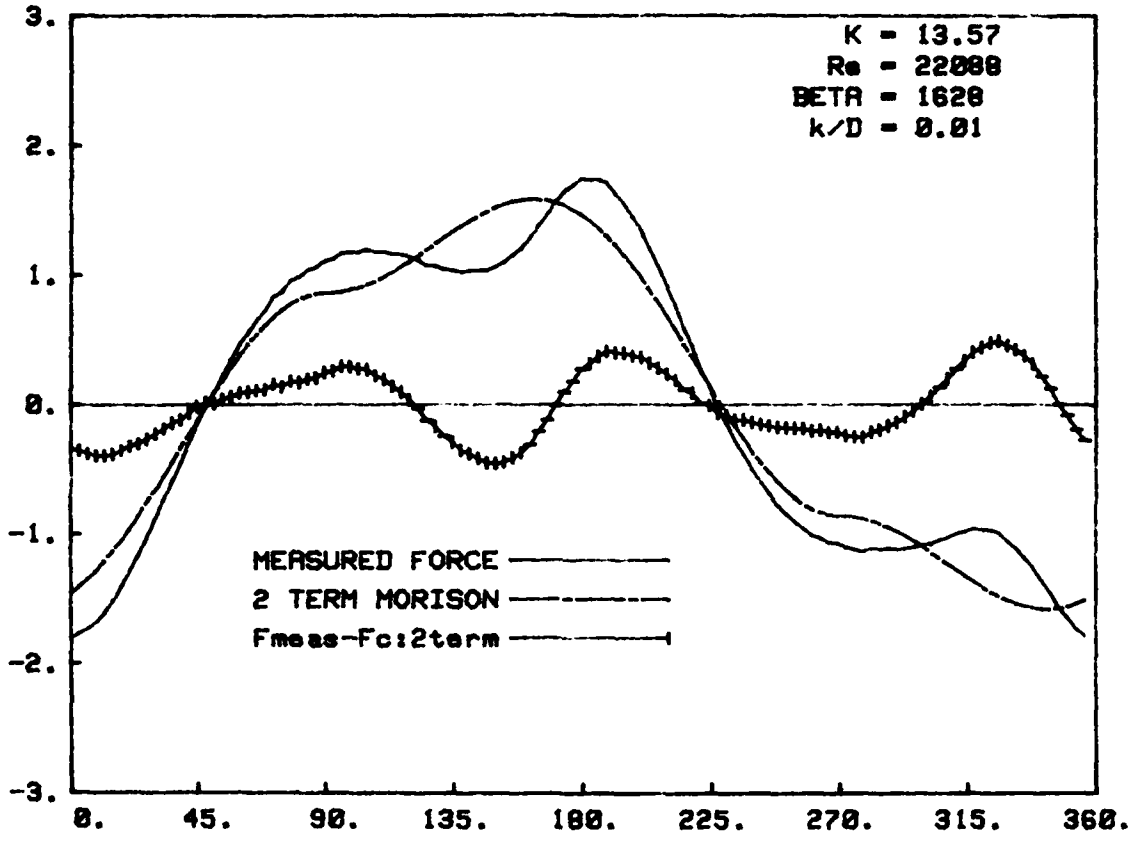

Fig. 44a Comparison of measured and calculated forces (Two-term MOJS Eq.)
K = 13.57

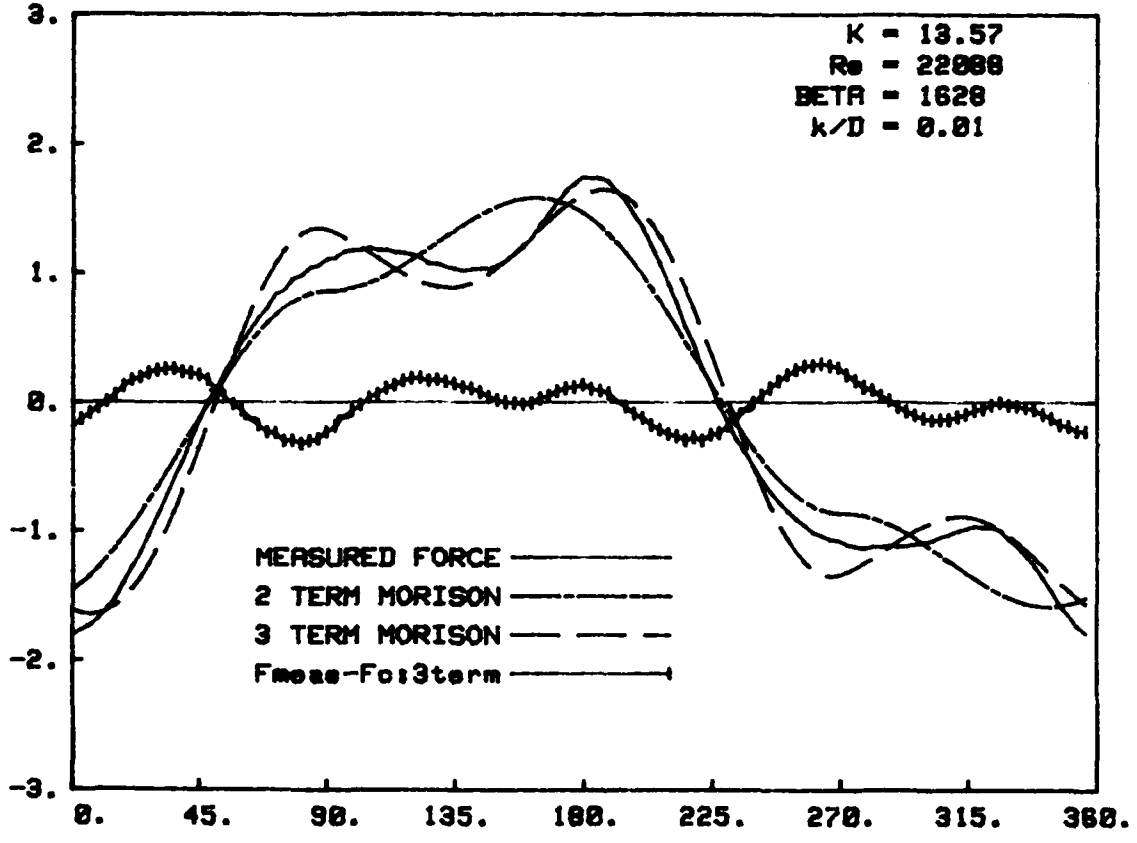

Fig. 44b Comparison of measured and calculated forces (Three-term MOJS Eq.)
K = 13.57

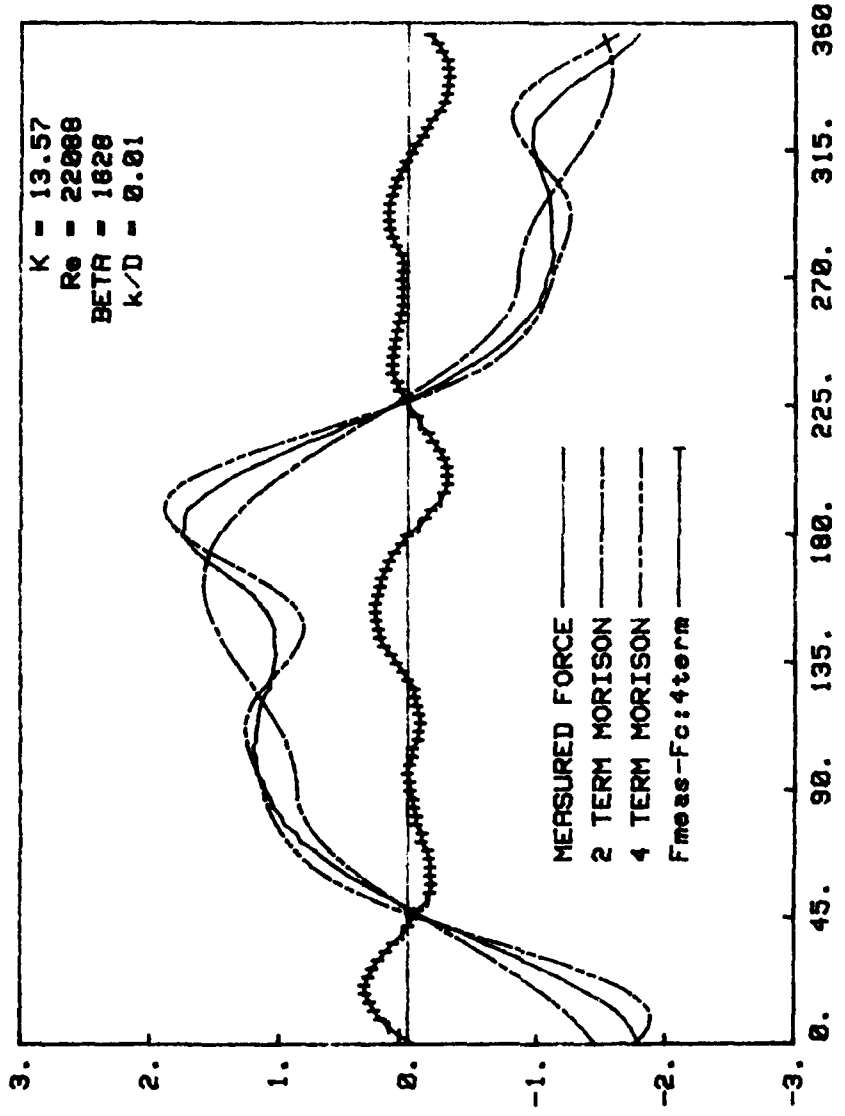

Fig. 44c Comparison of measured and calculated forces (Four-term MOJS Eq.)
K = 13.57

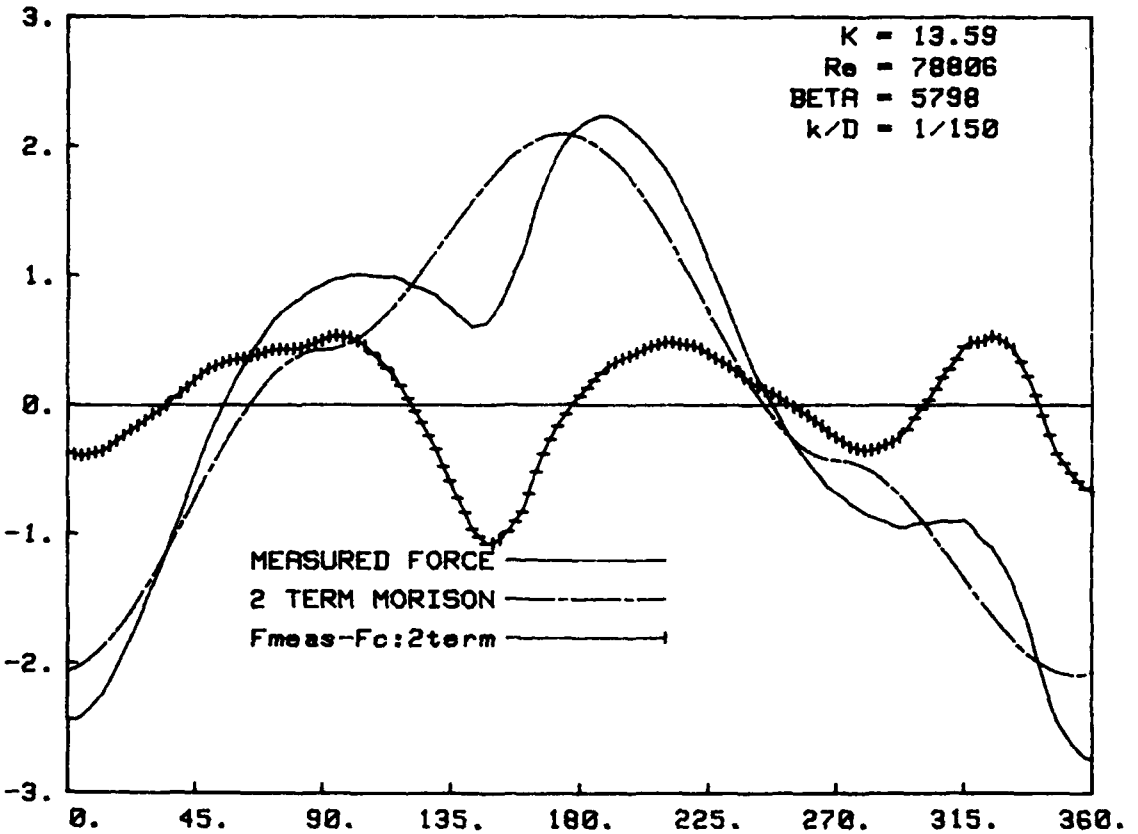

Fig. 45a Comparison of measured and calculated forces (Two-term MOJS Eq.)
K = 13.59

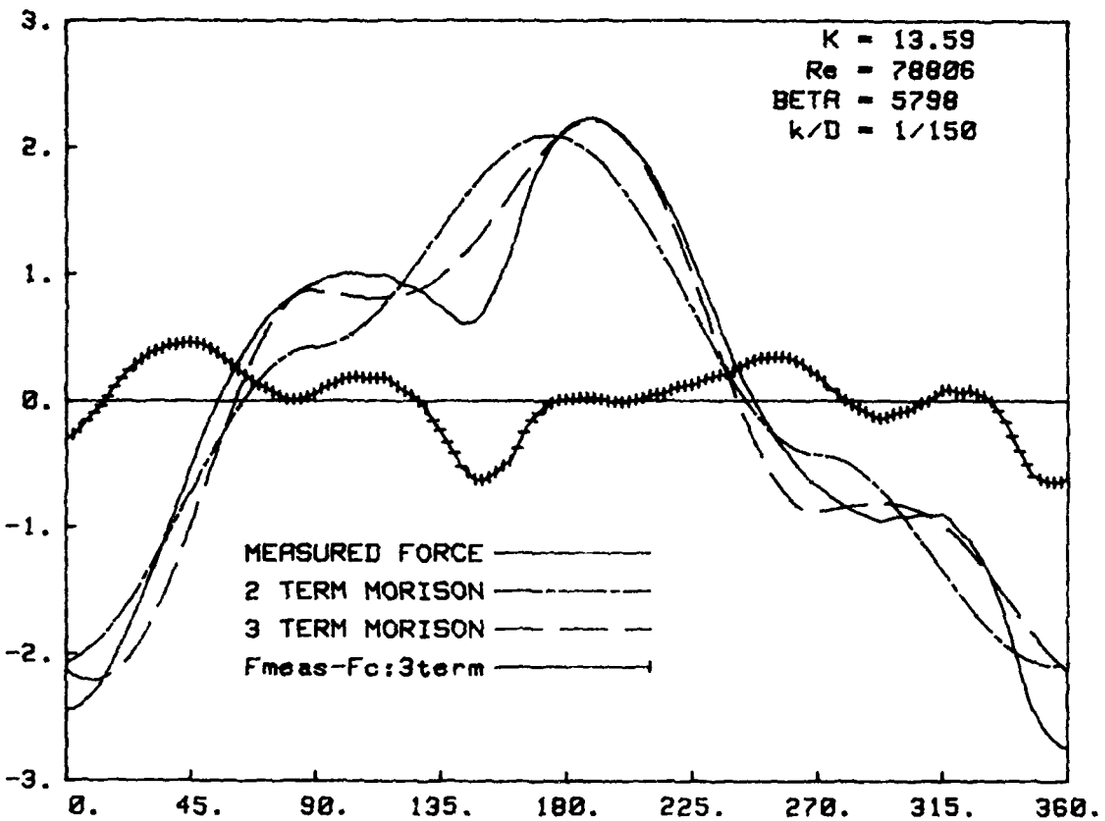

Fig. 45b Comparison of measured and calculated forces (Three-term MOJS Eq.)
K = 13.59

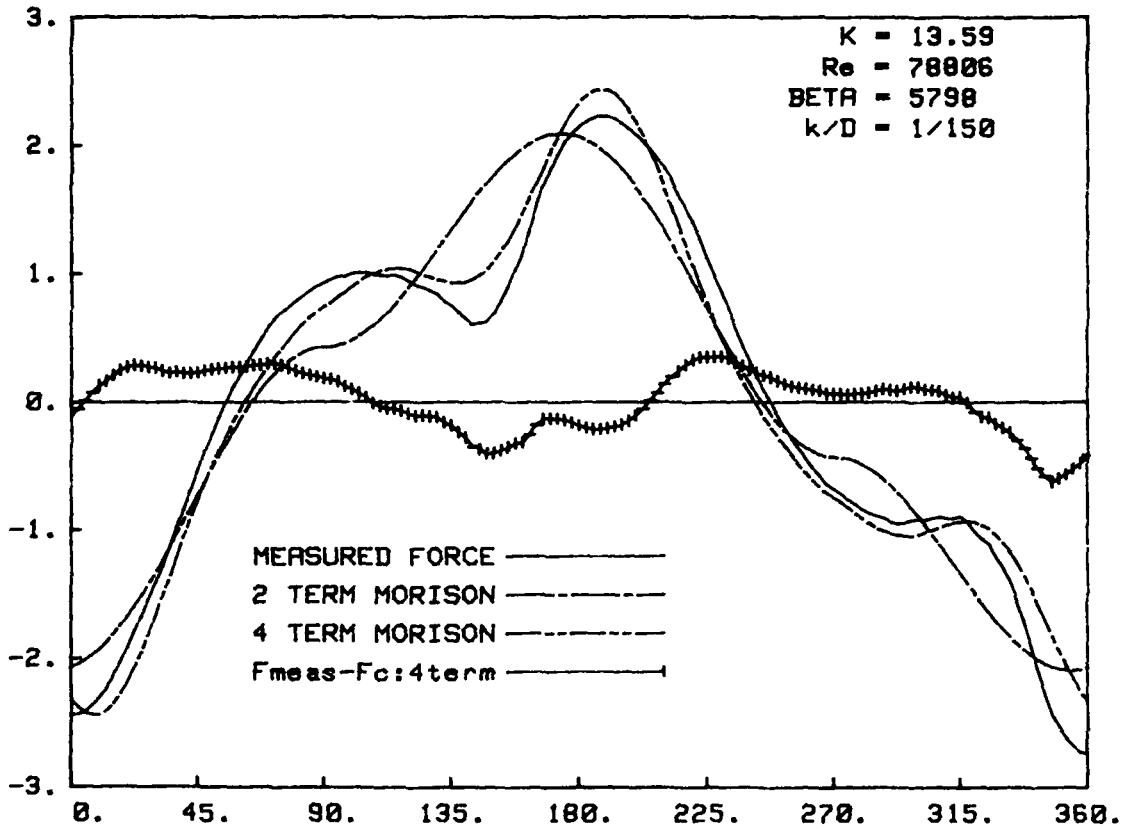

Fig. 45c Comparison of measured and calculated forces (Four-term MOJS Eq.) K = 13.59

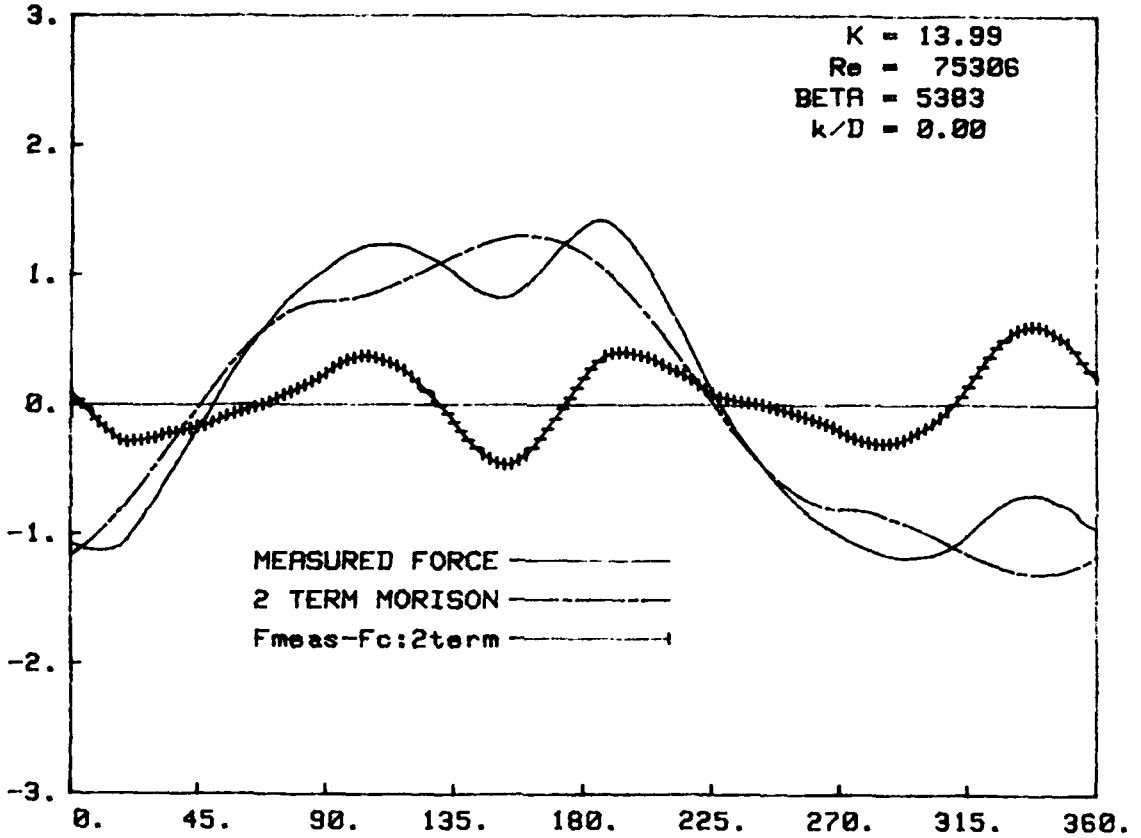

Fig. 46a Comparison of measured and calculated forces (Two-term MOJS Eq.)
K = 13.99

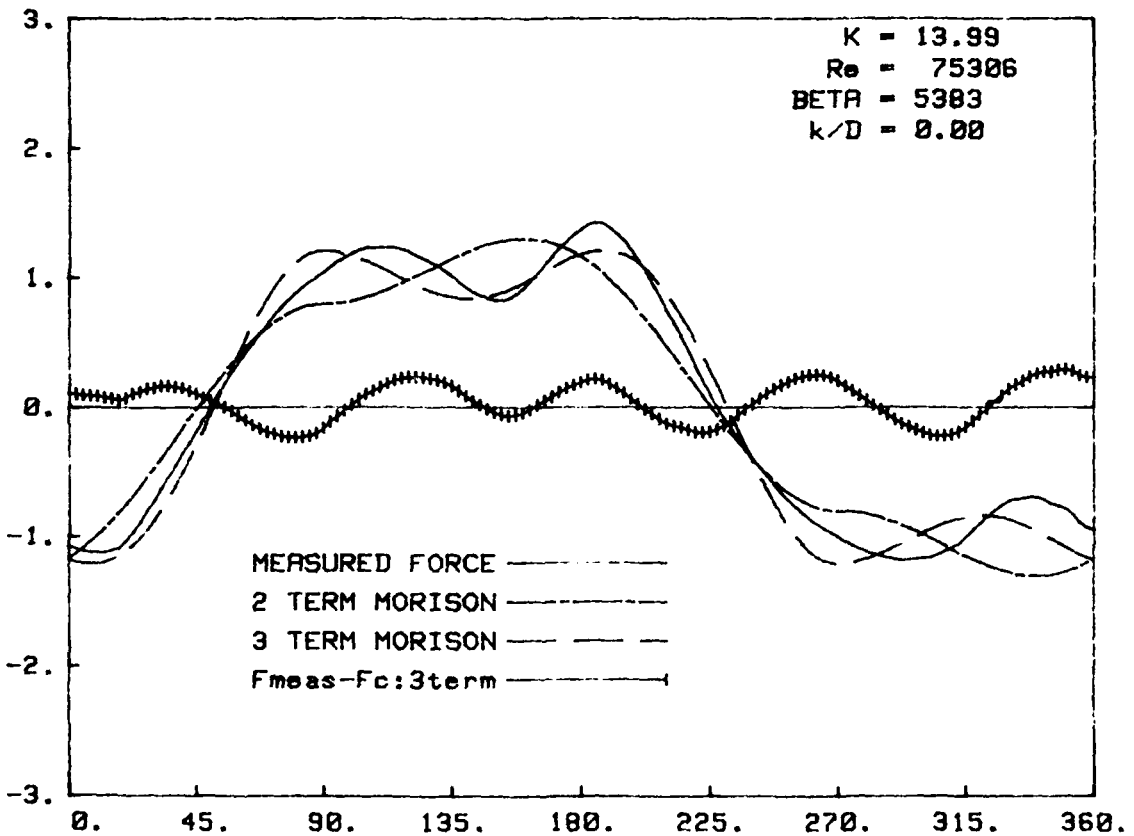

Fig. 46b Comparison of measured and calculated forces (Three-term MOJS Eq.)
K = 13.99

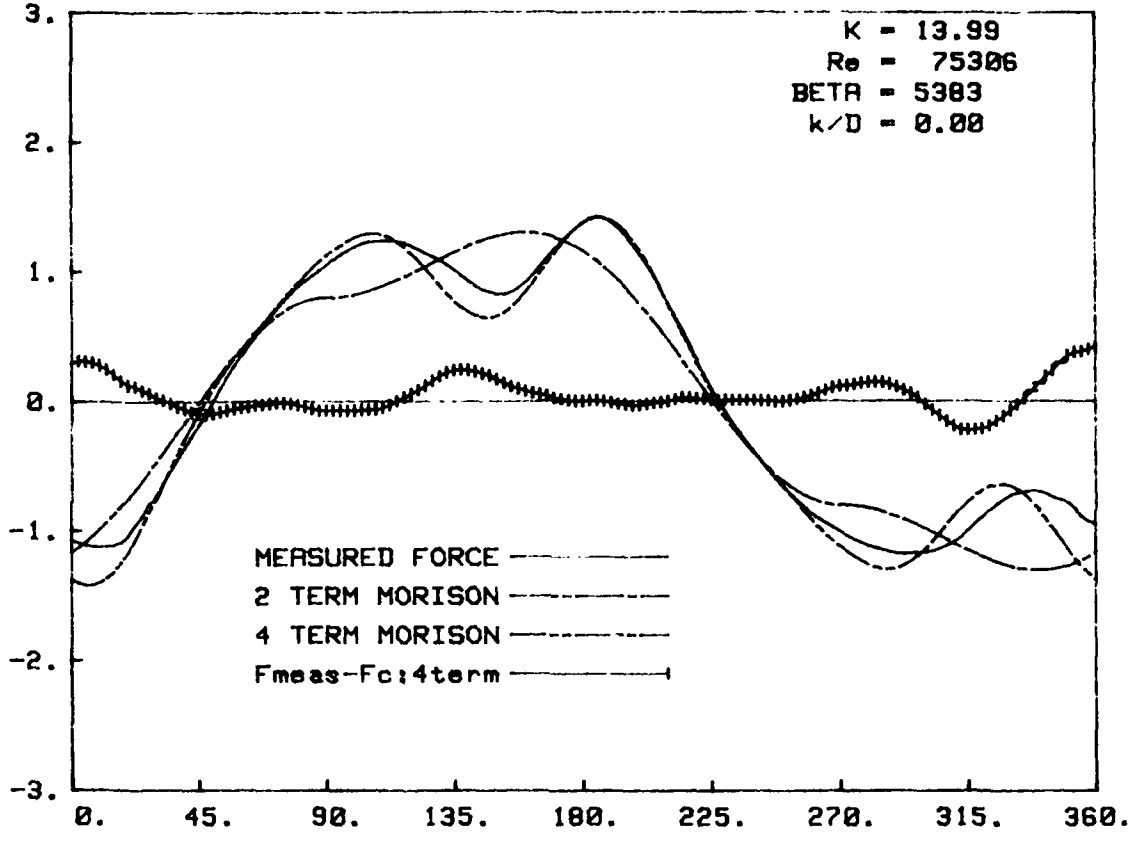

Fig. 46c Comparison of measured and calculated forces (Four-term MOJS Eq.)
K = 13.99

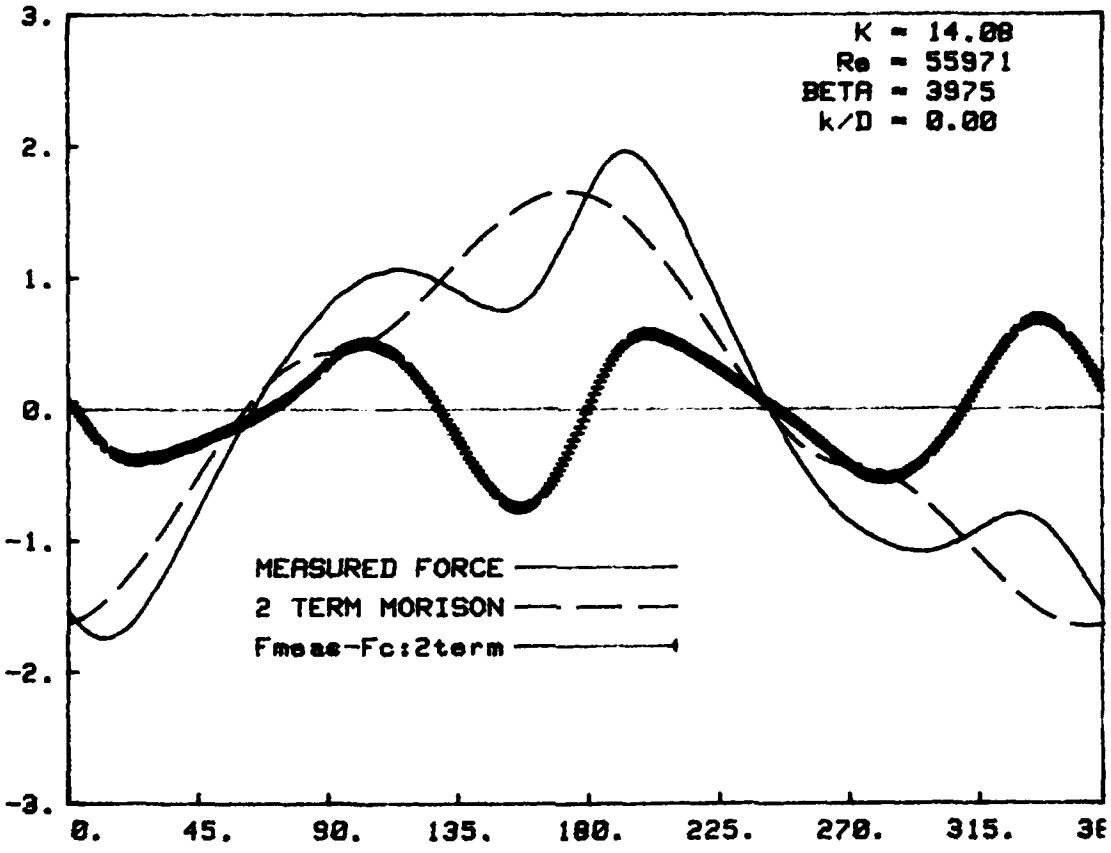

Fig. 47a Comparison of measured and calculated forces (Two-term MOJS Eq.)
K = 14.08

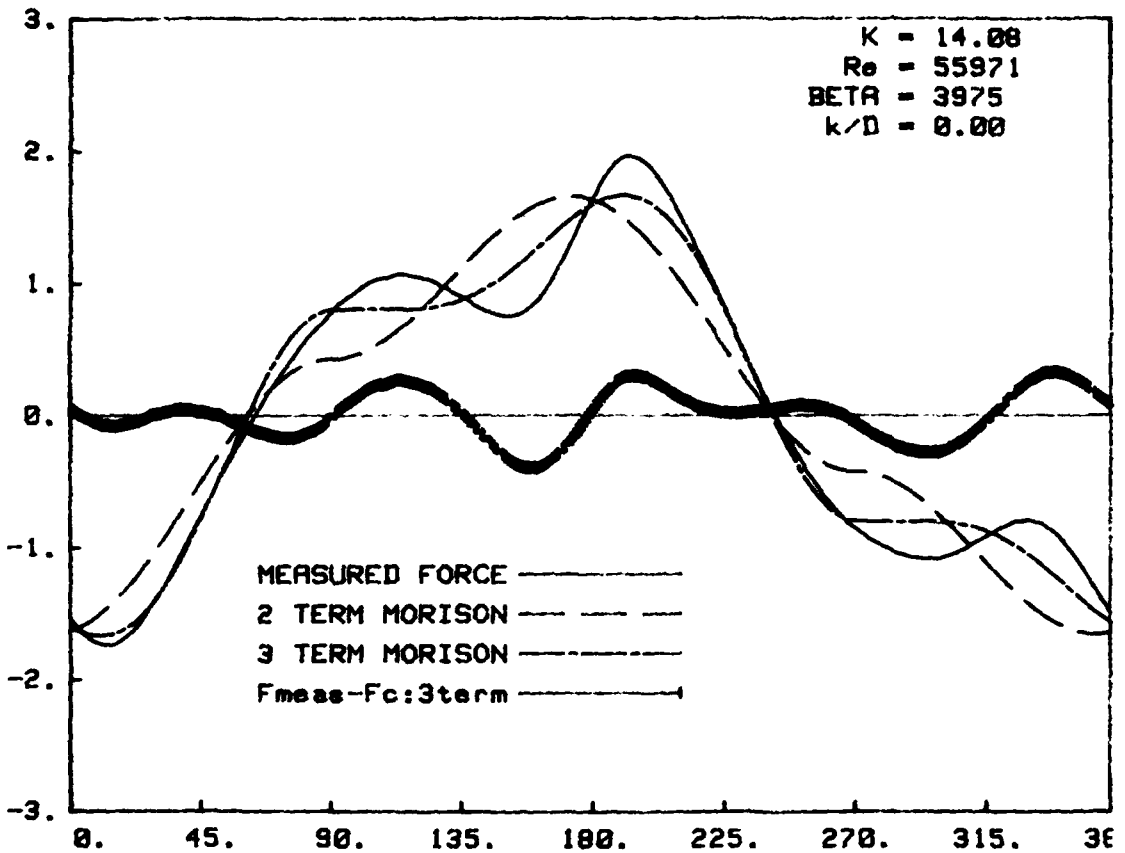

Fig. 47b Comparison of measured and calculated forces (Three-term MOJS Eq.)
K = 14.08

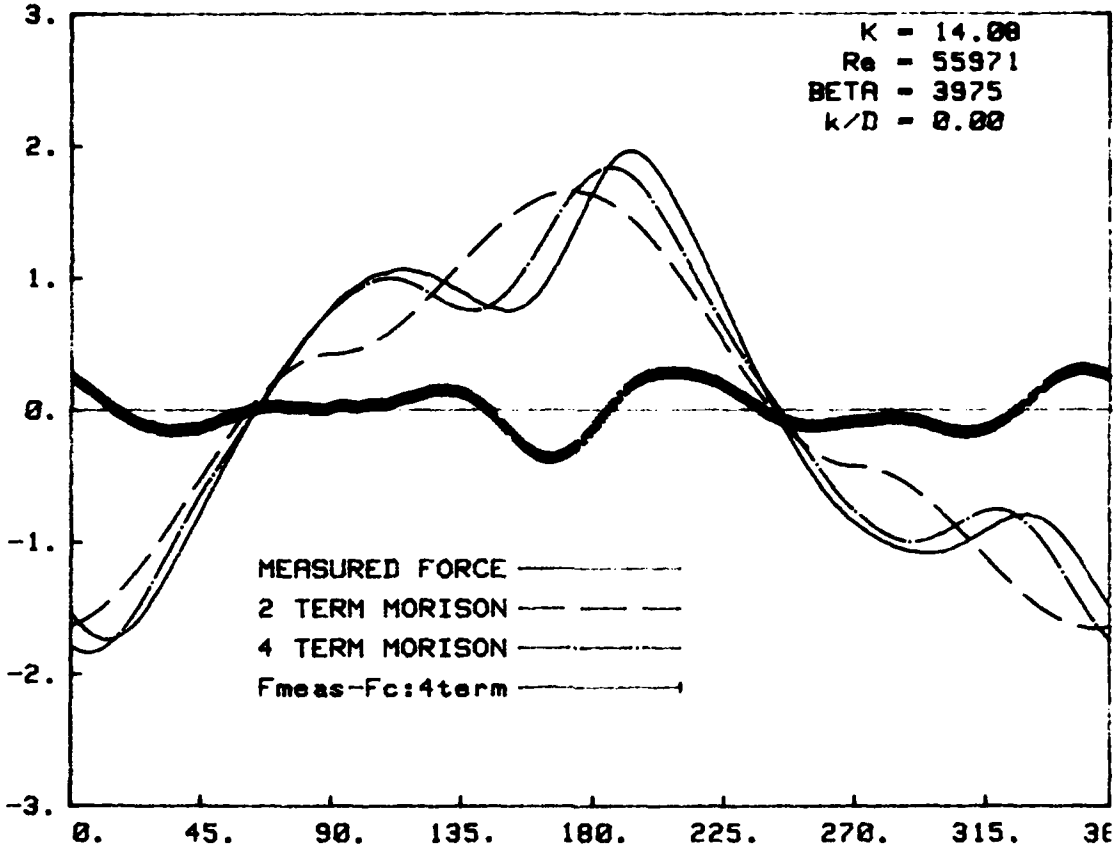

Fig. 47c Comparison of measured and calculated forces (Four-term MOJS Eq.)
K = 14.08

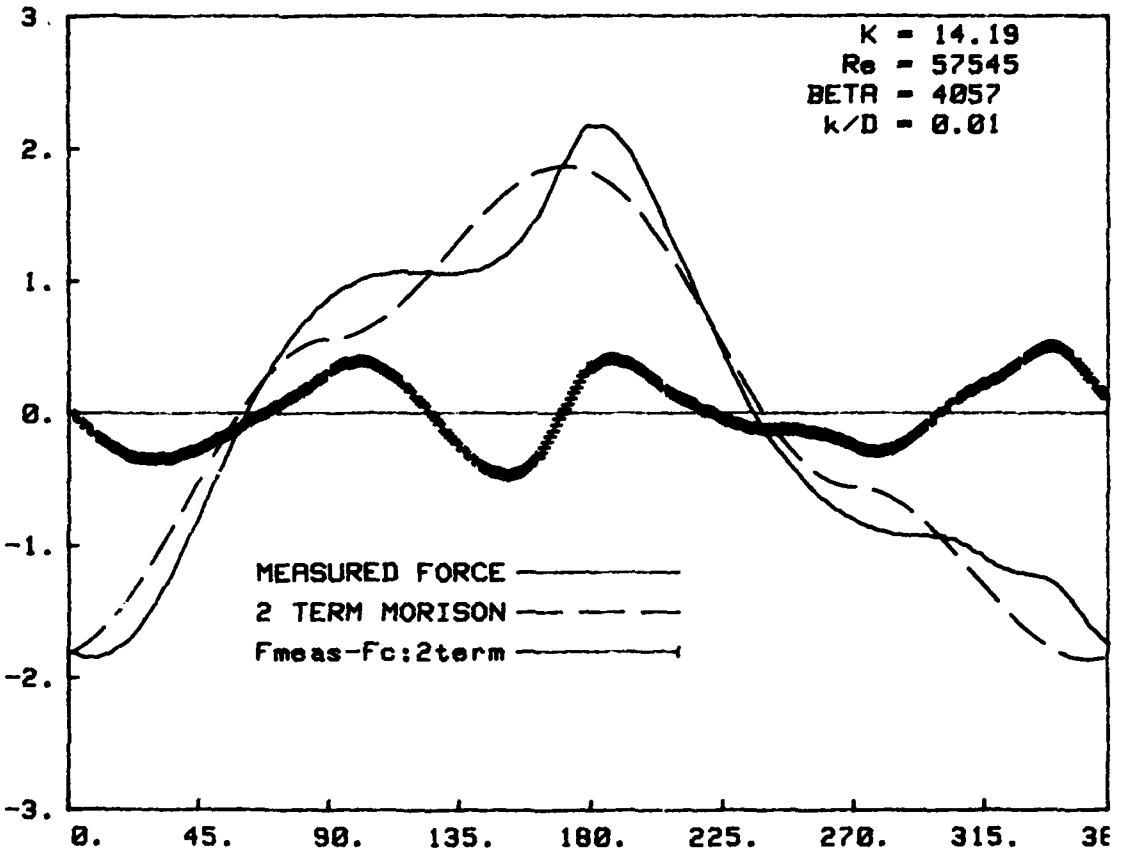

Fig. 48a Comparison of measured and calculated forces (Two-term MOJS Eq.)
K = 14.19

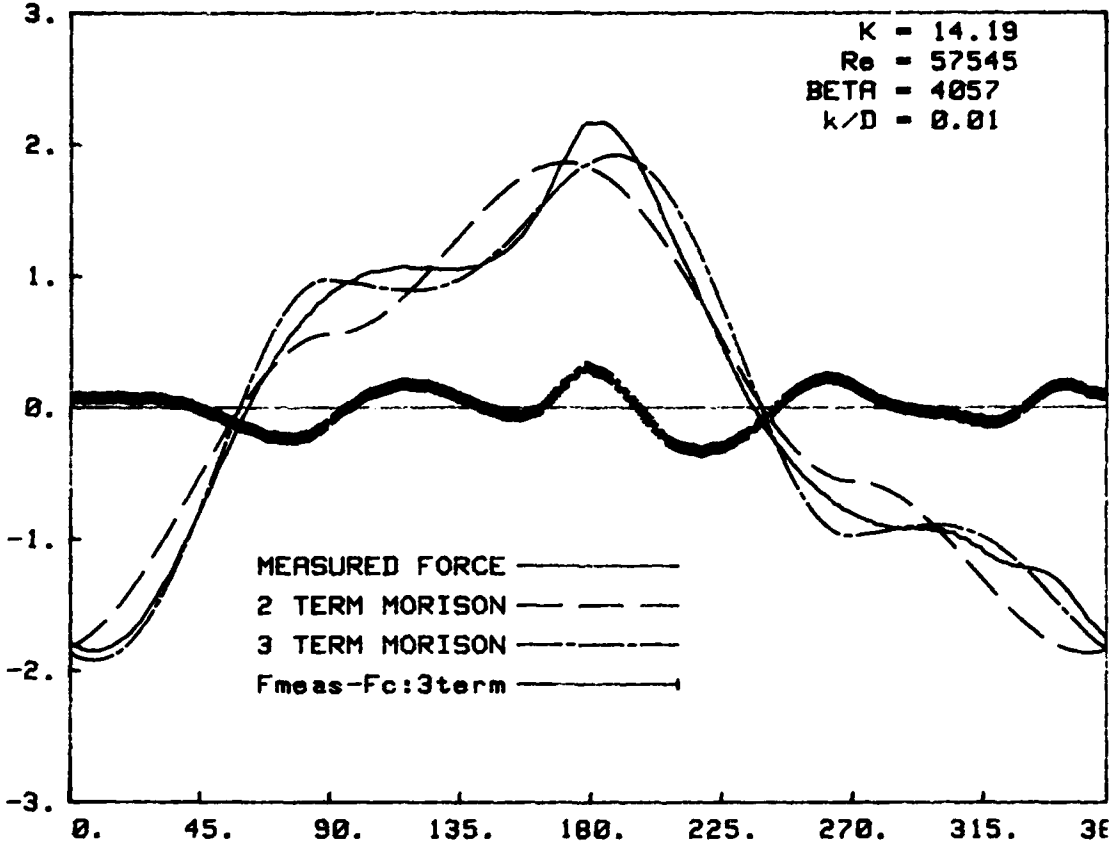

Fig. 48b Comparison of measured and calculated forces (Three-term MOJS Eq.)
K = 14.19

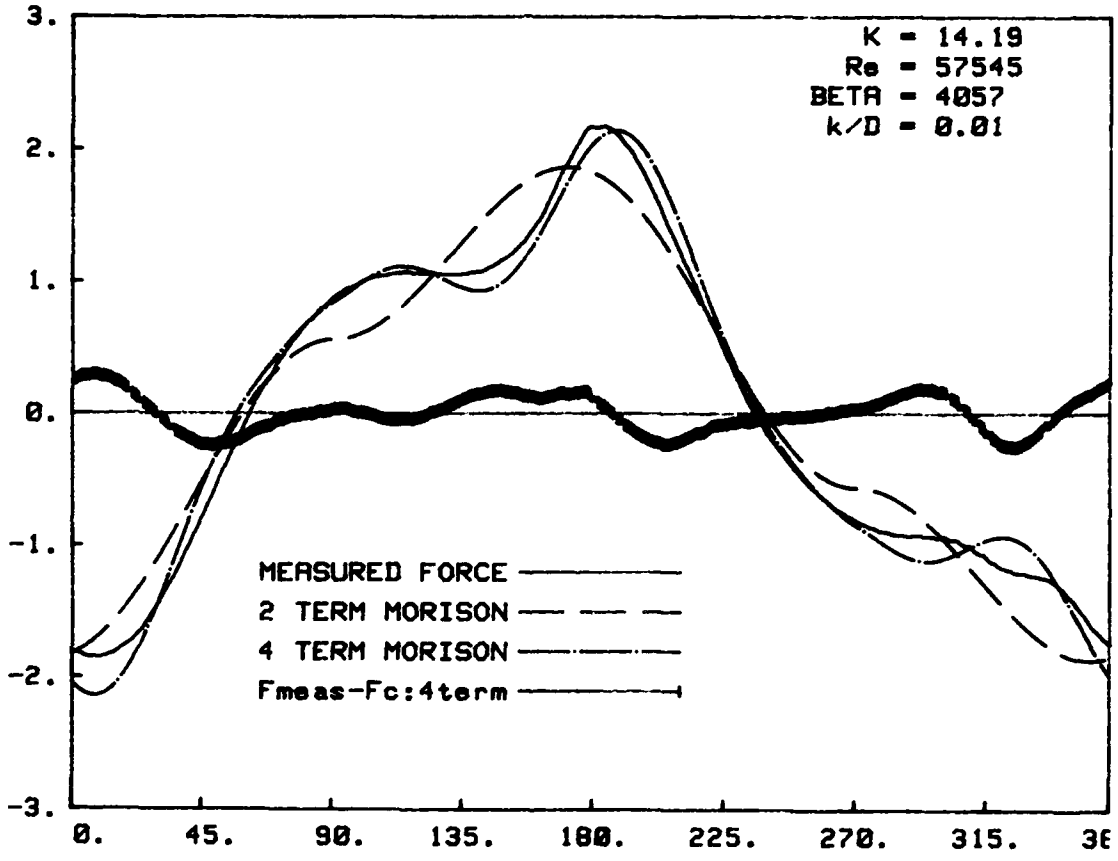

Fig. 48c Comparison of measured and calculated forces (Four-term MOJS Eq.)
K = 14.19

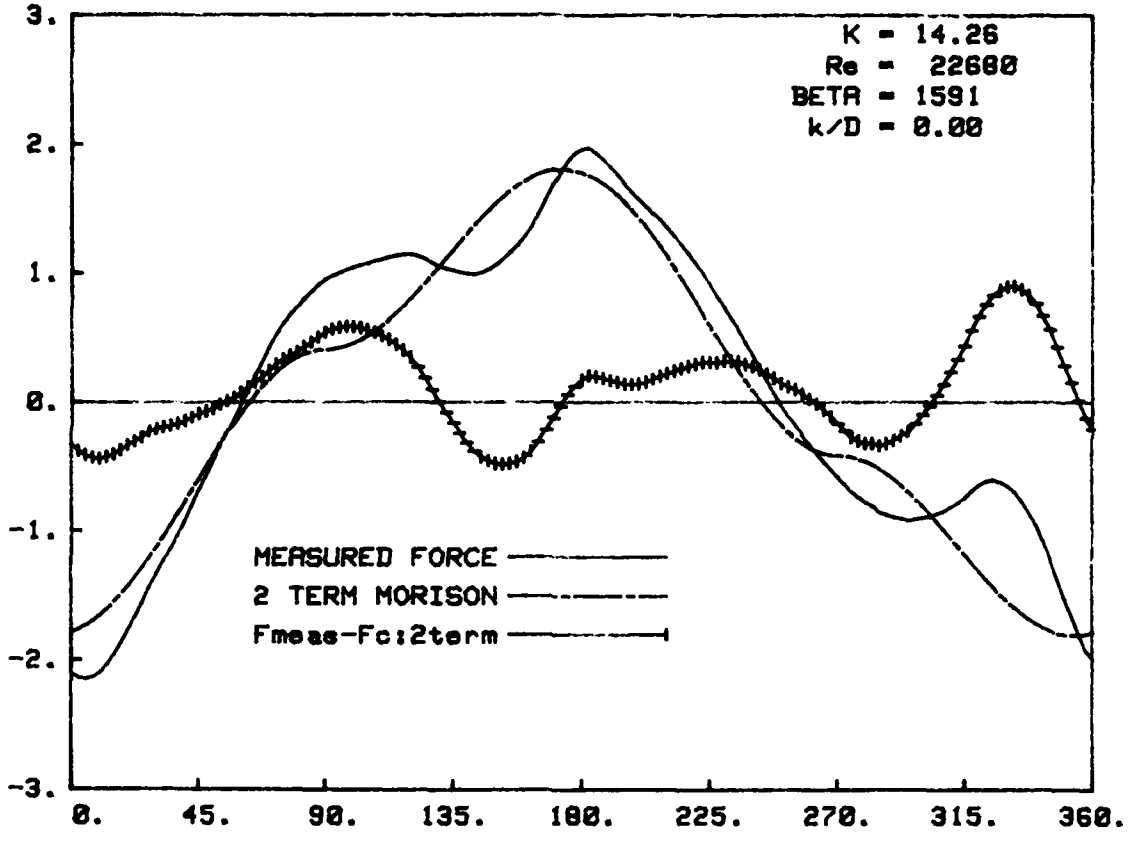

Fig. 49a Comparison of measured and calculated forces (Two-term MOJS Eq.)
K = 14.26, Re = 22680

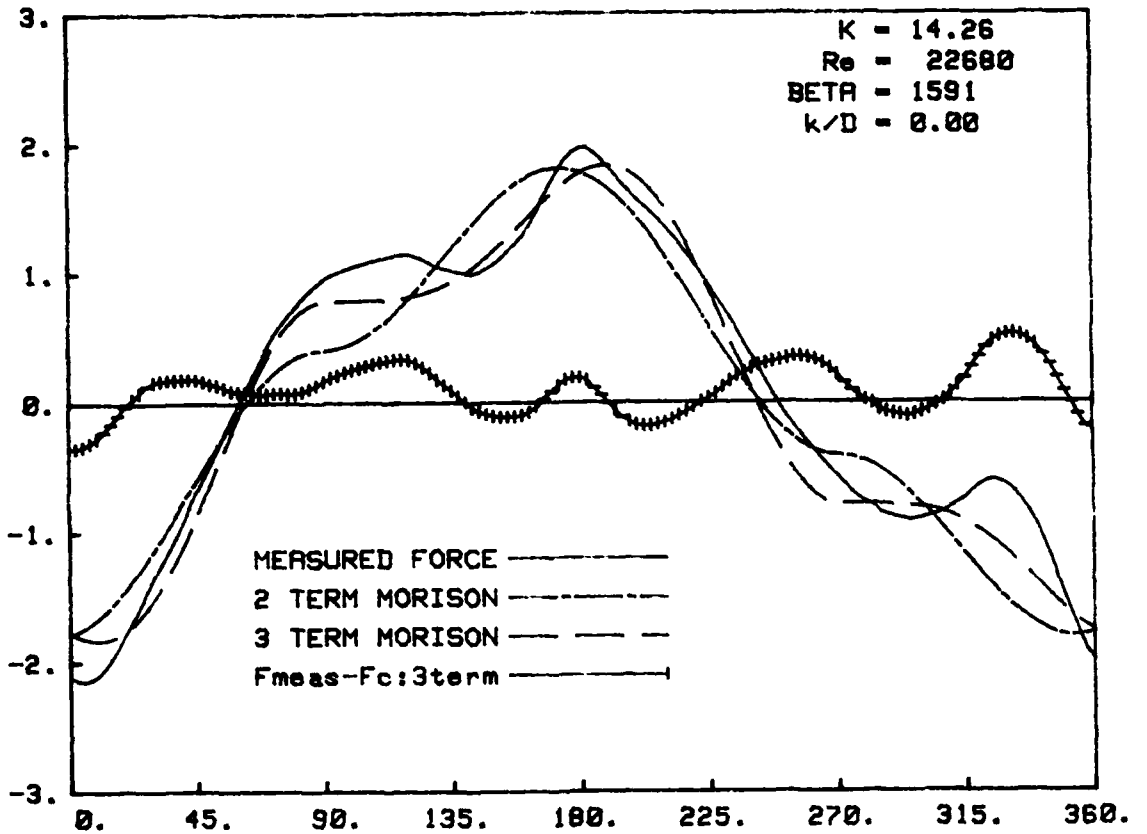

Fig. 49b Comparison of measured and calculated forces (Three-term MOJS Eq.)
K = 14.26, Re = 22680

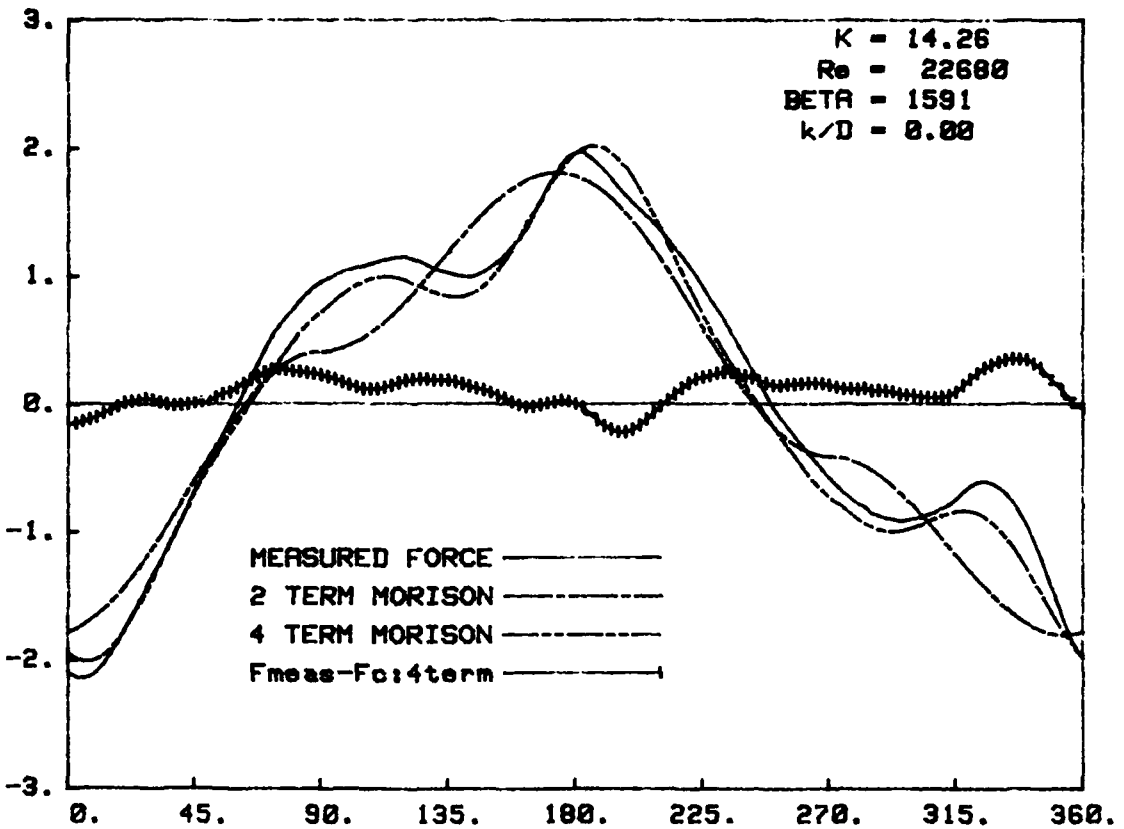

Fig. 49c Comparison of measured nd calculated forces (Four-term MOJS Eq.)
K = 14.26, Re = 22680

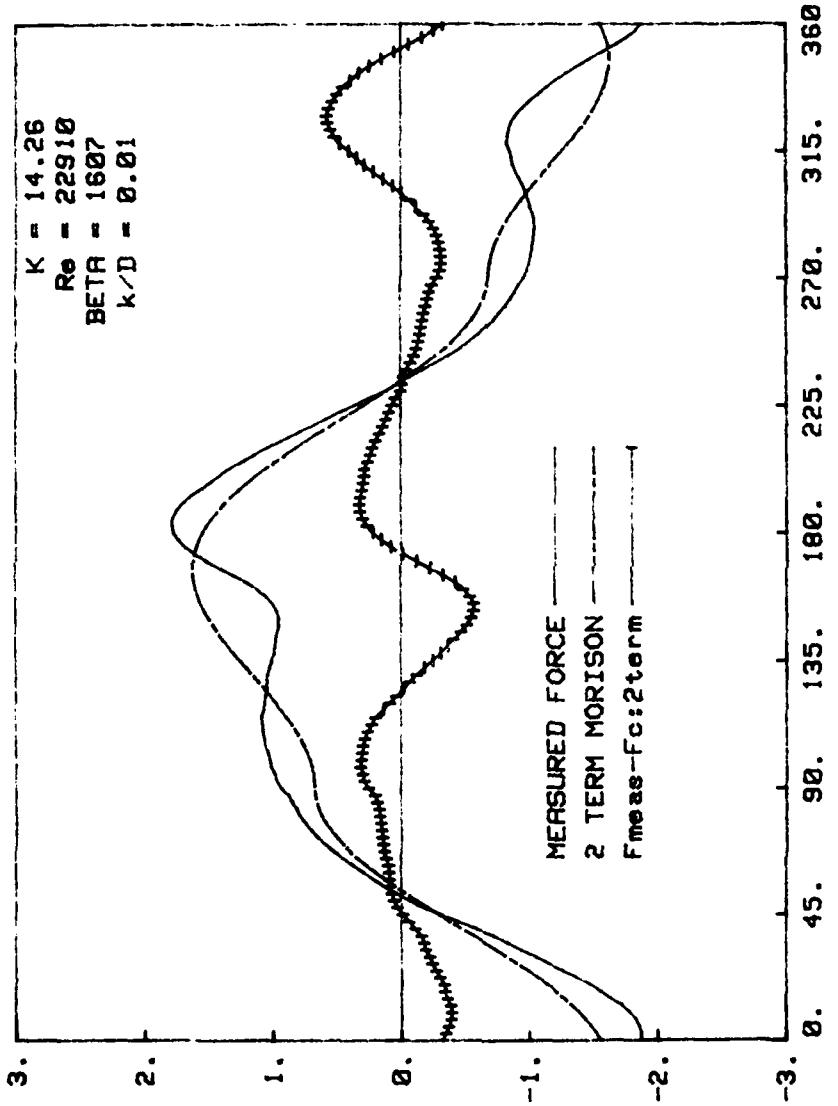

Fig. 50a Comparison of measured and calculated forces (Two-term MOJS Eq.)
K = 14.26, Re = 22910

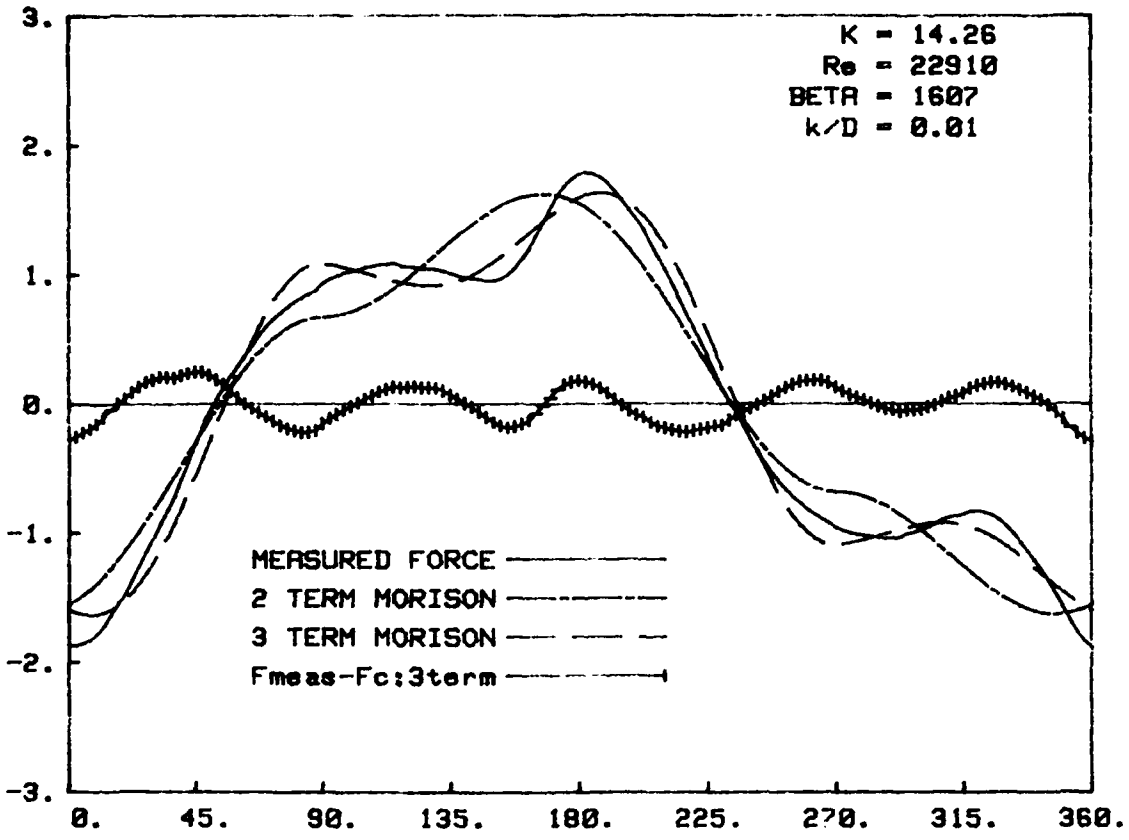

Fig. 50b Comparison of measured and calculated forces (Three-term MOJS Eq.)
K = 14.26 , Re = 22910

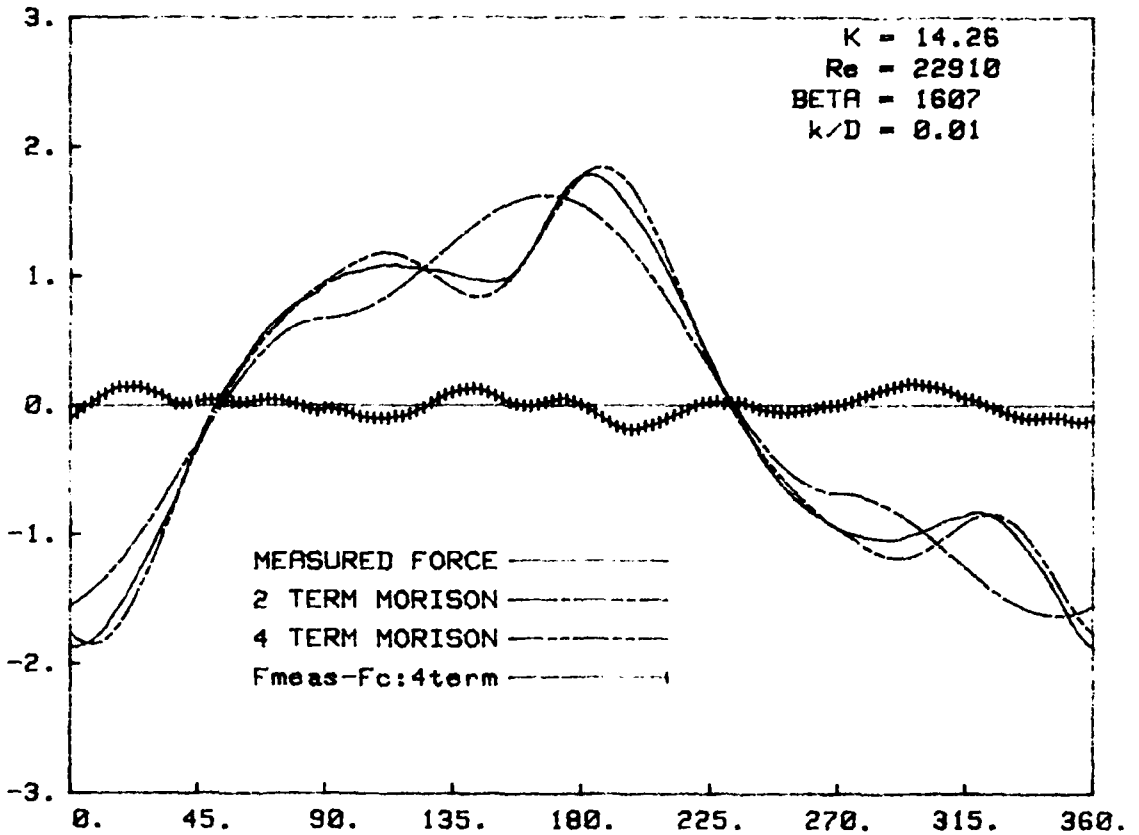

Fig. 50c Comparison of measured and calculated forces (Four-term MOJS Eq.)
K = 14.26 , Re = 22910

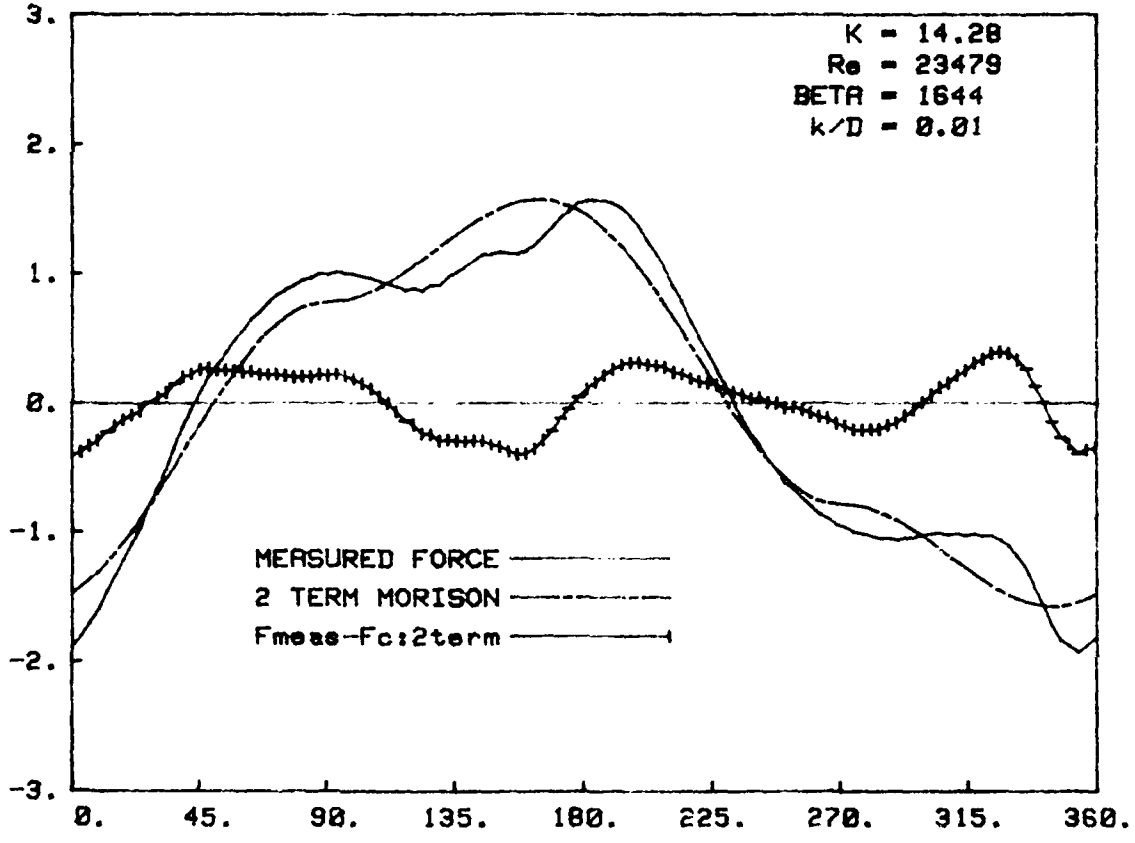

Fig. 51a Comparison of measured and calculated forces (Two-term MOJS Eq.)
K = 14.28

AD-A137 438 MORISON'S EQUATION AND THE WAVE FORCES ON OFFSHORE STRUCTURES(U) SARPKAYA (TURGUT) CARMEL CA T SARPKAYA DEC 81 NCEL-CR-82.008 N68305-80-C-0053 3/3

UNCLASSIFIED F/G 8/3 NL

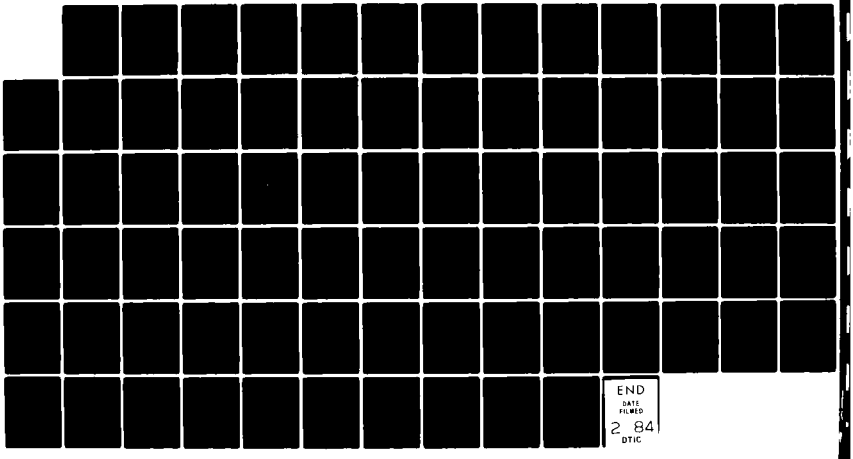

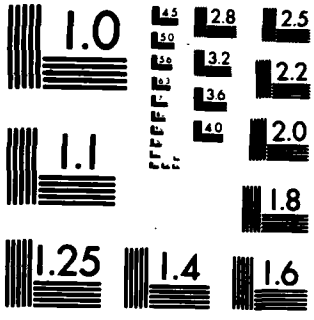

MICROCOPY RESOLUTION TEST CHART
NATIONAL BUREAU OF STANDARDS-1963-A

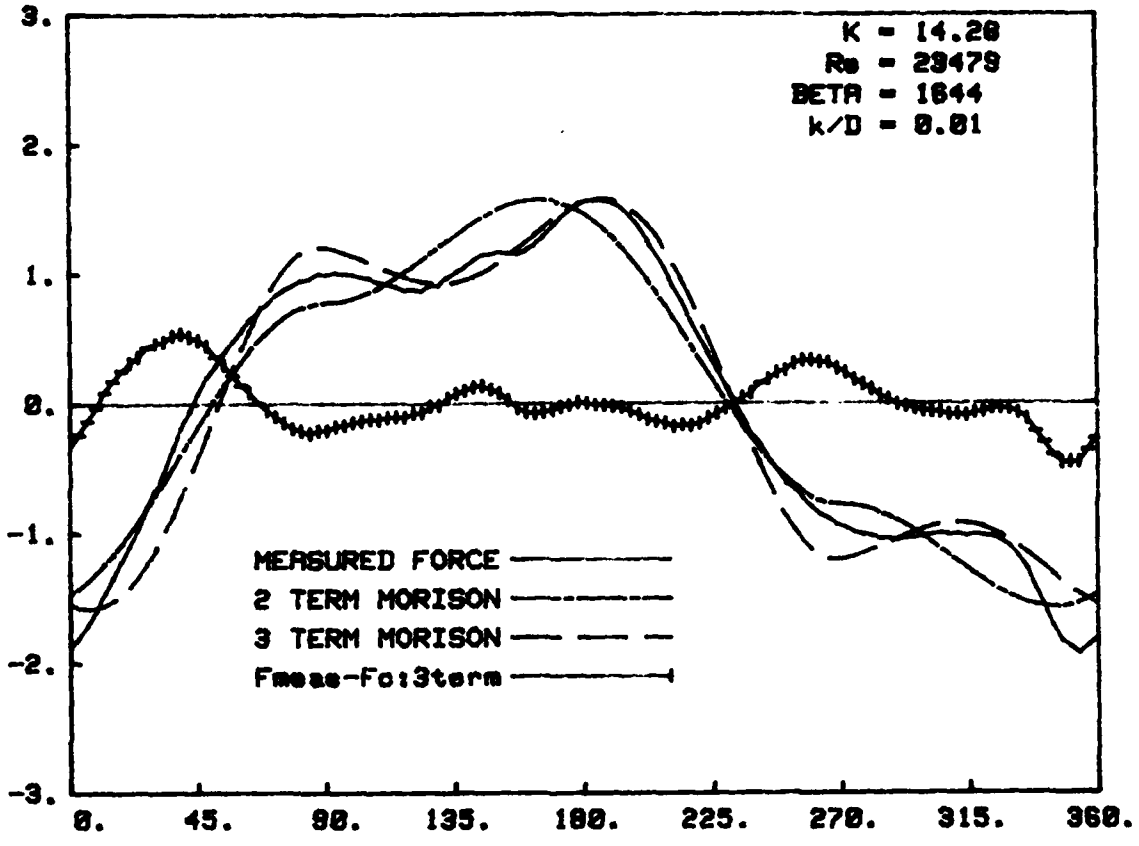

Fig. 51b Comparison of measured and calculated forces (Three-term MOJS Eq.)
K = 14.28

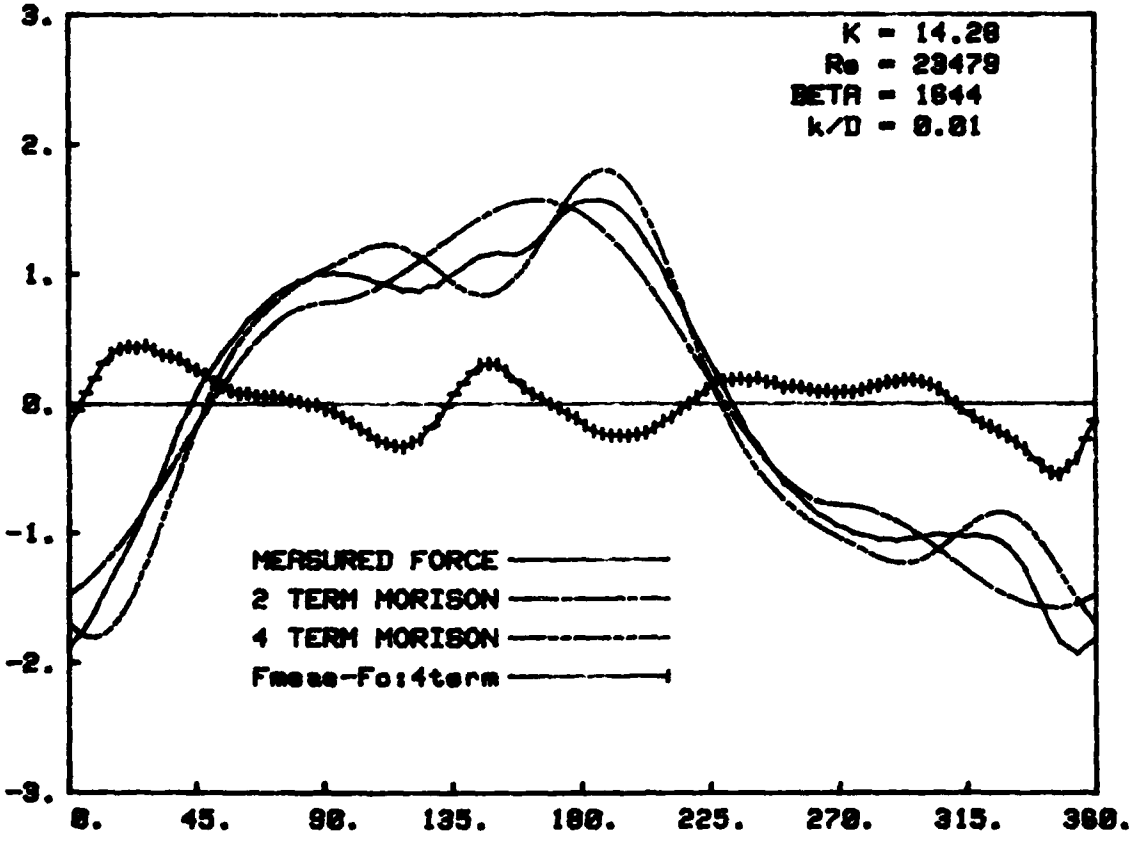

Fig. 51c Comparison of measured and calculated forces (Four-term MOJS Eq.)
K = 14.28

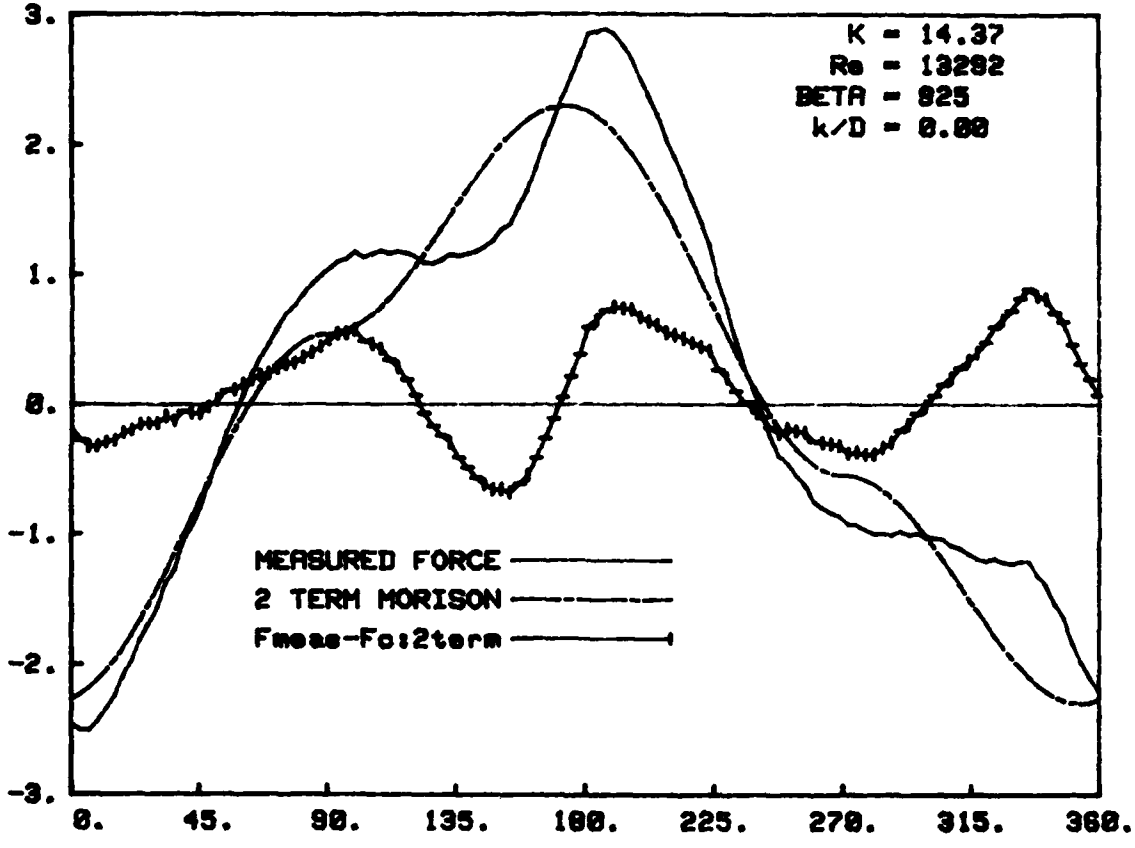

Fig. 52a Comparison of measured and calculated forces (Two-term MOJS Eq.)
K = 14.37

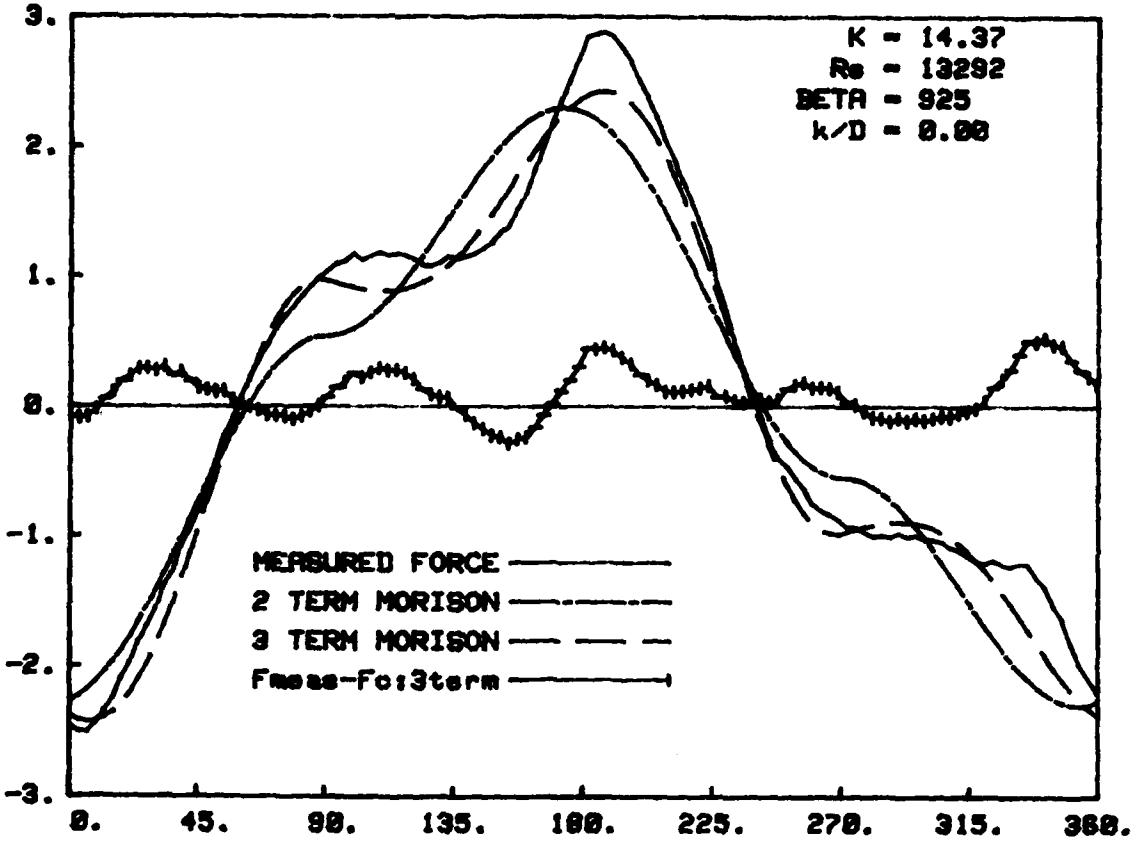

Fig. 52b Comparison of measured and calculated forces (Three-term MOJS Eq.)
K = 14.37

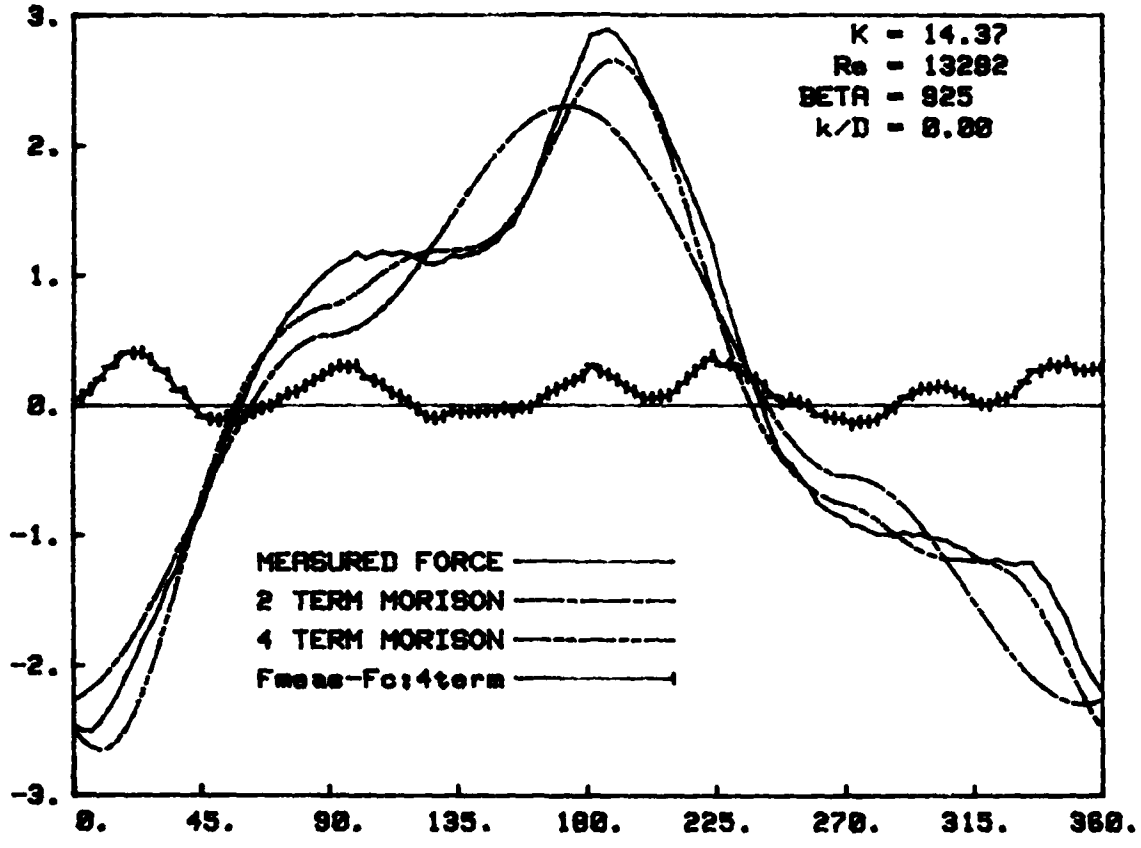

Fig. 52c Comparison of measured and calculated forces (Four-term MOJS Eq.)
K = 14.37

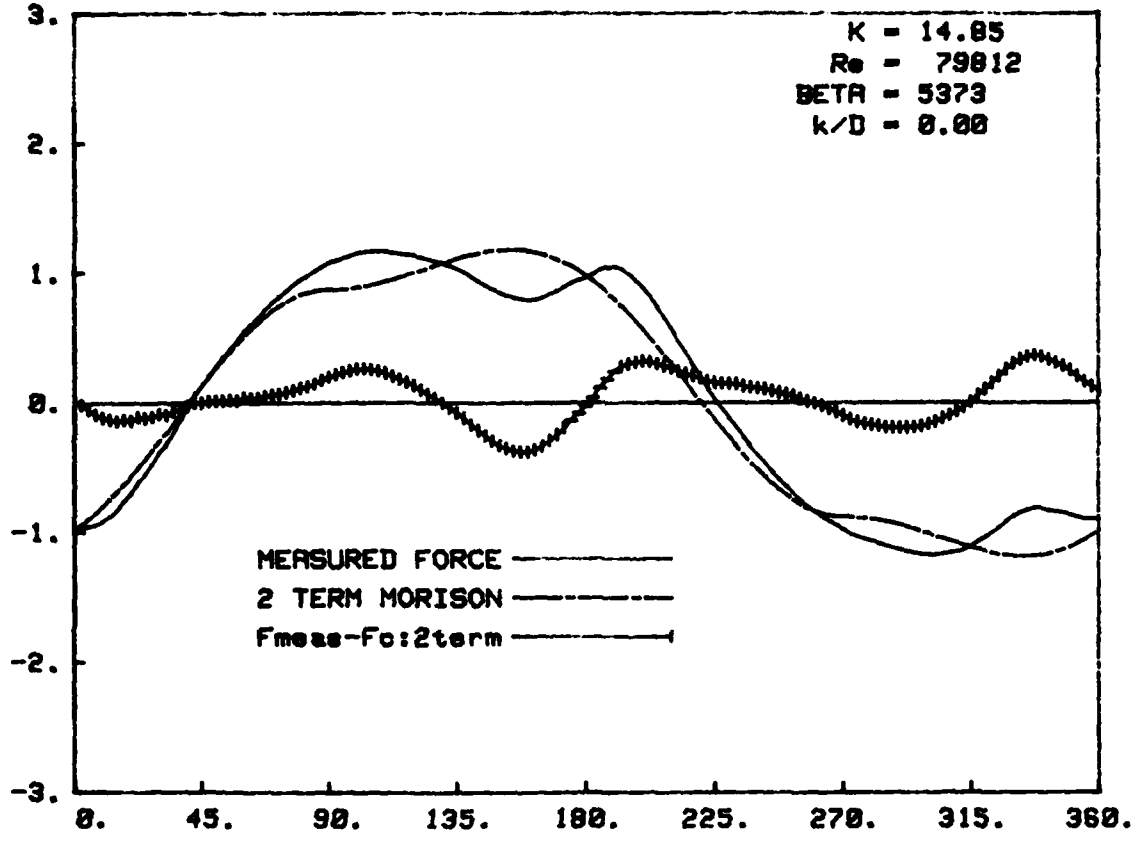

Fig. 53a Comparison of measured and calculated forces (Two-term MOJS Eq.)
K = 14.85

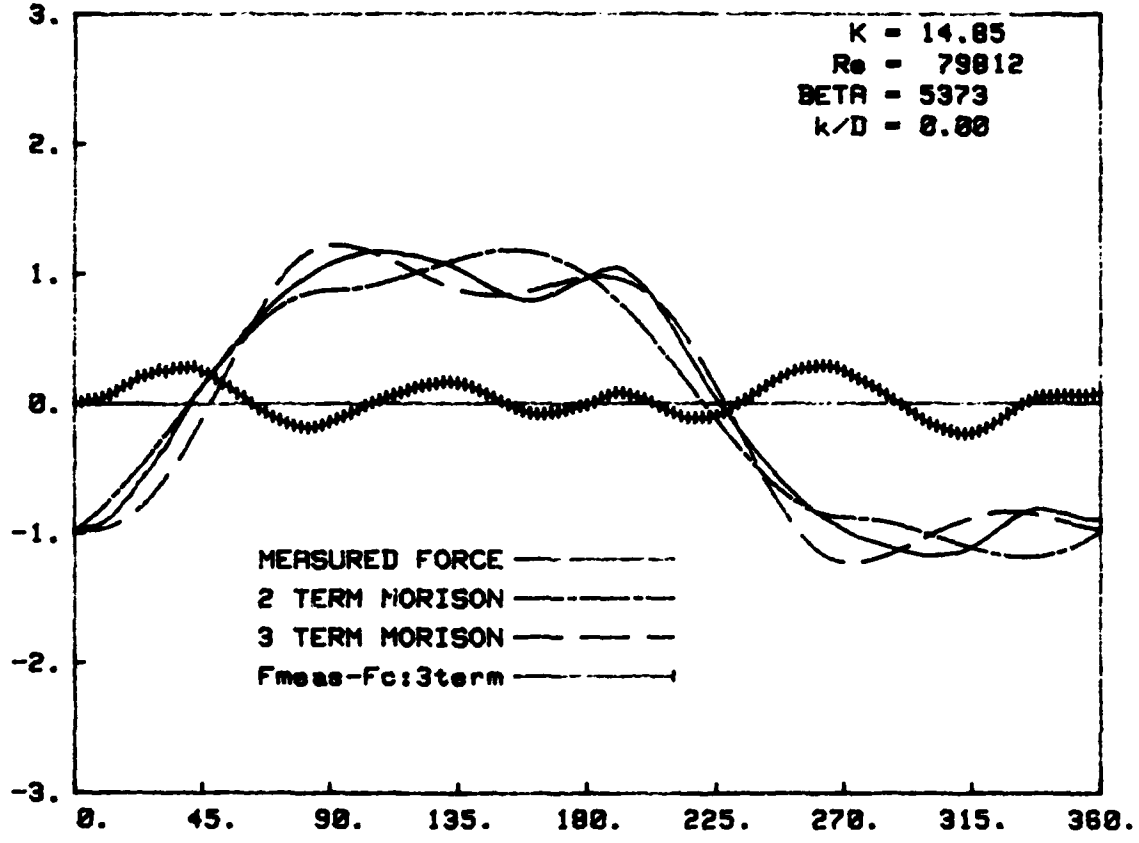

Fig. 53b Comparison of measured and calculated forces (Three-term MOJS Eq.)
K = 14.85

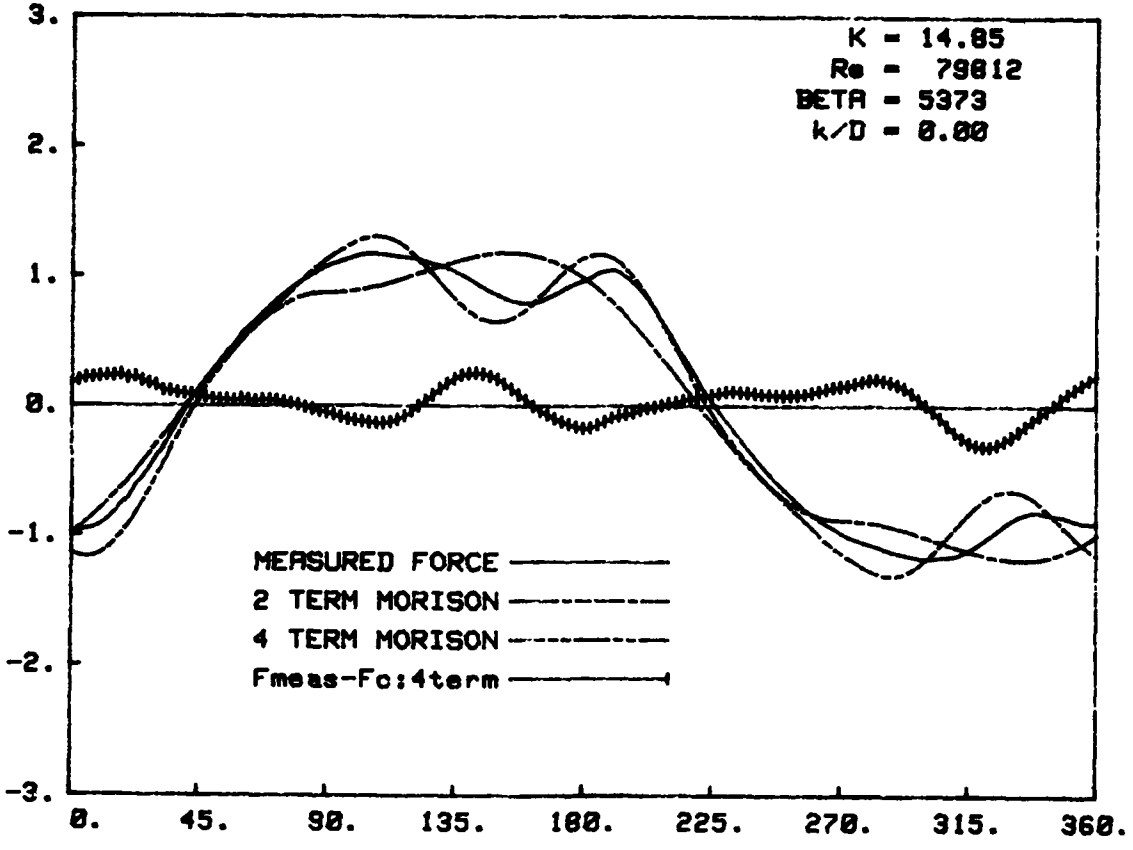

Fig. 53c Comparison of measured and calculated forces (Four-term MOJS Eq.)
K = 14.85

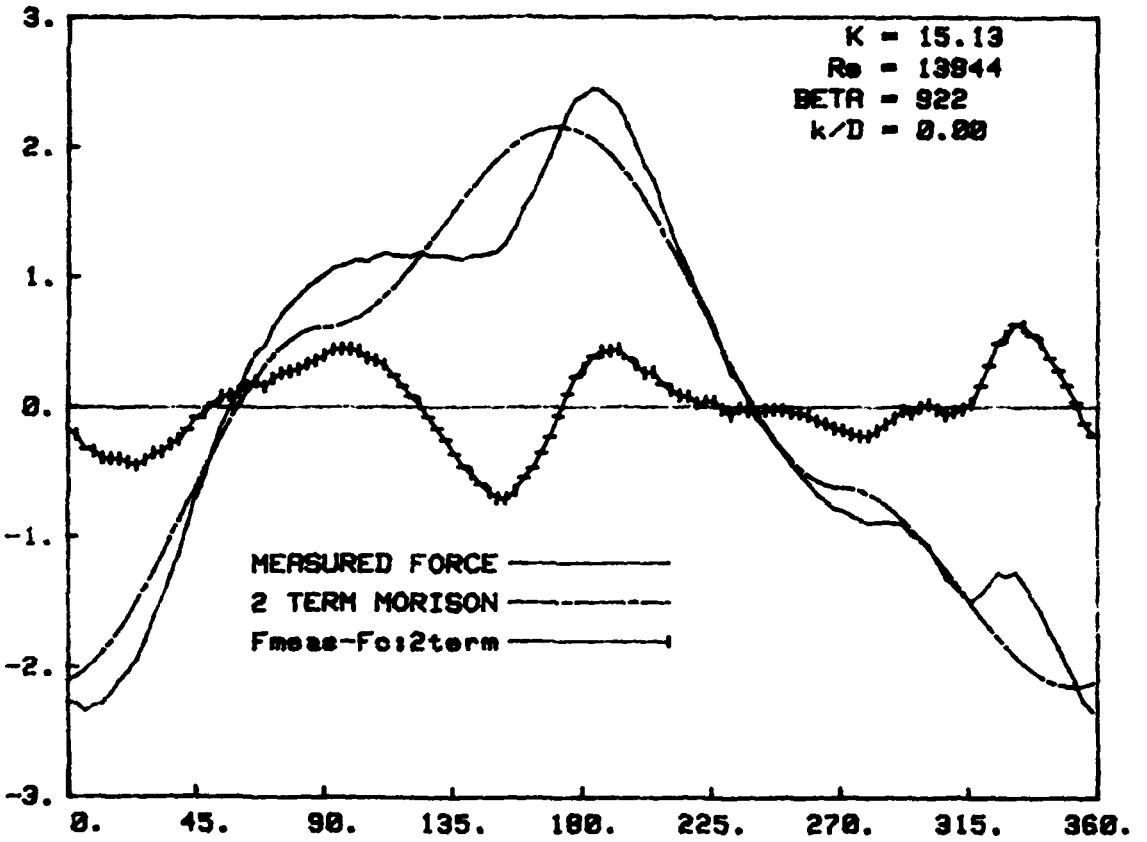

Fig. 54a Comparison of measured and calculated forces (Two-term MOJS Eq.)
K = 15.13

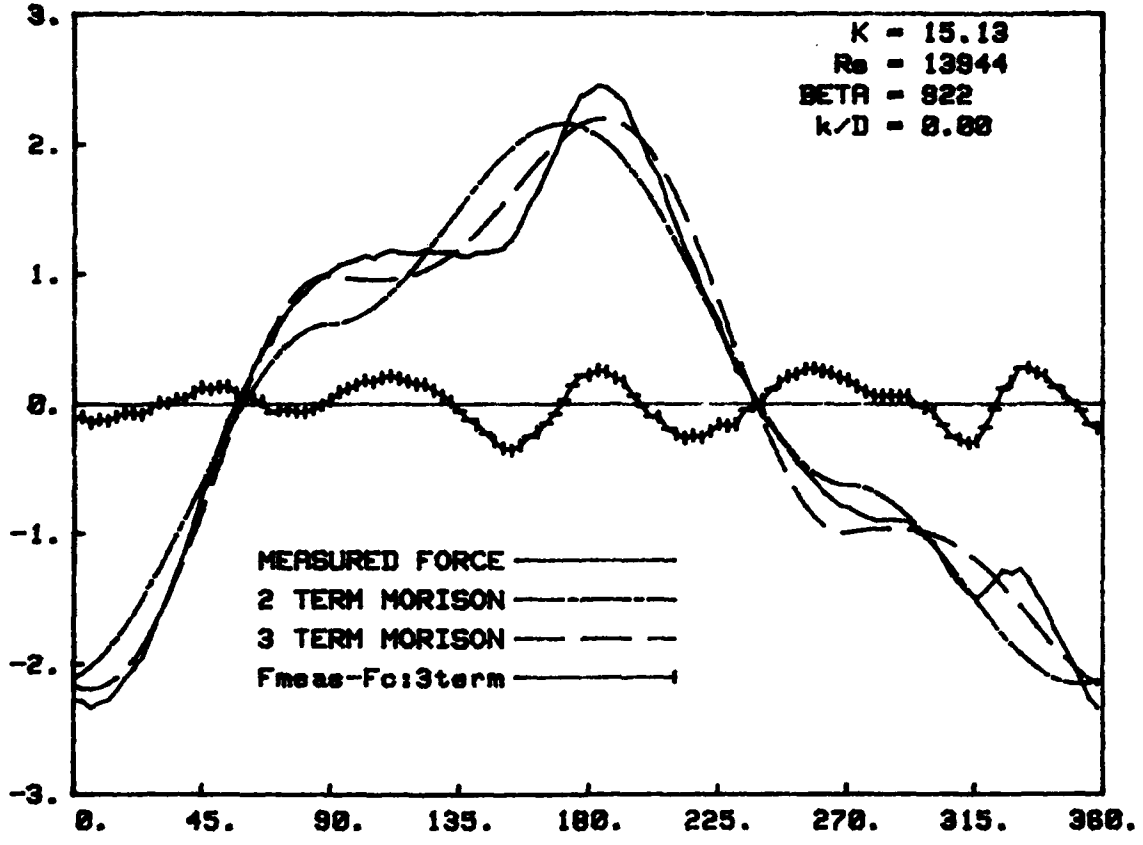

Fig. 54b Comparison of measured and calculated forces (Three-term MOJS Eq.)
K = 15.13

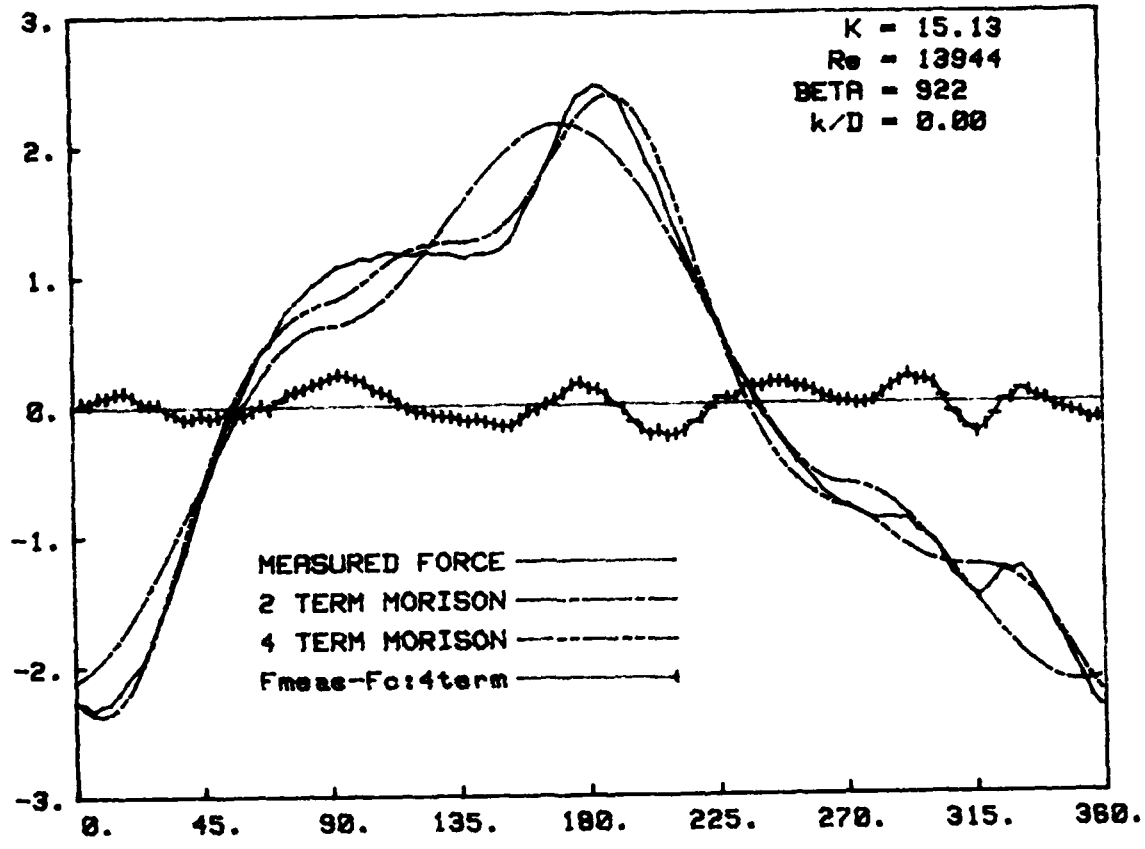

Fig. 54c Comparison of measured and calculated forces (Four-term MOJS Eq.) K = 15.13

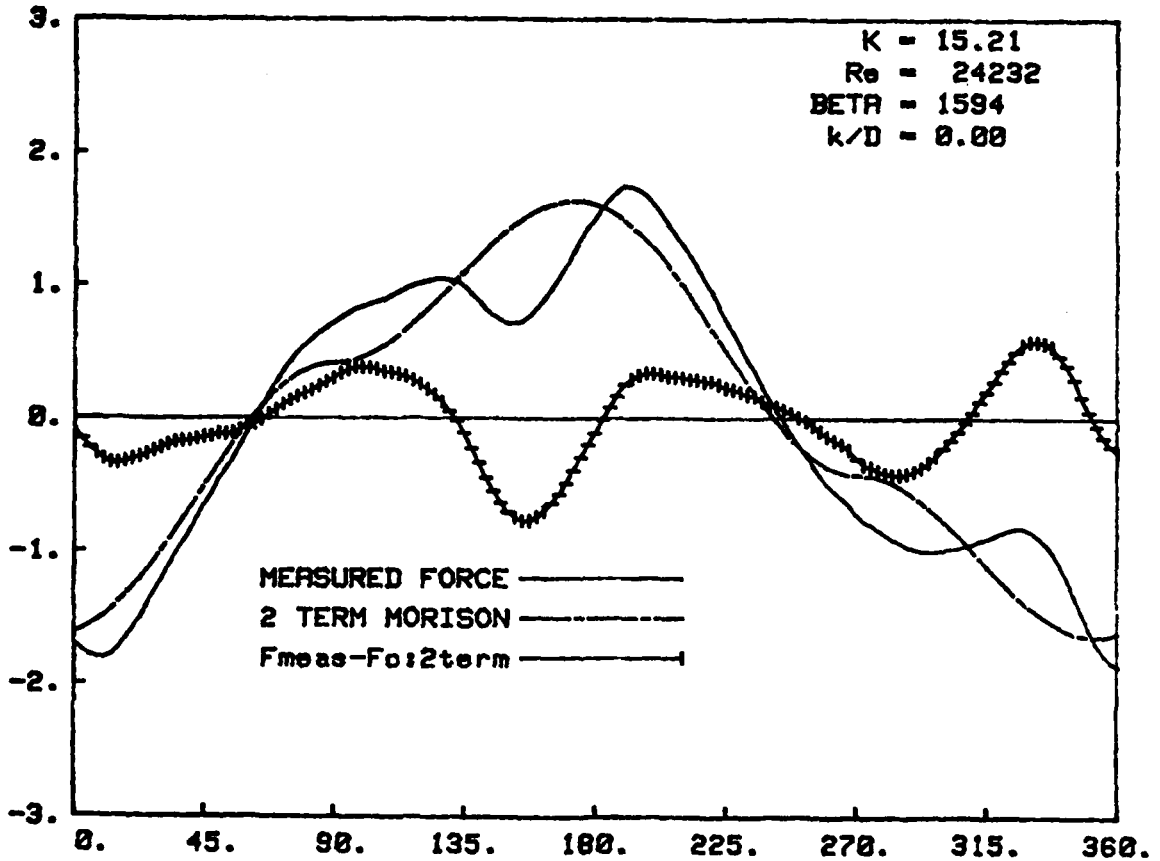

Fig. 55a Comparison of measured and calculated forces (Two-term MOJS Eq.)
K = 15.21

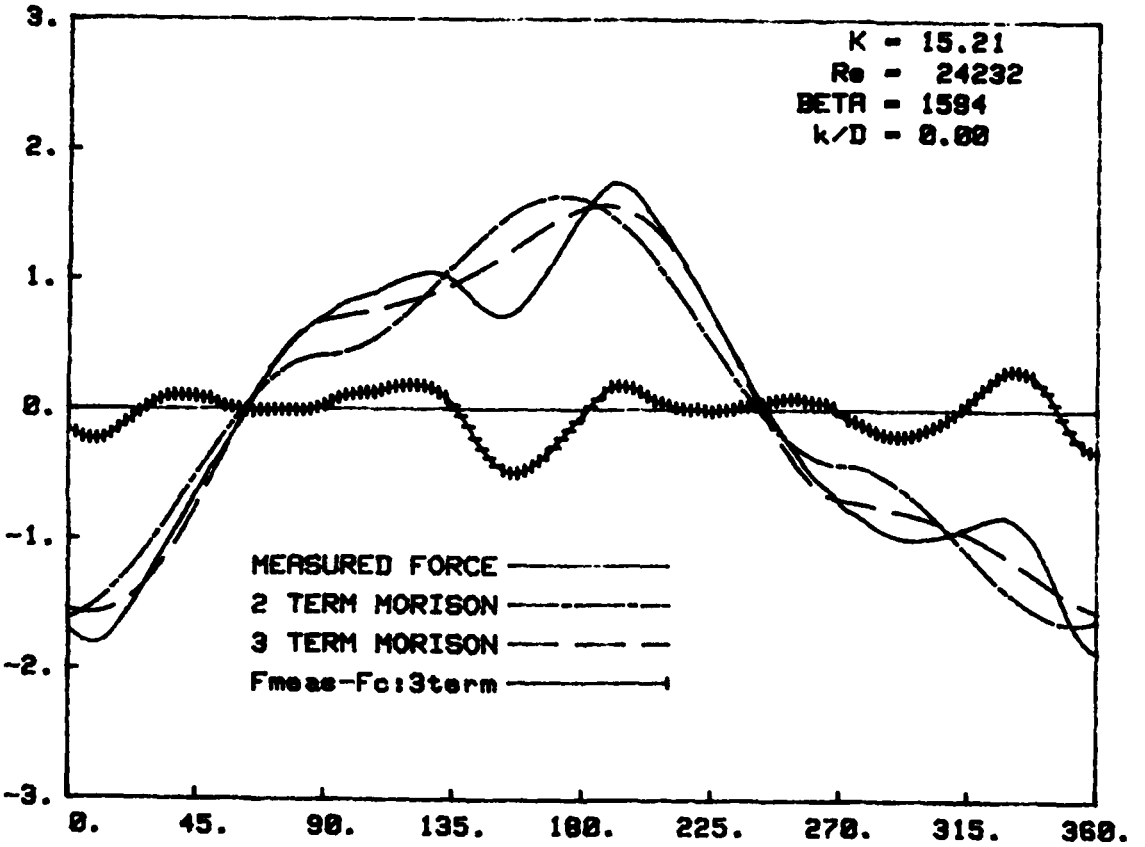

Fig. 55b Comparison of measured and calculated forces (Three-term MOJS Eq.)
K = 15.21

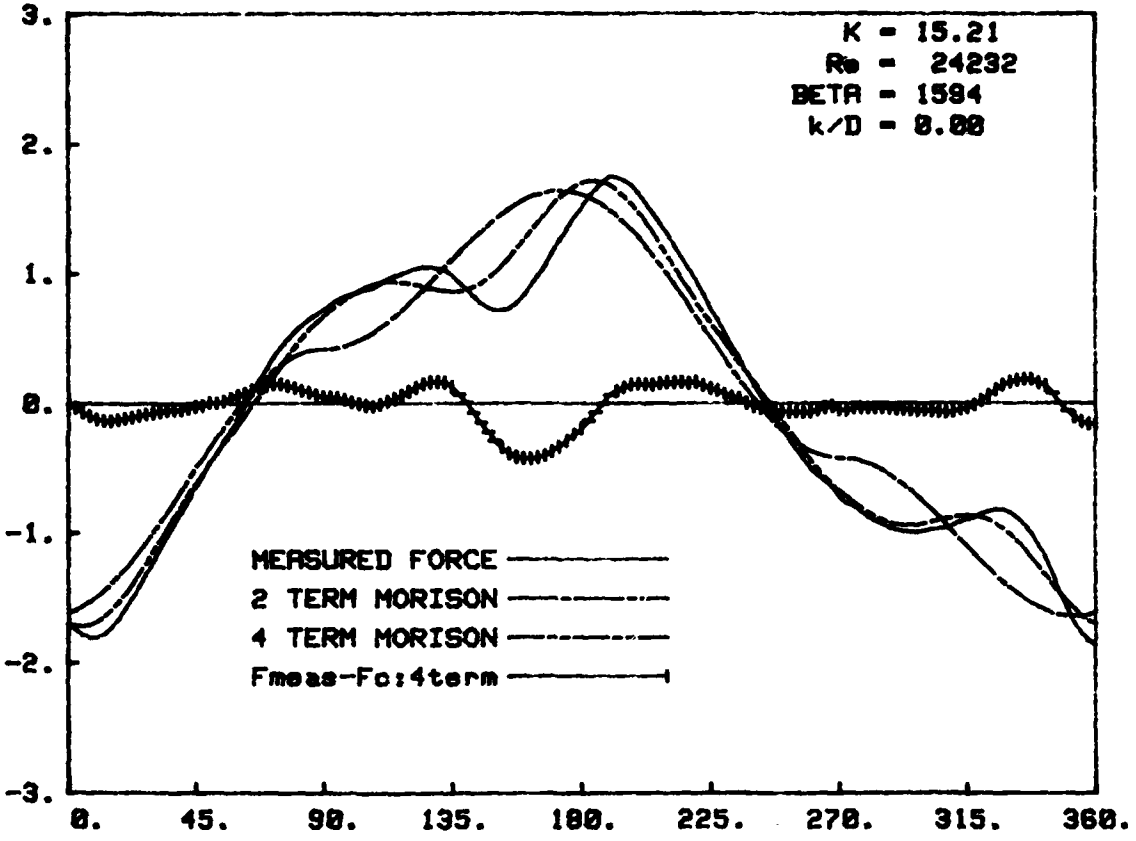

Fig. 55c Comparison of measured and calculated forces (Four-term MOJS Eq.)
K = 15.21

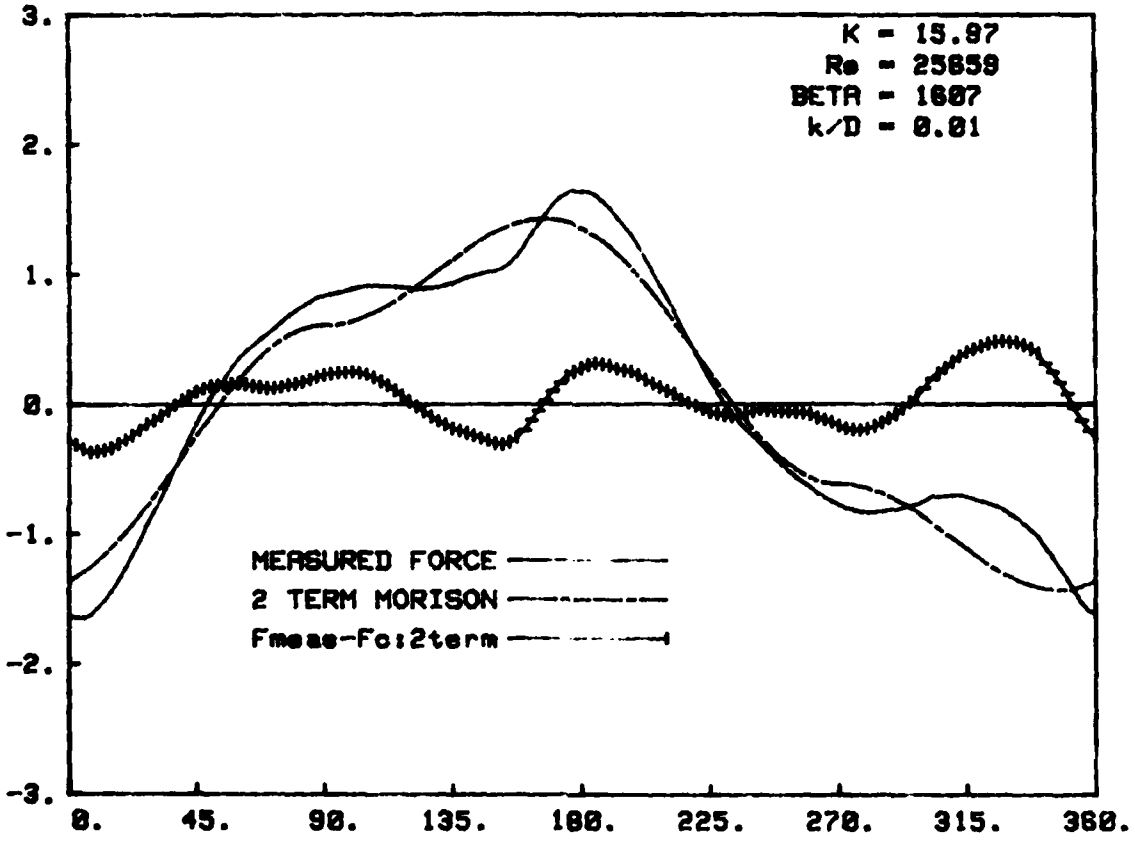

Fig. 56a Comparison of measured and calculated forces (Two-term MOJS Eq.)
K = 15.97

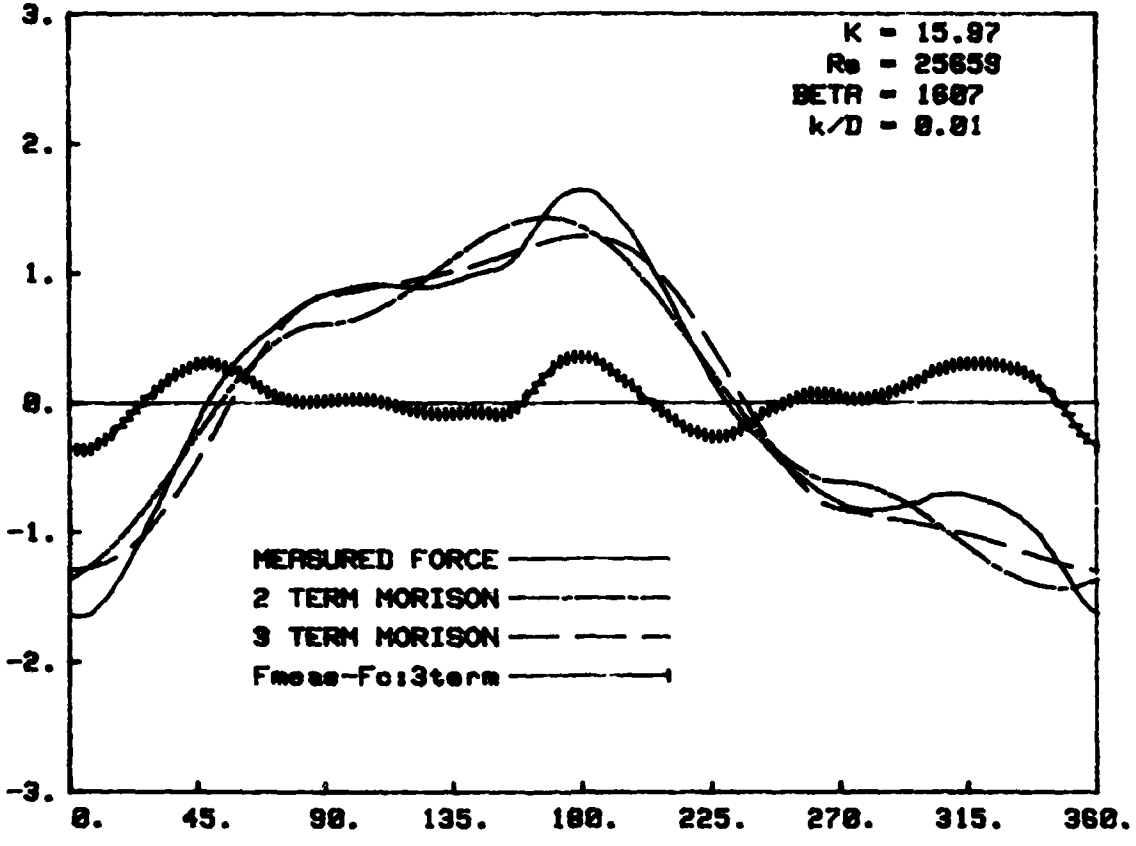

Fig. 56b Comparison of measured and calculated forces (Three-term MOJS Eq.)
K = 15.97

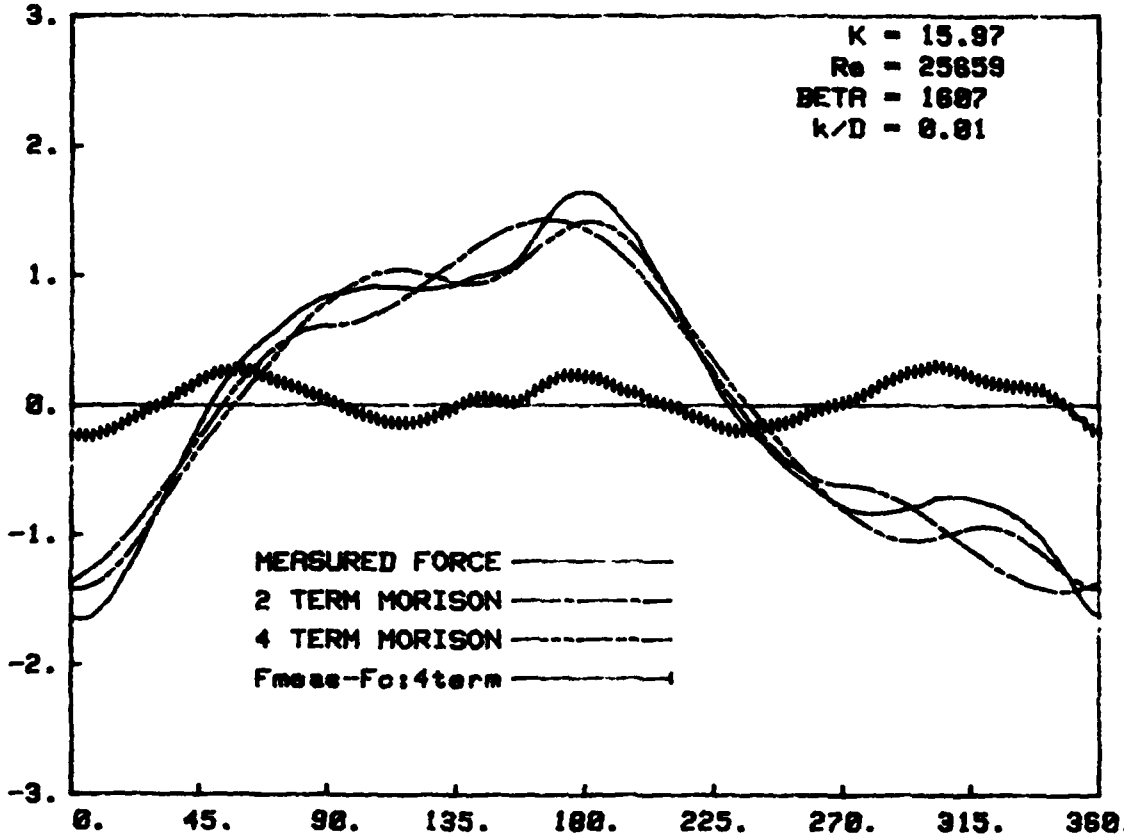

Fig. 56c Comparison of measured and calculated forces (Four-term MOJS Eq.)
K = 15.97

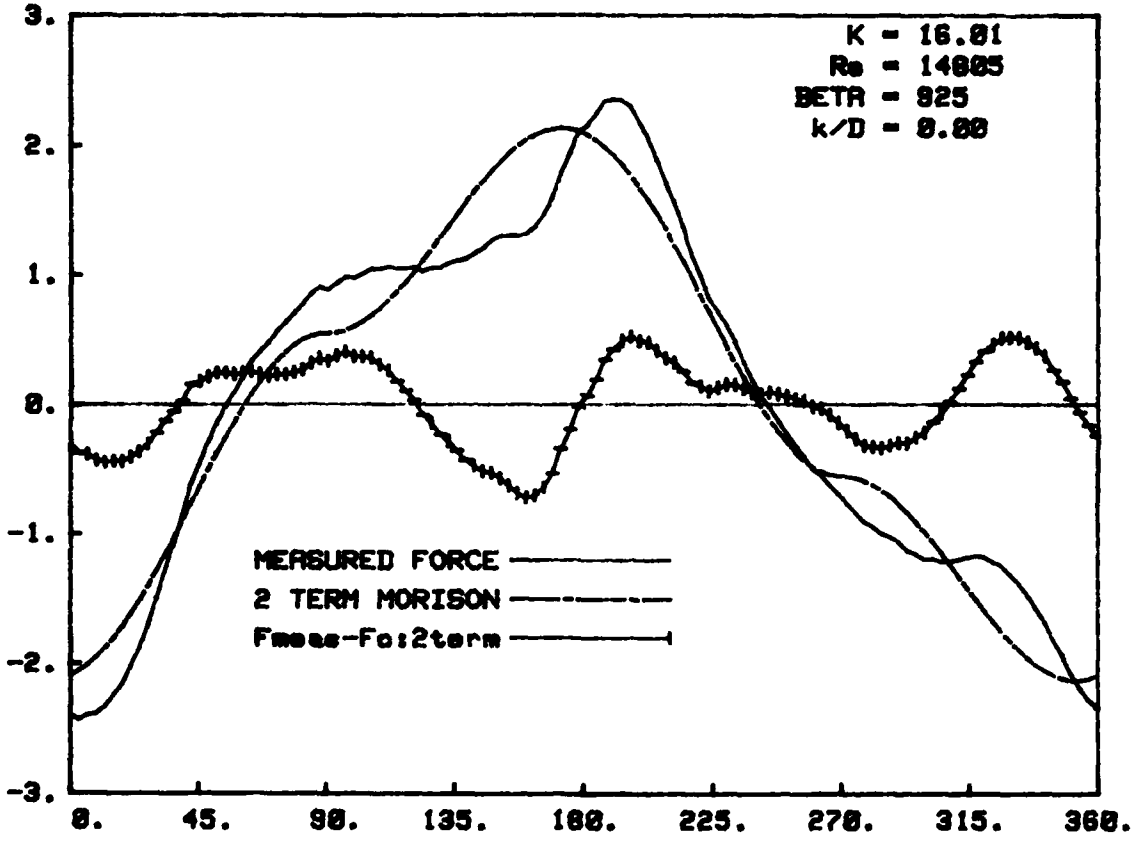

Fig. 57a Comparison of measured and calculated forces (Two-term MOJS Eq.)
K = 16.01

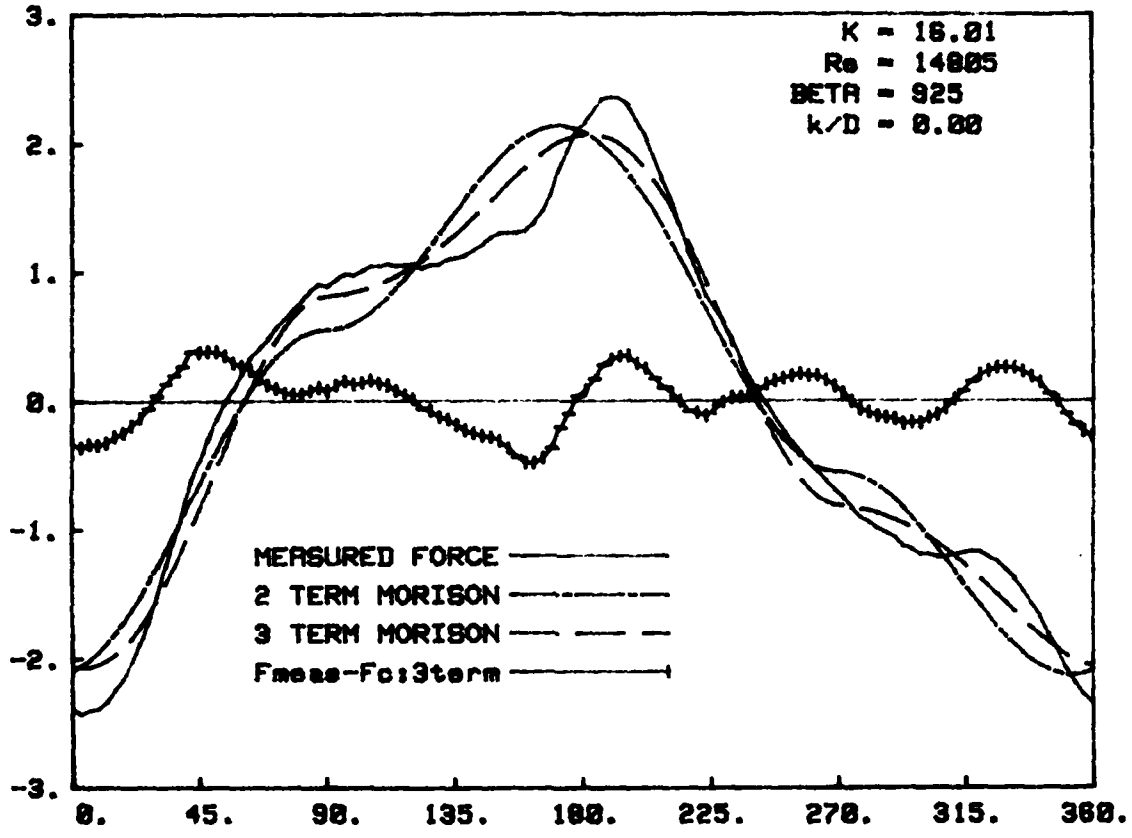

Fig. 57b Comparison of measured and calculated forces (Three-term MOJS Eq.)
K = 16.01

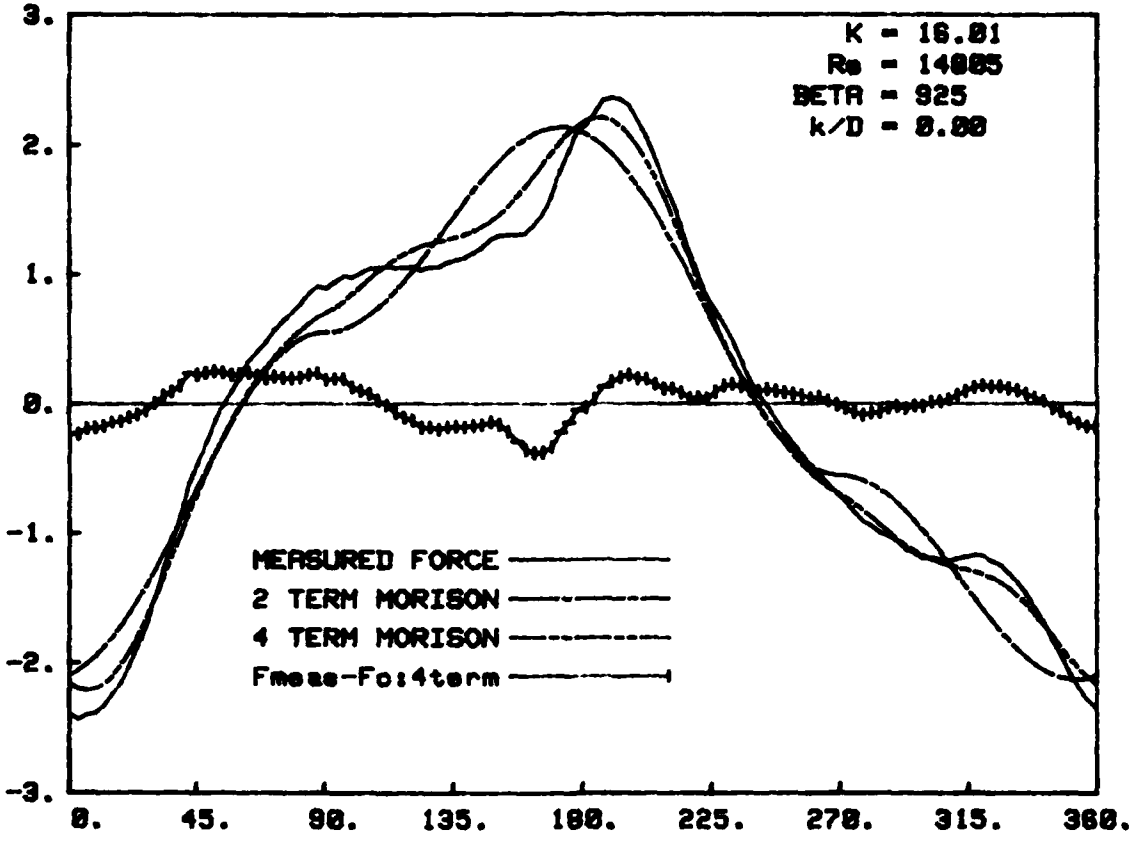

Fig. 57c Comparison of measured and calculated forces (Four-term MOJS Eq.)
K = 16.01

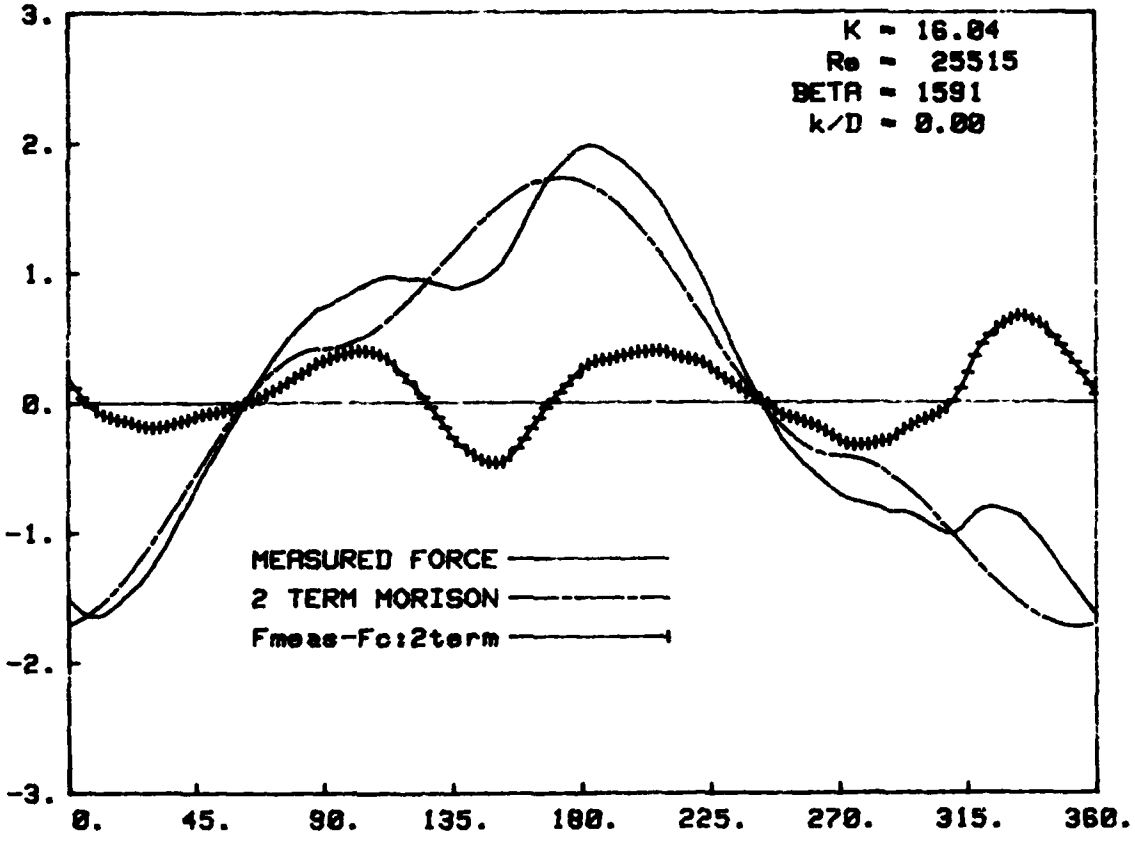

Fig. 58a Comparison of measured and calculated forces (Two-term MOJS Eq.)
K = 16.04

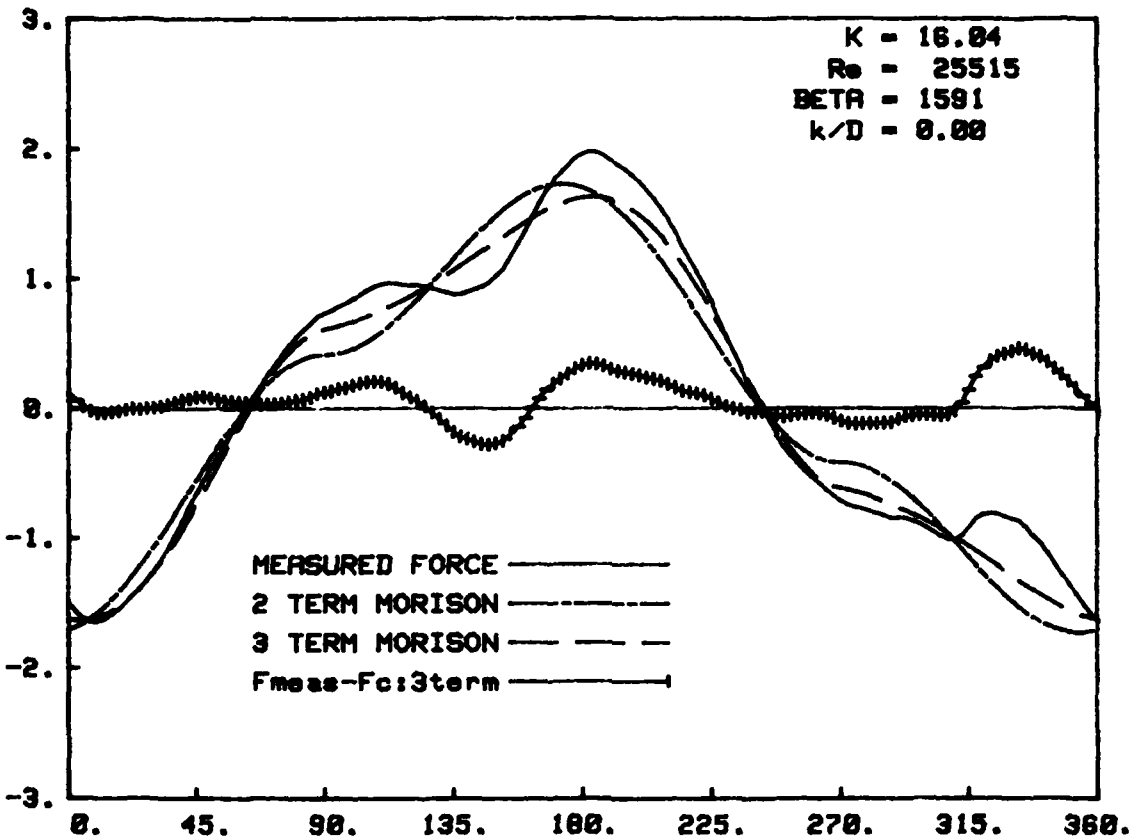

Fig. 58b Comparison of measured and calculated forces (Three-term MOJS Eq.)
K = 16.04

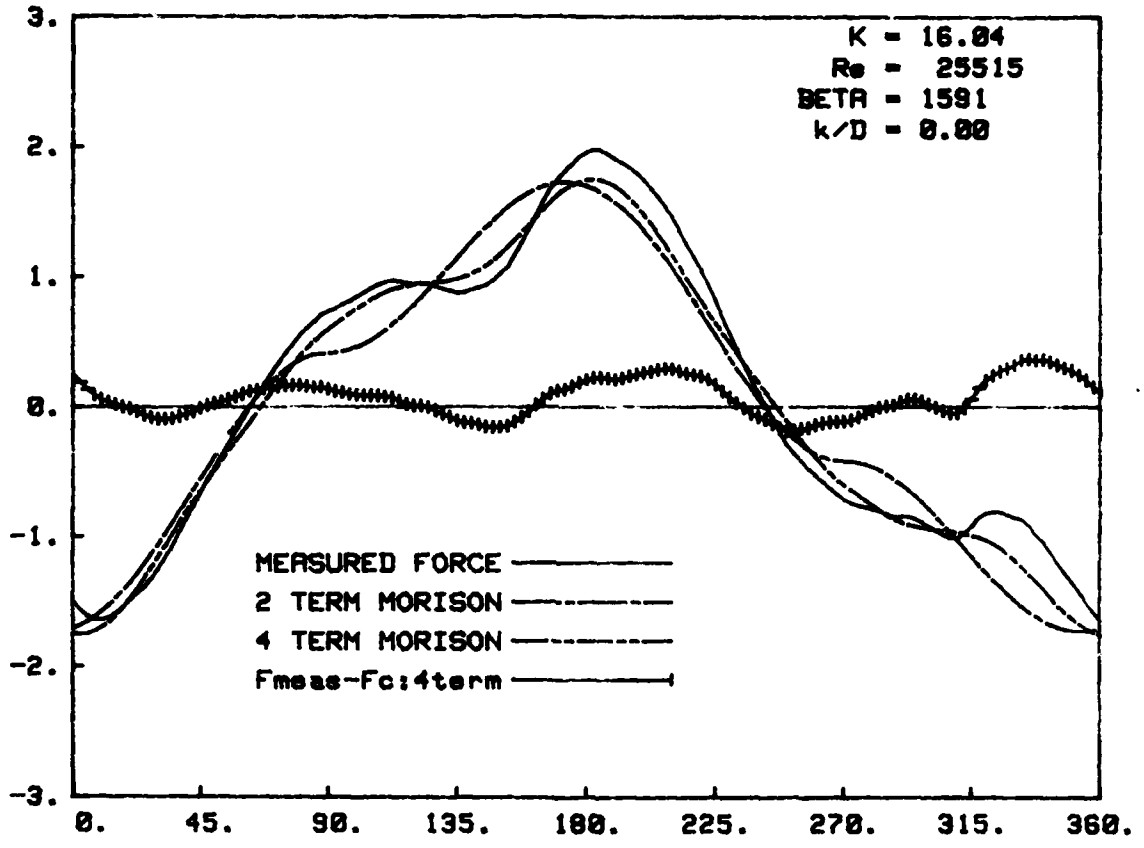

Fig. 58c Comparison of measured and calculated forces (Four-term MOJS Eq.)
K = 16.04

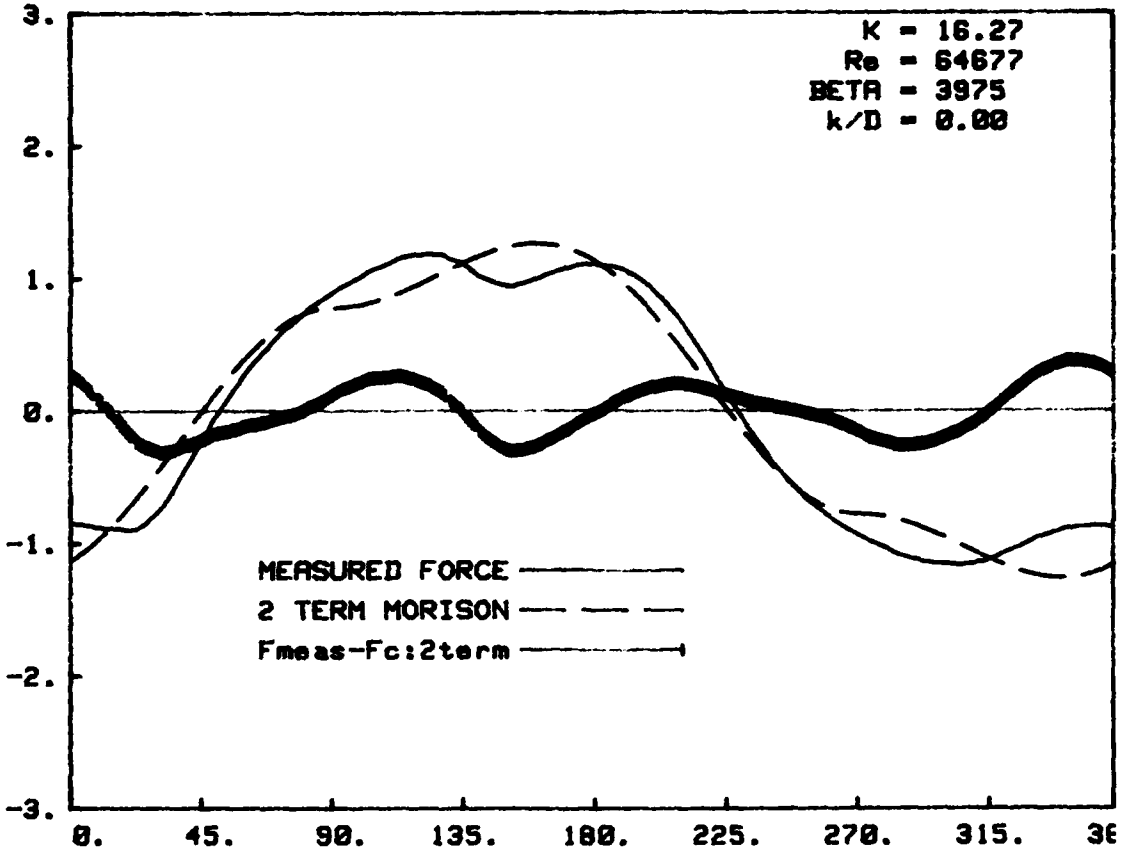

Fig. 59a Comparison of measured and calculated forces (Two-term MOJS Eq.)
K = 16.27

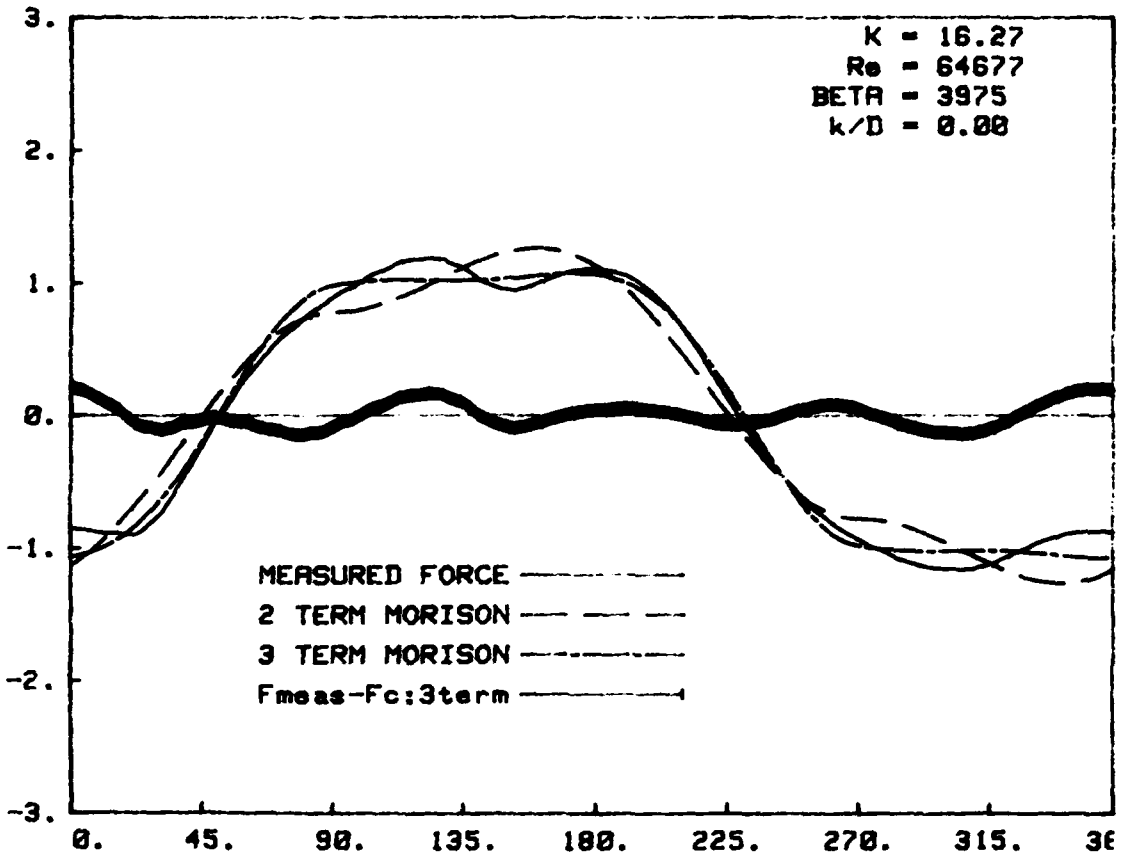

Fig. 59b Comparison of measured and calculated forces (Three-term MOJS Eq.)
K = 16.27

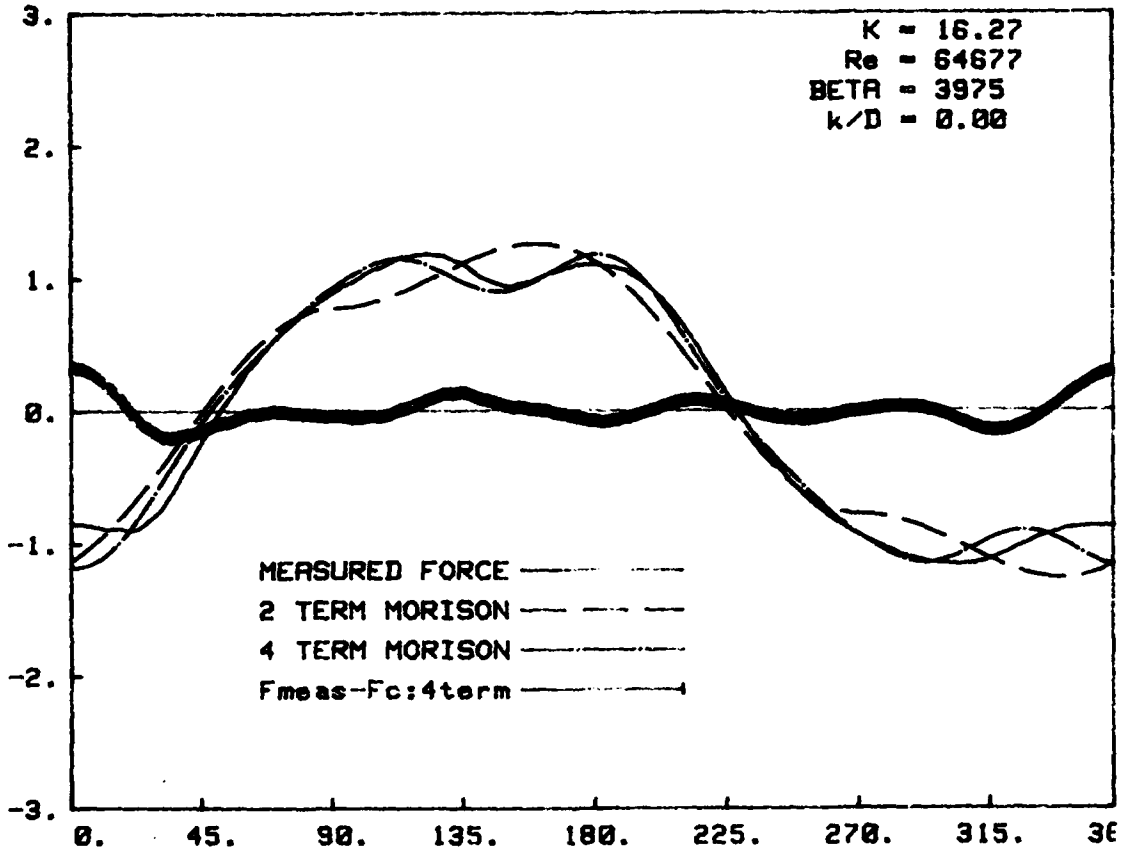

Fig. 59c Comparison of measured and calculated forces (Four-term MOJS Eq.)
K = 16.27

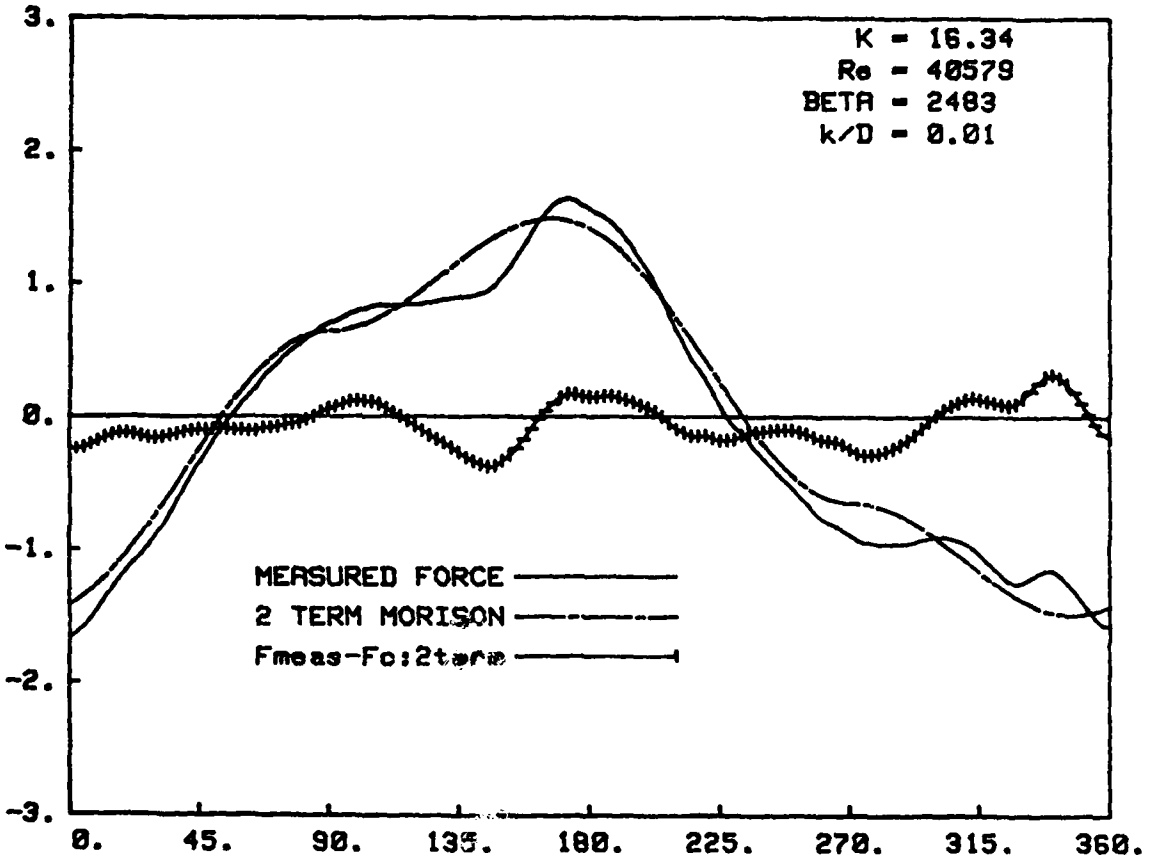

Fig. 60a Comparison of measured and calculated forces (Two-term MOJS Eq.)
K = 16.34

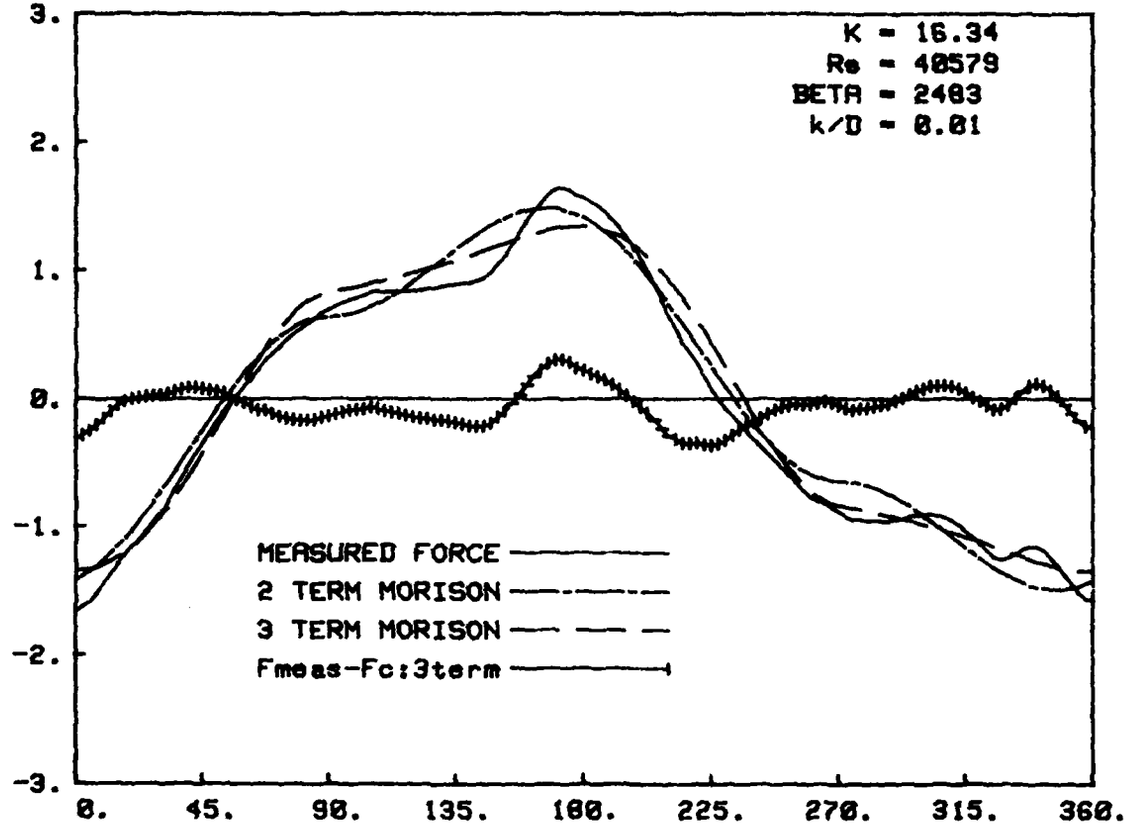

Fig. 60b Comparison of measured and calculated forces (Three-term MOJS Eq.)
K = 16.34

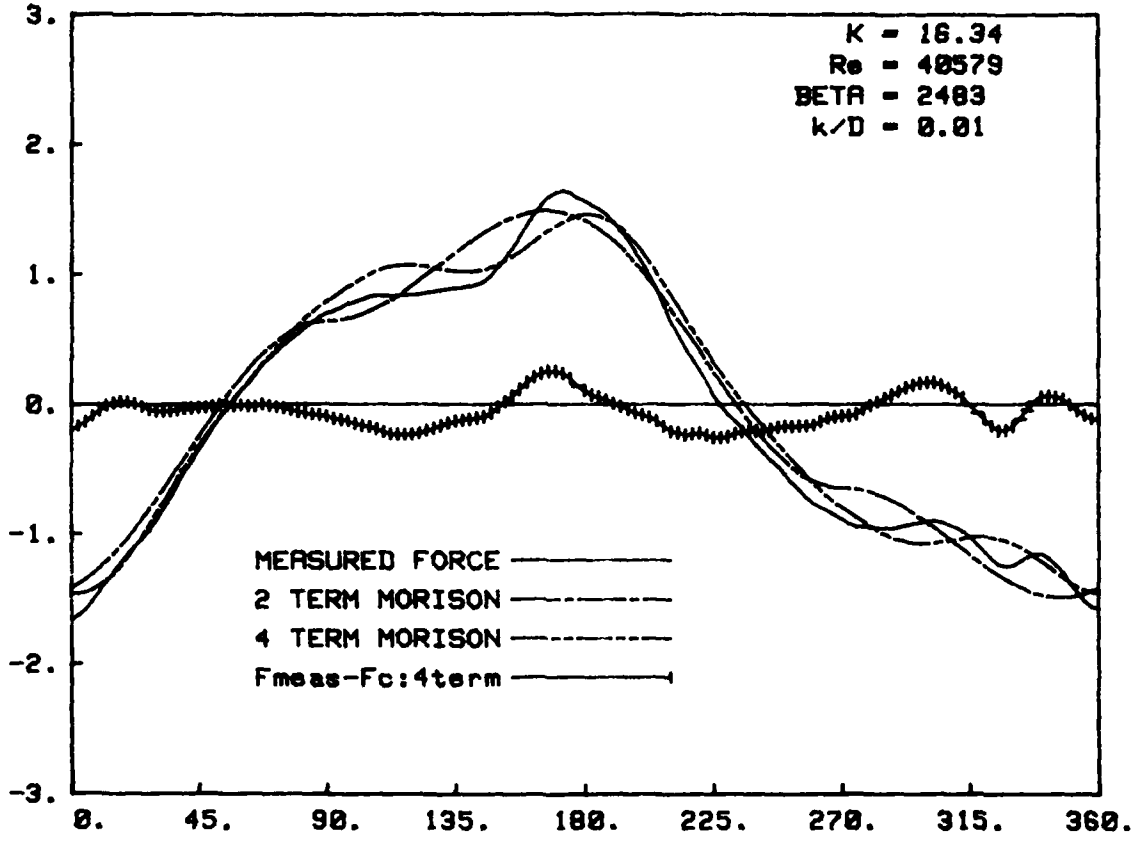

Fig. 60c Comparison of measured and calculated forces (Four-term MOJS Eq.)
K = 16.34

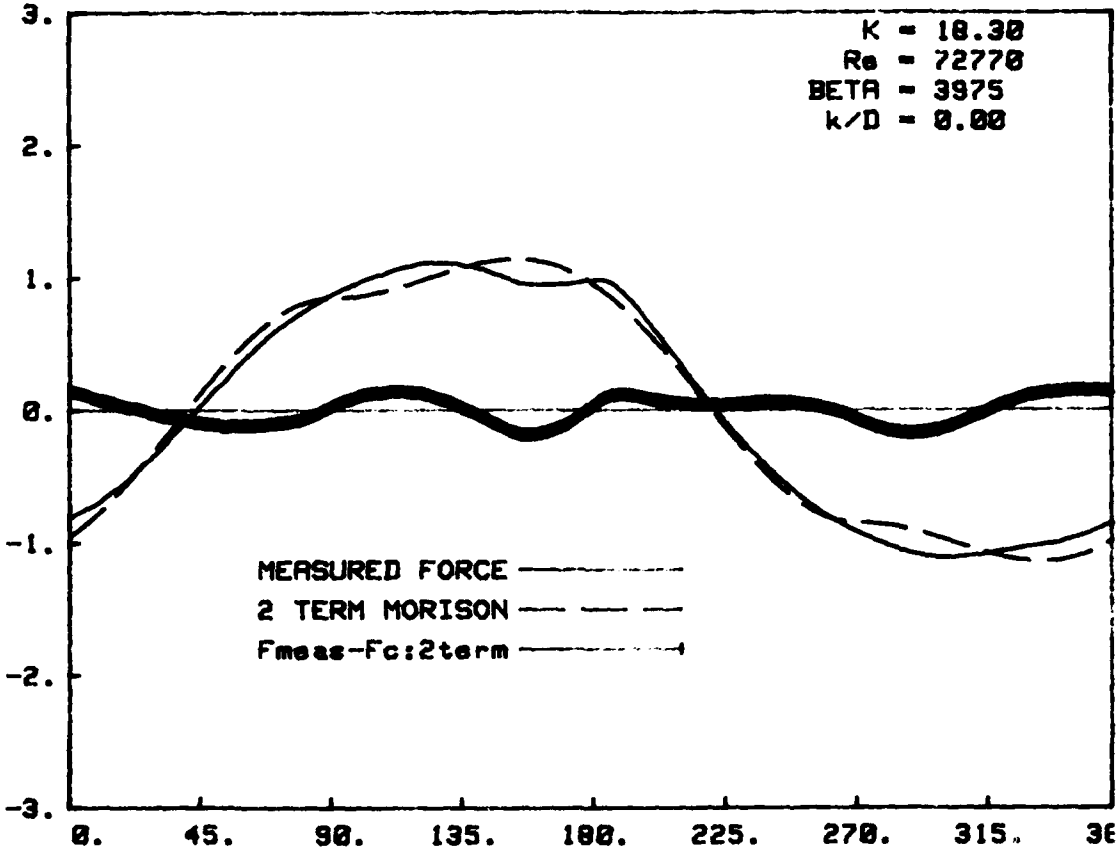

Fig. 61a Comparison of measured and calculated forces (Two-term MOJS Eq.)
K = 18.30

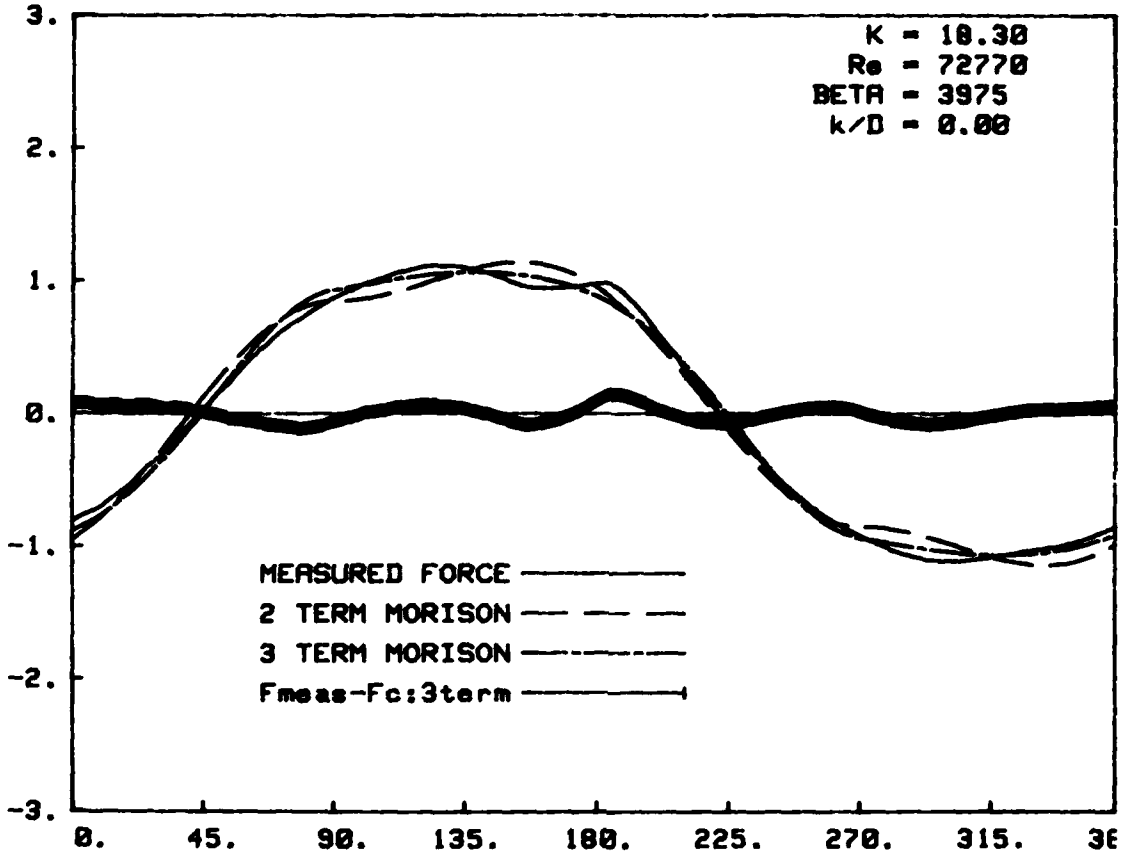

Fig. 61b Comparison of measured and calculated forces (Three-term MOJS Eq.)
K = 18.30

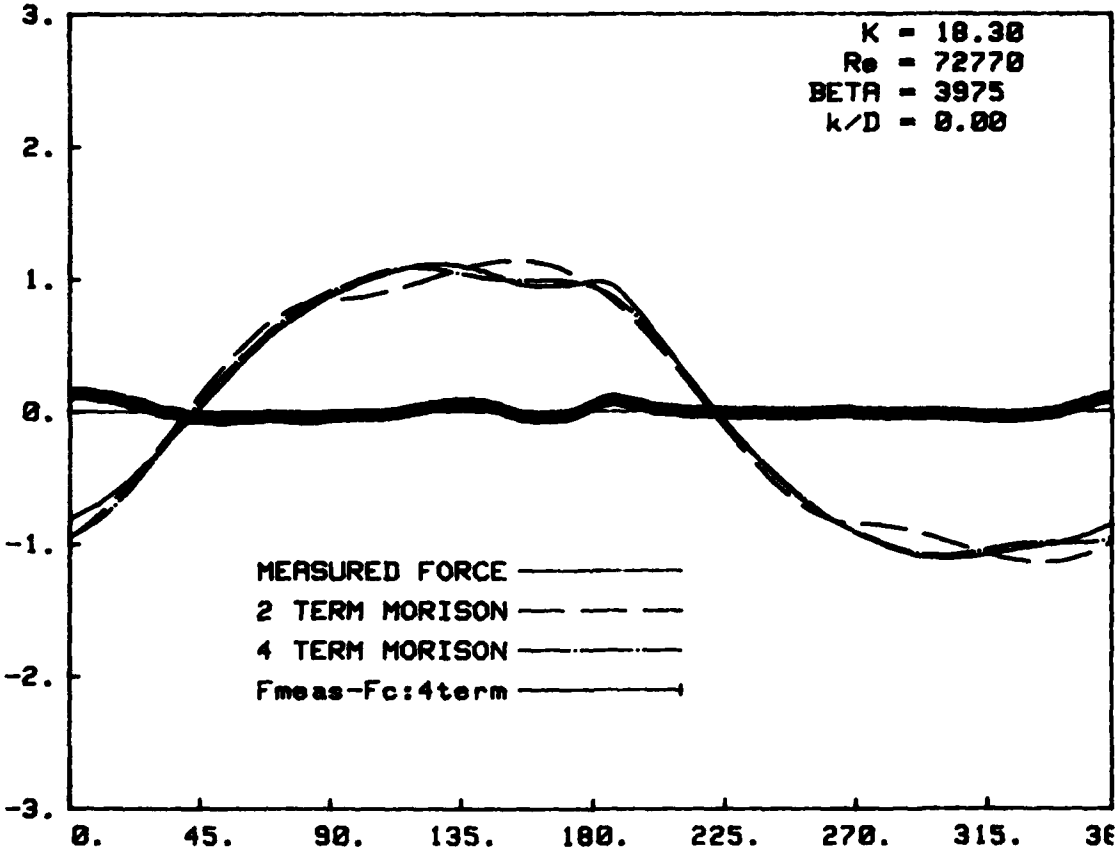

Fig. 61c Comparison of measured and calculated forces (Four-term MOJS Eq.)
K = 18.30

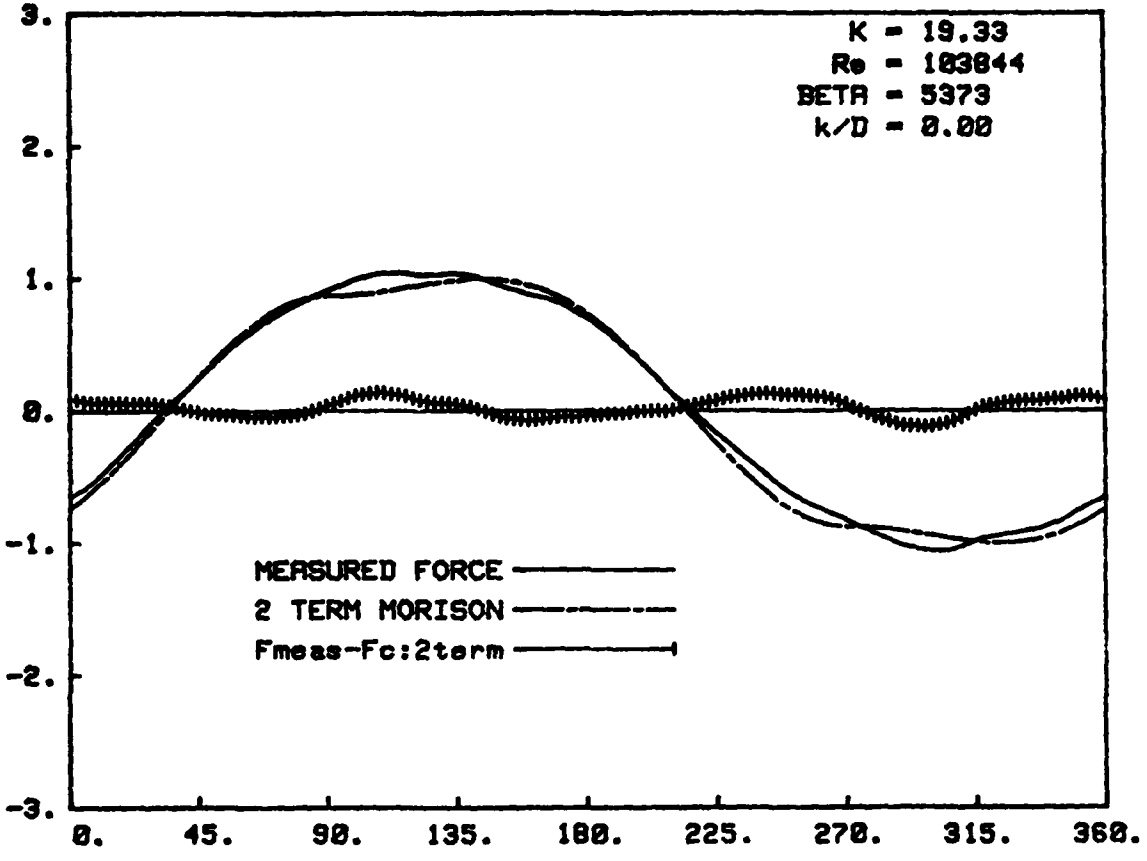

Fig. 62a Comparison of measured and calculated forces (Two-term MOJS Eq.)
K = 19.33

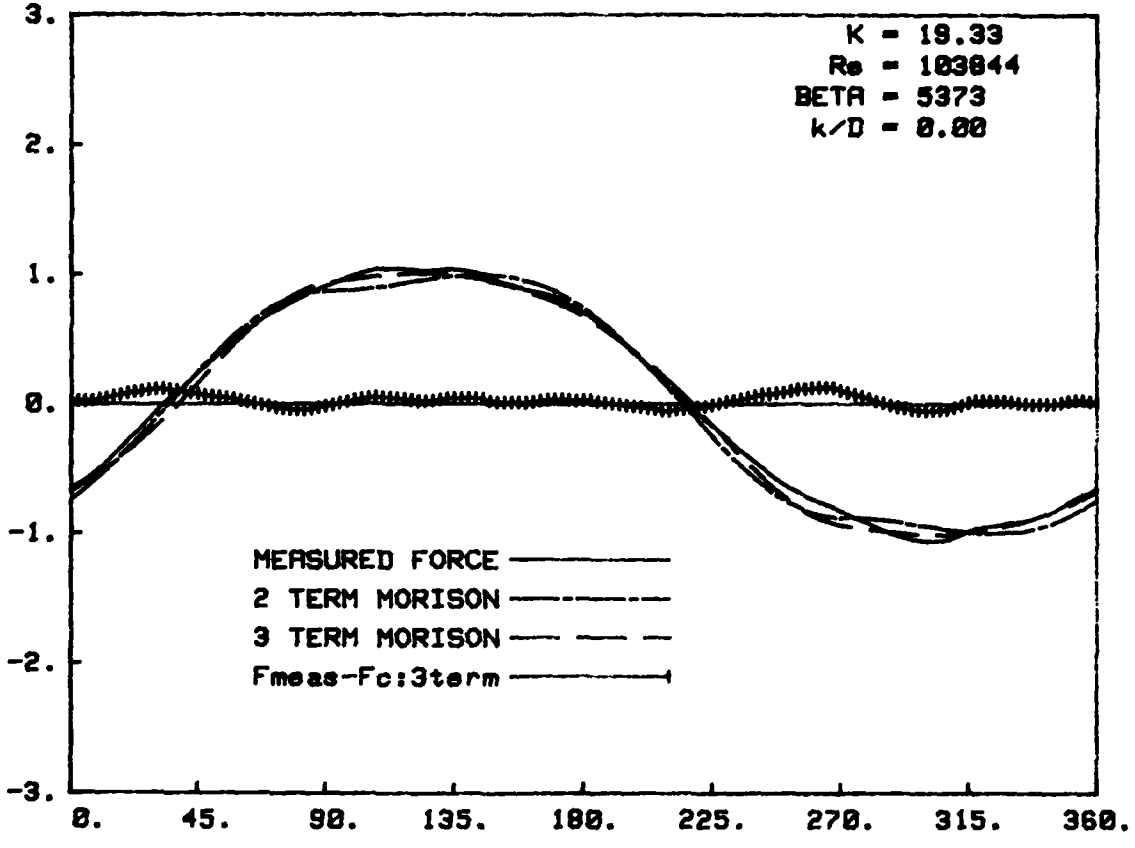

Fig. 62b Comparison of measured and calculated forces (Three-term MOJS Eq.)
K = 19.33

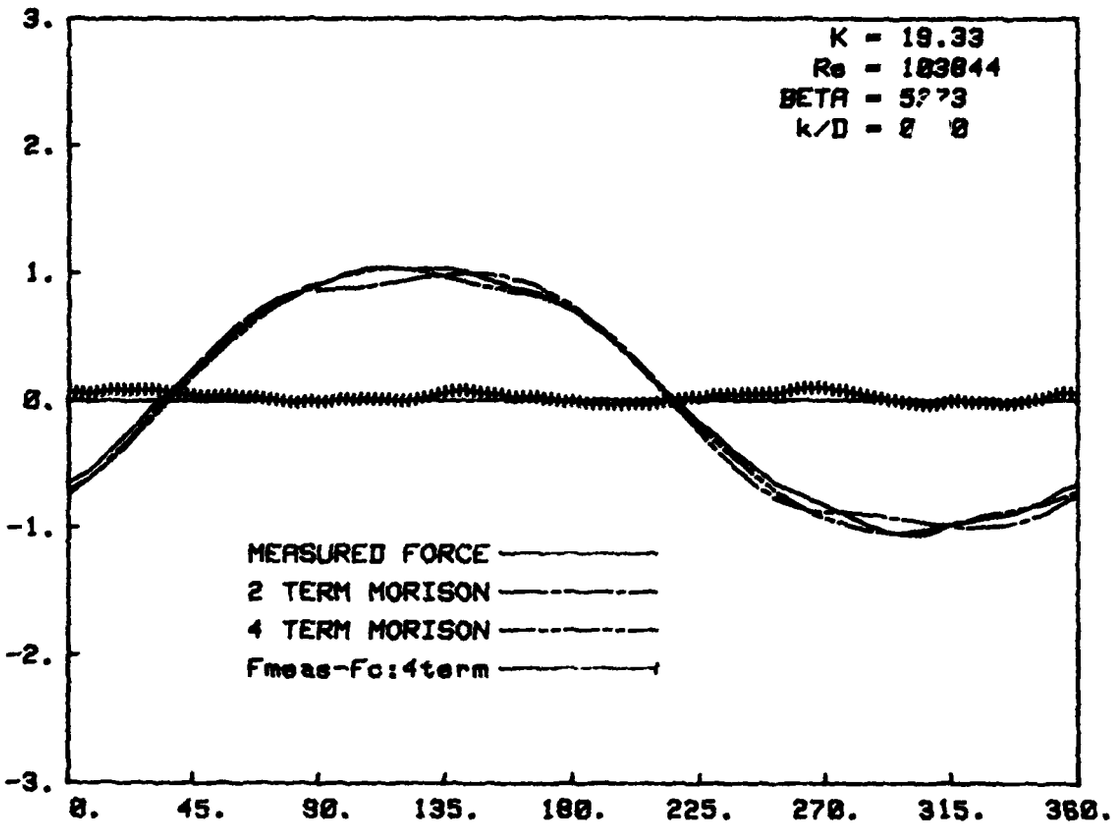

Fig. 62c Comparison of measured and calculated forces (Four-term MOJS Eq.)
K = 19.33

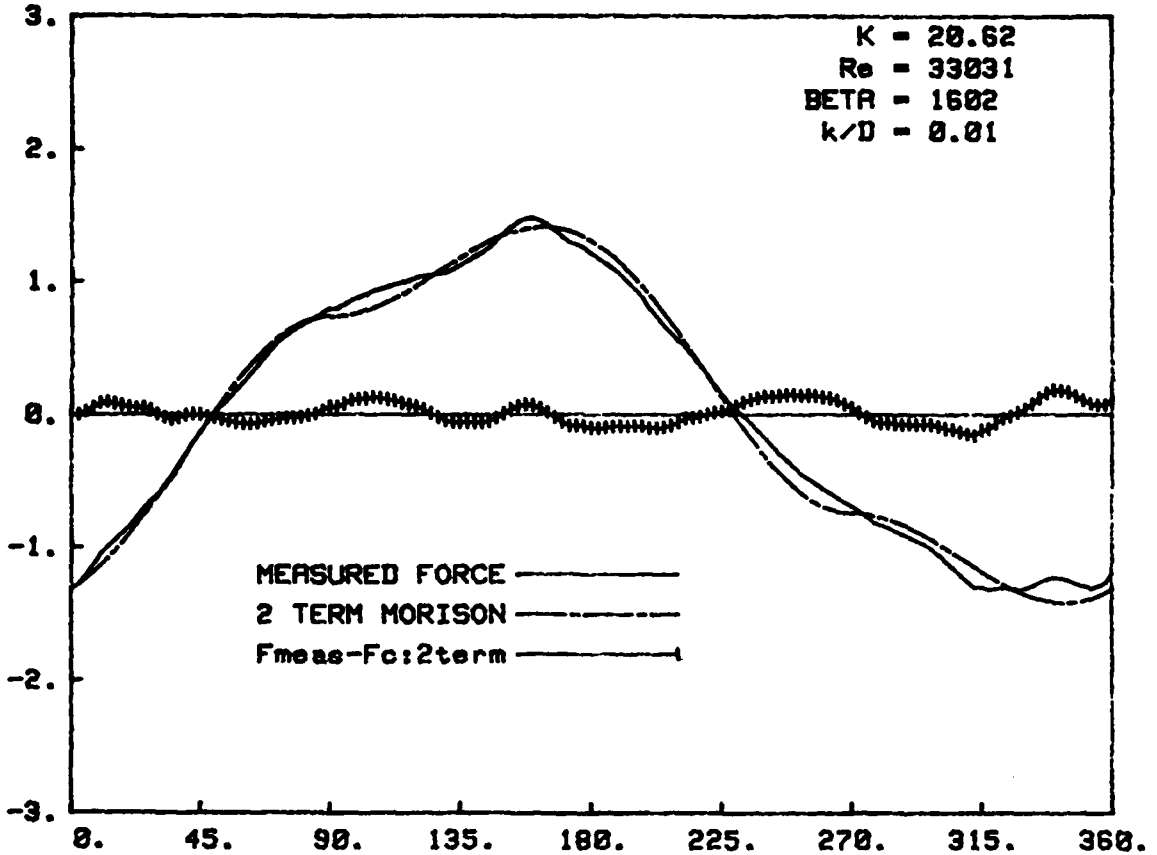

Fig. 63a Comparison of measured and calculated forces (Two-term MOJS Eq.)
K = 20.62

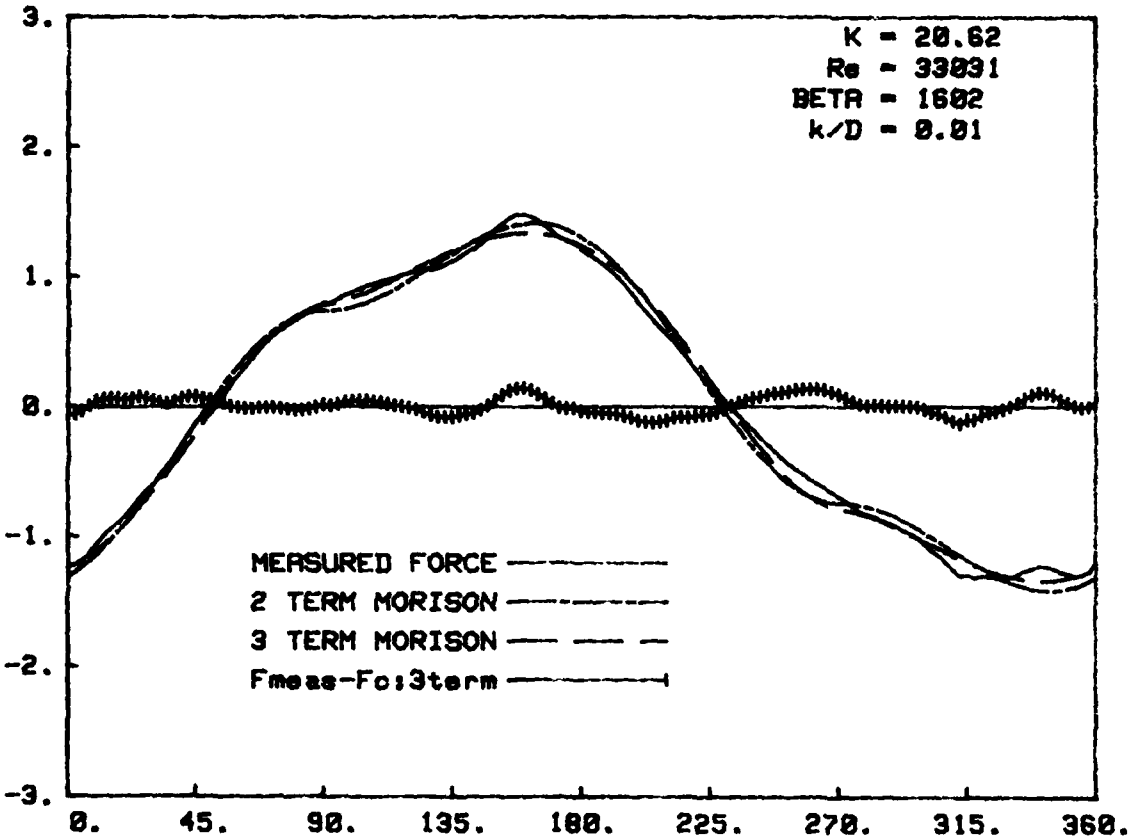

Fig. 63b Comparison of measured and calculated forces (Three-term MOJS Eq.)
K = 20.62

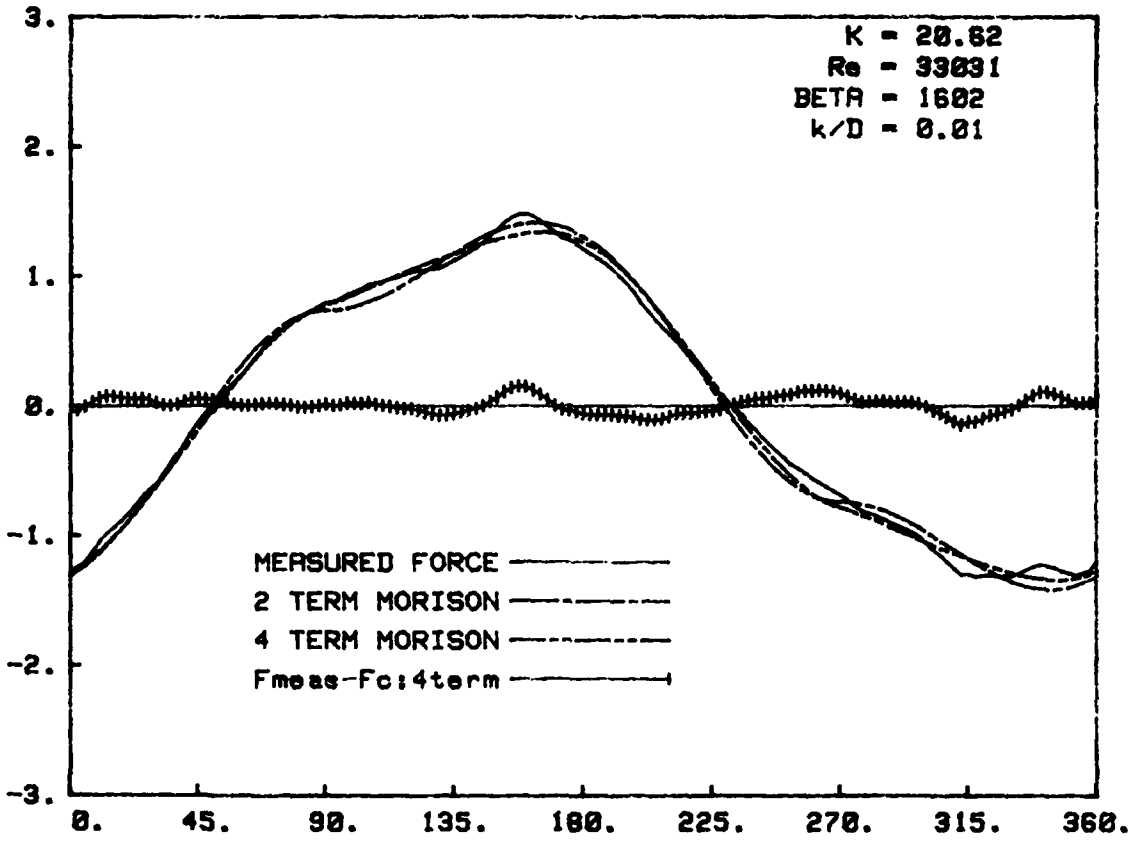

Fig. 63c Comparison of measured and calculated forces (Four-term MOJS Eq.)
K = 20.62

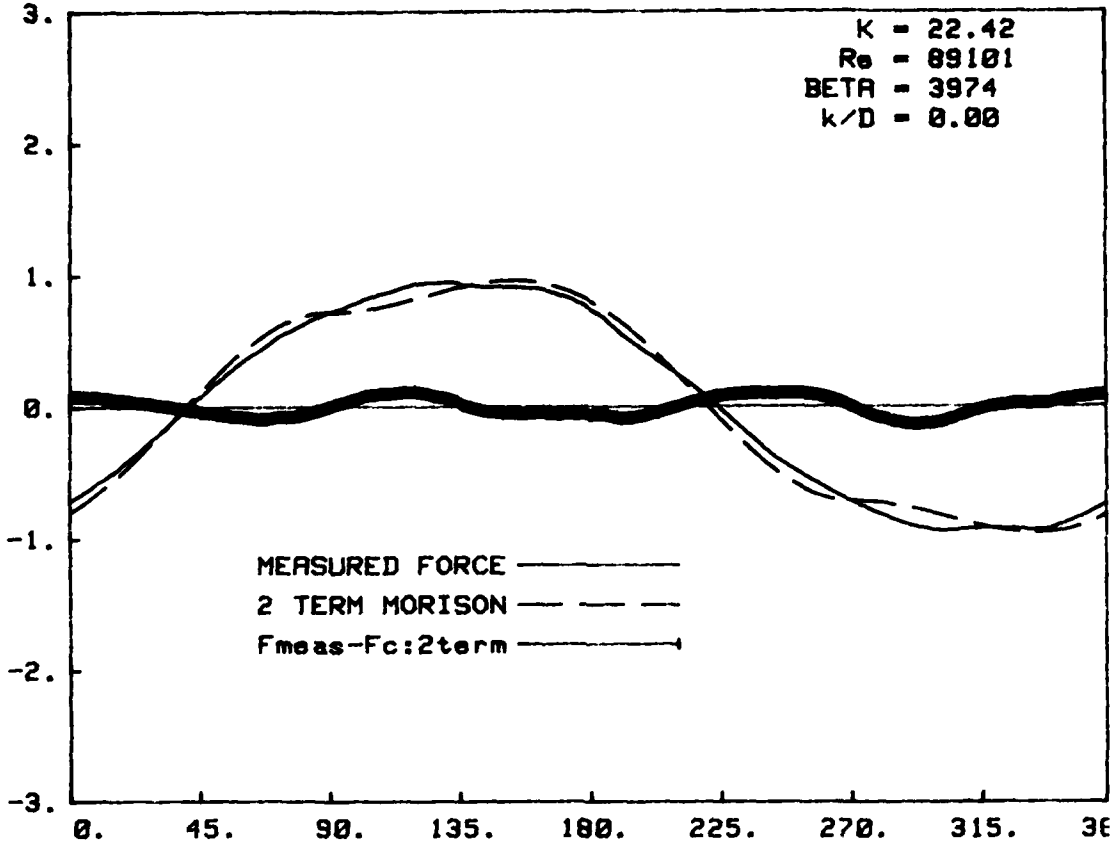

Fig. 64a Comparison of measured and calculated forces (Two-term MOJS Eq.)
K = 22.42

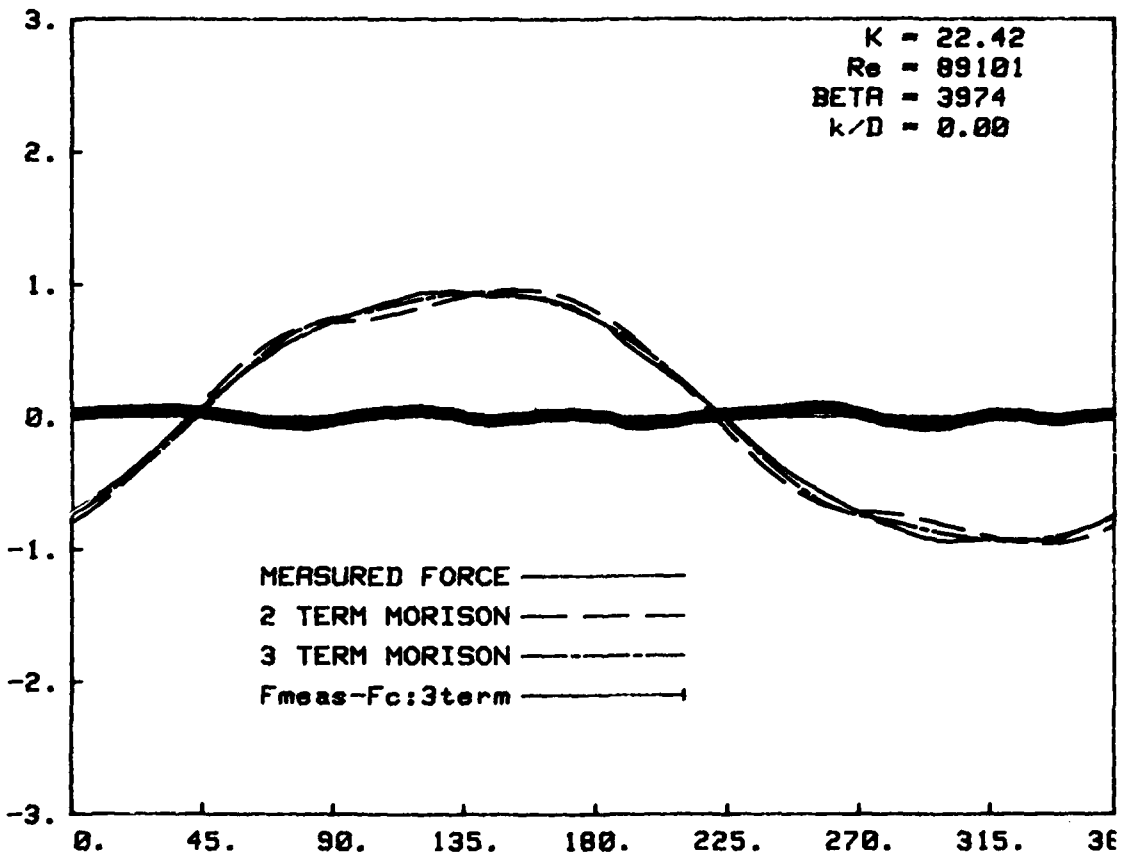

Fig. 64b Comparison of measured and calculated forces (Three-term MOJS Eq.)
K = 22.42

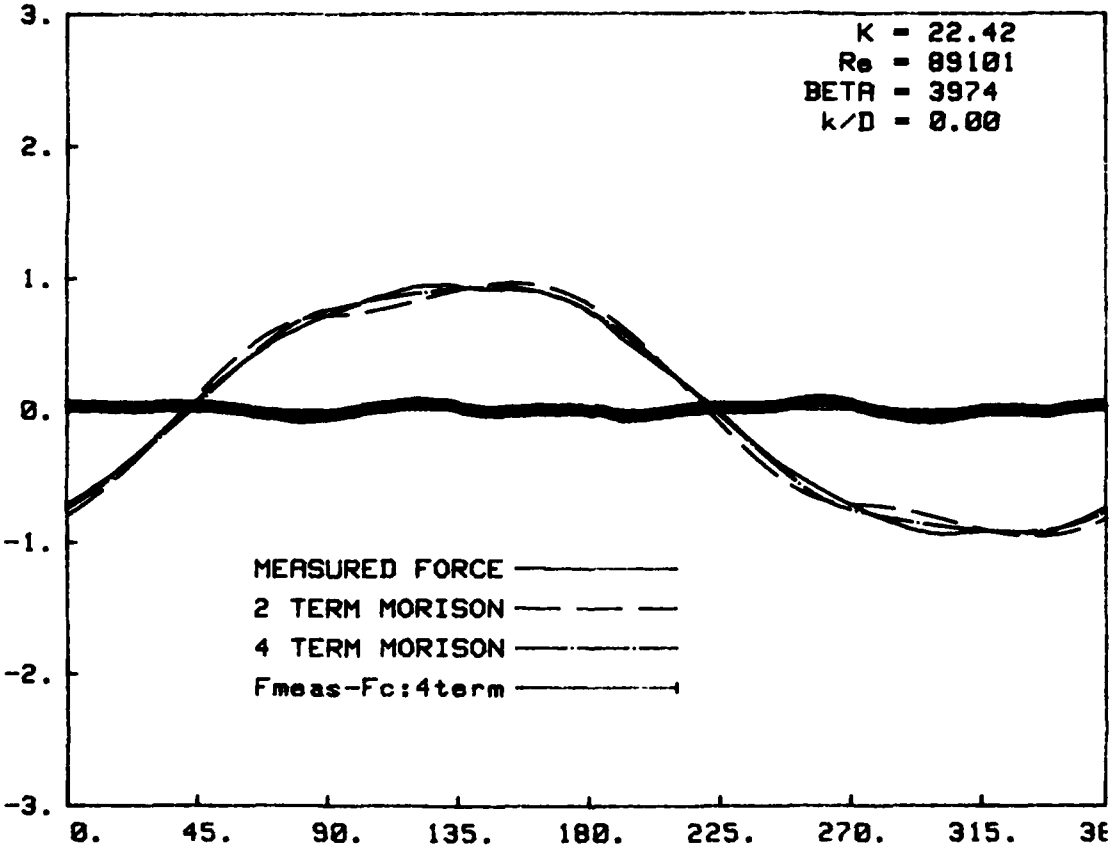

Fig. 64c Comparison of measured and calculated forces (Four-term MOJS Eq.)
K = 22.42

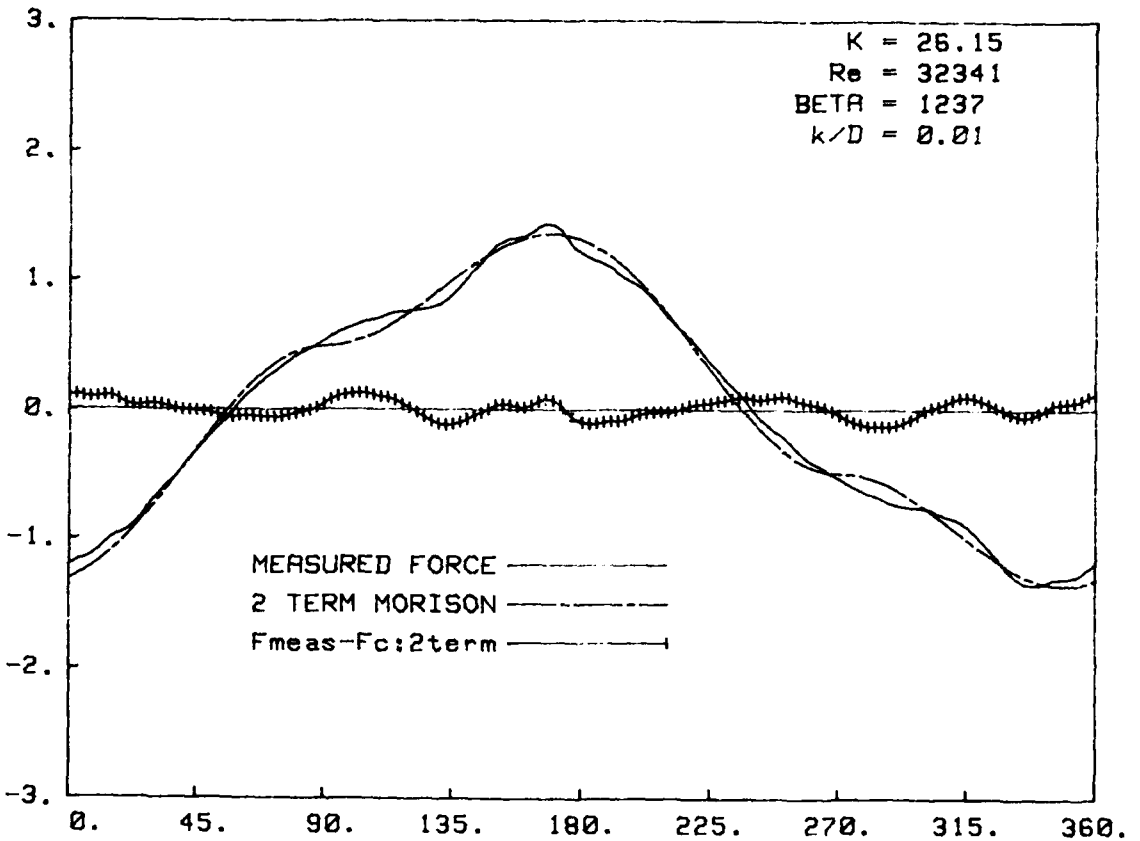

Fig. 65a Comparison of measured and calculated forces (Two-term MOJS Eq.)
K = 26.15

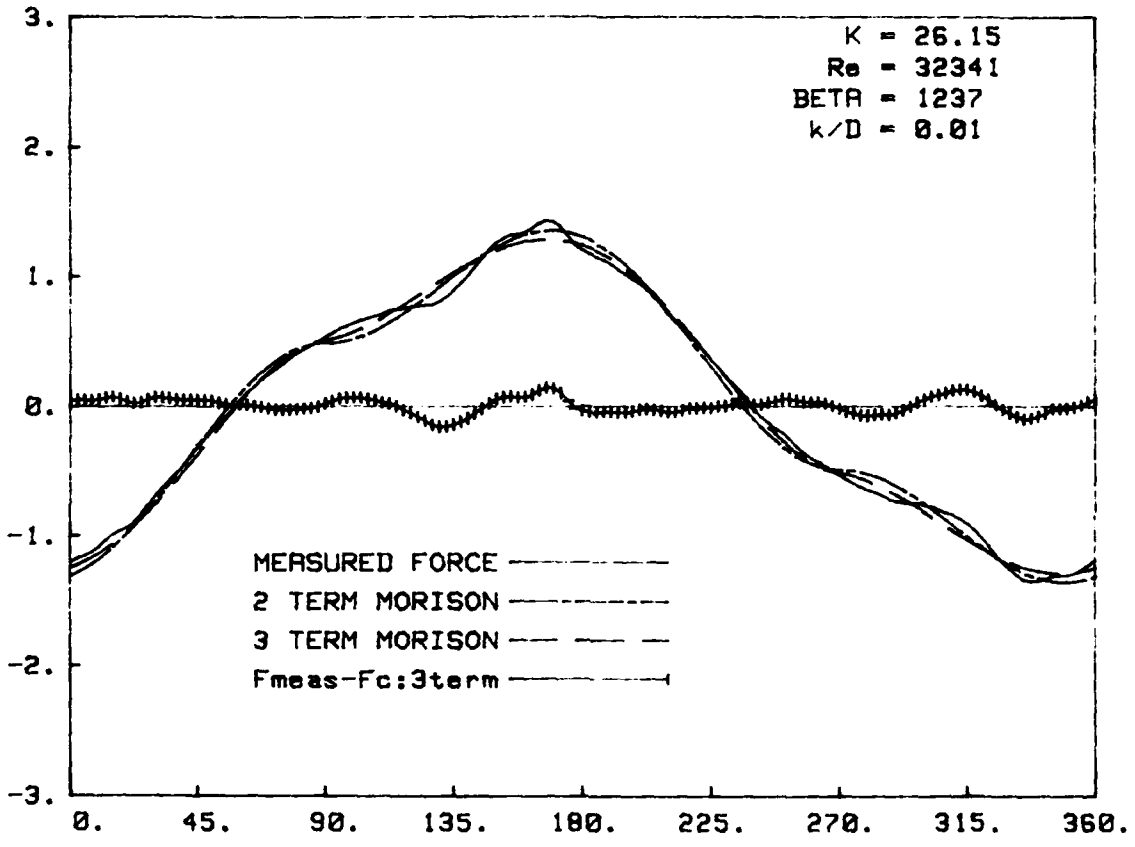

Fig. 65b Comparison of measured and calculated forces (Three-term MOJS Eq.)
K = 26.15

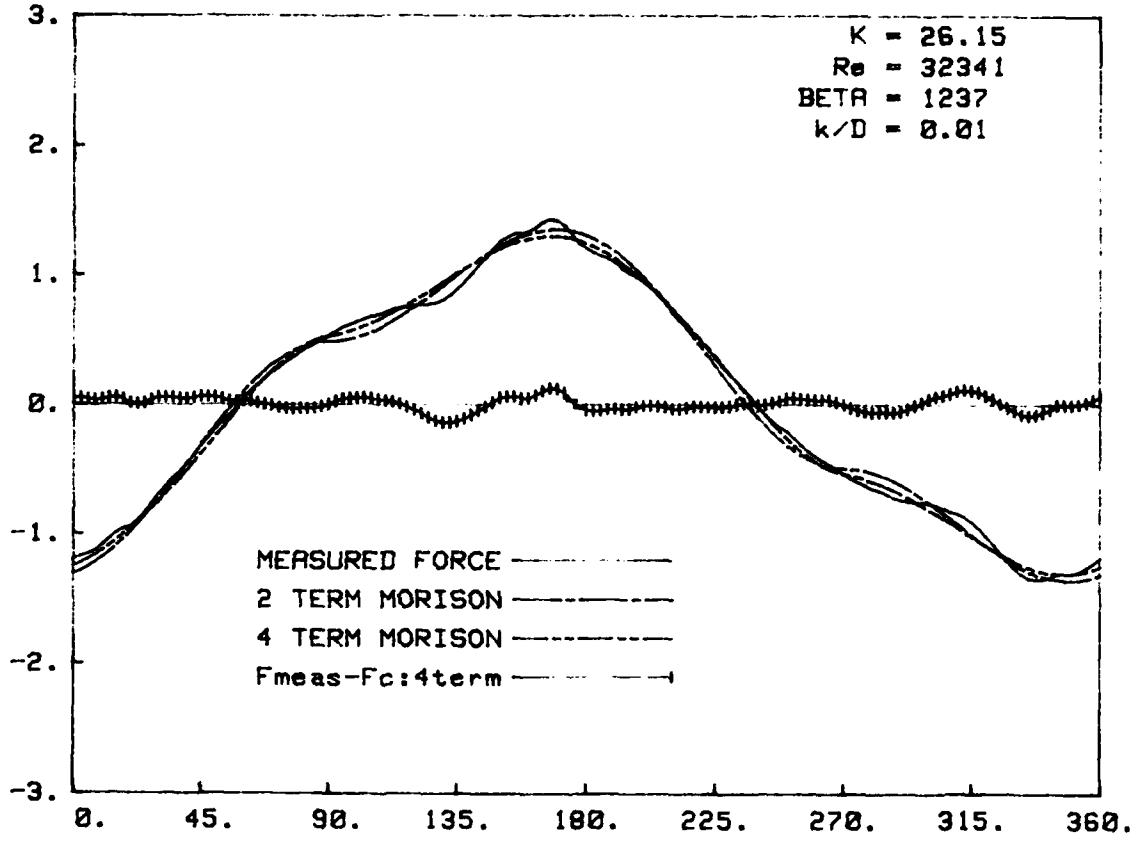

Fig. 65c Comparison of measured and calculated forces (Four-term MOJS Eq.)
K = 26.15

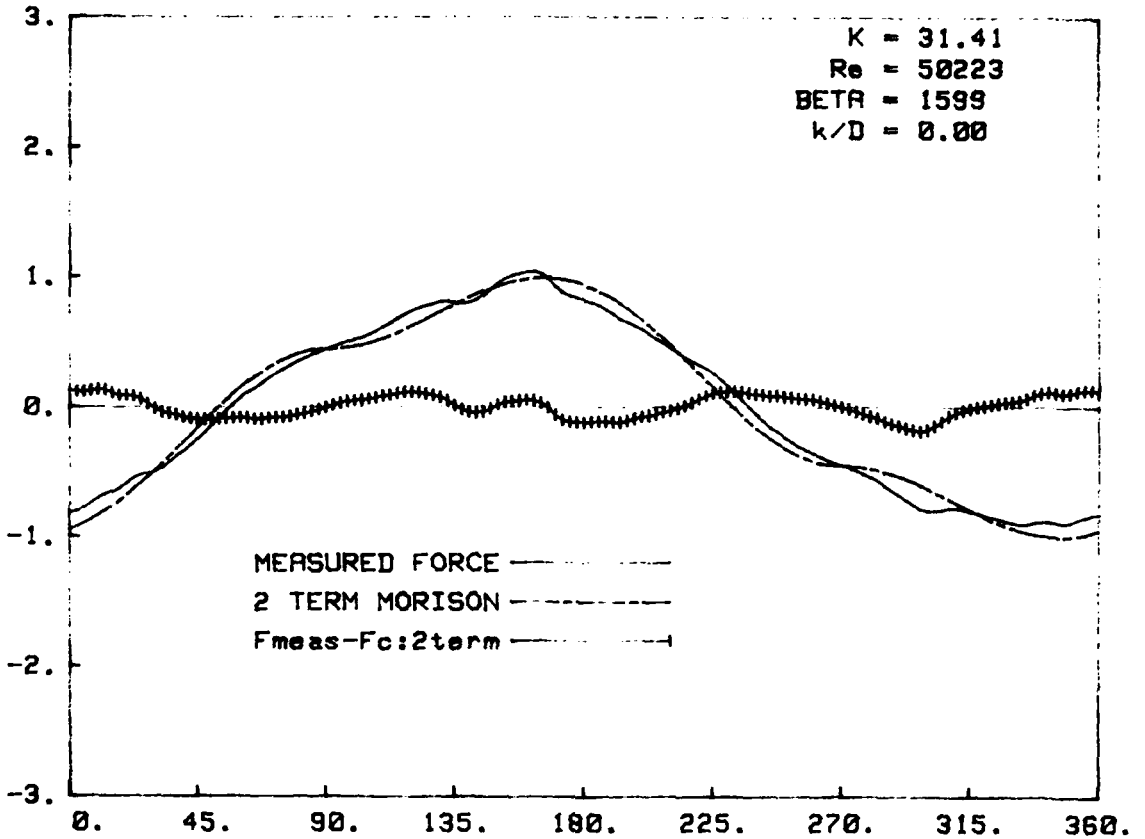

Fig. 66a Comparison of measured and calculated forces (Two-term MOJS Eq.)
K = 31.41

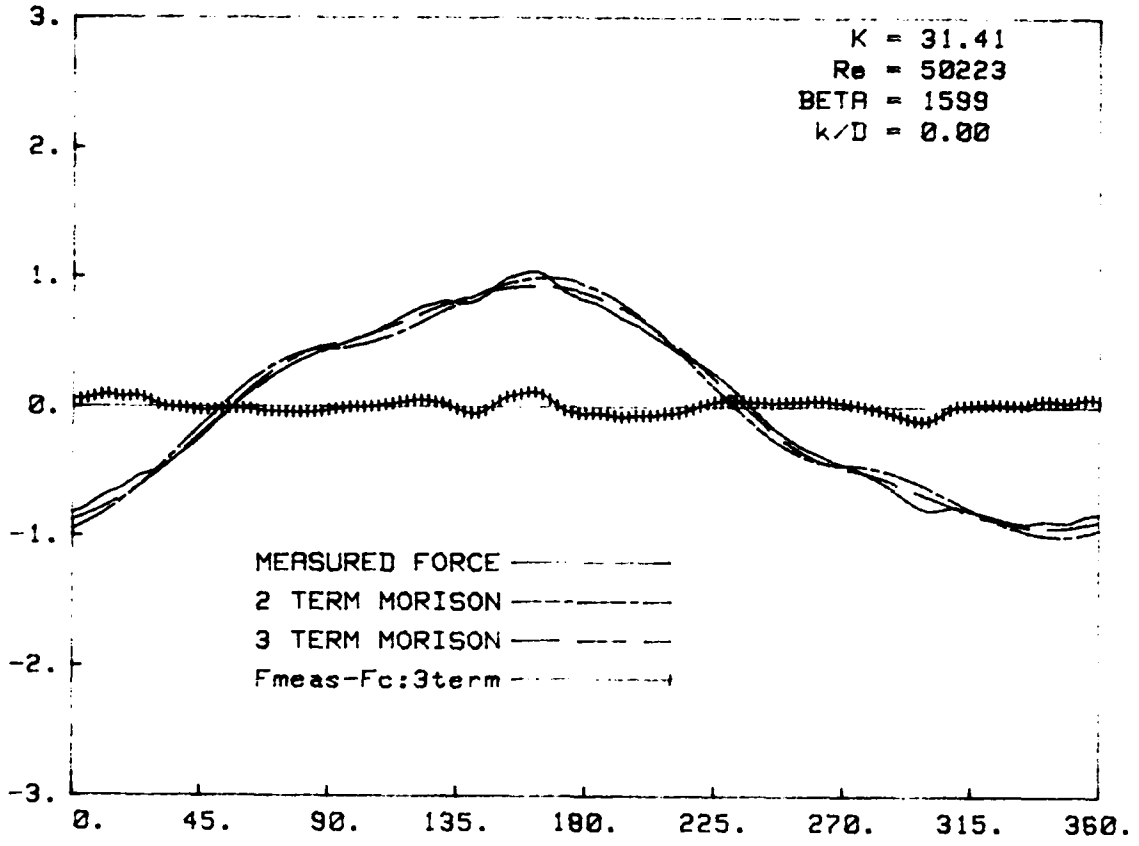

Fig. 66b Comparison of measured and calculated forces (Three-term MOJS Eq.)
K = 31.41

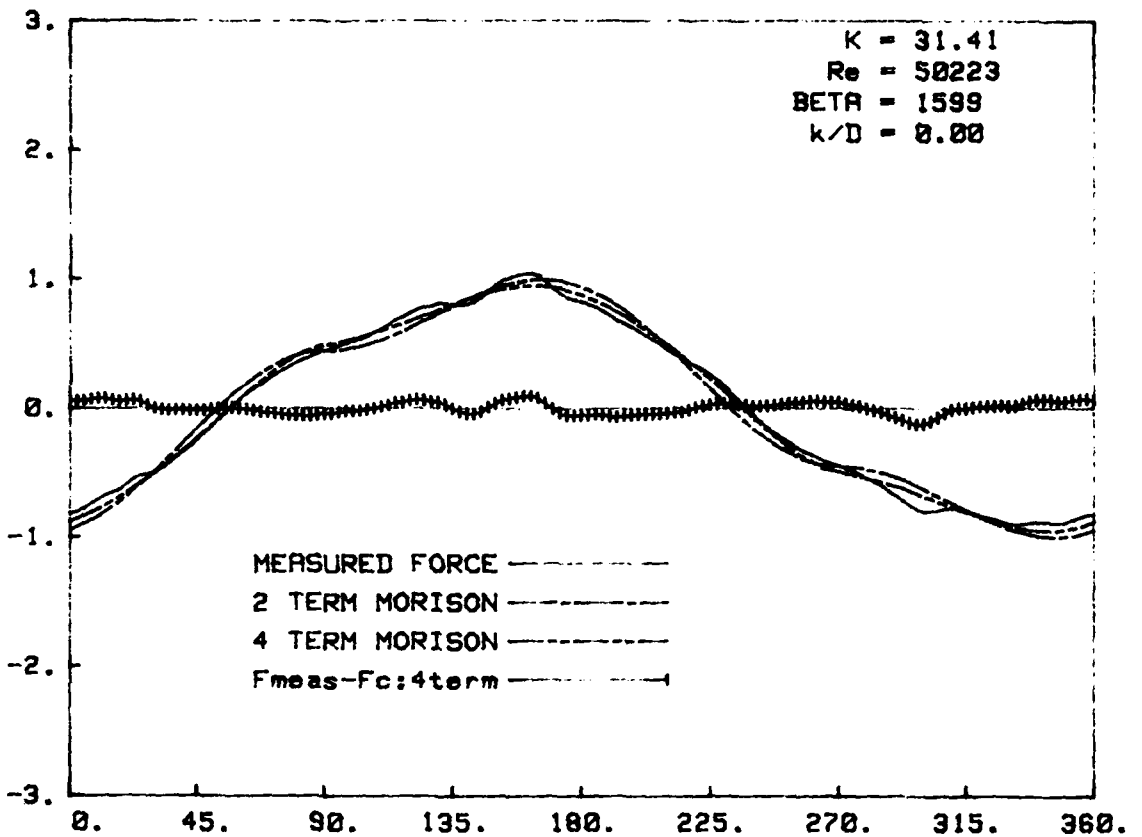

Fig. 66c Comparison of measured and calculated forces (Four-term MOJS Eq.)
K = 31.41

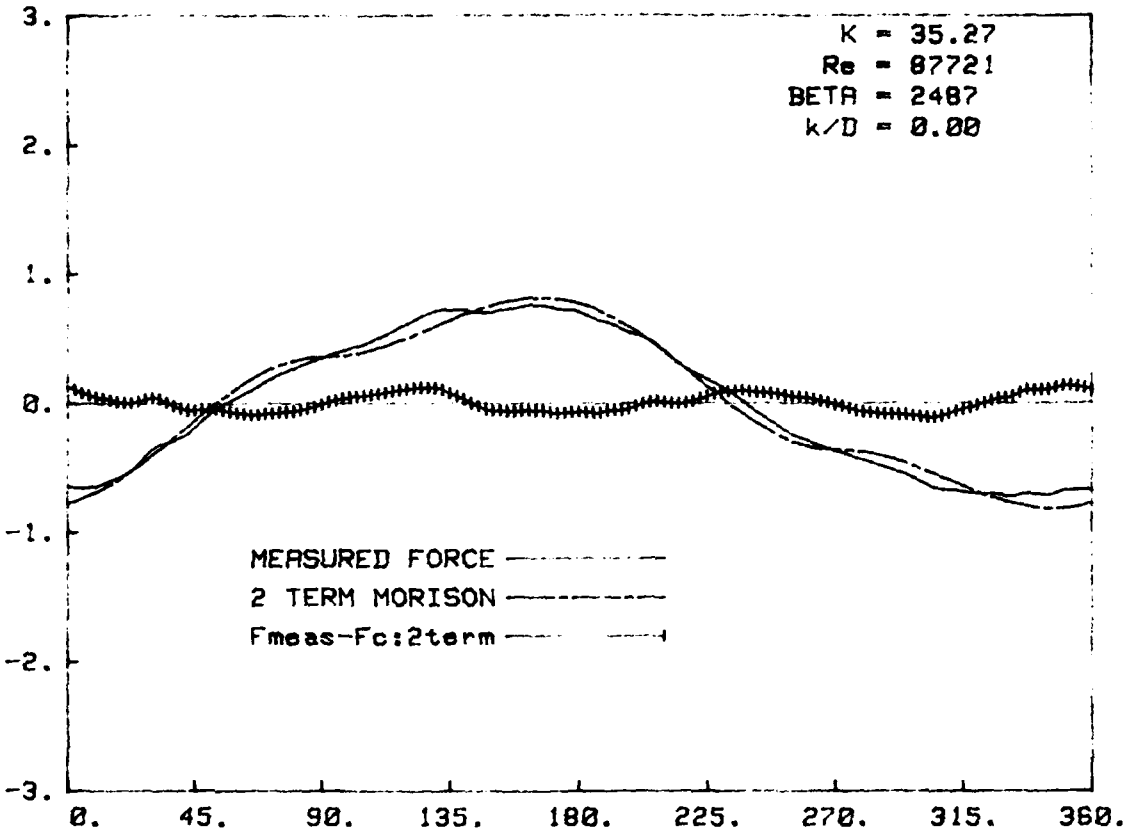

Fig. 67a Comparison of measured and calculated forces (Two-term MOJS Eq.)
K = 35.27

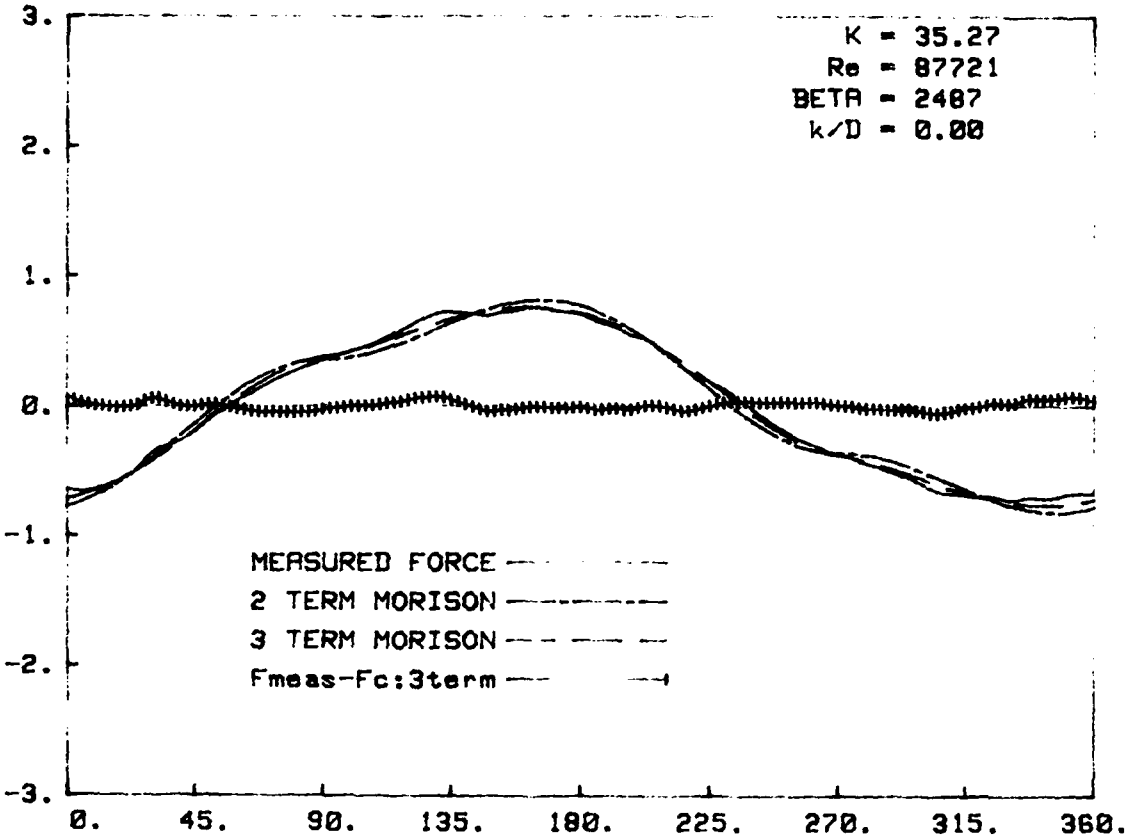

Fig. 67b Comparison of measured and calculated forces (Three-term MOJS Eq.)
K = 35.27

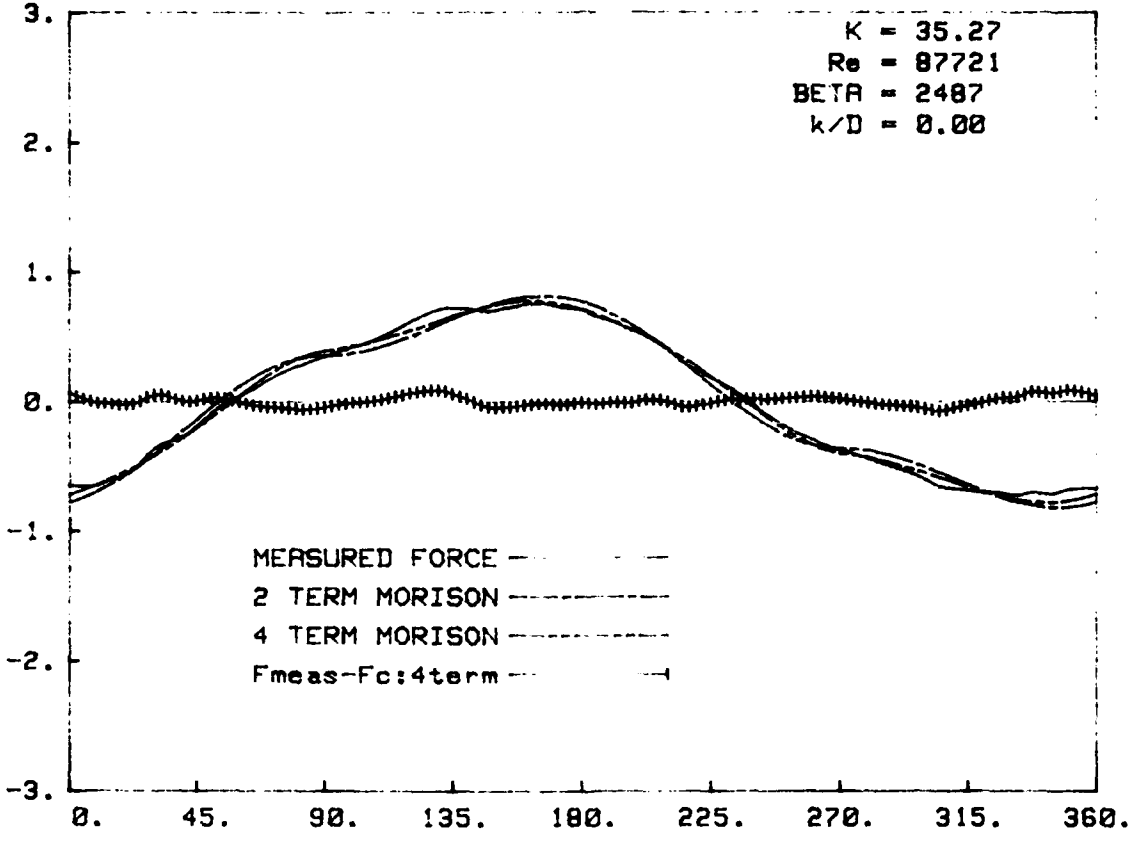

Fig. 67c Comparison of measured and calculated forces (Four-term MOJS Eq.)
K = 35.27

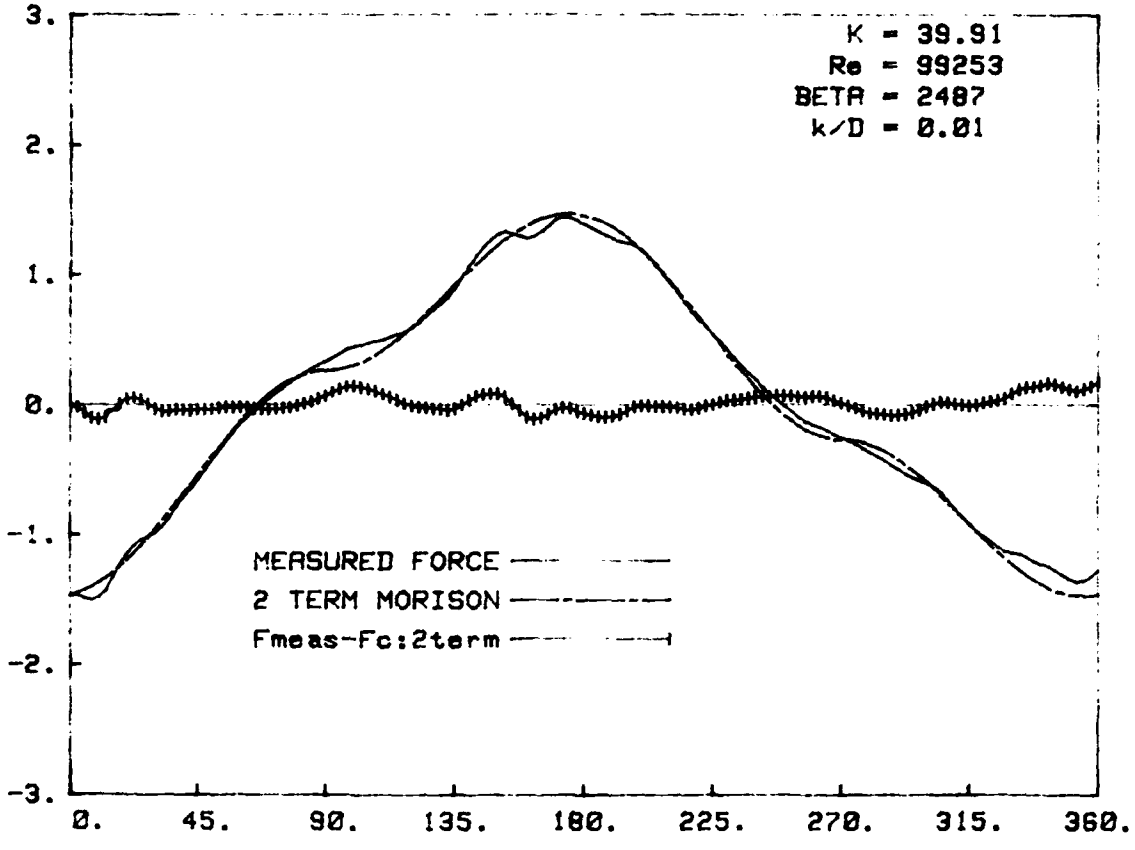

Fig. 68a Comparison of measured and calculated forces (Two-term MOJS Eq.)
K = 39.91

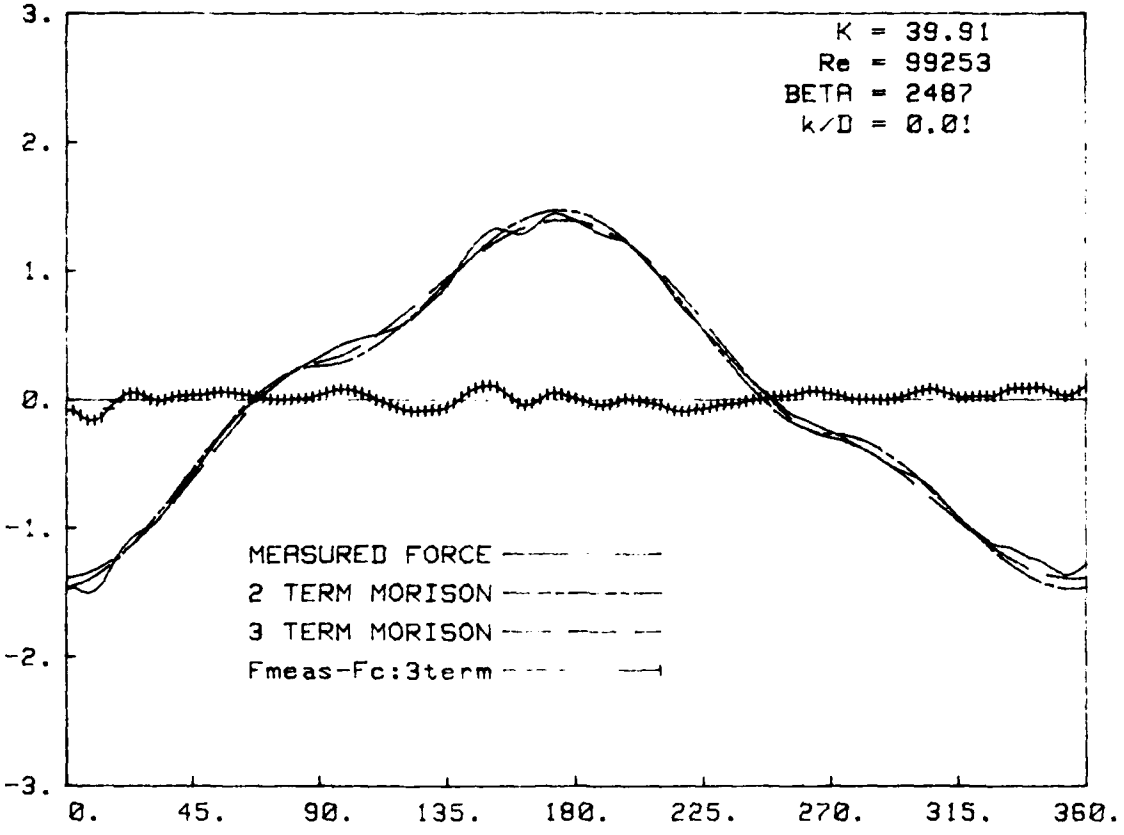

Fig. 68b Comparison of measured and calculated forces (Three-term MOJS Eq.)
K = 39.91

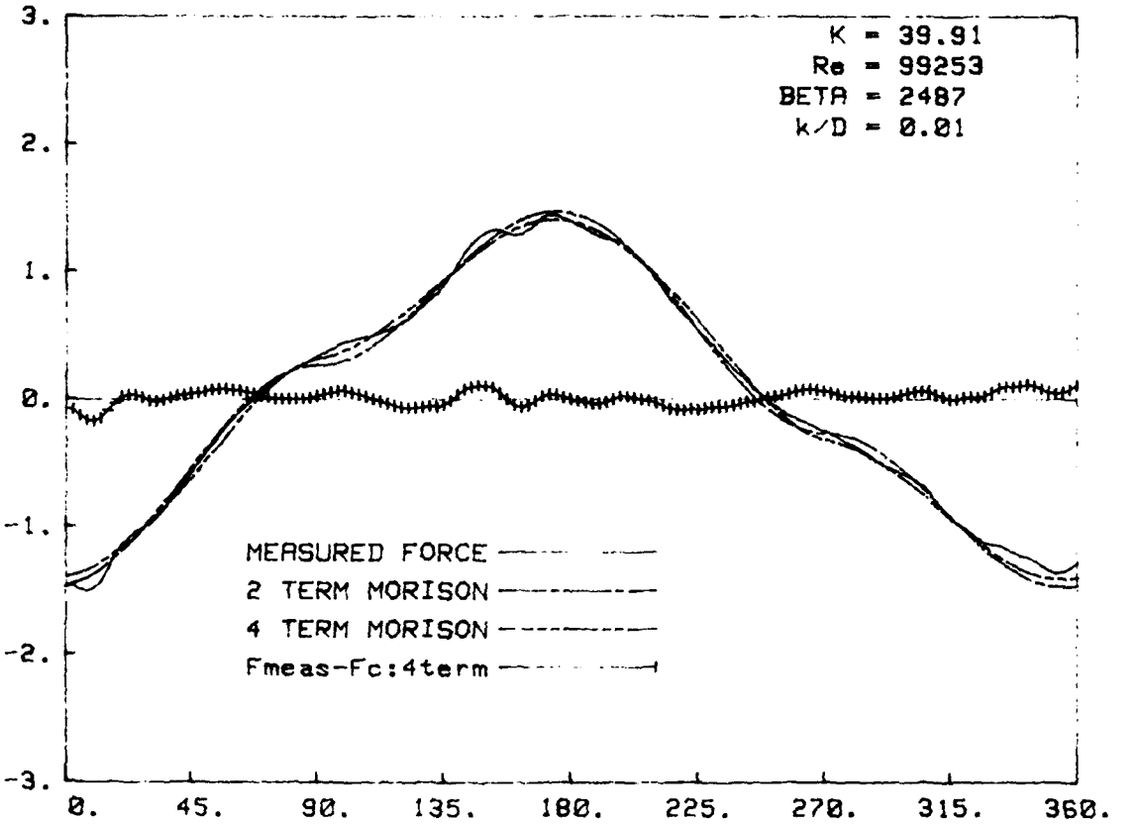

Fig. 6[illegible] Comparison of measured and calculated forces (Four-term MOJS Eq.)
K = 39.91

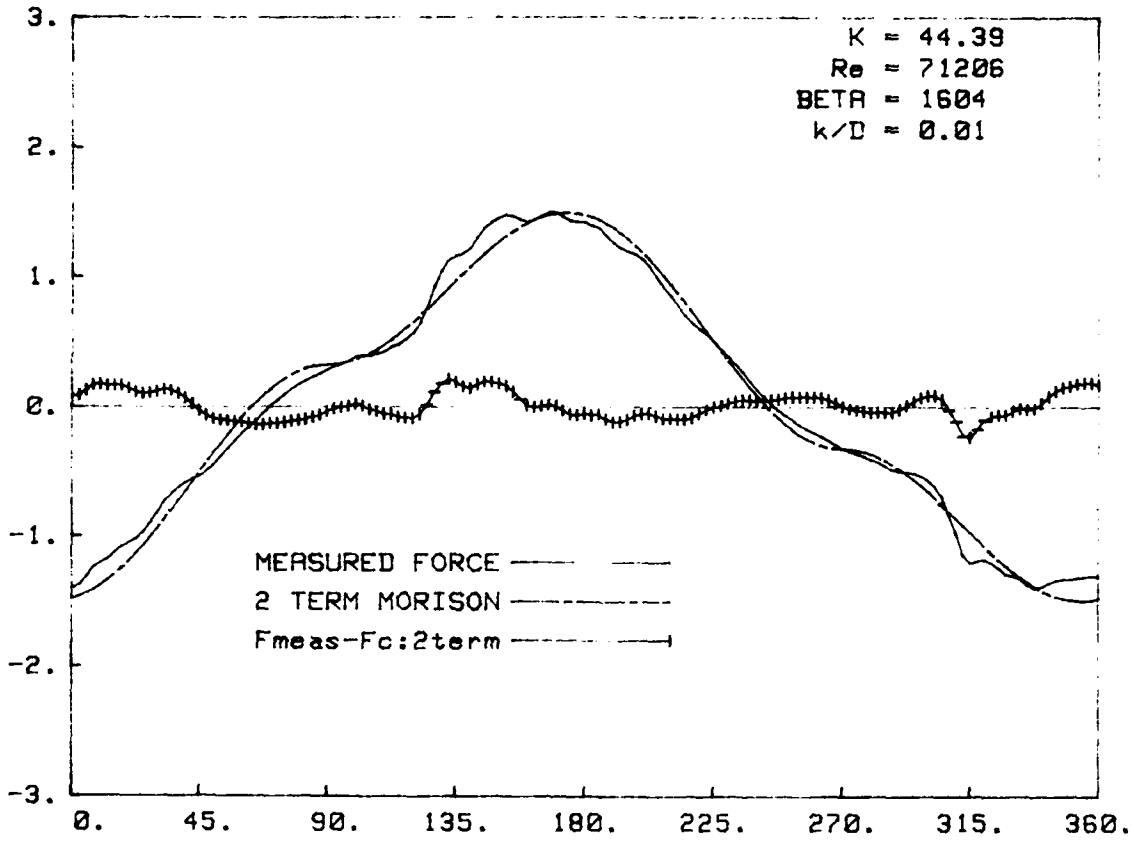

Fig. 69a Comparison of measured and calculated forces (Two-term MOJS Eq.)
K = 44.39

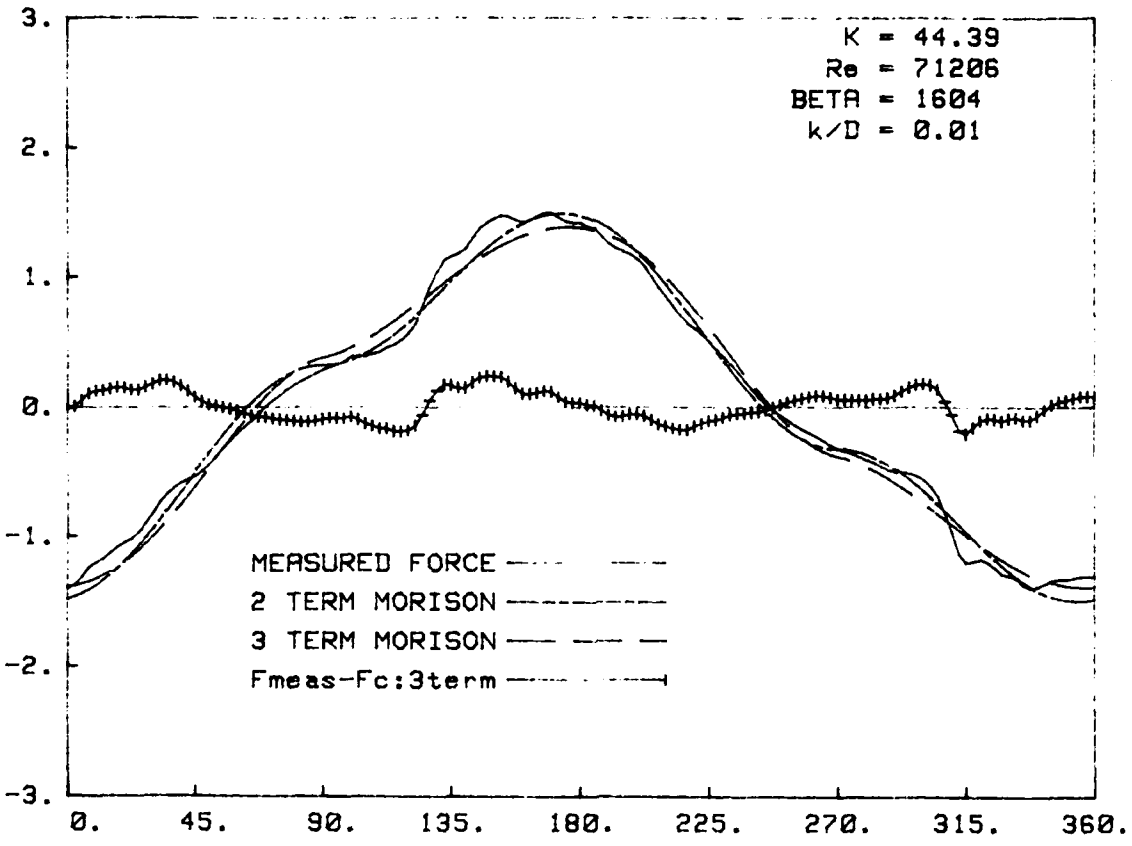

Fig. 69b Comparison of measured and calculated forces (Three-term MOJS Eq.)
K = 44.39

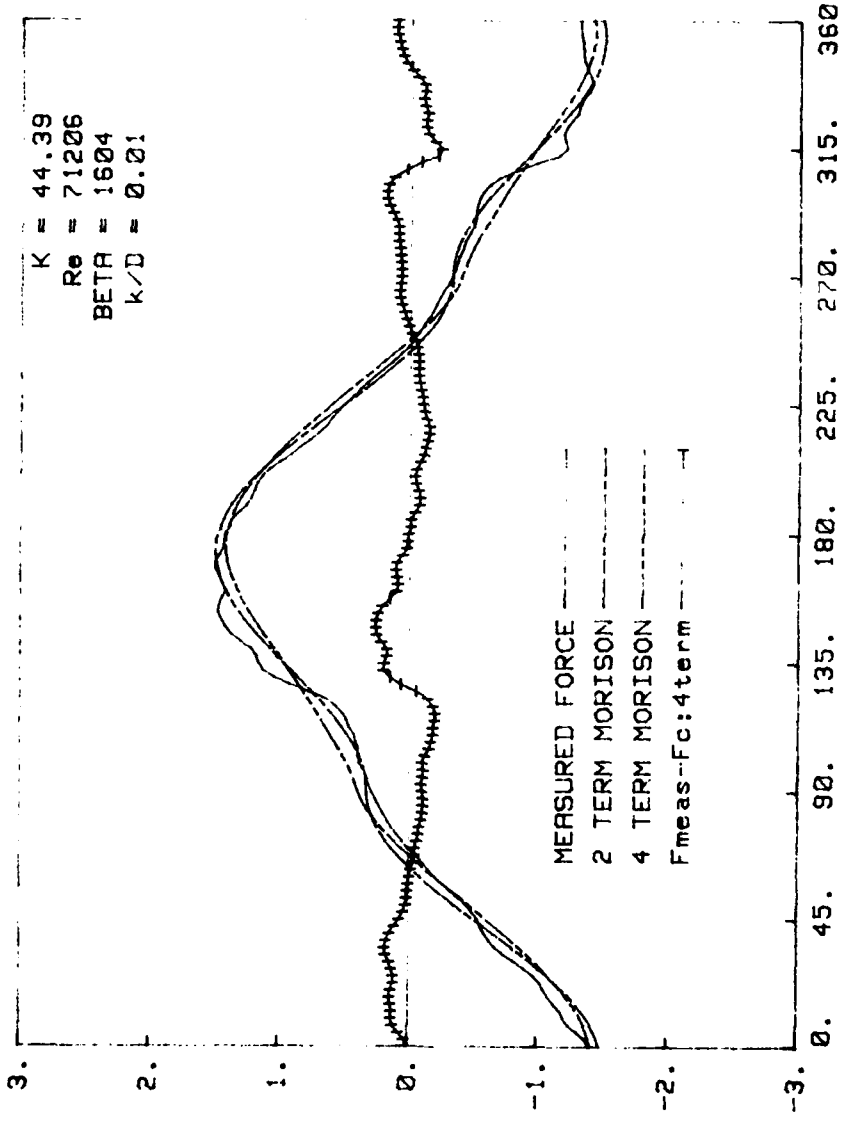

Fig. 69c Comparison of measured and calculated forces (Four-term MOJS Eq.)
K = 44.39

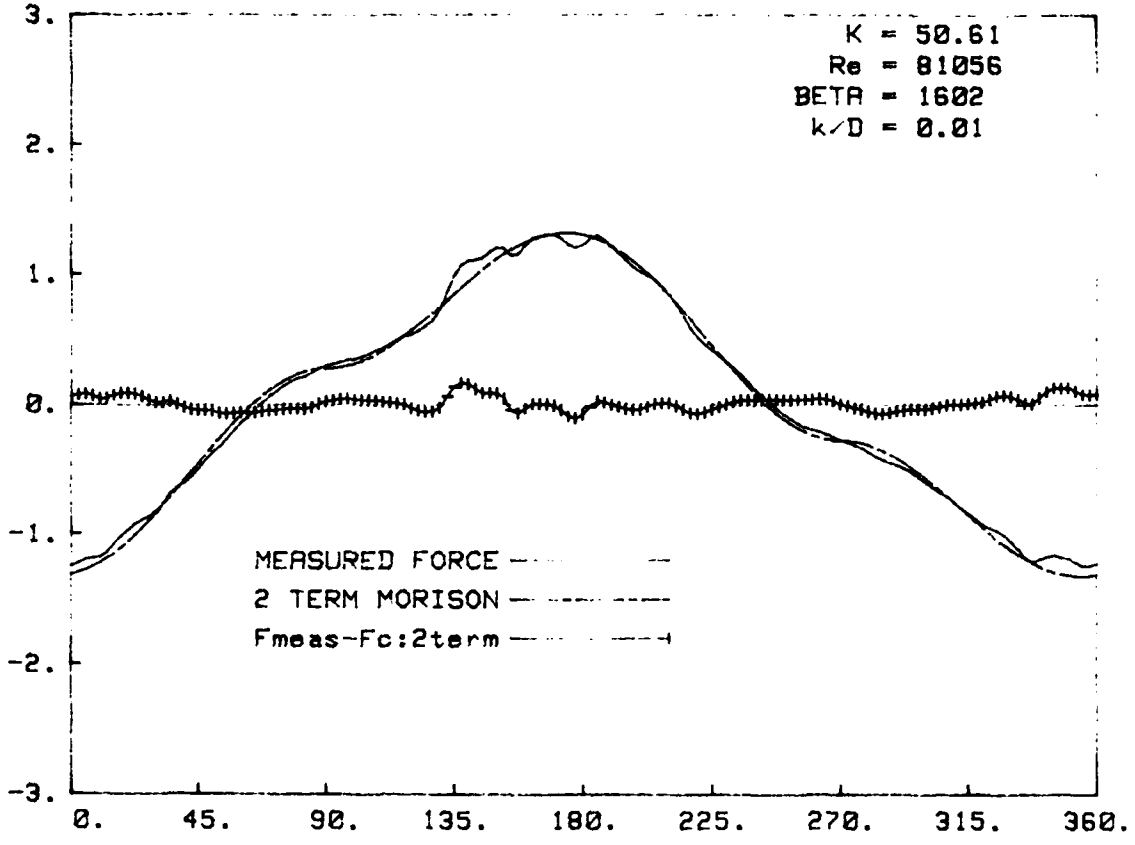

Fig. 70a Comparison of measured and calculated forces (Two-term MOJS Eq.)
K = 50.61

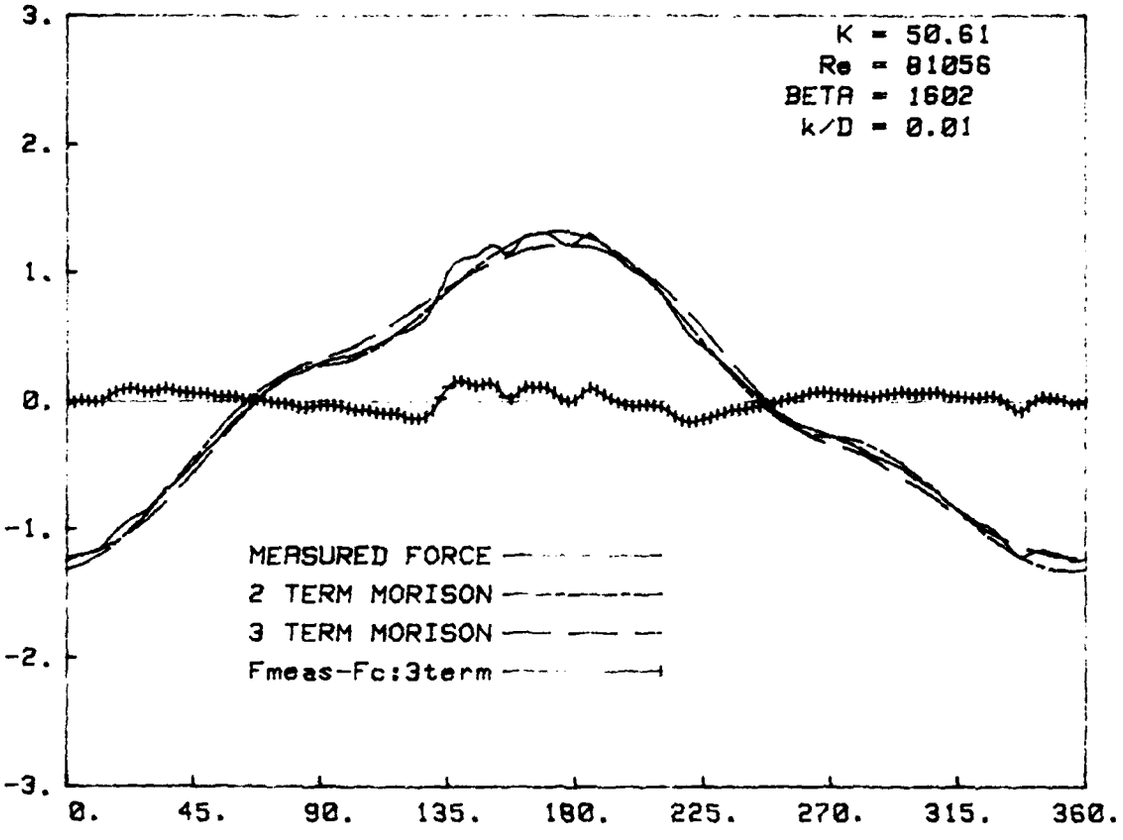

Fig. 70b Comparison of measured and calculated forces (Three-term MOJS Eq.)
K = 50.61

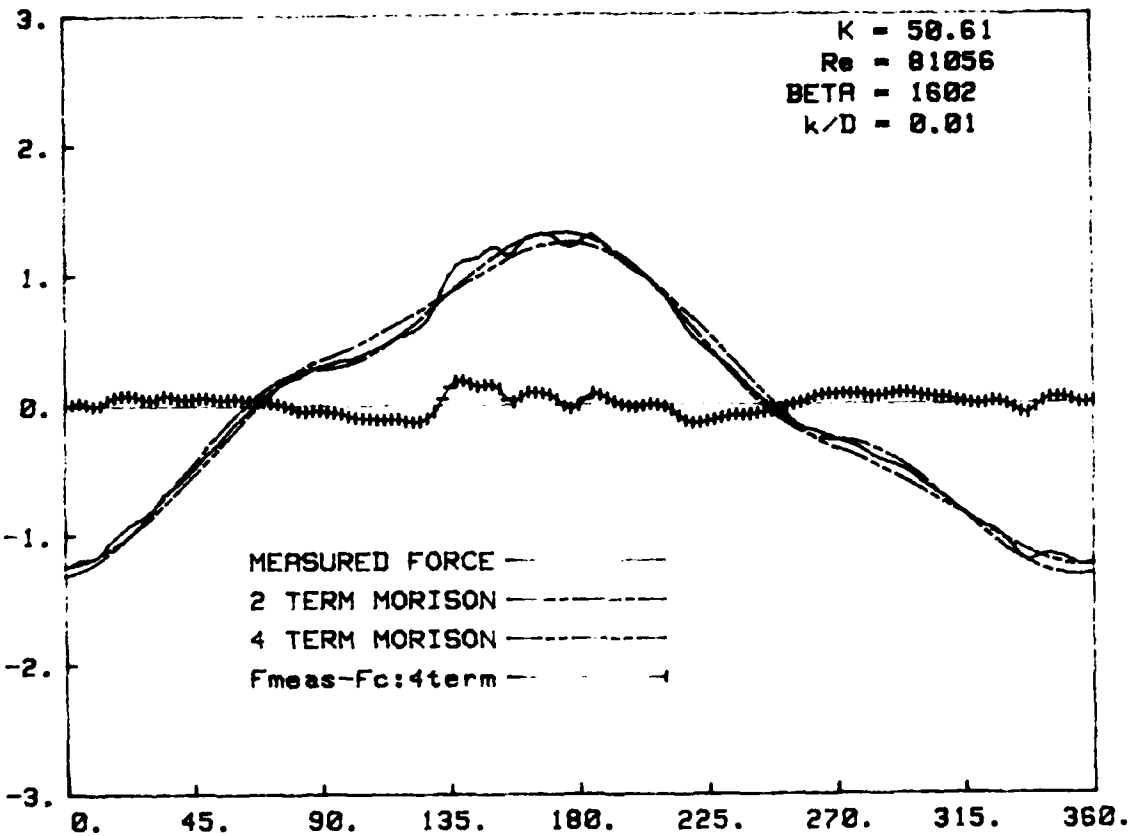

Fig. 70c Comparison of measured and calculated forces (four-term MOJS Eq.)
K = 50.61

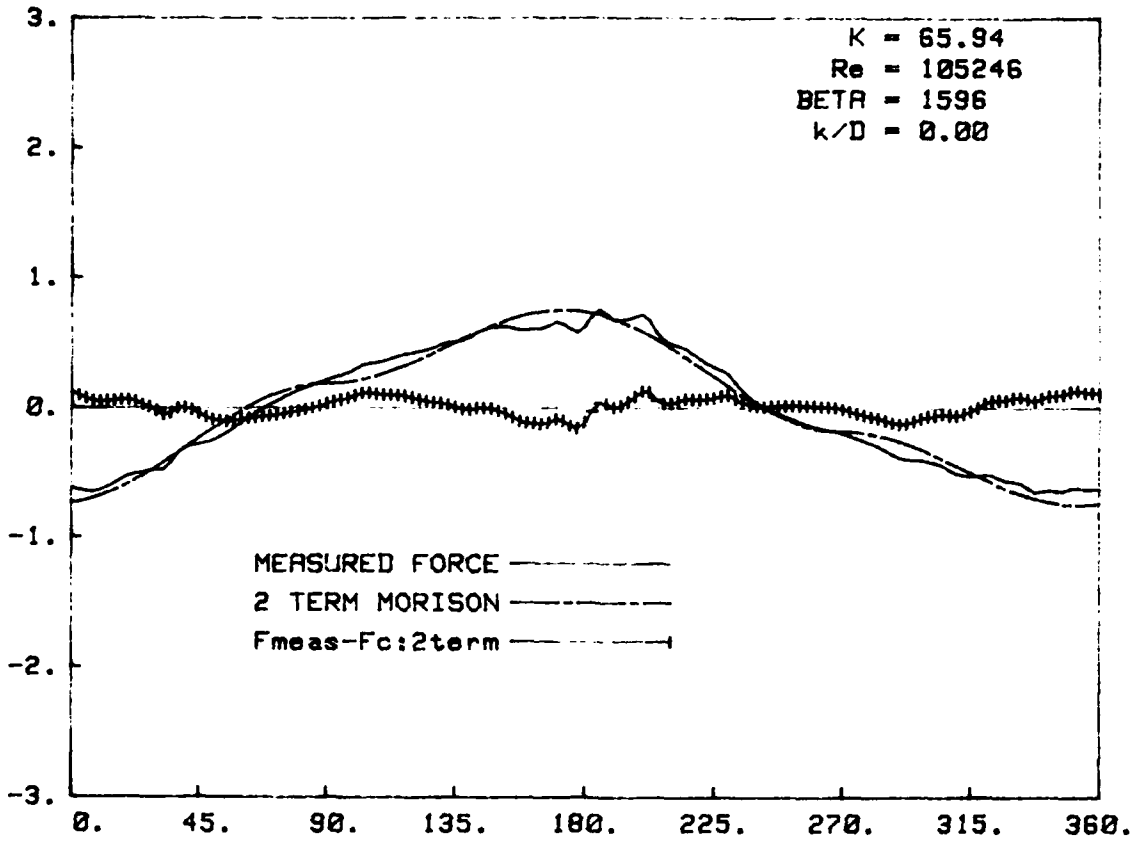

Fig. 71a Comparison of measured and calculated forces (Two-term MOJS Eq.)
K = 65.94

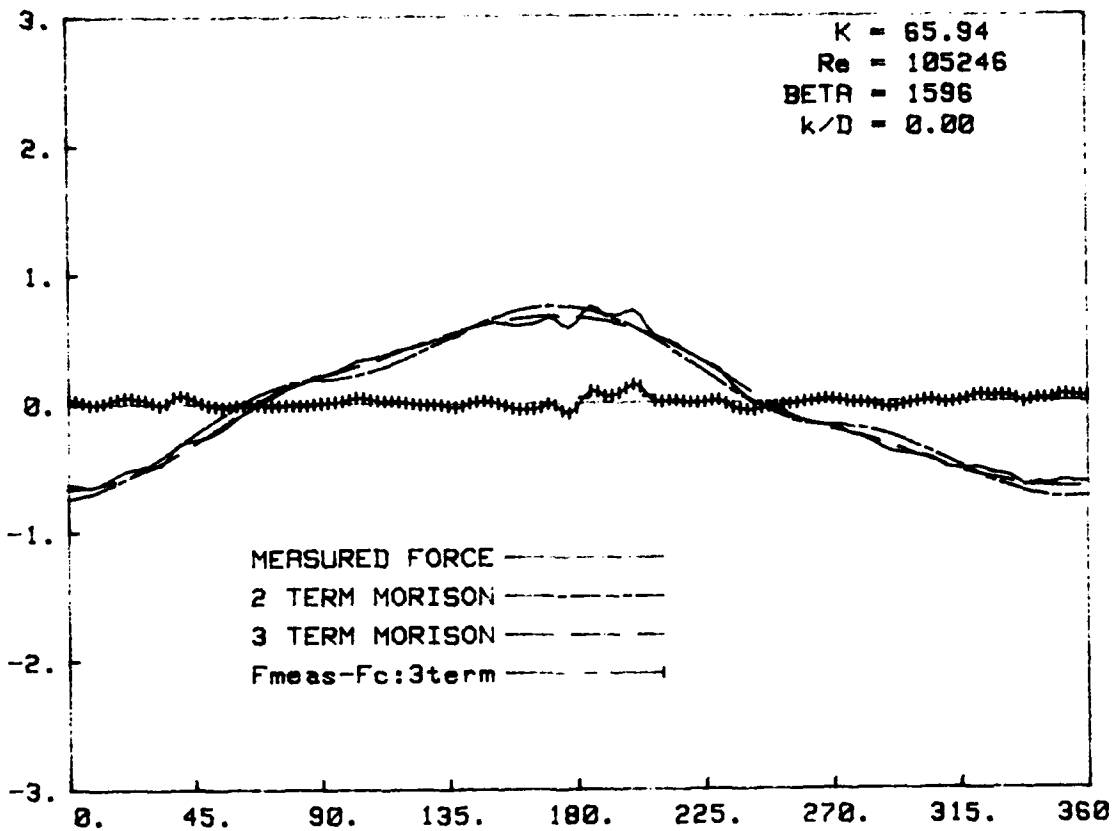

Fig. 71b Comparison of measured and calculated forces (Three-term MOJS Eq.)
K = 65.94

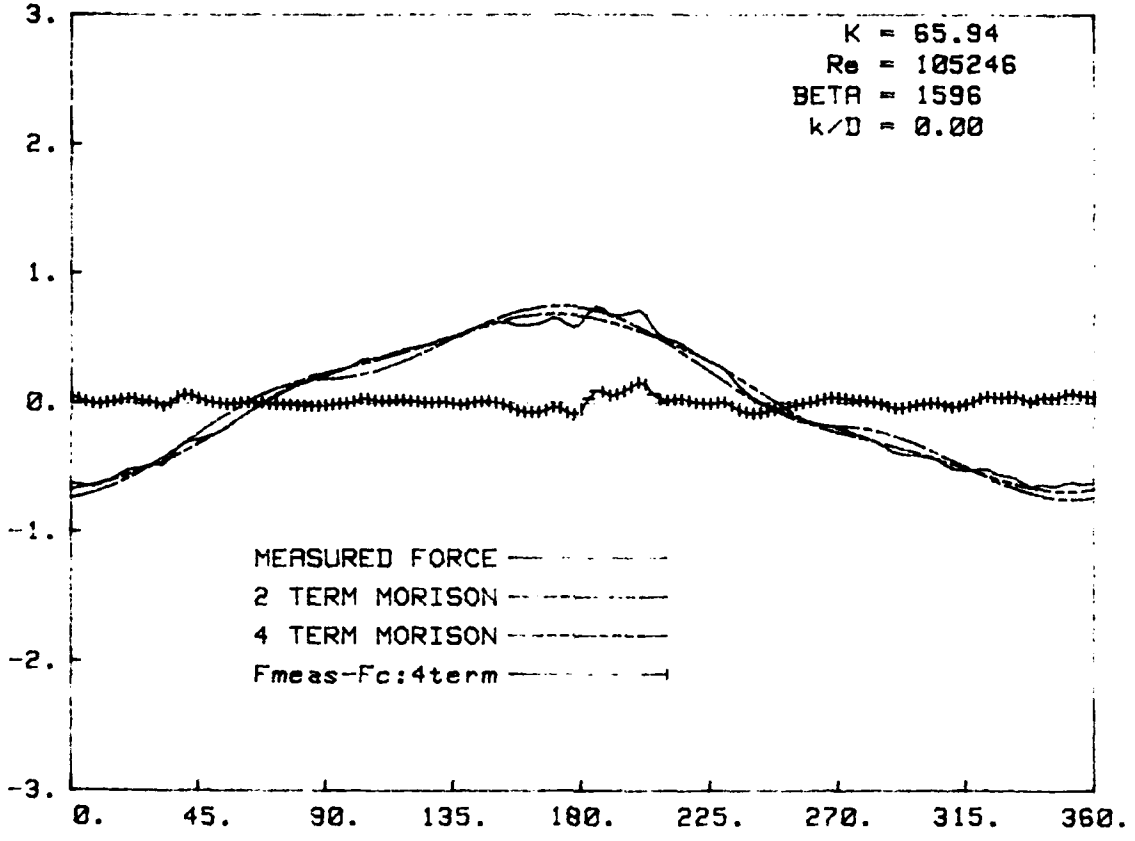

Fig. 71c Comparison of measured and calculated forces (Four-term MOJS Eq.)
K = 65.94

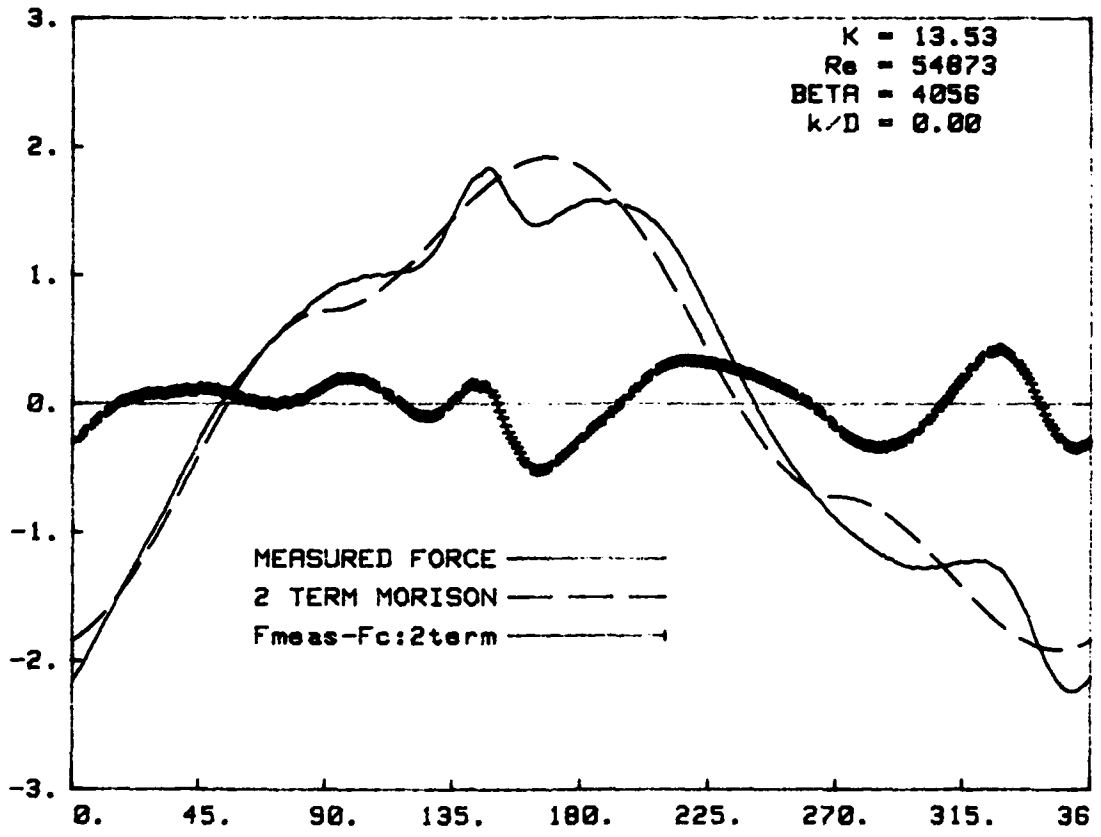

Fig. 72a Comparison of measured and calculated force (Two-term MOJS eq.)
K = 13.53

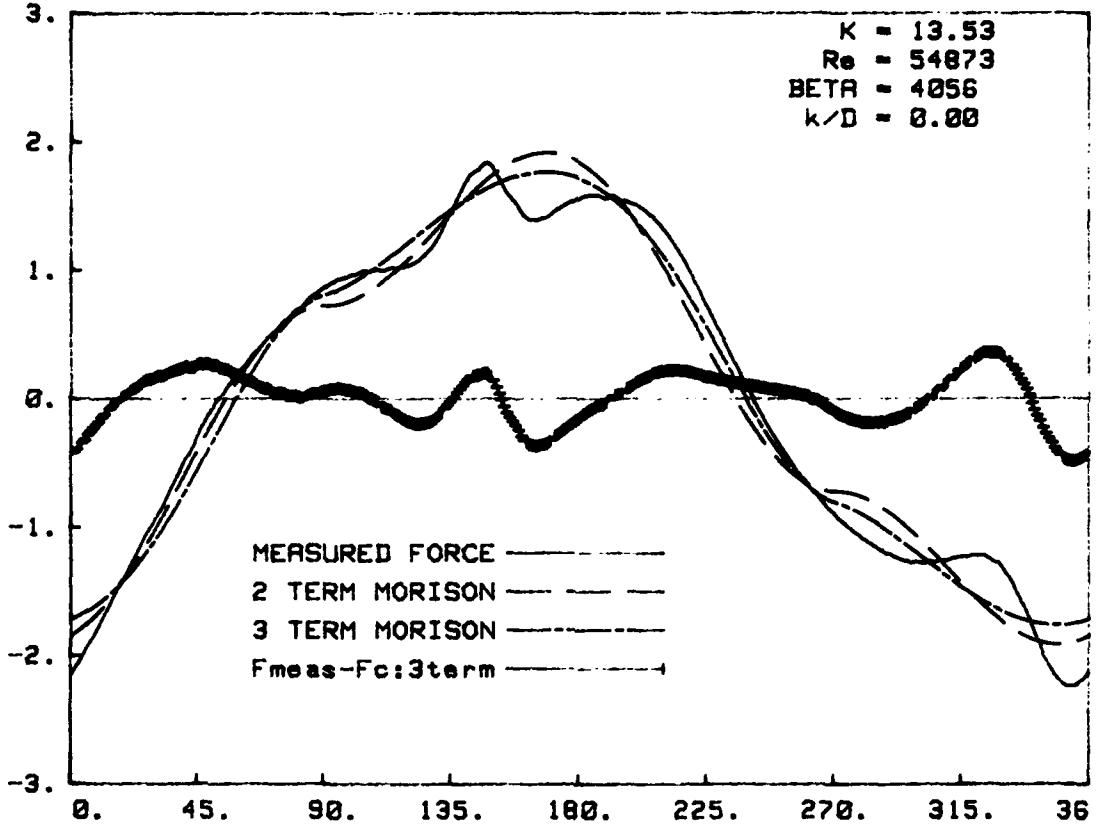

Fig. 72b Comparison of measured and calculated force (Three-term MOJS Eq.)
K = 13.53 and Ψ = 0.3

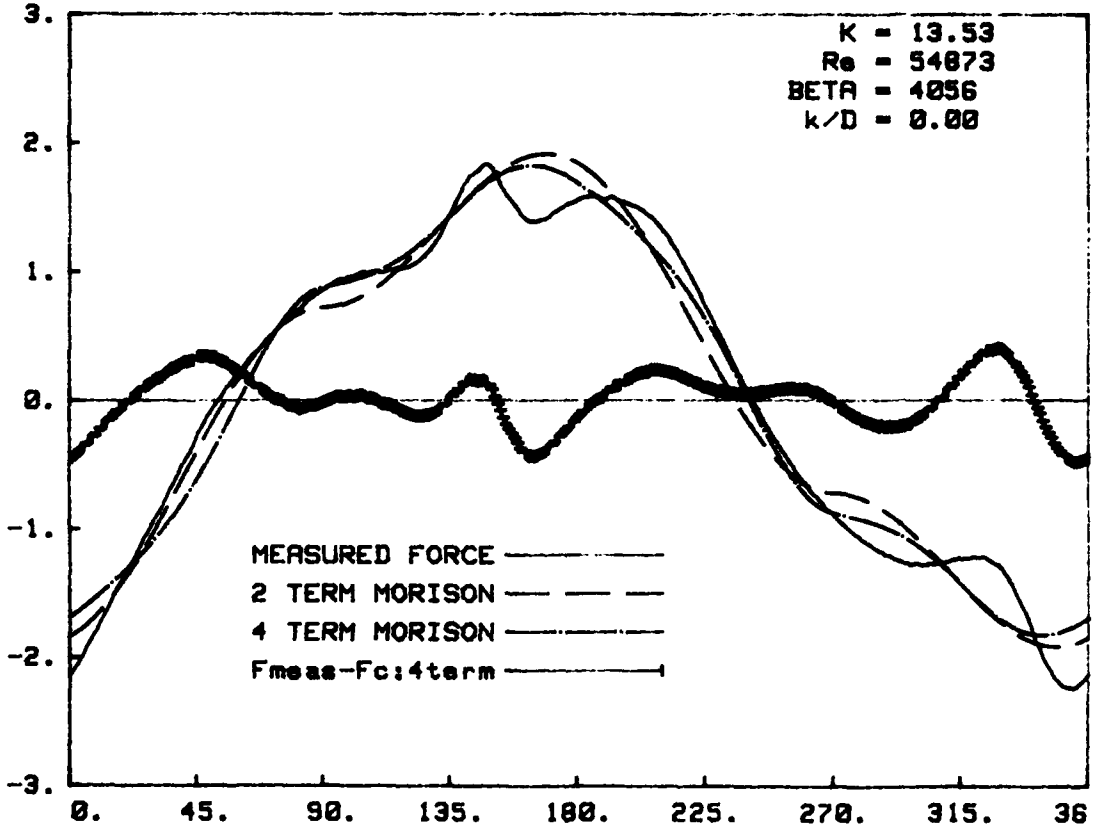

Fig. 72c Comparison of measured and calculated forces (Four-term MOJS Eq.)
K = 13.53 and Ψ = 0.3

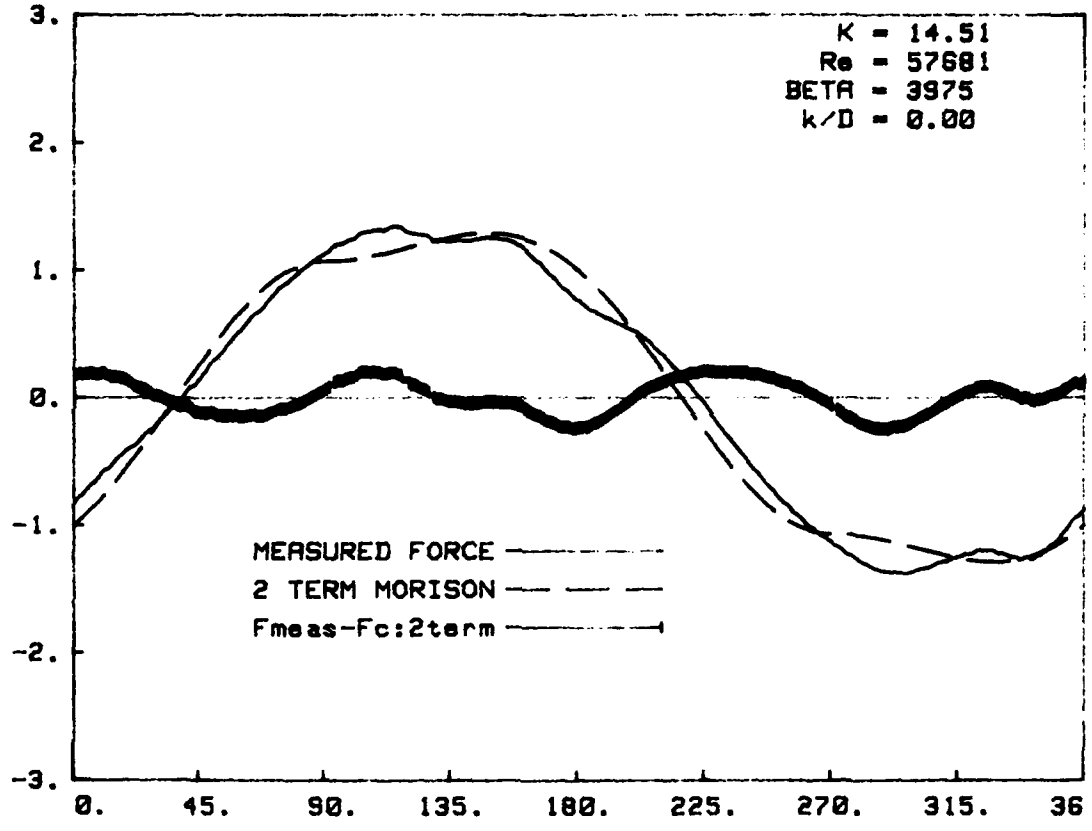

Fig. 73a Comparison of measured and calculated forces (Two-term MOJS Eq.)
K = 14.51

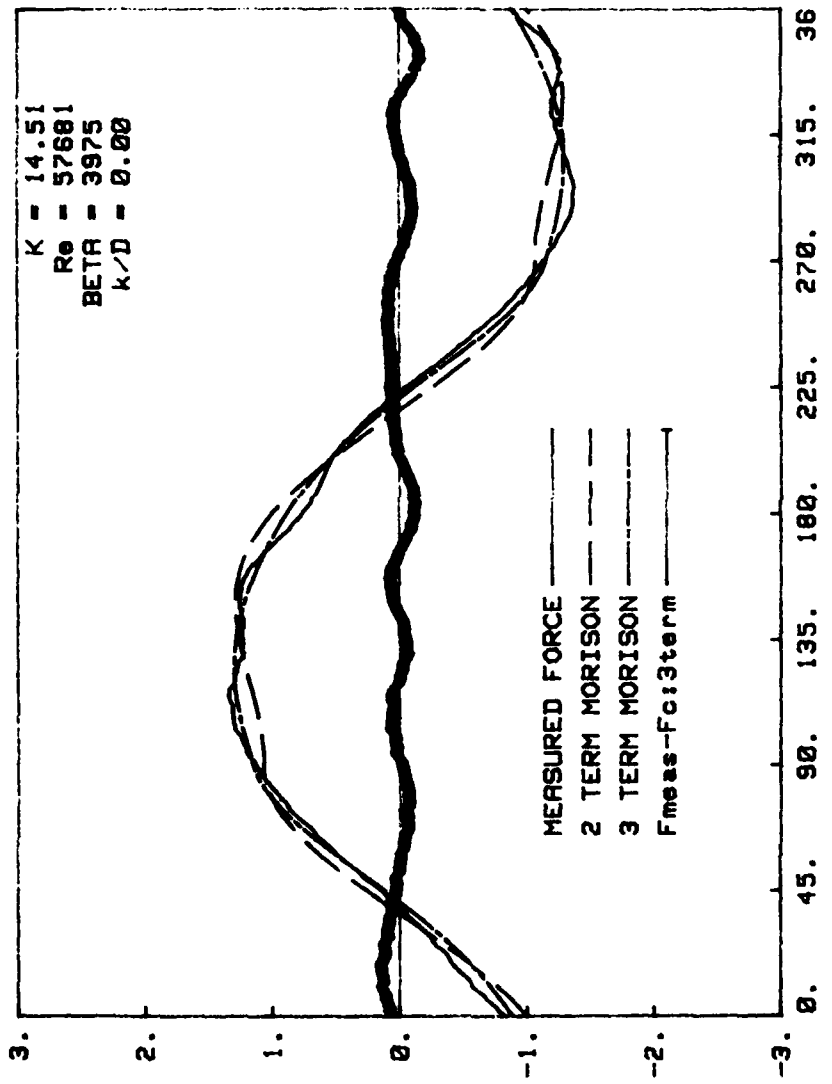

Fig. 73b Comparison of measured and calculated forces (Three-term MOJS Eq.)
K = 14.51 and ψ = 0.3

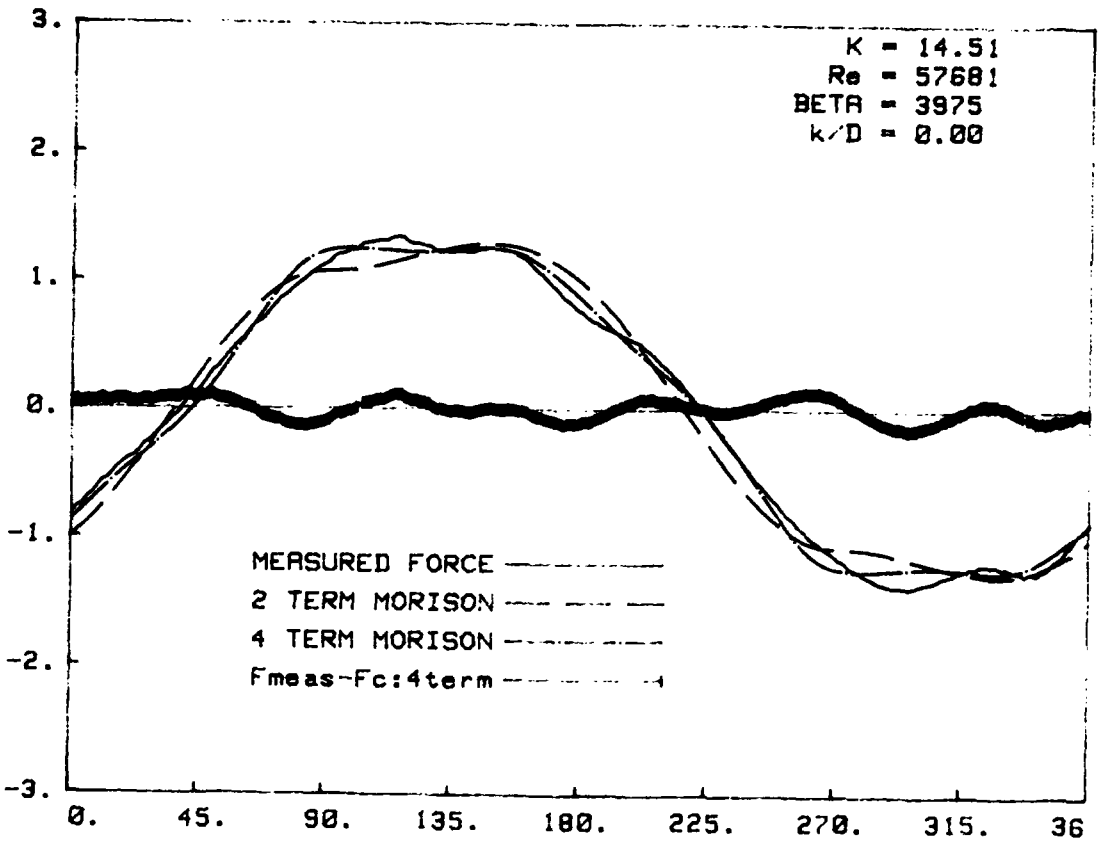

Fig. 73c Comparison of measured and calculated forces (Four-term MOJS Eq.)
K = 14.51 and Ψ = 0.3

Table 1. Fourier Coefficients for K = 6.47,
Re = 34763, k/D = 0.00

N	A(N)	B(N)	Magnitude	Phase [Deg]
1	.0030	-.0000	.0030	-.78
2	.0167	.0224	.0280	53.31
3	.2056	-.0286	.2076	-7.92
4	.0102	.0123	.0160	50.35
5	-.0042	-.0127	.0134	-108.42
6	.0001	.0039	.0039	88.17
7	.0054	.0007	.0054	7.60
8	.0029	.0022	.0036	36.26
9	-.0049	.0010	.0050	168.86
10	-.0009	.0003	.0010	161.11

Table 2. Fourier Coefficients for K = 8.64,
Re = 14181, k/D = 0.01

N	A(N)	B(N)	Magnitude	Phase [Deg]
1	.0031	-.0021	.0038	-33.80
2	.0144	-.0128	.0193	-41.48
3	.0101	-.0972	.0978	-84.07
4	-.0241	.0454	.0514	117.99
5	-.0935	-.0099	.0940	-173.96
6	.0123	.0323	.0346	69.07
7	-.0148	.0279	.0316	117.89
8	.0084	.0122	.0148	55.50
9	-.0048	.0177	.0183	105.14
10	.0058	.0081	.0100	54.55

Table 3. Fourier Coefficients for K = 9.41,
Re = 50442, k/D = 0.00

N	A(N)	B(N)	Magnitude	Phase [Deg]
1	.0101	-.0001	.0101	-.39
2	-.0057	-.0045	.0072	-142.00
3	.0329	-.2635	.2655	-82.89
4	.0081	-.0028	.0085	-18.93
5	-.1098	-.1125	.1572	-134.31
6	-.0091	.0044	.0101	154.36
7	-.0247	-.0241	.0344	-135.69
8	-.0083	.0054	.0099	146.82
9	-.0083	-.0065	.0106	-141.68
10	-.0026	-.0004	.0026	-171.60

Table 4. Fourier Coefficients for K = 10.45
Re = 55962, k/D = 0.00

N	A(N)	B(N)	Magnitude	Phase [Deg]
1	.0105	.0000	.0105	.24
2	.0959	-.0510	.1087	-28.01
3	.0476	-.4226	.4253	-83.58
4	.0650	-.0132	.0663	-11.50
5	-.1281	-.1233	.1778	-136.11
6	.0119	.0003	.0119	1.50
7	-.0211	-.0185	.0281	-138.86
8	.0001	.0126	.0126	89.40
9	-.0104	-.0029	.0108	-164.43
10	-.0022	.0056	.0060	111.60

Table 5. Fourier Coefficients for K = 11.43
Re = 61533, k/D = 0.00

N	A(N)	B(N)	Magnitude	Phase [Deg]
1	.0132	.0000	.0132	.16
2	.0115	-.0243	.0269	-64.62
3	.0227	-.4839	.4844	-87.32
4	.0392	-.0174	.0429	-23.97
5	-.1634	-.1477	.2202	-137.89
6	.0198	-.0166	.0258	-39.86
7	-.0294	-.0371	.0473	-128.42
8	.0068	-.0051	.0085	-37.05
9	-.0124	-.0129	.0179	-133.97
10	.0039	-.0061	.0073	-57.30

Table 6. Fourier Coefficients for K = 12.43,
Re = 20038, k/D = 0.00

N	A(N)	B(N)	Magnitude	Phase [Deg]
1	.0226	.0001	.0226	.18
2	.0093	.0120	.0152	52.37
3	-.0902	-.4687	.4773	-100.90
4	.0156	.0051	.0165	18.18
5	-.2741	-.0608	.2808	-167.48
6	.0109	-.0107	.0153	-44.35
7	-.0504	.0295	.0584	149.62
8	.0018	.0072	.0075	76.13
9	-.0282	.0204	.0348	144.20
10	-.0042	.0056	.0070	127.32

Table 7. Fourier Coefficients for K = 13.59,
Re = 78806, k/D = 1/150

N	A(N)	B(N)	Magnitude	Phase [Deg]
1	.0246	-.0002	.0246	-.38
2	-.1787	.2196	.2831	129.14
3	-.1066	-.4403	.4531	-103.61
4	-.0726	.0727	.1027	134.95
5	-.2032	-.0234	.2046	-173.44
6	.0057	.0278	.0284	78.46
7	-.0349	.0675	.0760	117.36
8	.0099	.0052	.0112	27.75
9	-.0143	.0411	.0435	109.14
10	-.0042	.0063	.0076	123.98

Table 8. Fourier Coefficients for K = 15.97, Re = 25659, k/D = 0.01

N	A(N)	B(N)	Magnitude	Phase [Deg]
1	.0149	-.0000	.0149	-.04
2	-.0090	-.0456	.0465	-101.22
3	-.1244	-.2275	.2593	-118.67
4	-.0202	-.0290	.0353	-124.91
5	-.1366	-.0535	.1467	-158.61
6	.0028	-.0060	.0066	-65.19
7	-.0087	-.0178	.0198	-115.95
8	-.0005	-.0089	.0089	-93.39
9	-.0245	.0054	.0251	167.66
10	-.0020	-.0081	.0083	-104.21

Table 9. Fourier Coefficients for K = 16.34, Re = 40579, k/D = 0.01

N	A(N)	B(N)	Magnitude	Phase [Deg]
1	.0147	.0000	.0147	.06
2	.0509	-.0418	.0658	-39.41
3	-.0513	-.1432	.1521	-109.69
4	.0428	-.0126	.0446	-16.48
5	-.1079	-.0035	.1079	-178.12
6	.0262	-.0232	.0350	-41.57
7	-.0041	-.0162	.0167	-104.23
8	-.0229	-.0278	.0360	-129.54
9	-.0239	.0015	.0240	176.42
10	-.0335	-.0105	.0351	-162.55

Table 10. Fourier Coefficients for K = 20.62, Re = 33031, k/D = 0.01

N	A(N)	B(N)	Magnitude	Phase [Deg]
1	.0100	.0001	.0100	.49
2	-.0134	.0099	.0166	143.57
3	.0854	.0028	.0855	1.90
4	.0280	-.0353	.0451	-51.58
5	-.0281	.0059	.0288	168.12
6	-.0120	-.0285	.0309	-112.85
7	.0069	-.0023	.0073	-18.82
8	-.0281	-.0009	.0281	-178.14
9	-.0075	-.0002	.0075	-178.39
10	-.0130	.0164	.0209	128.39


DATE
ILME